A MULTIDISCIPLINARY INVESTIGATION OF TUBERCULOSIS: MATHEMATICAL AND EXPERIMENTAL STUDIES OF NATURAL HISTORY, DRUG RESISTANCE BIOLOGY, AND MDR-TB TRANSMISSION

by
Phillip Parker Salvatore

A dissertation submitted to Johns Hopkins University in conformity with the requirements for the degree of Doctor of Philosophy

Baltimore, Maryland
April 2018

DISSERTATION ABSTRACT

Background: Tuberculosis (TB) is the ninth leading cause of death worldwide and the leading cause of death from an infectious agent. While control efforts have achieved gradual reductions in TB incidence globally, continuing these declines into the future will require the interface of many scientific and public health disciplines.

Methods: We conducted three investigations of TB biology and epidemiology in a multidisciplinary approach to public health research for infectious disease control. We articulated a novel framework for linking individual-level TB disease progression with population-level clinical outcomes; we investigated the molecular mechanisms of pyrazinamide action on TB inhibition; and we modeled the influence of multidrug resistant TB (MDR-TB) transmission efficiency on long-term projections of the TB epidemic.

Results: Our mathematical framework effectively links individual disease progression dynamics with clinical outcomes, and we demonstrate the impact of these dynamics on important epidemiological metrics. We identify a novel protein interaction between Ribosome Recycling Factor and bacterial protein RpsA, a potential target of pyrazinamide action. Finally, we demonstrate that predicted trends in future MDR-TB epidemics are highly sensitive to variations in MDR-TB transmission efficiency.

Conclusions: This dissertation provides a unique example of how research through multiple lenses of public health science may provide novel insight into infectious disease control.

DISSERTATION READERS AND FINAL ORAL EXAMINATION COMMITTEE

Jonathan E. Golub, Ph.D.

Committee Chair

Associate Professor

Division of Infectious Diseases, Department of Medicine, Johns Hopkins School of Medicine

Department of Epidemiology, Johns Hopkins Bloomberg School of Public Health

David W. Dowdy, M.D., Ph.D., Sc.M.

Dissertation Advisor

Associate Professor

Department of Epidemiology,

Department of International Health, Johns Hopkins School of Public Health

David J. Sullivan, M.D.

Advisor

Professor

Department of Molecular Microbiology & Immunology, Johns Hopkins School of Public Health

Fernando J. Pineda, Ph.D.

Associate Professor

Department of Molecular Microbiology & Immunology,

Department of Biostatistics, Johns Hopkins School of Public Health

Emily A. Kendall, M.D.

Assistant Professor

Division of Infectious Diseases, Department of Medicine, Johns Hopkins School of Medicine

ALTERNATE READERS

Arturo Casadevall, M.D., Ph.D., M.S.

Alfred & Jill Sommer Professor and Chair, Bloomberg Distinguished Professor

Professor

Department of Molecular Microbiology & Immunology, Johns Hopkins School of Public Health

Division of Infectious Diseases, Department of Medicine, Johns Hopkins School of Medicine

Robert H. Gilman, M.D.

Professor

Department of International Health,

Department of Molecular Microbiology & Immunology, Johns Hopkins School of Public Health

ACKNOWLEDGEMENTS

This dissertation describes a synthesis of my research activities over the course of the last four years that I have spent at the Johns Hopkins Bloomberg School of Public Health. In many ways, however, it represents to me a culmination of a much longer trajectory many years in the making. I am proud of the accomplishments I have achieved and the research I present here, but I must also emphatically state that none of it would have been possible without the support and contributions of a great many people. I wish I had the time and space to thank each one of you in turn for your part in shaping me into the scientist I am today. I hope you can permit me an abbreviated summary of those sentiments here. To anyone whom I neglect to thank directly, due to constraints of space or my own memory, I am grateful nonetheless.

I must begin by thanking David Dowdy, who took a chance on a PhD student in microbiology and guided me through the completion of my dissertation. David has always been the warmest and most receptive scientist that I know, and he has immeasurably improved the ways I work and how I think. The first person who recommended I reach out to him, during my first semester in Baltimore, used the word "wunderkind" to describe David and he has consistently lived up to – if not surpassed – that description. Even before he became my advisor formally, he was always willing to take time to look over my independent research and provide encouragement. When I joined his team after much administrative ado, he found funding for me on short notice and put me to work on one of the most rewarding research projects of my career. David is everything one could wish for in a mentor: patient, friendly, insightful, rigorous but not

demanding, swift but not rushed, and unfailingly, unconditionally supportive. Anyone who has spent time in David's orbit will know that he spontaneously attracts ranks of talented researchers to him, as if through sheer magnetism and strength of character. I am lucky to count myself one of those many, and am grateful to have had the opportunity to call him a mentor, a teacher, a colleague, and a friend. David, from the bottom of my heart, thank you.

I cannot expend one word more without thanking my partner, Samantha Almozara. She, too, has been unfailingly supportive of my pursuits since long before I knew anything about tuberculosis. In college, she put up with my pager blaring at all hours of the night when I worked graveyard shifts for the ambulance squad. When I left for Niger, Senegal, Chad, and everywhere else that my adventures took me, she was one of the few back home that I could depend on for a phone call or video message when things were roughest. When I enrolled at Harvard, it was no coincidence that we were but a stone's throw apart. Sam lived through six years of graduate school with me, and I know it took a toll on her beyond what it took on me. She has sacrificed more than I can repay to support me always. She left her job, her friends, and her home to join me in Baltimore, where we have found a new home together. I tell her this constantly: I could never do the things I do if Samantha did not do everything she does for me. Samantha, you are a shining light on a cloudy night. Thank you.

During my time here at Johns Hopkins, I have trod many paths and been part of many circles, but my roots were first and will forever remain in the Molecular Microbiology & Immunology department. I must thank the many faculty there who welcomed me and have supported and mentored me at different points of my studies:

Arturo Casadevall, Mary Hardwick, Gary Ketner, Sabra Klein, Dick Markham, Doug Norris, Andy Pekosz, Clive Schiff, Alan Scott, and many others. Fernando Pineda was in every oral exam and advisory committee meeting I undertook in my time here and deserves a multitude of thanks and recognition. Even when my research took on a decidedly mathematical bent, I never felt alone in the MMI department; I knew, at least, there would always be Fernando to keep me company. David Sullivan became my advisor and lent his support to my research with the Epidemiology department at a critical juncture in my studies, a seemingly small act that I will forever consider heroic. I must also extend my gratitude to all of the members of my thesis committee: David Dowdy, David Sullivan, Fernando Pineda, Emily Kendall, and Jonathan Golub. They sat through hours of research presentations and read through hundreds of pages of thesis drafts to improve the work contained here, for which they deserve many thanks. I would be remiss if I did not acknowledge Ying Zhang, who hosted me in his lab for several years while I collected data for Chapter III of my thesis. Wanliang Shi, who taught me to be a bacteriologist, who walked me through my first days in the BSL-3 lab, who remains one of the most astute and keen laboratorians I know, and who was the funniest lab supervisor I could hope for, will forever be my friend and mentor.

Those with doctorates are not the only ones in the MMI department who deserve my thanks. Rebecca Yee was the first labmate I had there and she continues to be a steadfast partner-in-crime. She has remained a true friend through thick and thin, and she is always the first person to whom I turn when I need academic and career advice. With my thesis completed, I can only hope that I can return some of the sage guidance she has given me over the years. Thank you. I cannot understate my thanks to the nine other PhD

students who joined the MMI department in my cohort. There were ten of us to start; only seven now remain. Brendan, Julia, Hannah, Kristin, Elizabeth, Jane, and Zach: I survived the gauntlet of courses here in the best of company, and I wish you the very best of luck in your years ahead. I have learned so much from this group of scientists, and I am grateful to have been one the cabal.

I am eternally thankful for having found a mentor, friend, and colleague in Bill Moss. Bill has allowed me to be a helping hand in his course every year in the Epidemiology department. I am always surprised at how entertaining his lectures remain, though I've heard each one four years straight. He has been kind enough to let me lead review sessions and provide lectures each year, and (I think) my skills in education and communication have improved notably as a result. I must also thank the many students who have sat through my classes over the years; you were figurative guinea pigs as I tested my didactic sea legs.

After having joined David Dowdy's team, I received an incredible amount of support from members of the Epidemiology department and the TB Center. Thank you to the current and past members of the team who have been terrific officemates and on whom I can always depend for an open ear and helpful feedback. There are far too many people to name, but I will try nonetheless: Austin, Brooke, Bud, Catherine, Colleen, Hae-Young, Hojoon, Parastu, Radhika, Sarah, Sourya, Todd, and Young-ji among many others. Jonathan Golub has been supportive of my cross-disciplinary goals since my first year in Baltimore, and is always willing to make room for my presentations at the TB Center Clinical & Epidemiology lunches. Other faculty at the TB Center have similarly supported my research over the years, and I am thankful for my many conversations with

Eric Nuermberger, Kelly Dooley, Petros Karakousis, Guyanu Lamichhane, Maunank Shah, and Dick Chaisson. Emily Kendall, a member of my thesis committee and a co-author on my manuscripts, is an incredible scientist and clinician from whom I always have more to learn. She is incisive with her feedback and tremendous in her acumen, and I am lucky to have the opportunity to work with her. Thank you for the years of support you've provided.

There are a multitude of individuals at Johns Hopkins to whom I am indebted, but I cannot forget the many people who imparted on me formative experiences which have taken me here. Ted Cohen was my mentor at Harvard and put my on the path of TB research. Friends I made during our first weeks in Niger, one of the more tumultuous experiences in my life: Phoebe Uricchio, Danielle Piccinini, Hailey Wright, Michele Hasit, Dan Hodson. Thank you for being steadfast in your support and for being the most hardy, resilient, and enduring of individuals I know. Kate Lawyer is an exemplar of conscientious international development and compassionate aide, and I'm not sure I would have pursued public health without such a role model. I have had excellent company in pursuing a career in health sciences from my time at Colgate University. Members of the ambulance squad – Dan Digiacomo and Sammy Rocks – still know how to throw a party, while members of our NIH study group – Dan, Dibs Datta, Hassan Mohammed, Joe Koos, Stanley Aladi – have made a rarified air of PhDs and MDs whose ranks I am proud to now join.

Lastly, my family and childhood friends were the first to set me on this path that I have walked. When we were perhaps six years old, Patrick Leehan told me that we would be scientists one day and I have never questioned his assessment since. That young man

had an outsized impact on my life and career, and he deserves my thanks for steering me on this road. My brother, Matt, is someone whom I have always looked up to and whom I am always keen to impress. I am lucky to have had someone to instill a competitive instinct from an early age, which has undoubtedly contributed to my success over the years. Finally, I have gratitude more than words can describe for my parents, Deena and Larry. They have always supported me and – when necessary – given me the push I needed. I never had reason to doubt their unconditional provision, which gave me the freedom and opportunity to pursue my passions through the years.

I am infinitely grateful for the many contributions and the unending support I have received from each of the individuals named above, and the many, many others who are not. From my core: thank you all.

TABLE OF CONTENTS

LIST OF TABLES

LIST OF FIGURES

CHAPTER I

INTRODUCTION

Sections of this chapter have been adapted from: Salvatore PP, Zhang Y. Tuberculosis: Molecular Basis of Pathogenesis. Ref Modul Biomed Sci. ***2017****; p. 1–15. DOI: 10.1016/B978-0-12-801238-3.95697-6.*

GLOBAL TUBERCULOSIS AND PUBLIC HEALTH

Tuberculosis (TB) represents one of the most significant causes of infectious disease morbidity and mortality worldwide. The World Health Organization (WHO) estimates that, in 2016, 10.4 million new cases of TB occurred, causing 1.6 million deaths [1]. It is the ninth leading cause of death globally, and the leading cause of death from an infectious agent. (By comparison, an estimated 1.1 million deaths associated with HIV/AIDS occurred in 2016, of which 370,000 were related to TB [2].) The etiologic agent of TB, the acid fast bacterium *Mycobacterium tuberculosis*, is estimated to currently infect 1.7 billion individuals – roughly 23% of the global population – of which 56 million are considered at high risk of developing disease in the near future [3].

Despite significant progress over the last half century, outcomes for TB patients remain inadequate. Approximately 72% of TB cases who go untreated are expected to die as a result [4]. Only 61% of TB cases are currently diagnosed, and still fewer are able to access appropriate treatment after diagnosis [1]. While many TB patients who start standard TB treatment regimens experience successful outcomes, such results are far from universal. Standardized short-course treatment regimens with directly observed therapy have improved cumulative treatment success for TB patients to 83% globally. However, in some patient populations, such as those with *M. tuberculosis* infections resistant to one or more first-line drugs, treatment success falls below 50% [1,5]. To address the heavy toll taken by TB worldwide and to fundamentally reduce the disability and loss of life caused by TB, the public health community must better understand the complexity of this disease from the fundamental biology of the pathogen to the epidemic spread of disease across vulnerable populations.

EPIDEMIOLOGY AND CONTROL OF TUBERCULOSIS

Infections with *M. tuberculosis* are transmitted through the inhalation of aerosolized droplet nuclei containing the bacterium; as a result, new infections are seeded by index cases infected with a high pulmonary burden of *M. tuberculosis* cells. Control of the TB epidemic and the prevention of new TB cases often focuses on minimizing the number of new infections caused through aerosol transmission, necessitating identification and treatment of existing infectious TB cases. Pulmonary TB cases were reported in 185 countries in 2016, and hundreds of thousands of cases occurred in each WHO region [1]. Most incident TB cases occurred in Southeast Asia, and three countries – India, Indonesia, and China – accounted for approximately 45% of all global TB cases. While the greatest numbers of TB cases occur in Asia, the greatest concentration of TB cases occurs in sub-Saharan Africa. There, 254 new TB cases occurred for every 100,000 individuals in the population, and incidence rates in some areas reached over 700 per 100,000 (e.g., in South Africa). While TB remains the leading cause of infection-related deaths worldwide, global TB incidence rates have declined since 2000 at an average rate 1.4% per year, though this rate must reach 4-5% per year by 2020 to achieve TB targets adopted by the World Health Assembly [1]. To reach these targets, TB control programs must use currently available measures to prevent and treat incident cases of TB.

Few tools can provide adequate protection against TB. The only widely used vaccine for TB – Bacillus Calmette–Guerin, first developed in 1921 [6] – is only 46% efficacious generally and likely only 13% efficacious in areas home to populations at greatest risk for TB [7]. For those who have been infected but remain asymptomatic –

commonly termed latent TB infection – the progression to symptomatic disease can be prevented with isoniazid preventive therapy (IPT). Such regimens require daily or weekly doses of antibiotics and are recommended for six months (up to nine months in low-burden settings), similar in duration to a treatment course for active TB [1]. IPT may reduce the risk of TB by more than 90% (provided that therapy is taken for 12 months or longer) [8]. Newer preventive regimens combining isoniazid and a rifamycin (such as rifampin or rifapentine) may shorten therapy for latent infection from nine months to twelve weeks [9]. These promising regimens demonstrate little significant reductions in efficacy, though at an increased cost for each TB case averted [10,11]. Importantly, such therapy does not prevent reinfection after the regimen is withdrawn, and in high-incidence areas, protection may diminish within 6 months after the end of therapy [12].

In the absence of effective prevention measures, most TB control strategies rely on the detection and treatment of infectious patients to minimize the transmission of *M. tuberculosis*. For patients infected with strains of *M. tuberculosis* susceptible to first-line anti-mycobacterial antibiotics, the WHO recommends the administration of a standardized combination regimen daily or weekly for six months [1]. In the intensive phase (the first two months) of the regimen, four drugs – isoniazid (INH), rifampin (RIF), pyrazinamide (PZA), and ethambutol – are given; thereafter, two of the drugs – INH and RIF – are given throughout the continuation phase (the subsequent four months) of treatment. When TB patients adhere to this standard therapy, long-term treatment success rates can reach over 90% [13]. Success can be diminished, however, by non-adherence or loss to follow-up during treatment. To address these issues, treatment regimens are also paired with directly observed therapy – in which a second observer monitors and records

the consumption of each scheduled dose of antibiotic – that can lead to treatment completion for 90% of TB patients [14]. However, this standard treatment regimen may fail to adequately cure TB patients who are infected with strains of *M. tuberculosis* genetically resistant to any of the four drugs in the regimen, particularly with infections resistant to both INH and RIF – termed multidrug resistant TB (MDR-TB). Even under optimal conditions, only 25-50% of MDR-TB patients are successfully treated with the standard regimen, many of whom will relapse with MDR-TB within two years after the end of therapy [15,16].

Attempts to replicate the success of six-month first-line therapy using second-line antibiotics have not been fruitful. One factor contributing to the inadequate efficacy of second-line regimens is the small pool of alternative antibiotics available to replace first-line agents [17]. A limited number of novel drugs with promising anti-tuberculosis activity have emerged in the last decade (e.g., bedaquiline, delaminid, and pretomanid), but whether they can achieve treatment success comparable with first-line agents remains unclear [18]. While longer (18-24 month) second-line regimens may improve treatment success for MDR-TB patients, such interventions place heavy financial burdens on patients and health systems, are associated with significant adverse side effects, and still fail to achieve durable cure for half of eligible patients [1,5]. A fruitful alternative may be the development of second-line agents which mirror the pharmacodynamics activity of first-line agents. For example, no single alternate agent may replace the sterilizing activity of PZA with comparable success [19], and no PZA analogues have been successfully developed. Unlike other first-line agents, the mechanism of action of PZA remains unclear, although recent studies suggest the involvement of a bacterial ribosomal

protein, *RpsA* [20]. Until such time when second-line regimens can effectively and rapidly treat drug resistant TB, these difficult cases will remain a heavy burden on TB control programs. As a result, control of the global TB epidemic may depend greatly on future trends in MDR-TB incidence.

NATURAL HISTORY AND PATHOGENESIS OF TUBERCULOSIS

M. tuberculosis exhibits a complex lifecycle in humans, often remaining clinically silent but occasionally manifesting in clinical pathologies. In the pre-antibiotic era, approximately 70% of microbiologically confirmed and clinically symptomatic infections led to death within 10 years of symptom onset, and most TB cases progressed to death or self-limited resolution of symptoms within approximately three years of symptom onset [4]. The complex molecular mechanisms underlying these clinical observations are described below, with particular emphasis on processes of initial *M. tuberculosis* infection, progression to clinical TB, and the role of HIV infection in pathogenesis.

Primary Infection

A productive *M. tuberculosis* infection originates following the inhalation of a single, aerosolized droplet nucleus containing 1-3 bacterial cells (Figure 1.1A) [21]. At the site of implantation, bacteria are phagocytosed by unactivated alveolar macrophages – which are ineffective in destroying the bacterium – where early rounds of replication occur in the immature phagosome (Figure 1.1B.1). If the infected macrophage is unable to destroy the phagocytosed bacillus, intracellular bacterial proliferation may lead to necrosis or apoptosis of the host cell (Figure 1.1B.2) [22].

Before the onset of the adaptive immune response, bacterial replication occurs relatively uninhibited in the airspaces and in the phagosomes of myeloid dendritic cells as well as newly-arrived alveolar macrophages and circulating monocytes [23]. Cytokines such as Tumor Necrosis Factor (TNF) released by innate immune cells act to

permeabilize the vascular endothelium and attract additional phagocytic cells to the site of infection (Figure 1.1B.3, Figure 1.2) [23]. The continuous influx of innate immune cells at the site of bacterial replication constitutes the formation of an early granuloma, a defining feature of pulmonary TB (Figure 1.1B.4, reviewed in [27]). The early granuloma is characterized by populations of highly motile roving macrophages as well as smaller populations of dendritic cells and polymorphonuclear leukocytes (PMNs), creating an environment for continuous cycles of phagocytosis and expulsion of replicating bacterial cells [28].

Figure 1.1: The Natural History of Tuberculosis Infection

(A) *M. tuberculosis* is transmitted via aerosolized droplet nuclei, each with an aerodynamic diameter smaller than 5μm and containing 1–3 bacterial cells. The small size of the particle facilitates deposition in the terminal alveoli of the lungs rather than in the tissues of the larger airways. (B) Upon deposition in an alveolus, *M. tuberculosis* is phagocytosed by unactivated alveolar macrophages (part 1). The bacterium eventually kills the infected macrophage by either necrosis or apoptosis, escaping into the alveolar tissues (part 2). Replication of the bacterium continues unabated in the extracellular space and within newly arrived dendritic cells and macrophages (part 3). Cytokine signaling attracts further macrophages, monocytes, and dendritic cells, which form the early granuloma (part 4). Upon arrival of mature T_H1 cells, macrophages become activated and can more effectively kill or contain the bacterium. Some of these macrophages become epithelioid, forming a capsule surrounding the necrotic region of bacterial survival and containing the infection from progressing further (part 5). Following immunologic suppression, the bacterial population may destroy immune cells at the luminal surface of the granuloma, causing the accumulation of caseous necrotic debris, which may liquefy and discharge, propagating transmission (part 6).

Figure 1.1: The Natural History of Tuberculosis Infection

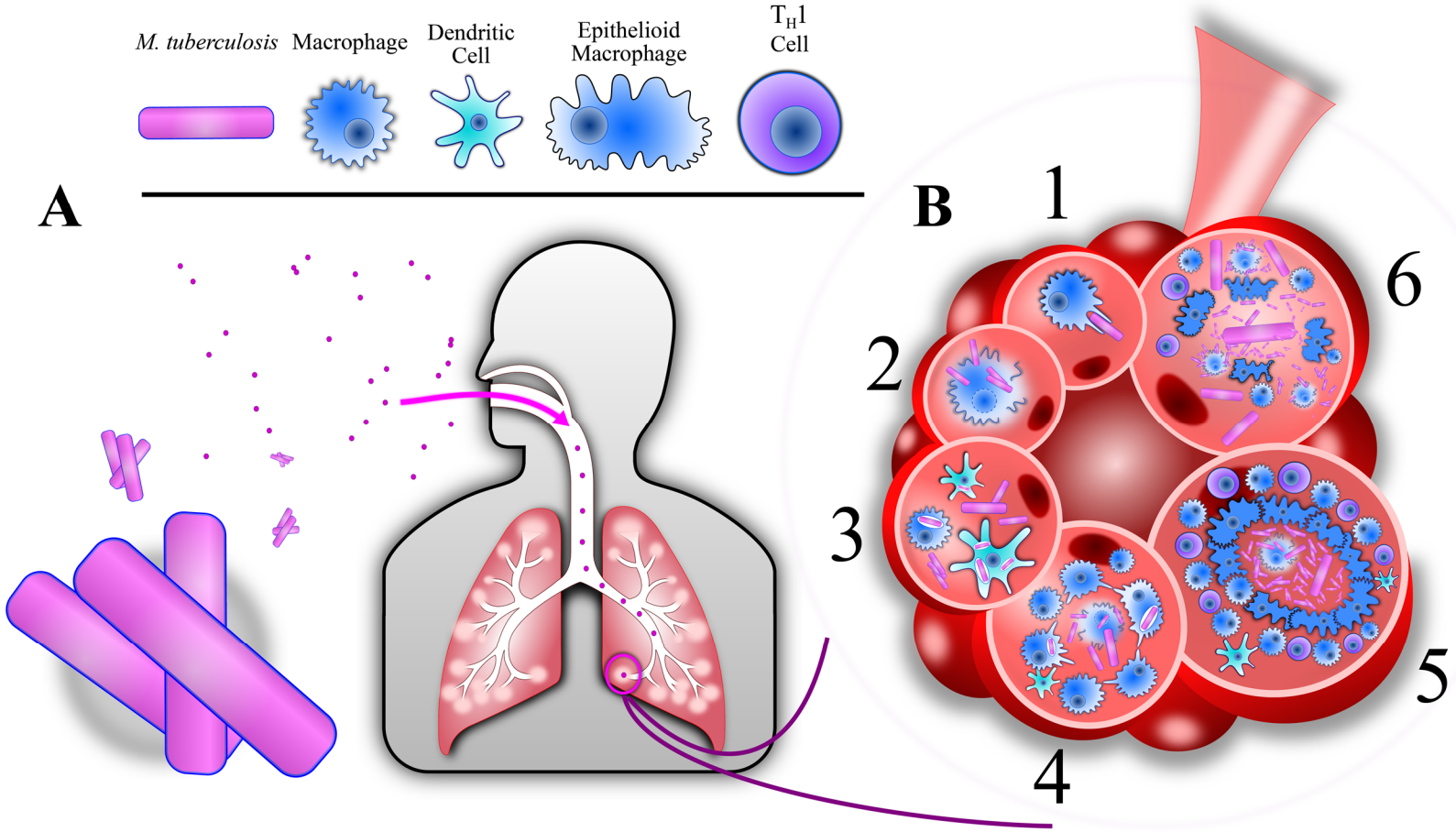

In some cases, bacteria are phagocytosed by macrophages or dendritic cells which traffic to the draining hilar lymph nodes, leading to lymphohematogenous dissemination and seeding of distal sites of infection [27,29]. At this time, approximately 3-8 weeks following initial implantation, dendritic cells presenting *M. tuberculosis* antigens via MHC-II molecules to immature $CD4^+$ T cells in the context of IL-12 and a costimulatory signal from B7:CD28 interactions triggers T cell maturation into T_H1 cells (Figure 1.2). As mature T_H1 cells traffic from the lymph nodes to the pulmonary and extrapulmonary sites of infection, they release IFN-γ which, with costimulation through CD40:CD40L interactions, activates local macrophages and monocytes and triggers oxidative bursts, phagolysosomal maturation, production of antimicrobial molecules (ROS, RNI, NO, NOS2, defensins, surfactants, etc.), secondary granule fusion, and epithelioid macrophage differentiation (Figure 1.2)

The cumulative effects of the onset of the adaptive immune response are to substantially reduce the net rate of bacterial growth to an equilibrium at the site of infection, limit extracellular survival of bacteria, and cause maturation of the granuloma to a fibro-epithelioid lesion (Figure 1.1B.5) [33–35]. In certain individuals, the adaptive immune response and concomitant granuloma maturation is sufficient to sterilize the infection, leaving only a healed, calcified lesion; in most cases, however, the bacterial population continues to survive. For a small number of individuals (~5% of those recently infected) [36], the infection will progress rapidly to active, symptomatic disease (termed primary progressive TB) within approximately 15-30 weeks [37] but potentially up to five years [38]. The vast majority of infections, however, will be contained in a

clinically silent, long-term latent state, of which 5-10% will eventually reactivate to cause symptomatic secondary TB [39,40].

Primary Progressive Tuberculosis

In roughly 5% of infections with *M. tuberculosis*, the infection is never sufficiently contained in the maturing granuloma [36]. As a result, these patients will rapidly develop symptomatic disease, termed primary progressive TB, over the course of weeks or months following the initial infection. In low-incidence settings, such disease makes up only 14% of prevalent cases of TB [41], but this may increase to 72% in high-incidence settings [42,43]. While this has been hypothesized to occur due to insufficient cellular immunity at the time of initial infection (particularly in children), further research is required to robustly test this hypothesis. Because the bacterial population is never contained in a mature granulomatous lesion, disease may disseminate diffusely throughout the lung or into the vasculature and throughout the body in a condition known as miliary TB.

Secondary Tuberculosis

Once an initial infection has been contained in a latent state, it can remain latent for years or decades and many patients will never report symptoms of TB during their lifetimes. In roughly 5-10% of latent infections, the infection may reactivate leading to gross necrosis in affected regions of the lung [49]. Many cases of reactivated secondary TB follow an insult to the immunological system responsible for continuously controlling and limiting the latent bacterial infection. The inciting insult may be to either innate

(inhibition of TNF) or adaptive immunity (reduction in $CD4^+$ T cells), and a nontrivial contributing role of multiple host genetic variants has also been identified (Figure 1.2) [31]. The following dysregulation may provide an advantage for bacterial cells to proliferate and destroy populations of macrophages at the luminal surface of the granuloma, leading to accumulation of caseous necrosis as nearby lesions enlarge and merge (Figure 1.1B.6) [34]. Key in this process is the secretion of host matrix metalloproteinases (MMPs) in response to the accumulation of mycobacterial products such as ESAT-6 which function to continuously degrade pulmonary collagen as well as to modulate host immune chemokines [50,51]. Eventually, these lesions may erode into larger respiratory airways, discharging the liquefied caseum from the necrotic cavities into the bronchial tree. Once the liquefied necrotic material has been evacuated, this material may seed bacteria in other sites of the lung and may lead to the aerosolization of droplet nuclei, continuing the chain of transmission.

Interactions with HIV

Following the emergence of HIV as a global pandemic in the 1980s, co-infection has appeared as one of the leading risk factors driving TB epidemiology. The most important effects of HIV infection are indirect: depletion of $CD4^+$ T_H1 cells leads to an increased risk of secondary TB in individuals with latent infection [47,55]. However, HIV infection may also have more direct effects on the pathophysiology of tuberculosis infections [56]. HIV has been shown to preferentially infect $CD4^+$ T cells specific to *M. tuberculosis* peptides, even in comparison with T cells specific for other opportunistic pathogens such as cytomegalovirus [57]. As macrophages also express CD4 and the

coreceptors CCR5 and CXCR4, HIV can also co-infect *M. tuberculosis*-infected macrophages leading to macrophage dysfunction and inhibited killing [58,59]. Within the granulomatous environment, HIV may interfere with TNF expression and lead to increased caseous necrosis [60,61]. Circulating monocytes infected with HIV upregulate production of the macrophage-attractant chemokine CCL2 and can skew the cellular immune response to a T_H2 phenotype [62,63]. Finally, because the typical immune response to TB involves production of proinflammatory cytokines (such as TNF, IL-1β, and IL-6) which favor replication of HIV, coinfection may trigger reciprocal effects which simultaneously exacerbate pathologies associated with each pathogen [64].

Figure 1.2: Immunologic Responses to *M. tuberculosis*

Following initial infection with *M. tuberculosis*, alveolar macrophages secrete the pro-inflammatory cytokine TNF. As the early granuloma forms, dendritic cells sample *M. tuberculosis* antigens and traffic to the secondary lymphatic tissues to begin antigen presentation. When an immature $CD4^+$ T cell successfully and specifically binds the dendritic cell's antigen/MHC-II complex and B7, the cell may mature into one of two phenotypes. In the presence of the costimulatory molecule IL-12, the cell will mature into an IFN-γ-producing T_H1 cell, while in the presence of IL-6 and TGF-β molecules, the cell will mature into an IL-17-producing T_H17 cell. The arrival of T_H1 cells carrying CD40L and secreting IFN-γ activates macrophages at the site of infection, producing an oxidative burst leading to the destruction of bacterial cells and maturation of the granuloma. As the infection progresses, a deficiency in the T_H1 response (particularly through reductions in TNF or IFN-γ signaling) may result in caseous necrosis, destruction of immune cells throughout the granuloma, and bacterial escape. T_H17 cells may contribute to the pathological damage of *M. tuberculosis* through secretion of IL-17, which stimulates the migration of PMNs, which produce a variety of oxidative species capable of damaging host cells. In addition, IL-17 contributes to the secretion of several matrix metalloproteinases by macrophages, PMNs, and epithelial cells. *TNF*, tumor necrosis factor; *MMP*, matrix metalloproteinase; *ROS*, reactive oxygen species; *RNI*, reactive nitrogen intermediates; *NO*, nitric oxide.

Figure 1.2: Immunologic Responses to *M. tuberculosis*

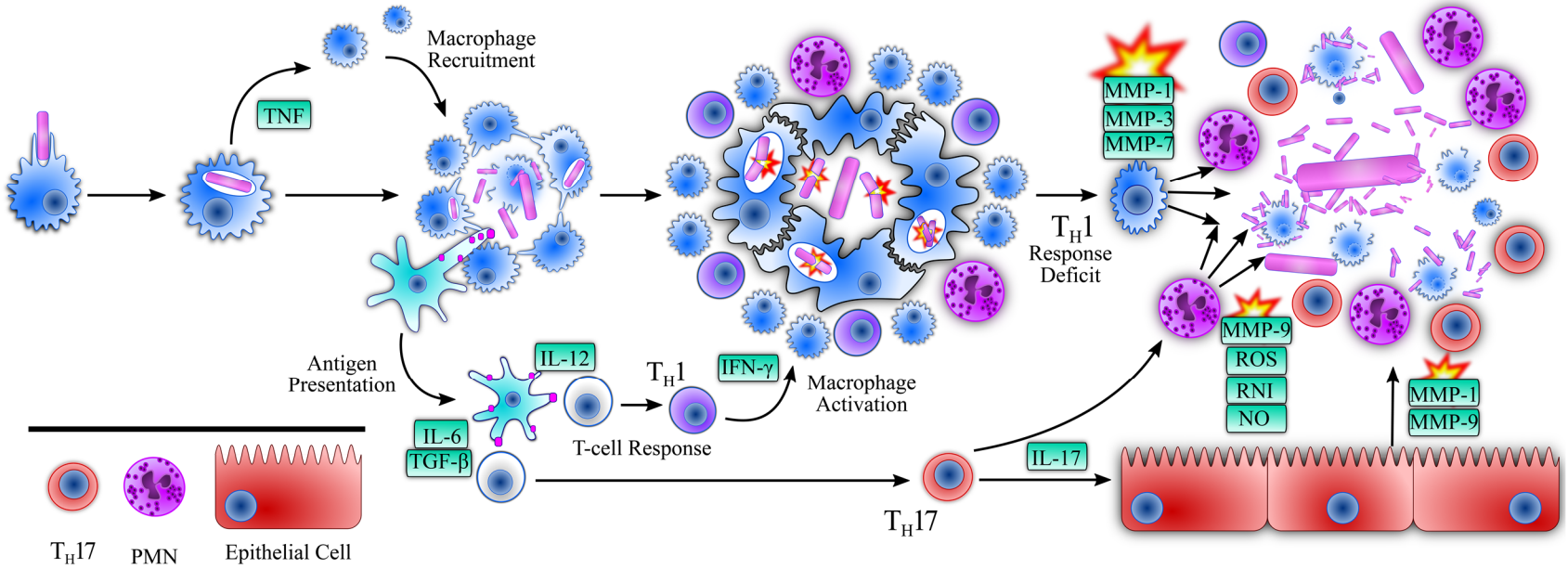

EXPERIMENTAL ANIMAL MODELS OF TUBERCULOSIS

Animal models represent important methodological tools in understanding – and ultimately controlling – human TB. Key insights from such studies have informed our understanding of TB transmission [21], immunology [25], pathogenesis [65], and treatment. The most common experimental model of *M. tuberculosis* infection is the mouse, which offers several distinct advantages in the study of TB: mice are inexpensive, can tolerate high infectious doses used in many experimental approaches, and a plethora of genetic and immunological tools exists for the manipulation and interrogation of biological processes in mice [66,67]. Despite these advantages, in several ways mice are poorly representative of TB pathology in humans. Most murine models do not develop caseating granulomas – a defining characteristic of human TB related to the production of infectious aerosols – and instead develop non-caseating necrotic lesions [68,69]; mice fail to develop true latent infections and instead develop long-term chronic pathology [70,71]; mice progress from initial infection to death much more rapidly than humans [72]; and mice are not known to self-resolve infections with *M. tuberculosis*, eventually progressing to death regardless of inoculating dose [72].

Alternative animal models are occasionally used in place of mice. Guinea pigs are particularly susceptible to infection and routinely develop caseating granulomas, making them a useful model for the study of TB inhalation and implantation [21,73]; however, relatively few molecular or immunological tools have been developed for the experimental manipulation of guinea pig immunology [66–68]. Rabbits similarly develop caseating granulomas as well as cavitary lesions but are relatively resistant to TB

infection – often substituted by infection with *M. bovis* in experimental studies – and most rabbits experience self-limited disease before spontaneously resolving [66–68]. Still, none of these animal models faithfully represent human sensitivity to infectious exposure; latent infection progressing to active disease; long durations between characteristic stages of infection; and heterogeneity in outcome (ranging from possible self-resolution or progression to death). Most of these distinct features of human disease are recapitulated by nonhuman primate models, but such models are prohibitively expensive for most experimental questions and inferences drawn from such studies are limited by small sample sizes. Despite the wealth of information about specific aspects of the pathological process learned from animal models, there remains a critical gap in connecting these processes to clinically-relevant outcomes in human populations.

DRUG RESISTANT TUBERCULOSIS

In *M. tuberculosis*, drug resistance emerges through the stepwise acquisition of individual chromosomal mutations, with no apparent acquisition through horizontal gene transfer [74]. As a result, a TB patient may be initially infected with an MDR-TB strain (termed primary resistance), or she may be initially infected with a drug susceptible strain which progressively develops into MDR-TB through *de novo* acquisition of mutations conferring resistance to INH and RIF (secondary resistance). Such secondary resistance may develop as a result of subtherapeutic drug regimens due to patient nonadherence, poor drug quality, and/or patient-dependent pharmacokinetic properties [75]. While improved treatment regimens for drug susceptible TB can minimize the probability of developing secondary resistance, the impact of primary resistance and the transmission of MDR-TB between patients remains widely debated.

Traditional TB dogma holds that phenotypic drug resistance in a bacterial population carries a physiological tradeoff [76,77]; therefore, mutations conferring drug resistance are likely to be accompanied by a reduction in reproductive fitness in the absence of the drug. This dogma dates to observations made in the 1950s that INH resistant clinical and laboratory strains of TB caused disease less frequently in guinea pigs than drug sensitive strains, and that this loss in virulence was inversely correlated with minimum inhibitory concentrations of INH [78,79]. These observations were corroborated in the following decades with both clinical isolates and laboratory mutants resistant to INH and/or RIF [80–82]. However, experimental evidence has also accrued which contradicts the fitness cost hypothesis. Screens of clinical isolates with varying

degrees of resistance to INH, RIF, and other antibiotics demonstrate that different isolates can be less virulent, equally virulent, or more virulent than drug sensitive strains in mice, and that the degree of virulence is not necessarily associated with any trends in drug resistance [83]. Multiple studies have confirmed that – within a given phenotype of drug resistance – the degree of laboratory fitness is highly dependent on the specific resistance-conferring chromosomal mutations present [77,82,84]. Genetic epistasis – in which secondary mutations (unrelated to antibiotic resistance) confer physiological benefits in the presence of resistance-conferring mutations – has also been shown to compensate physiological fitness costs [85–87].

Most studies of the fitness costs of drug resistance in *M. tuberculosis* have been conducted by assessing the growth of resistant organisms in co-culture with drug susceptible organisms, or by comparing the virulence of each strain in laboratory animals infected under controlled conditions. Yet for the purposes of public health, these assays do not capture many characteristics of the complex natural history of infection: the successful transmission of *M. tuberculosis* from an initial host to a secondary host in whom it establishes infection, replicates, and subsequently transmits again [88,89]. Extrapolating laboratory findings to humans is further limited by the animal models commonly used in the study of TB which, as described above, may fail to faithfully represent the TB disease process of humans [68]. *In vitro* or *in vivo* growth rates may or may not represent growth rates *in situ*, which in turn may not correlate with clinical virulence or population-level transmission dynamics.

To complement studies of physiological fitness costs in laboratory models, molecular epidemiological methods have also been employed. Studies of genetic

clustering investigate TB cases with genetically related *M. tuberculosis* infections as evidence of recent TB transmission. Such studies have found that MDR-TB strains cluster anywhere from 10-fold more to 10-fold less than drug sensitive TB strains in various studies and settings [90]. Phylogenetic analyses have been used to reconstruct extensive chains of MDR-TB transmission [91,92], and even extensively drug resistant TB (resistant to INH, RIF, as well as a fluoroquinolone and a second-line injectable agent) has been observed to cause explosive outbreaks [93].

How these characteristics may contribute to long-term MDR trends in the global TB epidemic are difficult to evaluate empirically, and thus dynamic mathematical models using differential calculus have been used to estimate the impacts of fitness costs on the spread of MDR-TB. Mathematical models developed assuming a significant fitness cost associated with drug resistant TB predict that such strains are unlikely to ever displace sensitive strains as the dominant burden of disease, provided drug sensitive TB is treated effectively [94], and that MDR-TB will remain a localized problem in areas where it develops [95]. However, when MDR-TB strains are considered to have variable fitness costs, MDR-TB may eventually outnumber drug sensitive cases [96,97], consistent with recent estimates which suggest that 95% of incident MDR-TB cases in recent years were attributable to transmission rather than secondary resistance [98].

DISSERTATION OBJECTIVES

The effective control of the global TB epidemic in coming decades will require the integration of both fundamental biology and epidemiology to develop novel tools for TB control and to effectively optimize and implement those tools already available. This work aims to provide an example of how these disciplines, often divided by methods and expertise, may be effectively linked in the practice of public health science. In Chapter II, we develop a theoretical framework for linking host-level pathogen dynamics with population-level clinical outcomes, demonstrating the utility of interrelating pathogen and epidemiological characteristics in understanding clinical TB. In Chapter III, we investigate the role of the bacterial ribosomal protein *RpsA* in the action of PZA and report a novel interaction with Ribosome Recycling Factor, representing a possible conserved bacterial function inhibited by PZA. In Chapter IV, we investigate how competing assumptions about the fitness costs of drug resistance influence long-term projections of the MDR-TB epidemic and demonstrate that the future of MDR-TB depends on the relative efficiency with which MDR-TB transmits infection. Finally, in Chapter V, we summarize these results in the context of current TB control and future scientific inquiry. Cumulatively, these studies offer an innovative approach to answering questions of public health relevance through the lenses of multiple scientific disciplines and provide a model for investigations in the field of TB control and beyond.

REFERENCES

1. Global Tuberculosis Report 2017. Geneva: World Health Organization, **2017**.
2. Ending Aids - Progress Towards the 90-90-90 Targets: Global AIDS Update 2017. Geneva: UNAIDS, **2017**.
3. Houben RMGJ, Dodd PJ. The global burden of latent tuberculosis infection: a re-estimation using mathematical modelling. PLoS Med. **2016**; 13(10):e1002152.
4. Tiemersma EW, van der Werf MJ, Borgdorff MW, Williams BG, Nagelkerke NJD. Natural history of tuberculosis: duration and fatality of untreated pulmonary tuberculosis in HIV negative patients: a systematic review. PLoS One. **2011**; 6(4):e17601.
5. Ahuja SD, Ashkin D, Avendano M, Banerjee R, Bauer M, Bayona JN, et al. Multidrug resistant pulmonary tuberculosis treatment regimens and patient outcomes: an individual patient data meta-analysis of 9,153 patients. PLoS Med. **2012**; 9(8): e1001300.
6. Behr MA, Small PM. A historical and molecular phylogeny of BCG strains. Vaccine. **1999**; 17(7–8):915–922.
7. Mangtani P, Abubakar I, Ariti C, Beynon R, Pimpin L, Fine PEM, et al. Protection by BCG vaccine against tuberculosis: a systematic review of randomized controlled trials. Clin Infect Dis. **2014**; 58(4):470–480.
8. Comstock GW. How much isoniazid is needed for prevention of tuberculosis among immunocompetent adults? Int J Tuberc Lung Dis. **1999**; 3(10):847–850.
9. Sterling TR, Villarino ME, Borisov AS, Shang N, Gordin F, Bliven-Sizemore E, et

al. Three months of rifapentine and isoniazid for latent tuberculosis infection. N Engl J Med. **2011**; 365(23):2155–2166.

10. Shepardson D, Marks SM, Chesson H, Kerrigan A, Holland DP, Scott N, et al. Cost-effectiveness of a 12-dose regimen for treating latent tuberculous infection in the United States. Int J Tuberc Lung Dis. **2013**; 17(12):1531–1537.
11. Pease C, Hutton B, Yazdi F, Wolfe D, Hamel C, Quach P, et al. Efficacy and completion rates of rifapentine and isoniazid (3HP) compared to other treatment regimens for latent tuberculosis infection: a systematic review with network meta-analyses. BMC Infect Dis. **2017**; 17(1):1–11.
12. Hermans SM, Grant AD, Chihota V, Lewis JJ, Vynnycky E, Churchyard GJ, et al. The timing of tuberculosis after isoniazid preventive therapy among gold miners in South Africa: a prospective cohort study. BMC Med. **2016**; 14(1):1–11.
13. Cox HS, Morrow M, Deutschmann PW. Long term efficacy of DOTS regimens for tuberculosis: systematic review. BMJ. **2008**; 336(7642):484–487.
14. Chaulk C, Kazandjian V. Directly observed therapy for treatment completion of tuberculosis: concensus statement of the Public Health Tuberculosis Guidelines Panel. JAMA. **1998**; 279(12):943–8.
15. Espinal MA, Kim SJ, Suarez PG, Kam KM, Khomenko AG, Migliori GB, et al. Standard short-course chemotherapy for drug-resistant tuberculosis: treatment outcomes in 6 countries. JAMA. **2000**; 283(19):2537–45.
16. Cox H, Kebede Y, Allamuratova S, Ismailov G, Davletmuratova Z, Byrnes G, et al. Tuberculosis recurrence and mortality after successful treatment: impact of drug resistance. PLoS Med. **2006**; 3(10): e384.

17. WHO treatment guidelines for drug-resistant tuberculosis - 2016 Update. Geneva: World Health Organiztion, **2016**.

18. Wong EB, Cohen KA, Bishai WR. Rising to the challenge: new therapies for tuberculosis. Trends Microbiol. **2013**; 21(9):493–501.

19. Fox W, Ellard GA., Mitchison DA. Studies on the treatment of tuberculosis undertaken by the British Medical Research Council Tuberculosis Units, 1946-1986, with relevant subsequent publications. Int J Tuberc Lung Dis. **1999**; 3(10 Supp 2):S231–S279.

20. Shi W, Zhang X, Jiang X, Yuan H, Lee JS, Barry CE, et al. Pyrazinamide inhibits trans-translation in *Mycobacterium tuberculosis*. Science. **2011**; 333(6049):1630–1632.

21. Riley R, Mills C, Nyka W, Weinstock N, Storey P, Sultan L, et al. Aerial dissemination of pulmonary tuberculosis: a two-year study of contagion in a tuberculosis ward. Am J Hyg. **1959**; 70:185–196.

22. Divangahi M, Behar S, Remold H. Dying to live: how the death modality of the infected macrophage macrophage modulates immunity to tuberculosis. Adv Exp Med Biol. **2013**; 783:103–120.

23. Wolf AJ, Linas B, Trevejo-Nuñez GJ, Kincaid E, Tamura T, Takatsu K, et al. *Mycobacterium tuberculosis* infects dendritic cells with high frequency and impairs their function in vivo. J Immunol. **2007**; 179:2509–2519.

24. Bean A, Roach D, Briscoe H, France M, Korner H, Sedgwick J, et al. Structural deficiencies in granuloma formation in TNF gene-targeted mice underlie the heightened susceptibility to aerosol *Mycobacterium tuberculosis* infection, which

is not compensated for by lymphotoxin. J Immunol. **1999**; 162:3504–3511.

25. Flynn JL, Goldstein MM, Chan J, Triebold KJ, Pfeffer K, Lowenstein CJ, et al. Tumor Necrosis Factor-alpha is required in the protective immune response against *Mycobacterium tuberculosis* in mice. Immunity. **1995**; 2(6):561–572.

26. Keane J, Gershon S, Wise R, Mirabile-levents E, Kasznica J, Schwieterman W, et al. Tuberculosis associated with infliximab, a Tumor Necrosis Factor A-neutralizing agent. N Engl J Med. **2001**; 345(15): 1098-1104.

27. Ramakrishnan L. Revisiting the role of the granuloma in tuberculosis. Nat Rev Immunol. **2012**; 12(5):352–366.

28. Davis JM, Ramakrishnan L. The role of the granuloma in expansion and dissemination of early tuberculous infection. Cell. **2009**; 136(1):37–49.

29. Krishnan N, Robertson BD, Thwaites G. The mechanisms and consequences of the extra-pulmonary dissemination of *Mycobacterium tuberculosis*. Tuberculosis. **2010**; 90(6):361–366.

30. Casanova JL, Abel L. Genetic dissection of immunity to mycobacteria: the human model. Annu Rev Genomics Hum Genet. **2002**; 20:581–620.

31. Fernando SL, Britton WJ. Genetic susceptibility to mycobacterial disease in humans. Immunol Cell Biol. **2006**; 84(2):125–137.

32. Moller M, Hoal EG. Current findings, challenges and novel approaches in human genetic susceptibility to tuberculosis. Tuberculosis. **2010**; 90(2):71–83.

33. Gil O, Diaz I, Vilaplana C, Tapia G, Diaz J, Fort M, et al. Granuloma encapsulation is a key factor for containing tuberculosis infection in minipigs. PLoS One. **2010**; 5(4): e10030.

34. Kaplan G, Post FA, Moreira AL, Wainwright H, Kreiswirth BN, Tanverdi M, et al. *Mycobacterium tuberculosis* growth at the cavity surface: a microenvironment with failed immunity. Infect Immun. **2003**; 71(12):7099–7108.

35. Orme IM, Basaraba RJ. The formation of the granuloma in tuberculosis infection. Semin Immunol. **2014**; 26(6):601–609.

36. Sutherland I. The evolution of clinical tuberculosis in adolescents. Tubercle. **1966**; 47:305–314.

37. ten Asbroek AH, Borgdorff MW, Nagelkerke NJ, Sebek MM, Deville W, van Embden JD, et al. Estimation of serial interval and incubation period of tuberculosis using DNA fingerprinting. Int J Tuberc Lung Dis. **1999**; 3(5):414–420.

38. Sutherland I, Švandová E, Radhakrishna S. The development of clinical tuberculosis following infection with tubercle bacilli. Tubercle. **1982**; 63(4):255–268.

39. Vynnycky E, Fine PEM. Lifetime risks, incubation period, and serial interval of tuberculosis. Am J Epidemiol. **2000**; 152(3):247–263.

40. Comstock GW, Livesay VT, Woolpert SF. The prognosis of a positive tuberculin reaction in childhood and adolescence. Am J Epidemiol. **1974**; 99(2):131–138.

41. Yuen C, Kammerer S, Marks K, Navin T, France AM. Recent transmission of tuberculosis — United States, 2011-2014. PLoS One. **2016**; 11(4): e0153728.

42. Verver S, Warren RM, Munch Z, Vynnycky E, van Helden PD, Richardson M, et al. Transmission of tuberculosis in a high incidence urban community in South Africa. Int J Epidemiol. **2004**; 33(2):351–357.

43. Glynn JR, Crampin AC, Yates MD, Traore H, Mwaungulu FD, Ngwira BM, et al. The importance of recent infection with *Mycobacterium tuberculosis* in an area with high HIV prevalence: a long-term molecular epidemiological study in Northern Malawi. J Infect Dis. **2005**; 192(3):480–487.

44. Fok A, Numata Y, Schulzer M, FitzGerald MJ. Risk factors for clustering of tuberculosis cases: A systematic review of population-based molecular epidemiology studies. Int J Tuberc Lung Dis. **2008**; 12(5):480–492.

45. Houben RMGJ, Crampin AC, Ndhlovu R, Sonnenberg P, Godfrey-Faussett P, Haas WH, et al. Human Immunodeficiency Virus associated tuberculosis more often due to recent infection than reactivation of latent infection. Int J Tuberc Lung Dis. **2011**; 15(1):24–31.

46. Nava-Aguilera E, Andersson N, Harris E, Mitchell S, Hamel C, Shea B, et al. Risk factors associated with recent transmission of tuberculosis: systematic review and meta-analysis. Int J Tuberc Lung Dis. **2009**; 13(1):17–26.

47. Selwyn PA, Hartel D, Lewis VA, Schoenbaum EE, Vermund SH, Klein RS, et al. A prospective study of the risk of tuberculosis among intravenous drug users with Human Immunodeficiency Virus infection. N Engl J Med. **1989**; 320(9):545–50.

48. Basu Roy R, Whittaker E, Kampmann B. Current understanding of the immune response to tuberculosis in children. Curr Opin Infect Dis. **2012**; 25(3):250–257.

49. Frieden TR, Sterling TR, Munsiff SS, Watt CJ, Dye C. Tuberculosis. Lancet. **2003**; 362(9387):887–899.

50. Monin L, Khader SA. Chemokines in tuberculosis: the good , the bad and the ugly. Semin Immunol. **2014**; 26:552–558.

51. Volkman HE, Pozos TC, Zheng J, Davis JM, Rawls JF, Ramakrishnan L. Tuberculous granuloma induction via interaction of a bacterial secreted protein with host epithelium. Science. **2010**; 327(5964):466–9.

52. Hunter RL. Pathology of post primary tuberculosis of the lung: an illustrated critical review. Tuberculosis. **2011**; 91(6): 497-509.

53. Hunter RL. Tuberculosis as a three-act play: a new paradigm for the pathogenesis of pulmonary tuberculosis. Tuberculosis. **2016**; 97: 8-17.

54. Orme IM. A new unifying theory of the pathogenesis of tuberculosis. Tuberculosis. **2014**; 94(1):8–14.

55. Lawn S, Myer L, Edwards D, Bekker L-G, Wood R. Short-term and long-term risk of tuberculosis associated with CD4 cell recovery during antiretroviral therapy in South Africa. AIDS. **2009**; 23(13):1717–1725.

56. Diedrich CR, Flynn JL. HIV-1/*Mycobacterium tuberculosis* coinfection immunology: How does HIV-1 exacerbate tuberculosis? Infect Immun. **2011**; 79(4):1407–1417.

57. Geldmacher C, Ngwenyama N, Schuetz A, Petrovas C, Reither K, Heeregrave EJ, et al. Preferential infection and depletion of *Mycobacterium tuberculosis*-specific CD4 T cells after HIV-1 infection. J Exp Med. **2010**; 207(13):2869–2881.

58. Patel NR, Zhu J, Tachado SD, Zhang J, Wan Z, Saukkonen J, et al. HIV impairs TNF-mediated macrophage apoptotic response to *Mycobacterium tuberculosis*. J Immunol. **2007**; 179(10):6973–6980.

59. Patel NR, Swan K, Li X, Tachado SD, Koziel H. Impaired *M. tuberculosis*-mediated apoptosis in alveolar macrophages from HIV+ persons: potential role of

IL-10 and BCL-3. J Leukoc Biol. **2009**; 86(1):53–60.

60. Bezuidenhout J, Roberts T, Muller L, Helden P van, Walzl G. Pleural tuberculosis in patients with early HIV infection is associated with increased TNF-alpha expression and necrosis in granulomas. PLoS One. **2009**; 4(1).

61. Noronha ALL de, Bafica A, Nogueira L, Barral A, Barral-Netto M. Lung granulomas from *Mycobacterium tuberculosis*/HIV-1 co-infected patients display decreased in situ TNF production. Pathol Res Pract. **2008**; 204(3):155–161.

62. Ansari AW, Heiken H, Meyer-Olson D, Schmidt RE. CCL2: a potential prognostic marker and target of anti-inflammatory strategy in HIV/AIDS pathogenesis. Eur J Immunol. **2011**; 41(12):3412–3418.

63. Ansari AW, Kamarulzaman A, Schmidt RE. Multifaceted impact of host C-C chemokine CCL2 in the immuno-pathogenesis of HIV-1/*M. tuberculosis* co-infection. Front Immunol. **2013**; 4(312):1–7.

64. Shankar EM, Vignesh R, Ellegård R, Barathan M, Chong YK, Bador MK, et al. HIV-*Mycobacterium tuberculosis* co-infection: a “danger-couple model” of disease pathogenesis. Pathog Dis. **2014**; 70(2):110–118.

65. Kauffman KD, Sallin MA, Sakai S, Kamenyeva O, Kabat J, Weiner D, et al. Defective positioning in granulomas but not lung-homing limits CD4 T-cell interactions with *Mycobacterium tuberculosis*-infected macrophages in rhesus macaques. Mucosal Immunol. **2017**; July: 1–12.

66. O’Toole R. Experimental models used to study human tuberculosis. Adv Appl Microbiol. **2010**; 71(10):75–89.

67. Gupta UD, Katoch VM. Animal models of tuberculosis. Tuberculosis. **2005**;

85:277–293.

68. Dharmadhikari AS, Nardell EA. What animal models teach humans about tuberculosis. Am J Respir Cell Mol Biol. **2008**; 39(5):503–508.

69. Lanoix J, Lenaerts A, Nuermberger E. Heterogeneous disease progression and treatment response in a C3HeB/FeJ mouse model of tuberculosis. Dis Model Mech. **2015**; 8:603–610.

70. Shi C, Shi J, Xu Z. A review of murine models of latent tuberculosis infection. Scand J Infect Dis. **2011**; 43(11–12):848–856.

71. Rhoades E, Frank A, Orme I. Progression of chronic pulmonary tuberculosis in mice intravenously infected with ethambutol resistant *Mycobacterium tuberculosis*. Tuber Lung Dis. **1997**; 78(1):57–66.

72. Medina E, North R. Resistance ranking of some common inbred mouse strains to *Mycobacterium tuberculosis* and relationship to major histocompatibility complex haplotype and Nramp1 genotype. Immunology. **1998**; 93:270–274.

73. Dharmadhikari AS, Mphahlele M, Venter K, Stoltz A, Mathebula R, Masotla T, et al. Rapid impact of effective treatment on transmission of multidrug-resistant tuberculosis. Int J Tuberc Lung Dis. **2014**; 18(9):1019–1025.

74. Zhang Y, Yew W-W. Mechanisms of drug resistance in *Mycobacterium tuberculosis* - update 2015. Int J Tuberc Lung Dis. **2015**; 19(11):1276–89.

75. Lipsitch M, Levin BR. The population dynamics of antimicrobial chemotherapy. Antimicrob Agents Chemother. **1997**; 41(2):363–73.

76. Zhang Y, Garbe T, Young D. Transformation with katG restores isoniazid-sensitivity in *Mycobacterium tuberculosis* isolates resistant to a range of drug

concentrations. Mol Microbiol. **1993**; 8(3):521–524.

77. Pym AS, Saint-Joanis B, Cole ST. Effect of katG mutations on the virulence of *Mycobacterium tuberculosis* and the implication for transmission in humans. Infect Immun. **2002**; 70(9):4955–4960.

78. Middlebrook G, Cohn M. Some observations on the pathogenicity of isoniazid-resistant variants of tubercle bacilli. Science. **1953**; 118(3063):297–299.

79. Barnett M, Busby SR, Mitchison DA. Tubercle bacilli resistant to isoniazid: virulence and response to treatment with isoniazid in guinea-pigs and mice. Br J Exp Pathol. **1953**; 34(5):568–81.

80. Li Z, Kelley C, Collins F, Rouse D, Morris S. Expression of katG in *Mycobacterium tuberculosis* is associated with its growth and persistence in mice and guinea pigs. J Infect Dis. **1998**; 177(4):1030–5.

81. Davies AP, Billington OJ, Bannister BA, Weir WR, McHugh TD, Gillespie SH. Comparison of fitness of two isolates of *Mycobacterium tuberculosis*, one of which had developed multi-drug resistance during the course of treatment. J Infect. **2000**; 41(2):184–7.

82. Gagneux S, Long CD, Small PM, Van T, Schoolnik GK, Bohannan BJM. The competitive cost of antibiotic resistance in *Mycobacterium tuberculosis*. Science. **2006**; 312(5782):1944–6.

83. Ordway DJ, Sonnenberg MG, Donahue S a, Belisle JT, Orme IM. Drug-resistant strains of *Mycobacterium tuberculosis* exhibit a range of virulence for mice. Infect Immun. **1995**; 63(2):741–3.

84. Billington OJ, McHugh TD, Gillespie SH. Physiological cost of rifampin

resistance induced in vitro in *Mycobacterium tuberculosis*. Antimicrob Agents Chemother. **1999**; 43(8):1866–9.

85. Sherman D, Mdluli K, Hickey M, Barry CI, Stover C. AhpC, oxidative stress and drug resistance in *Mycobacterium tuberculosis*. Biofactors. **1999**; 10:211–217.

86. Comas I, Borrell S, Roetzer A, Rose G, Malla B, Kato-Maeda M, et al. Whole-genome sequenceing of rifampicin-resistant *M. tuberculosis* strains identifies compensatory mutations in RNA polymerase. Nat Genet. **2011**; 44(1):106–110.

87. Safi H, Lingaraju S, Amin A, Kim S, Jones M, Holmes M, et al. Evolution of high-level ethambutol-resistant tuberculosis through interacting mutations in decaprenylphosphoryl-β-D-Arabinose biosynthetic and utilization pathway genes. Nat Genet. **2013**; 45(10):1190–1197.

88. Day T, Alizon S, Mideo N. Bridging scales in the evolution of infectious disease life histories - theory. Evolution. **2011**; 65(12):3448–61.

89. Mideo N, Alizon S, Day T. Linking within- and between-host dynamics in the evolutionary epidemiology of infectious diseases. Trends Ecol Evol. **2008**; 23(9):511–7.

90. Borrell S, Gagneux S. Infectiousness, reproductive fitness and evolution of drug-resistant *Mycobacterium tuberculosis*. Int J Tuberc Lung Dis. **2009**; 13(12):1456–1466.

91. Casali N, Nikolayevskyy V, Balabanova Y, Harris SR, Ignatyeva O, Kontsevaya I, et al. Evolution and transmission of drug-resistant tuberculosis in a Russian population. Nat Genet. **2014**; 46(3):279–86.

92. Cohen KA, Abeel T, Manson McGuire A, Desjardins CA, Munsamy V, Shea TP,

et al. Evolution of extensively drug-resistant tuberculosis over four decades: whole genome sequencing and dating analysis of *Mycobacterium tuberculosis* isolates from KwaZulu-Natal. PLoS Med. **2015**; 12(9): e1001880.

93. Gandhi NR, Moll A, Sturm AW, Pawinski R, Govender T, Lalloo U, et al. Extensively drug-resistant tuberculosis as a cause of death in patients co-infected with tuberculosis and HIV in a rural area of South Africa. Lancet. **2006**; 368(9547):1575–1580.

94. Blower SM, Gerberding JL. Understanding, predicting and controlling the emergence of drug-resistant tuberculosis: a theoretical framework. J Mol Med. **1998**; 76(9):624–36.

95. Dye C, Espinal M. Will tuberculosis become resistant to all antibiotics? Proc Biol Sci. **2001**; 268(1462):45–52.

96. Cohen T, Murray M. Modeling epidemics of multidrug-resistant *M. tuberculosis* of heterogeneous fitness. Nat Med. **2004**; 10(10):1117–21.

97. Knight GM, Colijn C, Shrestha S, Fofana M, Cobelens F, White RG, et al. The distribution of fitness costs of resistance-conferring mutations is a key determinant for the future burden of drug-resistant tuberculosis: a model-based analysis. Clin Infect Dis. **2015**; 61(S3):S147–S154.

98. Kendall EA, Fofana MO, Dowdy DW. Burden of transmitted multidrug resistance in epidemics of tuberculosis: a transmission modelling analysis. Lancet Respir Med. **2015**; 3(12):963–972.

CHAPTER II

LINKING INDIVIDUAL NATURAL HISTORY TO POPULATION OUTCOMES IN TUBERCULOSIS

Phillip P. Salvatore[1], Alvaro Proaño[2], Emily A. Kendall[3,4], Robert H. Gilman[2,5,6], David W. Dowdy[4,6,7]

1. Department of Molecular Microbiology and Immunology, The Johns Hopkins Bloomberg School of Public Health, Baltimore, MD, USA
2. Laboratorio de Investigación en Enfermedades Infecciosas, Laboratorio de Investigación y Desarrollo, Facultad de Ciencias y Filosofía, Universidad Peruana Cayetano Heredia, Lima, Peru
3. Division of Infectious Diseases, The Johns Hopkins University School of Medicine, Baltimore, MD, USA
4. The Center for Tuberculosis Research, The Johns Hopkins University School of Medicine, Baltimore, MD, USA
5. Asociación Benéfica PRISMA, Lima, Peru
6. Department of International Health, The Johns Hopkins Bloomberg School of Public Health, Baltimore, MD, USA
7. Department of Epidemiology, The Johns Hopkins Bloomberg School of Public Health, Baltimore, MD, USA

This chapter was previously published as: Salvatore PP, Proaño A, Kendall EA, Gilman RH, Dowdy DW. Linking individual natural history to population outcomes in tuberculosis. J Infect Dis. ***2017*** *Dec 27;217(1):112-121. DOI: 10.1093/infdis/jix555.*

ABSTRACT

Background: Substantial individual heterogeneity exists in the clinical manifestations and duration of active tuberculosis. We sought to link the individual-level characteristics of TB disease to observed population-level outcomes.

Methods: We developed an individual-based, stochastic model of TB disease in a hypothetical cohort of patients with smear-positive TB. We conceptualized the disease process as consisting of two states – progression and recovery – including transitions between the two. We then used a Bayesian process to calibrate the model to clinical data from the pre-chemotherapy era, thus identifying the rates of progression and recovery (and probabilities of transition) consistent with observed population-level clinical outcomes.

Results: Observed outcomes are consistent with slow rates of disease progression (median doubling time: 84 days, 95% uncertainty range 62-104) and a low, but nonzero, probability of transition from disease progression to recovery (median 16% per year, 95% uncertainty range 11%-21%). Other individual-level dynamics were less influential in determining observed outcomes.

Conclusions: This simplified model identifies individual-level dynamics – including a long doubling time and low probability of immune recovery – that recapitulate population-level clinical outcomes of untreated TB patients. This framework may facilitate better understanding of the population-level impact of interventions acting at the individual host level.

INTRODUCTION

Tuberculosis (TB) remains one of the leading causes of death worldwide, with an estimated 23% of the world's population infected and 1.4 million individuals dying of TB in 2015 [1,2]. The spectrum of disease caused by *Mycobacterium tuberculosis* demonstrates marked heterogeneity in terms of pathological presentation [3], incubation period [4], infectiousness [5], treatment responses [6], and other key clinical characteristics. While experimental studies have described underpinning biological mechanisms [7], and epidemiological studies have identified risk factors for TB progression at the population level [8], integrating these distinct approaches remains a complex task.

Epidemiological models are often utilized to make inferences about dynamics of complex systems, such as transmission of drug-resistant TB [9] and population-level impacts of various interventions [10]. In many such models, however, individual-level temporal dynamics and pathological processes (such as disease onset, progression, cure, and death) are simplified as population-level rates or probabilities. In contrast, within-host models can help disentangle individual-level dynamics of *M. tuberculosis* replication, host immune cell responses, cytokine signaling, pathology, and bacterial metapopulations [11–15]. Most within-host models of TB have uncertain applicability to human epidemics, however, as they draw on biological observations of experimental animal infection that have important dissimilarities with key aspects of human disease – including long-term asymptomatic latency, spontaneous self-resolution, and heterogeneity in disease outcome [16]. There is therefore a critical gap in our

understanding, namely the linkage of individual-level pathological processes to population-level clinical outcomes. Filling this gap could help to better predict the population-level effects of interventions – from better treatment for drug-resistant TB to earlier diagnosis and linkage to care – for which individual-level biological effects may be easier to measure.

In this study, we present a mathematical framework to address this knowledge gap using a simplified biological representation of TB progression across a population of individuals with incipient active TB. In developing this framework, we aimed to create the simplest possible representation of biological processes that could be compared against observed population-level clinical outcomes. We then calibrate this system to characteristics of the natural history of TB observed in empirical studies of patients in the pre-chemotherapy era. The primary objective of this study is to identify individual-level characteristics of TB disease progression which could – when simulated in a simplified system over large populations of immunocompetent individuals – successfully recapitulate clinical outcomes of untreated TB at the population level.

METHODS

Objective

To better simulate the temporal dynamics and heterogeneous outcomes of disease progression in clinical populations, we developed an individual-based, stochastic mathematical model of pulmonary tuberculosis progression in the human host. To link this model to population-level clinical outcomes, we drew upon data from epidemiological studies describing the natural history of TB before the worldwide introduction of modern anti-mycobacterial therapy (or the emergence of the HIV/AIDS pandemic) [17]. A systematic review of these studies estimated that, among adults diagnosed with sputum smear-positive TB, the average duration of disease was three years, 55% would die within five years, and 28% would eventually spontaneously resolve without chemotherapy [17]. We therefore sought to ascertain the individual-level characteristics of TB progression and resolution that could replicate similar clinical outcomes in large simulated populations.

Conceptual Framework

To construct a conceptual framework to address the primary objective, we made the simplifying assumption that, once infected, individuals exist in one of two clinical phases: disease progression or stabilization/recovery (Figure 2.1A). During these phases, the disease burden may increase and symptoms worsen (progression), or the disease burden may stabilize and symptoms either improve or worsen only slowly (recovery). To capture the myriad host and pathogen modifiers which influence an individual's disease

phenotype [18–20], rates of progression and recovery are modeled at the individual level to allow for variability from one individual to the next (see rate distributions in Figure 2.1B). Each individual's course of disease may then be simulated as a rate of progression, a rate of recovery, and a set of Markov probabilities which define the transitions between these two phases (see Figure 2.1C).

While these conceptual phases of progression and recovery are simplifications of the complex pathophysiology of TB infection [21], they are analogous to experimentally observable dynamics of bacterial replication and immune responses *in vivo* [7]. Unlike biological within-host models of TB [11–14,22], this model does not attempt to capture the complex and diverse immunological and pathophysiological mechanisms which influence clinical outcomes in any given individual. Rather, for simplicity and ease of understanding, we use "disease burden" as a mathematical benchmark that is likely associated with clinical outcomes (e.g., individuals who develop a higher burden may experience more severe symptoms, increased risk of mortality, and other pathological characteristics such as increased infectiousness) [18,23,24]. In this framework, "disease burden" should not be interpreted as a direct representation of bacillary load; instead, disease burden in this model represents a composite measure of characteristics of TB disease – such as pulmonary pathology, cough frequency, immunological exhaustion, chronic weight loss, etc., in addition to bacillary load – that correlate with the progression of clinical disease in patients. In this context, the simulated disease burden is not a verifiable quantity *per se*, but rather an instrument to relate the observable rates of progression and recovery in human populations to potentially measurable analogues of bacillary growth and decline in experimental systems.

We next define a conceptual "symptom threshold" as the disease burden above which active TB becomes symptomatic and clinically recognizable (i.e., as would be observable in pre-chemotherapy studies of smear-positive TB patients) [17]. Inversely, an infection in which the disease burden falls below this threshold represents an apparent self-resolution of symptomatic TB. Similarly, we define a "death threshold" – another conceptual construct – as the disease burden beyond which death would occur. (Similar techniques have been used to define "detectability" and "life-threatening" thresholds in models of cancer progression [25].) Using disease burden as a reference frame for clinical characteristics thus allows the duration and clinical status of each simulated case to be tracked.

Individual-Level Dynamics

Each patient is assumed to start at a disease burden of 1 (arbitrary) unit in the progression phase. The start of each simulation therefore represents the time at which a pathophysiological process toward progression to symptomatic, active disease (i.e., "incipient" TB) begins. Therefore, each patient is considered clinically silent and epidemiologically undetectable in our analyses until the patient's disease burden exceeds the symptom threshold for the first time. In calculating the disease burden at each discrete time step, we assume that progression and recovery follow the properties of a simple exponential process, with a single rate constant describing net growth (or decay) over time for a given individual in a given phase. We assume that the range of plausible growth rates during the progression phase (Figure 2.1B, purple distribution) is higher than the range of plausible growth (or decay) rates during the recovery phase (Figure

2.1B, blue distribution). While the disease progression of two simulated patients may exhibit different exponential growth and decay rates, the simulated disease within each individual host is assigned a single representative rate for the progression phase and a single representative rate for the recovery phase, sampled from the plausible ranges of each distribution (illustrated as the vertical lines on each curve in Figure 2.1B).

Figure 2.1: Individual-Level Model Framework of Progression and Recovery in Tuberculosis

(A) Each patient's disease is modeled through time as a sequence of transitions between disease progression and disease recovery. (B) A patient may take her rate of progression and her rate of recovery from a range of plausible rates, represented by probability densities across possible values of progression (purple density) and recovery (blue density). The shape of these densities is determined by the specific value of the rate mode parameters. Within each cohort, a value from each of these densities (depicted by vertical lines in the plot) is stochastically sampled to characterize each patient's infection. (C) In the case of an arbitrary simulated Patient A, disease development begins in the progression phase during which growth is characterized by the patient's sampled rate of progression. At any time (with a given weekly probability), the infection may transition to recovery, during which growth/decay is characterized by the patient's sampled rate of recovery. Similarly, at any subsequent time, the infection may transition from recovery to the progression phase, with the same rate of progression as sampled previously. The concomitant changes in Patient A's disease burden are represented in Figure 2.2.

Figure 2.1: Individual-Level Model Framework of Progression and Recovery in Tuberculosis

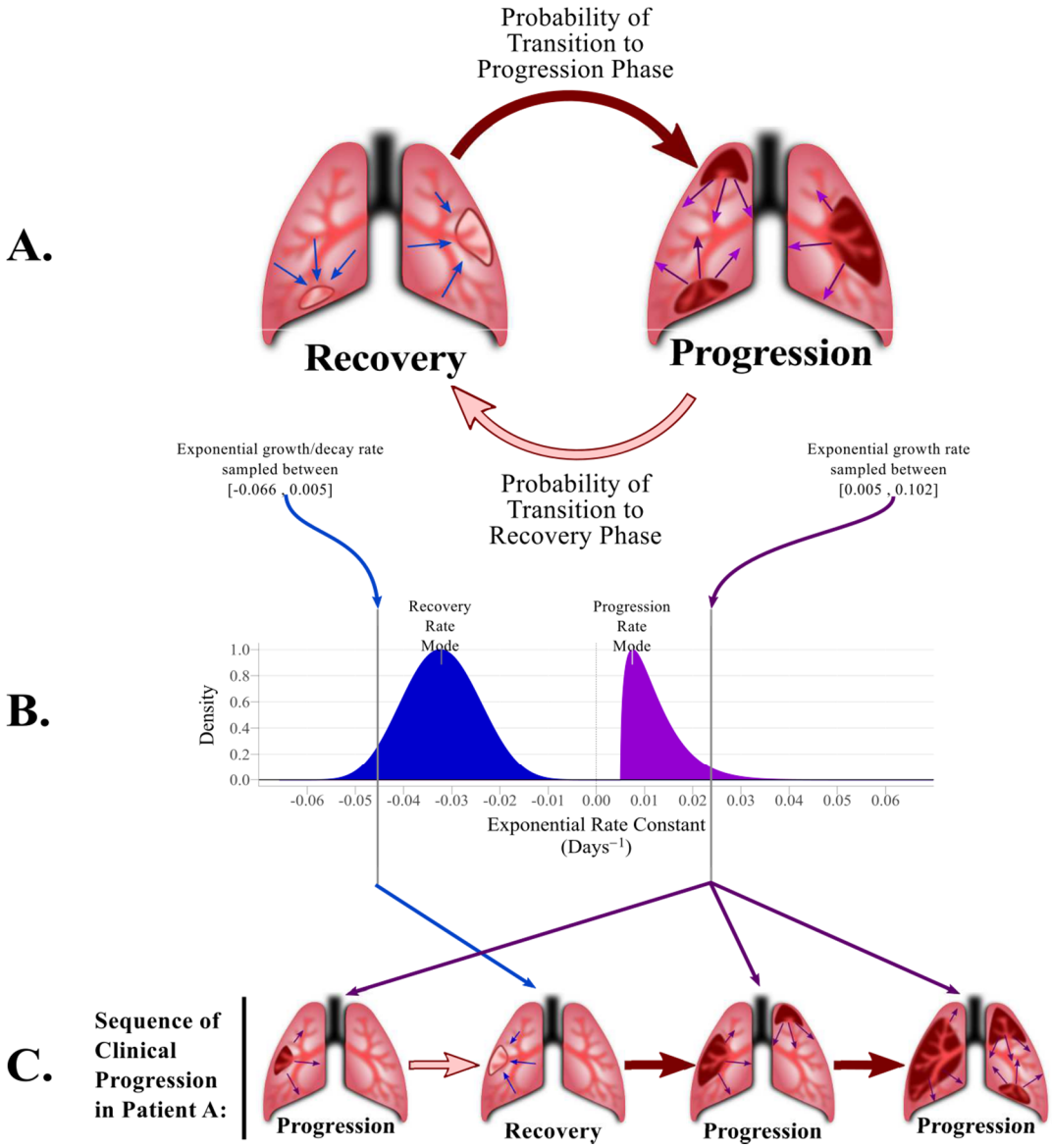

As a simulated course of disease progresses, each individual may transition between progression and recovery phases (illustrated for an arbitrary simulated "Patient A" in Figure 2.1C). Mathematically, these transitions occur probabilistically, independent of disease burden or history, and correspond to switches from the progression rate to the recovery rate, or vice versa (blue and purple arrows in Figure 2.1B-C). If, at any point, the disease burden of a symptomatic patient exceeds the "death threshold", the patient is classified as having died of TB. Conversely, a patient whose burden declines below the "symptom threshold" is classified as an apparently self-resolved case; these cases may relapse with symptomatic TB during the five years of simulation (see "Patient A" in Figure 2.2). Patients whose disease burden declines below the starting value of 1 unit are classified as cured, with no further possibility of disease progression. Thus, for each patient the duration of disease can be calculated as the continuous time spent with a disease burden between the "symptom threshold" and the "death threshold." A cohort of simulated patients is then assembled to estimate population-level clinical characteristics such as TB mortality, spontaneous resolution, and disease duration, accounting for variation in progression/recovery rates from one patient to the next as well as stochastic transition events from progression to recovery and back. A representative cohort of 250 simulated patient trajectories (representing a single set of population-level parameter distributions) is illustrated in Figure 2.2; emphasized is the infection trajectory of "Patient A" (diagramed qualitatively in Figure 2.1C).

Figure 2.2: Disease Burdens of a Simulated Population over Time

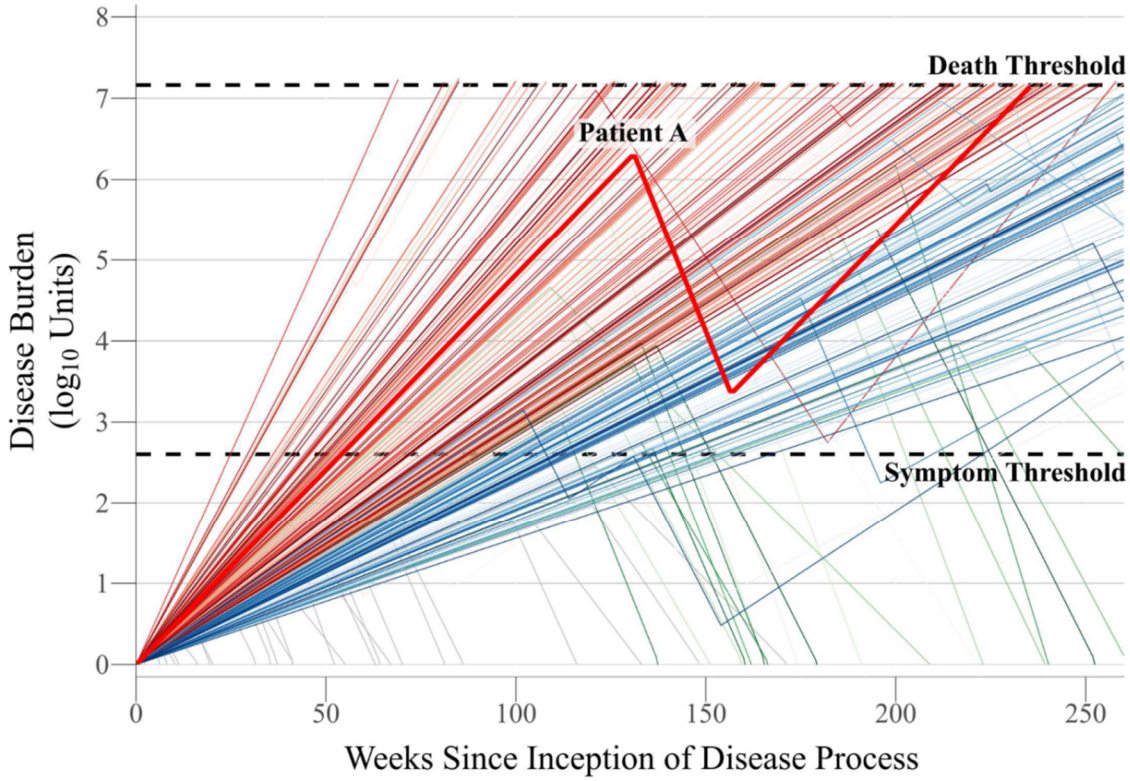

Patients whose infections exceed the "symptom threshold" (a mathematical benchmark) are tracked until death (when the bacillary burden exceeds a mathematical "death threshold", colored in red) or self-resolution (when the burden falls below the "symptom threshold", colored in green). Patients who continue to experience active TB (i.e., without exceeding the death threshold or experiencing self-resolution) after five years are colored in blue. Patients who never develop symptomatic disease (i.e., never surpass the symptom threshold) are plotted in grey. All disease burdens depicted were generated using the same model parameters and represent the population variability in progression/recovery rates as well as stochastic transitions between phases of infection. The disease burden of an arbitrary Patient A quantitatively depicts the progression of disease diagrammed graphically in Figure 2.1C; note that the rate (slope) of progression for Patient A is the same throughout her life (i.e., both before and after recovery).

Analytic Methods

To evaluate the likely values of model parameters (progression/recovery rates and phase transition probabilities), we implemented a Bayesian sampling-importance-resampling algorithm [26]. In this approach, a range of reasonable ("prior") values was defined for each model parameter (see Table 1). These prior ranges were taken as uniform distributions, on either the logarithmic- or log-modulus-transformed scales [27], bounded as shown in Table 1. Latin hypercube sampling [28] was then utilized to randomly draw two million sets of parameter values; each set was subsequently used to simulate a population of 1,000 patients with untreated TB using the drawn values for the two transition probabilities to inform stochastic realizations of the sequence of progression and recovery in each individual patient. The drawn values of the progression rate and recovery rate for the cohort represented the cohort's population modal progression and recovery rate, respectively, with each individual's rates drawn from a beta distribution (chosen to provide central tendency within defined upper and lower bounds) around each mode. Beta distributions were parameterized by the modal value and a concentration parameter of $\kappa=20$ to maintain a clear central tendency in each population. Individuals who never reached the symptom threshold over five years were dropped from the analysis. All other individuals were simulated until death (reaching the death threshold, colored in red in Figure 2.2), spontaneous recovery (again falling below the symptom threshold, colored in green in Figure 2.2), or five years of symptomatic disease (colored in blue in Figure 2.2) – reflecting the five-year mortality/recovery data to which our model was calibrated [17]. Outcomes in each cohort were aggregated to calculate the population-level simulated outcomes described below.

Table 2.1: **Parameter Values Used to Define Upper and Lower Bounds of Sampling Ranges**

Parameter	Sampled Range	References	Notes
Death threshold	7.0-10.0[a] ($\log_{10}$ units)[b]	[37–39]	Burdens in animal models rarely measure greater than 10^9 units per lung.
Width of the window between symptom and death thresholds	4.0-7.0[a] ($\log_{10}$ units)[b]	[39–41]	Burdens in animals with asymptomatic infection may be as high as 10^3 units.
Progression to Recovery transition rate	0.001-0.35 per week[a,c]	Derived	Assume 5% transition per year, and no more than 75% transition per month.
Recovery to Progression transition rate	10^{-5}-10^{-4} per week[a,d]	[42]	Probability of reactivation in latent infections estimated to be 0.8% per year.
Mode of the progression phase growth rate	0.035-0.714 per week[e,f]	[39–41]	Assume patients progress from onset to death in 3-60 months, assuming 10^4 unit symptom window.
Mode of the recovery phase growth rate	(-0.462)-0.035 per week[e,g]	[43]	Assume patients self-resolve at ¼ the rate of chemotherapeutic recovery (as defined by time to sputum conversion).

[a]Range sampled uniformly on the $\log_{10}$ scale

[b]The symptom threshold in a given simulation is derived by value of the death threshold and the value of the symptom window width.

[c]A 0.35 weekly rate of transition is equivalent to a 75% monthly probability of transition

[d]Rates in this range are equivalent to 0.05-5.0% probabilities of transition

[e]Range sampled uniformly on the log-modulus scale

[f]Progression rates in this range are equivalent to net population doubling times in the range of 6-137 days

[g]Progression rates in this range are equivalent to the range of a population half-life of 11 days to a population doubling time of 137 days

To identify those parameter values most consistent with observed population-level data, we assigned each cohort a pseudo-likelihood, defined as the joint probability density of the simulated cohort's population-level characteristics according to estimated density functions for three key summary statistics of observed pre-chemotherapy era cohorts: 55% case-fatality ratio within 5 years of symptom onset, median symptom duration of 3 years, and spontaneous resolution of ≥10% of cases [17]. (For further details, see "Importance Resampling" in the Supplementary Methods.) After assigning a pseudo-likelihood to each simulated cohort, we resampled two million cohorts, with replacement, proportional to the pseudo-likelihood [26]. The resampled (posterior) distribution therefore represents – in weighted fashion – those cohorts (and their corresponding parameter values) with the best fit to historical data. We define 95% uncertainty ranges (UR) as the 2.5^{th} and 97.5^{th} percentiles of each parameter's value, across the posterior distribution.

A multivariate sensitivity analysis was performed by computing the partial rank correlation coefficient (PRCC) between each of the six input parameters (two transition probabilities, modal progression rate, modal recovery rate, symptom threshold, and death threshold) and the pseudo-likelihood of each plausible cohort. This analysis identifies those parameters that most strongly influence the ability of the simulated data to fit the observed data, adjusting for all other parameters simultaneously. Based on the results of this sensitivity analysis, an additional post-hoc non-parametric Spearman correlation was tested between the probability of transitioning from progression to recovery and the modal progression rate.

Mathematical formulae, prior distributions, likelihood functions, importance resampling, and further technical details are provided in the Supplementary Methods. All statistical computing was performed using R version 3.2.2 (R Foundation for Statistical Computing, Vienna, Austria).

RESULTS

Of the two million simulated patient cohorts, 551,100 (27%) had results deemed consistent with historical estimates of TB natural history (i.e., non-zero pseudo-likelihoods, see the Supplementary Results for further details). Figure 2.3 presents the case-fatality ratios and median durations of disease of all simulated cohorts; the 551,100 plausible cohorts are colored according to the pseudo-likelihood of each. After weighting (resampling) cohorts according to these pseudo-likelihoods, the median case fatality ratio was 55% [Interquartile range (IQR): 54%, 56%], the median duration of disease for the 50^{th} percentile of cohorts was 2.5 years [IQR: 2.1, 2.8], and the median proportion of self-resolving cases was 28% [IQR: 19%, 37%] – consistent with empirical calibration targets (55% case fatality, mean three-year symptom duration, 28% self-resolved over 10 years) [17].

The correlation between each input parameter value and the fit between simulated and observed data is presented in Figure 2.4. The probability of transition from the progression phase to the recovery was also strongly correlated with model fit, and plausible models are consistent with a median yearly transition probability of 16% [95% UR: 11%, 21%; Figure 2.5A] The most important determinant of model fit was the rate of disease progression, and plausible results indicate a median progression rate of 0.0083 per day [95% UR: 0.0066, 0.011], equivalent to an exponential doubling time of 84 days [95% UR: 62, 104; Figure 2.5B, purple posterior]. This range can be interpreted as the doubling times of TB "disease burden" that are consistent with observed data on case-fatality, duration of clinical disease, and probability of self-resolution [17]. The rate of

disease progression and the probability of transition from progression to recovery were correlated among plausible cohorts (Spearman's $\rho = 0.68$, $p<0.01$).

The association between the rate of recovery and model fit to observed data was less strong (Figure 2.4). Model results suggest a median recovery rate of -0.014 per day [95% UR: -0.032, -0.0052], equivalent to an exponential half-life of 48 days [95% UR: 22, 133; Figure 2.5A, blue posterior]. Sensitivity analysis indicated that model fit was not associated with the value of the symptom threshold, death threshold, or probability of transition from recovery to progression ($|PRCC|<0.02$ for each, see also Supplementary Figures S1.1-S1.3).

To illustrate the potential application of this framework for investigating the impacts of individual-level interventions, we simulated cohorts with various diagnostic strategies (detailed further in the Supplementary Methods). In this example, our model was able to recapitulate global estimates of case fatality in the presence of partial diagnosis and treatment coverage (17.3%) [2] and illustrate how those gains in mortality could be achieved without observing substantial reductions in incidence (see the Supplementary Results for further details).

Figure 2.3:Weighting Process of Two Million Simulated Cohorts, According to Fit with Observed Clinical Data

Each point represents the results of a cohort of 1,000 simulated patients, plotted according to the 5-year case fatality ratio and median duration of disease amongst symptomatic patients who die or self-resolve. Each point is colored according to its weight (probability of being resampled to generate the final, or posterior, distribution), measured from 0 to 1 (the maximum likelihood of cohort results). Points colored in grey represent those cohorts with joint likelihoods equal to zero. (Not depicted are the 5% of simulations in which no patients developed symptoms.)

Figure 2.3:Weighting Process of Two Million Simulated Cohorts, According to Fit with Observed Clinical Data

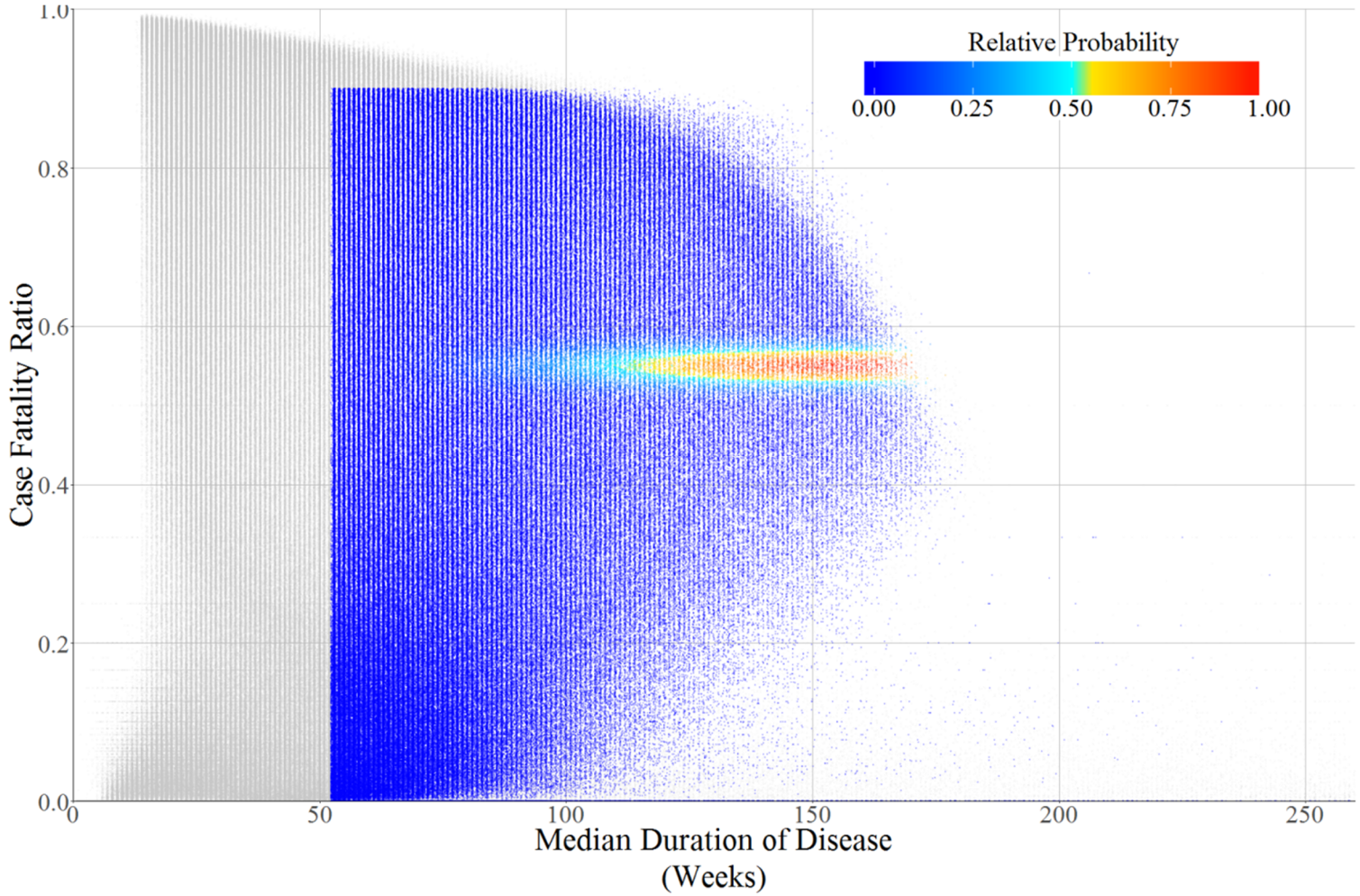

Figure 2.4: Association between Key Model Parameters and Population-Level Clinical Results

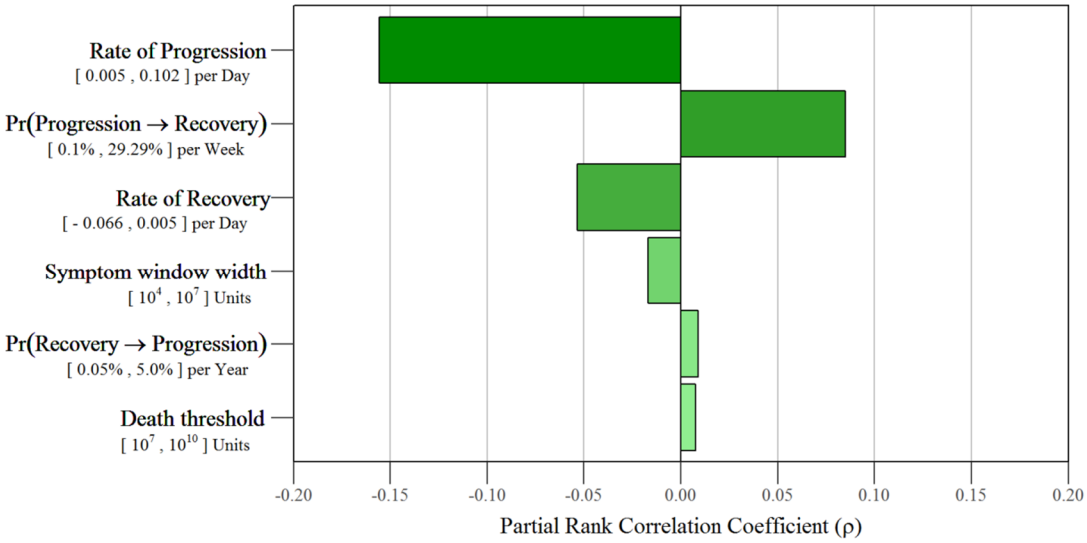

Each bar represents the partial rank correlation coefficient of the association between each model parameter and the joint likelihood of cohort results (i.e., how closely each cohort fits the observed data). Beneath each parameter label is the sampling range from which parameter values were sampled.

Figure 2.5: Values of Key Parameters Consistent with Observed Cohort Data

Model input values (prior distributions) were sampled uniformly on log-transformed or log-modulus-transformed scales between reasonable bounds selected on an a-priori basis (denoted by vertical dashed lines). Histogram densities show the proportion of 2 million weighted parameter values that were most consistent with observed cohort data from the pre-chemotherapy era (posterior distributions). (A) Distributions of probabilities of transition from progression phase to recovery phase on weekly and annualized scales. Simulations most consistent with observed data therefore primarily contain transition probabilities in the lower half of the initially sampled range (i.e., left-hand portion of the graph). The median transition probability among these data-consistent simulations (16% per year) implies that 50% of patients transition within 4.2 years ($0.5=e^{-0.16\times4.2}$), provided they survive that long. (B) Distributions of progression rates and recovery rates during the progression phase (purple) and the recovery phase (blue). In this graph, a progression/recovery rate of zero implies no change in disease burden with time. Recovery rates less than zero are therefore also displayed as half-lives (i.e., duration of time required for the disease burden to be cut in half), while progression rates are displayed as doubling times (i.e., duration of time required for the disease burden to double).

Figure 2.5: Values of Key Parameters Consistent with Observed Cohort Data

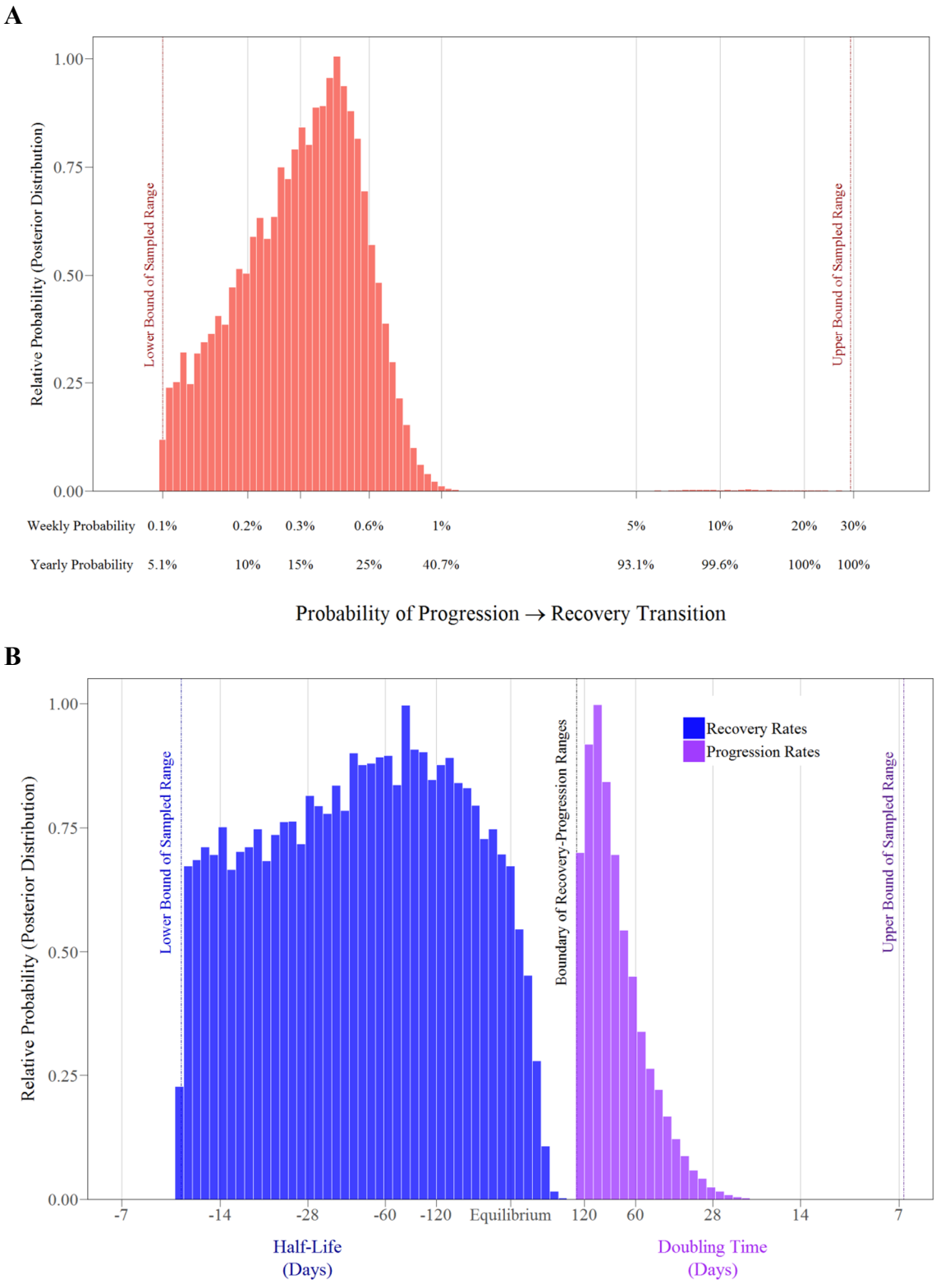

DISCUSSION

This study sought to identify individual-level TB disease characteristics that were consistent with historical population-level clinical outcomes, using a simplified model. As our model is calibrated to clinical characteristics of symptomatic TB, it should be interpreted as representative of incipient and active TB (but not long-term latency). The simulated case-fatality (median 55%), duration of disease (median 129 weeks), and proportion of self-resolved cases (median 28%) indicate that this simplified structure can capture the basic dynamics of clinical TB progression in human populations. Our primary results suggest that, under physiological conditions in realistic populations, active TB may reasonably be represented as a slow rate of disease progression (median 84-day doubling time) and a low probability of transitioning from progression to recovery (16% per year).

This modeling approach deliberately utilized a minimal parameterization of complex disease processes, but many possible complex models may also be consistent with observed clinical characteristics of TB progression. Therefore, the results presented here must be interpreted in the context of this framework and the analytical approach utilized.

It may be useful to provide intuitive context for these results. For example, we fit our model to a review of pre-chemotherapy era studies suggesting that TB patients experienced symptoms for an average of 3 years before death or symptom resolution [17]. Our estimated median doubling time of 84 days (Figure 2.5A, purple posterior) would generate a net 10^4 unit increase in disease burden (the minimum difference

between the "symptom threshold" and "death threshold") in 3.1 years of continuous progression. Our estimated 16% yearly probability – equivalent to a 29% probability of transition in the first two years – likewise reflects the empirical estimate (to which our data were fit) that 28% of untreated TB patients experience spontaneous resolution [17].

The data from this model also offer useful context with which to view experimental results from *in vitro* and *in vivo* models. For example, murine data suggest much faster disease progression (physiological doubling times of 2-3 days [29,30]) and shorter duration of disease (median durations of 31 weeks [31]) compared to our results (doubling times of 84 days and median disease duration of 2.5 years). Additionally, our results indicate that most patients who transition from progression to recovery experience sustained reductions in disease burden whereas bacillary burden in murine models may eventually plateau [29,30] but never declines. This discrepancy illustrates some of the implicit limitations of murine models in the study of human TB: without treatment, all mice eventually die from TB, whereas many human patients may naturally self-resolve [17]. Our simulation framework – with parameter values calibrated to clinical data in human populations – thus provides an important complement to data from animal models.

A primary limitation of this model framework is its simplification of the complex internal pathophysiological mechanisms of host-pathogen interactions. For example, changes in disease burden are simplified as generalized exponential growth and decay, and transitions between progression and recovery are represented as stochastic processes depending only on the current phase of disease. These simplifications necessarily limit the ability to draw precise mechanistic inference; however, they also allow for simulation

of a conceptually tractable measure (disease burden), thereby quantitatively linking individual-level data on disease progression and recovery with observable population-level clinical outcomes. Similarly, we also use mathematical constructs of symptom and death thresholds that have no direct physiological meaning. Importantly, these constructs were not significant determinants of our primary outcome (see Figure 2.4 and Supplementary Figures S1.1-S1.3). Our model is also not capable of calculating the single ("identifiable") parameter values that are most likely to result in the observed clinical data to which our model was fit. Rather, we sampled from *a priori* defined ranges and evaluated multiple sets of parameter values that might be consistent. Finally, our calibration strategy used data from historical studies with distinct demographic and epidemiological characteristics; while use of data-driven evidence is an advantage of the methodology, differences in these characteristics between historical and modern populations may limit the generalizability of these results in the contemporary epidemiology of TB (e.g., including HIV, diabetes, and changing age structures).

The development of a model linking individual-level and population-level outcomes opens a variety of avenues for future research and may also help to ground predictions of the population-level impacts of interventions which hinge on the temporal dynamics of individual-level TB outcomes. For example, the impact of scale-up of screening and diagnostic interventions may be heavily influenced by the distribution of individuals detectable by such interventions, as demonstrated in our simulation of diagnostic and treatment interventions. When patients with high simulated disease burdens are more likely to be diagnosed and treated than patients with low disease burdens, our model accurately reproduced 2015 global estimates of case fatality with

high precision, without predicting a major reduction in transmission (see the Supplementary Results). Linking clinical data with this mathematical framework may also be relevant to the transmission of TB, where a small number of patients (with prolonged symptoms and/or large disease burdens) may generate a majority of new infections [32]. For example, our simulation of diagnosis and treatment implied passive clinical interventions alone may not significantly reduce disease morbidity (as measured by disease burden over time), which may correlate with infectious potential in a population. Identifying such patients with measurable correlates of "disease burden" – such as cough frequency, cavitary lesions, sputum grade, aerosol dispersion, and time to positivity of cultures [33–35] – may augment the impact of diagnostic and treatment interventions on transmission, an effect our model may be able to quantitatively characterize. Finally, this framework holds potential for application to other infections which can be conceptualized as a sequence of transitions between states of varying pathogenesis [36].

In summary, this novel model linking individual-level and population-level outcomes suggests a range of parameters related to TB progression and recovery that might be consistent with observed clinical outcomes. Among these, we estimate the doubling time of disease burden as 84 days during the progression phase, a half-life of 47 days during recovery, and a probability of transition to recovery of 16% per year. Thus, in human populations, TB disease burden is likely to grow at a very slow rate, with a relatively low probability of switching from progression to recovery in the absence of intervention. While limited by pathological and mechanistic simplifications, this model

links within-host and population-level processes to better understand the complex interactions which influence human pathology and disease.

REFERENCES

1. Houben RM, Dodd PJ. The global burden of latent tuberculosis infection: a re-estimation using mathematical modelling. PLoS Med. **2016**; 13(10): e1002152.
2. Global tuberculosis report 2016. Geneva: World Health Organization, **2016**.
3. Sandgren A, Hollo V, van der Werf MJ. Extrapulmonary tuberculosis in the European Union and European Economic Area, 2002 to 2011. Eurosurveillance. **2013**; 18(12):1–9.
4. Vynnycky E, Fine PEM. Lifetime risks, incubation period, and serial interval of tuberculosis. Am J Epidemiol. **2000**; 152(3):247–263.
5. Fennelly KP, Jones-López EC, Ayakaka I, et al. Variability of infectious aerosols produced during coughing by patients with pulmonary tuberculosis. Am J Respir Crit Care Med. **2012**; 186(5):450–457.
6. Lalande L, Bourguignon L, Bihari S, et al. Population modeling and simulation study of the pharmacokinetics and antituberculosis pharmacodynamics of isoniazid in lungs. Antimicrob Agents Chemother. **2015**; 59(9):5181–5189.
7. Kim WS, Kim J, Cha S Bin, et al. Virulence-dependent alterations in the kinetics of immune cells during pulmonary infection by *Mycobacterium tuberculosis*. PLoS One. **2015**; 10(12): e0145234.
8. Selwyn PA, Hartel D, Lewis VA, et al. A prospective study of the risk of tuberculosis among intravenous drug users with Human Immunodeficiency Virus infection. N Engl J Med. **1989**; 320(9):545–50.
9. Knight GM, Colijn C, Shrestha S, et al. The distribution of fitness costs of

resistance-conferring mutations is a key determinant for the future burden of drug-resistant tuberculosis: a model-based analysis. Clin Infect Dis. **2015**; 61(S3):S147–S154.

10. Kendall EA, Shrestha S, Cohen T, et al. Priority-setting for novel drug regimens to treat yuberculosis: an epidemiologic model. PLoS Med. **2017**; 14(1): e1002202.
11. Wigginton JE, Kirschner D. A model to predict cell-mediated immune regulatory mechanisms during human infection with *Mycobacterium tuberculosis*. J Immunol. **2001**; 166(3):1951–1967.
12. Sud D, Bigbee C, Flynn JL, Kirschner DE. Contribution of CD8+ T cells to control of *Mycobacterium tuberculosis* infection. J Immunol. **2006**; 176(7):4296–314.
13. Gong C, Linderman JJ, Kirschner D. A population model capturing dynamics of tuberculosis granulomas predicts host infection outcomes. Math Biosci Eng. **2015**; 12(3):625–642.
14. Ganguli S, Gammack D, Kirschner DE. A metapopulation model of granuloma formation in the lung during infection with *Mycobacterium tuberculosis*. Math Biosci Eng. **2005**; 2(3):535–560.
15. Alavez-Ramírez J, Castellanos J, Esteva L, et al. Within-host population dynamics of antibiotic-resistant *M. tuberculosis*. Math Med Biol. **2007**; 24:35–56.
16. O'Toole R. Experimental models used to study human tuberculosis. Adv Appl Microbiol. **2010**; 71(10):75–89.
17. Tiemersma EW, van der Werf MJ, Borgdorff MW, Williams BG, Nagelkerke NJD. Natural history of tuberculosis: duration and fatality of untreated pulmonary

tuberculosis in HIV negative patients: a systematic review. PLoS One. **2011**; 6(4): e17601.

18. Dormans J, Burger M, Aguilar D, et al. Correlation of virulence , lung pathology , bacterial load and delayed type hypersensitivity responses after infection with different *Mycobacterium tuberculosis* genotypes in a BALB/c mouse model. Clin Exp Immunol. **2004**; 137:460–468.
19. Salie M, van der Merwe L, Möller M, et al. Associations between human leukocyte antigen class i variants and the *Mycobacterium tuberculosis* subtypes causing disease. J Infect Dis. **2014**; 209:216–223.
20. Caws M, Thwaites G, Dunstan S, et al. The influence of host and bacterial genotype on the development of disseminated disease with *Mycobacterium tuberculosis*. PLoS Pathog. **2008**; 4(3):e1000034.
21. Salvatore PP, Zhang Y. Tuberculosis: molecular basis of pathogenesis. Ref Modul Biomed Sci. **2017**; p. 1–15.
22. Alavez-Ramírez J, Castellanos JRA, Esteva L, et al. Within-host population dynamics of antibiotic-resistant *M. tuberculosis*. Math Med Biol. **2007**; 24(1):35–56.
23. Lopez B, Aguilar A, Orozco H, et al. A marked difference in pathogenesis and immune response induced by different *Mycobacterium tuberculosis* genotypes. Clin Exp Immunol. **2003**; 133:30–37.
24. Marquina-Castillo B, Garcia-Garcia L, Ponce-de-Leon P, et al. Virulence , immunopathology and transmissibility of selected strains of *Mycobacterium tuberculosi*s in a murine model. Immunology. **2009**; 128(1):123–133.

25. Botesteanu D, Lee J, Levy D. Modeling the dynamics of high-grade serous ovarian cancer progression for transvaginal ultrasound-based screening and early detection. PLoS One. **2016**; 11(6):e0156661.

26. Smith AFM, Gelfand AE. Bayesian statistics without tears: a sampling-resampling perspective. Am Stat. **1992**; 46(2):84–88.

27. John J, Draper N. An alternative family of transformations. Appl Stat. **1980**; 29(2):190–197.

28. Stein M. Large sample properties of simulations using Latin hypercube sampling. Technometrics. **1987**; 29(2):143–151.

29. Gill WP, Harik NS, Whiddon MR, Liao RP, Mittler JE, Sherman DR. A replication clock for *Mycobacterium tuberculosis*. Nat Med. **2009**; 15(2):211–214.

30. McDaniel MM, Krishna N, Handagama WG, Eda S, Ganusov V. Quantifying limits on replication, death, and quiescence of *Mycobacterium tuberculosis* in mice. Front Microbiol. **2016**; 7:862.

31. Medina E, North R. Resistance ranking of some common inbred mouse strains to *Mycobacterium tuberculosis* and relationship to major histocompatibility complex haplotype and Nramp1 genotype. Immunology. **1998**; 93:270–274.

32. Dowdy DW, Golub JE, Chaisson RE, Saraceni V. Heterogeneity in tuberculosis transmission and the role of geographic hotspots in propagating epidemics. Proc Natl Acad Sci USA. **2012**; 109(24):9557–9562.

33. Proaño A, Bravard MA, Tracey BH, et al. Protocol for studying cough frequency in people with pulmonary tuberculosis. BMJ Open. **2016**; 6(4):e010365.

34. Proaño A, Xu Z, Caligiuri P, Mollura DJ, Gilman RH. Computer automated

algorithm to evaluate cavitary lesions in adults with pulmonary tuberculosis. J Thorac Dis. **2017**; 9(7):93–96.

35. Proaño A, Bravard MA, López JW, et al. Dynamics of cough frequency in adults undergoing treatment for pulmonary tuberculosis. Clin Infect Dis. **2017**; 64(9):1174–1181.

36. Casadevall A, Pirofski L. The damage-response framework of microbial pathogenesis. Nat Rev. **2003**; 1(1):17–24.

37. Orme IM. A mouse model of the recrudescence of latent tuberculosis in the elderly. Am Rev Respir Dis. **1988**; 137(3):716–718.

38. Cooper AM, Dalton DK, Stewart TA, Griffin JP, Russell DG, Orme IM. Disseminated tuberculosis in interferon gamma gene-disrupted mice. J Exp Med. **1993**; 178:2243–2247.

39. Lin PL, Rodgers M, Smith L, et al. Quantitative comparison of active and latent tuberculosis in the cynomolgus macaque model. Infect Immun. **2009**; 77(10):4631–4642.

40. Capuano SV, Croix DA, Pawar S, et al. Experimental *Mycobacterium tuberculosis* infection of cynomolgus macaques closely resembles the various manifestations of human *M. tuberculosis* infection. Infect Immun. **2003**; 71(10):5831–5844.

41. Lin PL, Coleman T, Carney JPJ, et al. Radiologic responses in cynomolgus macaques for assessing tuberculosis chemotherapy regimens. Antimicrob Agents Chemother. **2013**; 57(9):4237–4244.

42. Shea KM, Kammerer JS, Winston CA, Navin TR, Horsburgh CR. Estimated rate of reactivation of latent tuberculosis infection in the United States, overall and by

population subgroup. Am J Epidemiol. **2014**; 179(2):216–225.

43. Kanda R, Nagao T, Tho N Van, et al. Factors affecting time to sputum culture conversion in adults with pulmonary tuberculosis: a historical cohort study without censored cases. PLoS One. **2015**; 10(11):e0142607.

CHAPTER III

TB TREATMENT, PYRAZINAMIDE ACTION, AND THE ROLE OF RIBOSOME RECYCLING FACTOR

Phillip P. Salvatore[1], David W. Dowdy[2-4]

1. Department of Molecular Microbiology and Immunology, The Johns Hopkins Bloomberg School of Public Health, Baltimore, MD, USA
2. The Center for Tuberculosis Research, The Johns Hopkins University School of Medicine, Baltimore, MD, USA
3. Department of International Health, The Johns Hopkins Bloomberg School of Public Health, Baltimore, MD, USA
4. Department of Epidemiology, The Johns Hopkins Bloomberg School of Public Health, Baltimore, MD, USA

ABSTRACT

Background: The mechanism of action of PZA in TB chemotherapy remains unsettled, though evidence suggests it inhibits the action of the bacterial protein RpsA. We reviewed the evidence for different models of PZA action and investigated protein binding partners of RpsA.

Methods: Recombinant RpsA was expressed and purified in *E. coli*. *M. tuberculosis* cells were lysed via sonication or French Press methods to obtain whole cell lysate. Purified bait RpsA was used to isolate putative binding partners using affinity chromatography. Protein identities were confirmed by mass spectrometry. Binding partners were overexpressed in *M. tuberculosis* culture and the minimal inhibitory concentration of POA was measured.

Results: RpsA bound several *M. tuberculosis* whole cell lysate proteins with high affinity. The most significant binding partner was found in lysate obtained via sonication but not by French Press and was identified as Ribosome Recycling Factor (RRF). When overexpressed in *M. tuberculosis* culture, RRF did not increase the sensitivity of cells to inhibition by POA.

Conclusions: These observations offer the first suggestion of a role of PZA in the inhibition of multiple conserved ribosome stress response pathways.

INTRODUCTION

While infections with strains of *Mycobacterium tuberculosis* susceptible to antibiotics may be successfully treated with a standardized short-course combination regimen, treatment of drug resistant tuberculosis (TB) requires longer regimens with additional, more expensive antibiotics often administered by injection [1]. Even after 18-24 months of combination treatment with second-line drugs, multidrug resistant TB (MDR-TB, resistant to at least two first-line drugs – rifampin and isoniazid) remains uncured in roughly half of treated patients [1]. Such treatments are complicated by the difficulty in detecting clinically meaningful drug resistance at the time of TB diagnosis. A critical component of long-term TB control programs will be the development and implementation of novel agents with anti-mycobacterial activity [2]. One strategy in the development of novel drugs and improvement in the detection of drug resistance involves identifying the mechanisms of action of current antibiotics used in the first-line treatment of TB. In the introduction of Chapter III, mechanisms of action of current first-line drugs are reviewed and the unique role of pyrazinamide in this regimen is explored for future study.

Short-course Chemotherapy for TB

Resistance to anti-mycobacterial therapies has existed as long as such antibiotics have been in use. In the first clinical trial of streptomycin for use in treating pulmonary tuberculosis (TB) in 1947, 35 of 41 surviving patients who received the antibiotic were later found to have developed infections that were insensitive to clinical concentrations of

streptomycin [3]. Much of the clinical research that followed those early studies was devoted to maximizing the effectiveness of TB treatment regimens, in large part by reducing the probability of acquiring drug resistance during treatment. Combining streptomycin and para-amino salicylic acid was found to reduce the probability of developing resistance to either drug individually, the first use of combination therapy to treat TB [4]. Isoniazid (INH), a more potent bactericidal drug, soon became a cornerstone of any first-line combination therapy [5]. While combinations of fast-acting bactericidal drugs like INH and ethambutol [6] were able to rapidly kill large bacterial populations in the first weeks of therapy [6,7], treatment courses of 12 months or longer were required to achieve adequate rates of long-term, relapse-free survival [8]. Rifampin (RIF), when included in combination with other bactericidal agents , could reduce the duration of treatment needed to achieve relapse-free cure from 12 months to 9 months [5,9].

Bacterial Populations and Drug Action

Of the four drugs utilized in the standard short-course first-line treatment of TB – INH, RIF, ethambutol, and pyrazinamide – three may be replaced with other agents that act in similar pharmacodynamics fashion. Actively replicating cells, targeted by the bactericidal actions of INH and ethambutol, may alternatively be killed by fluoroquinolones such as levofloxacin or moxifloxacin which inhibit DNA gyrase [10]. Rifampin may be effectively replaced by rifabutin when needed to avoid interactions with non-nucleoside reverse transcriptase inhibitors or protease inhibitors [11], and additional drug classes which mimic the activity of RIF continue to be developed for clinical use

[12]. Pyrazinamide (PZA), however, targets a unique population of cells unlike any other known class of antibiotics.

PZA demonstrates low bactericidal activity in clinical trials. At doses required to demonstrate appreciable rates of sputum conversion, PZA proved too hepatotoxic and was therefore removed from standard regimens [13]. However, in combination with more bactericidal drugs, lower-dose PZA improved rates of long-term relapse-free cure, demonstrating its sterilizing activity [5]. This sterilizing activity is likely accomplished through an altogether different modality than that of RIF. When PZA was added to combination regimens already containing RIF, rather than providing redundant sterilization without added effect, PZA was able to further shorten regimens from nine months to the six-month regimen still recommended today [5]. Despite the improvement provided by PZA in a six-month regimen, it was found that no benefit was gained when adding PZA beyond the first two months, suggesting that the bacterial population which is sterilized by PZA is effectively neutralized in the first eight weeks of therapy [14].

Experimental evidence further supports the assertion that PZA acts on a unique population of bacterial cells. Under laboratory conditions, PZA demonstrates poor inhibitory activity against *M. tuberculosis* in broth cultures at neutral pH [15], similar to the expected environment for actively replicating cells in lung cavities and interstitium. Similar observations are noted in commonly used murine models of TB [7,16]. However, at acid pH, PZA activity is greatly enhanced [17]. Recent data indicate that the minimal effect observed in murine models may result from crucial differences in pathology between TB in mouse and humans. While humans develop characteristic caseating necrosis and cavitary lesions, most mouse models develop a more diffuse (and non-

caseating) cellular infiltration [18,19]. Unlike other murine models, in C3HeB/FeJ mice – an inbred mouse strain which develops caseating necrosis in response to *M. tuberculosis* infection – PZA demonstrates significant antibiotic effect, albeit with notable inter-animal variability [16,20,21]. This observation has been explained by variability in caseum pH, with animals that exhibit more acidic caseum also demonstrating a greater dose-response to PZA [22]. Cumulatively, these findings define the role of PZA in accelerating sterilization in clinical regimens: by targeting a unique population of bacterial cells in a discrete acid compartment incompletely sterilized by RIF alone, PZA hastens the elimination of subsets of the bacterial population that would otherwise survive in an inactive state through the intensive bactericidal phases of therapy until the acidic environment of the caseum is eliminated [23]. Considering that there are no effective alternatives to PZA for sterilizing bacterial populations in acidic environments, it is vital to better understand the mechanism of action of PZA if we are to identify novel drugs to emulate its activity in cases of PZA-resistant infections.

Models of Pyrazinamide Action: Membrane Disequilibrium

Speculation about the specific molecular mechanism through which PZA exerts its antibiotic effects has persisted for several decades. Pyrazinamide, like INH, is administered as a prodrug which is converted to its active form, pyrazinoic acid (POA) by the bacterial nicotinamidase pncA [24,25]. As a result, most genetic resistance to PZA occurs through inactivating mutations to *pncA*, and a collection of various *pncA* mutations have been observed in clinical isolates [26]. The precise site and mode of action of POA, however, remains uncertain.

After PZA is converted to POA within *M. tuberculosis* cells, POA accumulates extracellularly at neutral pH, possibly through active transport efflux mechanisms [27]. Only when cells are treated with PZA in weakly acidic media (pH≤5.5) does POA begin to accumulate intracellularly, and the peak intracellular concentration is inversely proportional to pH [27]. Notably, this intracellular accumulation is not observed in inherently PZA-resistant *M. smegmatis* at acid pH, suggesting the antibiotic effect of PZA is dependent on the inability of *M. tuberculosis* cells to maintain low intracellular concentrations of POA in acid conditions. Efflux pump inhibitors such as reserpine and ion transport inhibitors (hence ATP production inhibitors) such as valinomycin increase the intracellular accumulation of POA in both *M. tuberculosis* and *M. smegmatis* at neutral pH [27,28], furthering the hypothesis that PZA activity is dependent on active efflux mechanisms which falter in acid conditions. These observations led to a model of POA action through a cascade of nonspecific toxic effects due to membrane disequilibrium. This framework asserts that the accumulation of protonated HPOA in an acidic extracellular environment at equilibrium results in an imbalanced influx of HPOA, resulting in disrupted membrane function, cytoplasmic acidification, and energy depletion due to loss in proton motive force across the membrane [13,29]. Consistent with this hypothesis are observations that the accumulation of intracellular POA is associated with reduced cross-membrane potential and that inhibitors of membrane-bound ATPases and cytochrome *c* oxidases enhance the activity of PZA in acid conditions [28].

This model, however, is incomplete. The dependence of intracellular POA accumulation on diffusion of protonated HPOA has not been confirmed experimentally,

and recent findings indicate that – unlike known ionophores CCCP and monensin – POA and PZA have no effect on cytoplasmic pH in acidic media [30]. The extracellular accumulation of HPOA has only been deduced theoretically using the Henderson-Hasselbach equation, assuming equilibrium between anionic POA^- and HPOA [31]. The hypothetical equilibrium conditions required for the Henderson-Hasselbach relationship to hold have not been empirically tested *in vitro* and are unlikely to hold *in vivo*. The extracellular accumulation of HPOA, which could provide evidence in favor of this hypothesis, has not been demonstrated experimentally. Recent studies have contested the finding that POA exposure reduces membrane potential [30]. Finally, nonspecific effects related to intracellular POA accumulation – such as reduced uptake of environmental amino acids and nucleotides [28] and increased sensitivity to weak acids and ultraviolet radiation [32] – may also be consistent with alternative models of PZA action.

Models of Pyrazinamide Action: Fatty Acid Pathways

Several additional models of PZA/POA action have been postulated. In multiple mycobacterial species, resistance to a PZA derivative, 5-chloro-pyrazinamide, may be conferred through overexpression of the Fatty Acid Synthase I gene *fas1*, a component in lipid biogenesis pathways [33]. Further investigation has demonstrated that both PZA and POA exert an inhibitory effect on FASI pathway products in acidic but not neutral pH [33,34]. Interestingly, in a cell-free assay, *M. smegmatis* FASI was inhibited by both POA and unmetabolized PZA, suggesting a possible direct antibiotic effect of PZA itself [35], though these results were contradicted in an *M. tuberculosis* system [36]. In a saturation transfer difference NMR system, POA and PZA were found to compete with

NADH for multiple binding sites on purified *M. tuberculosis* FASI [37]. Further support for a fatty acid synthesis model is provided by studies of Coenzyme A (CoA) metabolism, a precursor in long-chain fatty acid synthesis. Isolates of PZA-resistant *M. tuberculosis* generated through experimental culture have been shown to occasionally possess mutations in *panD*, an enzyme involved in biosynthesis of pantothenate and CoA [38,39], and intrinsically PZA-resistant *M. bovis* BCG displays POA sensitivity upon disruption of the long-chain fatty acyl-CoA ligase *fadD2* [40]. However, while supplemental pantothenate and CoA metabolites were found to mitigate the effects of PZA and POA [41,42], PZA remained active against *M. tuberculosis* strains lacking functional *panD*, indicating that PZA does not function primarily through *panD* inhibition [42]. Nevertheless, POA treatment was found to deplete CoA levels downstream of PanD action [39,43] and, more directly, POA was found to bind directly with purified PanD by isothermal titration calorimetry [43]. Despite the promise of these findings in molecular investigations, the direct connection between inhibition of fatty acid synthesis and the specific sterilizing effects on unique bacterial subpopulations – the critical role fulfilled by PZA in clinical regimens [23] – remains unrefined. A novel model, however, may serve to better articulate the mechanism of action of POA in fulfilling this specific role.

Models of Pyrazinamide Action: Trans-Translation

In light of the limitations of existing models of PZA/POA action, alternative methods of investigation have been pursued. A POA derivative, 5-hydroxyl-2-pyrazine carboxylic acid, linked to a sepharose matrix was found to bind specifically to several

novel protein partners in *M. tuberculosis* whole cell lysate [44]. Mass spectrometric analysis subsequently identified one of these partners as the small ribosomal subunit protein S1 encoded by the gene *RpsA*. No fatty acid synthesis pathway enzymes were detected in the same pull-down experiment. Furthermore, POA was found to bind specifically to purified wild-type RpsA with a $K_a > 7 \times 10^7$ M^{-1} as measured by isothermal titration calorimetry [44]. Later studies would identify two POA binding sites on *M. tuberculosis* RpsA using X-ray crystallography [45]. Overexpression of *RpsA* on a plasmid vector increased the minimum inhibitory concentration (MIC) – the concentration of drug required to prevent visible bacterial growth on solid media – of PZA five-fold in acidic *in vitro* conditions [44]. Several clinically PZA-resistant *M. tuberculosis* isolates carrying wild-type *pncA* genes were found to carry RpsA mutations at either N-terminal or C-terminal amino acid positions, and one such RpsA mutant (as well as RpsA from intrinsically PZA-resistant *M. smegmatis*) failed to bind specifically with POA by titration calorimetry. Cumulatively, these observations provided convincing evidence that, once POA has sufficiently accumulated intracellularly in acidic conditions, its antibiotic effect may be exerted through binding RpsA; when RpsA is mutated and POA cannot bind, the antibiotic effect is lost.

Functional studies provide a more detailed mechanism of inhibition through RpsA than alternative models suggested. While RpsA is an essential component of canonical translation and ribosome function, studies in other bacteria such as *Escherichia coli* have found that RpsA also plays a critical role in rescuing ribosomes under unique conditions [46]. When a ribosome stalls on a truncated mRNA, in the absence of a stop codon termination complexes cannot act to release the incomplete peptide or disengage the

ribosomal subunits. Specialized RNA complexes which possess dual transfer and messenger characteristics (hence referred to as transfer-messenger RNAs or tmRNAs) may enter the ribosomal A-site, tag the incomplete peptide for degradation using a poly-alanine sequence, and subsequently rescue the stalled ribosome for recycle and re-use [47]. This process is known as trans-translation or ribosome rescue. Cell-free translation assays and *in vitro* depletion experiments indicate that RpsA is an essential component of trans-translation and may bind tmRNA outside the ribosome [48].

On the basis of these observations, interactions between RpsA and tmRNA in *M. tuberculosis* were assessed. When purified RpsA and tmRNA are co-incubated, gel mobility assays reveal tmRNA migrates at a much larger molecular weight than expected, suggesting it is bound by RpsA [44]. When these complexes are incubated in the presence of POA, tmRNA migrates closer to its expected molecular weight (proportional to the concentration of POA present), indicating that POA inhibits the interaction of RpsA and tmRNA. No comparable inhibition is observed when tmRNA is incubated with mutant RpsA from POA-resistant clinical isolates [44,45]. Peptide assays of cell-free translation systems confirmed that trans-translated peptides from *M. tuberculosis* ribosomes are not produced in the presence of POA, but canonical translation is unaffected. These data illustrate a direct and detailed mechanistic description of PZA's antibiotic effect through the inhibition of ribosome rescue. That some bacteria implement ribosome stalling and rescue as a form of metabolic regulation under stress conditions [49] lends further credence to this model as the mechanism through which PZA functions to sterilize specific bacterial subpopulations in acidic or other stress conditions [23].

Experimental Rationale

Pyrazinamide is an essential component of first-line short course regimens used to treat TB. No other drug or drug class acts to sterilize bacterial populations in acidic compartments, and no effective replacement for PZA can reduce TB treatment from nine to six months while maintaining low rates of relapse. If novel chemotherapies are to be developed which can emulate the therapeutic role of PZA in combination therapy, it is essential to better understand the mechanism of action of PZA in *M. tuberculosis.* The most detailed model of PZA action indicates its ability to inhibit the rescue of stalled ribosomes under stress conditions, specifically by inhibiting the interactions between RpsA and tmRNA. As the function of RpsA has never been investigated thoroughly in *M. tuberculosis*, RpsA may offer novel targets for agents which could one day supplement PZA and further hasten therapy or replace PZA in the case of drug resistance. We therefore proposed to identify to protein binding partners of RpsA in *M. tuberculosis***.**

METHODS

Protein Purification

Based on X-ray crystallographic findings that POA binds RpsA in the protein's C-terminal region (residues K303, F307, F310, and R357) [45], we restricted our investigation to binding partners of the C-terminal domain of RpsA comprising the protein's fourth RNA-binding S1 domain and a flexible alpha-helix of unknown function (residues 292-481), denoted $RpsA^{292}$. Polymerase chain reaction was used to amplify *M. tuberculosis* genomic $RpsA^{292}$ with an N-terminal hexa-histidine tag which was cloned into an IPTG-inducible pET-SUMO vector as previously described [44]. This vector was transformed into *E. coli* DH5α chemically competent cells according to the manufacturer's protocol. Transformed cultures were plated on LB agar containing 50μg/mL kanamycin to identify transformed clones. Correct $RpsA^{292}$ insertion was confirmed by Sanger DNA sequencing.

Prior to overexpression, clones were grown to stationary phase overnight in liquid LB media with kanamycin at 35°C and shaking at 250rpm. Cultures were then transferred 1:100 into fresh media and grown to mid-log phase under the same conditions, at which point 400μg/mL isopropyl β-D-1-thiogalactopyranoside (IPTG) was used to induce protein overexpression. Cultures were then grown for four hours under the same conditions.

Induced cells were harvested by centrifugation at 4000rpm and washed with PBS. Resuspended cells were lysed via sonication. Homogenates were separated by centrifugation at 16000rpm for 20 minutes at 4°C. Cell lysate supernatants were

incubated with nickel-nitrilotriacetic acid (Ni-NTA) resin for 60 minutes at 4°C. Charged resin was then washed with PBS plus 20mM imidazole to remove contaminants. Purified $RpsA^{292}$ was then eluted from the resin using PBS plus 250mM imidazole. Purity was confirmed by SDS-PAGE. Imidazole was removed from purified protein buffers using dialysis cassettes 1:1000 in PBS overnight.

Cell Lysis

Single colonies of wild-type *M. tuberculosis* strain H37Ra (ATCC 25177) were inoculated into Middlebrook 7H9 liquid media with 0.2% (v/v) glycerol, 0.05% Tween 80, and 10% filtered albumin-dextrose-catalase. Cultures were grown to mid-log phase over 14-21 days. Cells were harvested via centrifugation at 9000rpm for 10 minutes at 4°C. Pellets were washed three times in PBS and resuspended. Cells were lysed either through sonication or French press lysis [50]. Lysis using sonication followed the protocol described above for *E. coli*.

In its native state, RpsA is associated with the 30S ribosomal subunit, a large macromolecular complex composed of both protein and nucleic acids [51]. Sonication, a common method of obtaining cell lysate which was utilized above, exposes whole cells to high energy ultrasonic pulses causing cytoplasmic cavitation and cell rupture [50]. As a result of these forces, large non-covalently-bound complexes may be separated into their constituent components and unique binding properties of the joint complex may be lost. French press lysis is an alternative method which ruptures cell walls and membranes through mechanical shearing and barotrauma but leaves larger complexes intact [50]. We

therefore also tested the binding partners of purified $RpsA^{292}$ in *M. tuberculosis* lysates obtained through French press lysis

For French press lysis, a Thermo Scientific Pressure Homogenizer was used. Cell suspensions were loaded into the pressure chamber at 4°C, pressure was gradually increased to 2000 PSI and ejected homogenate was collected. Pressurization was repeated three times total. After either lysis method, homogenates were centrifuged for 30 minutes at 20,000rpm at 4°C and lysate supernatants were collected.

Protein Interactions

Protein binding partners of $RpsA^{292}$ were assessed via Ni-NTA pulldown. A total of 5mg of *M. tuberculosis* H37Ra cell lysate supernatant were incubated with 200µg purified $RpsA^{292}$ for 2.5 hours at 4°C with gentle rocking. In experiments with POA, either 300µg/mL POA or DMSO as control was incubated with lysate supernatants for 15 minutes prior to the addition of $RpsA^{292.}$ Then, Ni-NTA resin was added to the mixture 1:10 by volume and incubated for one hour further. As controls, $RpsA^{292}$ alone, cell lysate alone, and PBS alone were incubated with resin under the same conditions. Unbound lysate products were removed from the resin using microfuge columns spun at 800rpm or using gravity columns, depending on the size of the preparation. Resin was then washed twice with PBS plus 20mM imidazole. Products bound to RpsA or to the resin matrix were eluted with PBS plus 250mM imidazole. Eluents were mixed with sodium dodecyl sulfate and heated to 100°C for 10 minutes to denature protein products, and precipitates were removed by centrifugation. Samples were then loaded into 1% polyacrylamide gels and electrophoresed at 100V for 1.5 hours. PAGE gels were

developed using colloidal Coomassie Blue stains at room temperature for 10 minutes. Bands of interest were excised from gels and submitted to the Johns Hopkins Mass Spectrometry and Proteomic facility for liquid chromatography FTFT tandem mass spectrometric analysis. Data was processed using Proteome Discoverer (v1.4 Thermo Fisher Scientific) and analyzed using Mascot v.2.5 Matrix Science.

Genetic Cloning

Wild-type *M. tuberculosis* genomic ribosome recycling factor (Rv2882c) was amplified via polymerase chain reaction using the following primers: 5' – GGT TTAATTAA GAA GGA GAT ATA CAT ATG ATT GAT GAG GCT CTC – 3' (forward) and 5' – GATATC CTA GAC CTC CAG CAG CTC – 3' (reverse). Purified PCR products were confirmed by Sanger DNA sequencing. Products were digested using NEB PacI and EcoRV double digestion restriction endonucleases in CutSmart Buffer for 15 minutes at 37°C according to manufacturer instructions. The tetracycline-inducible vector pUV15tetORM (ATCC Plasmid # 17975) was digested under the same conditions. Ligation of PCR products into the digested vector was performed using NEB T4 DNA Ligase at room temperature overnight, followed by inactivation at 65°C for 15 minutes according to manufacturer instructions. Ligation products were transformed into *E. coli* DH5α chemically competent cells according to the protocol described above. Plasmids were isolated from transformed cells and correct insertion and orientation was confirmed by Sanger DNA sequencing.

Purified pUV15tetORM-RRF isolated from *E. coli* was subsequently transformed into *M. tuberculosis* H37Ra and H37Rv cells according to standard protocols [52]. All

work involving live *M. tuberculosis* H37Rv was performed in the Johns Hopkins Bloomberg School of Public Health Biosafety Level 3 facility according to standard operating procedures. Competent cells were created by inoculating starter cultures into Middlebrook 7H9 liquid media with glycerol, Tween 80, and filtered albumin-dextrose-catalase and incubating at 37°C to log phase for 7 days. Cells were harvested by centrifugation at 4000rpm for 10 minutes. Cell pellets were resuspended in sterile distilled water and washed three times with 10% glycerol in water, and finally resuspended 100:1 in 10% glycerol in water. Purified plasmids (containing cloned RRF or empty vector) were added to cell suspensions for 1 minute at room temperature before electroporation (one pulse at 2.5kV). Transformed suspensions were then incubated in fresh Middlebrook 7H9 liquid media at 37°C overnight, before plating on Middlebrook 7H11 solid media with 50 μg/mL hygromycin. Plates were incubated at 37°C until single colonies were visible (approximately 3 weeks).

Antibiotic Sensitivity Testing

Transformed single colonies of *M. tuberculosis* were grown to log phase in sequential cultures of Middlebrook 7H9 liquid media with glycerol, Tween 80, filtered albumin-dextrose-catalase, and hygromycin. Agar plates containing Middlebrook 7H11 solid media with glycerol, Tween 80, and filtered albumin-dextrose-catalase were prepared containing increasing concentrations of POA up to 600μg/mL and/or increasing concentrations of the inducing agent anhydrotetracycline (ATc) up to 100ng/mL. Log phase transformed cultures were then spread uniformly on solid media and incubated at 37°C for up to 6 weeks. Growth on all plates was assessed on the same day.

RESULTS

Based on the observations that POA interacts with RpsA in its C-terminal domain [44,45], we purified an N-truncated recombinant *M. tuberculosis* RpsA (residues 292 to 481). To facilitate our affinity chromatography methodology, we included an N-terminal polyhistidine tag on the truncated peptide. Sample purity was confirmed by SDS-PAGE (Figure 3.1), indicating a band of high intensity at the expected fragment size of 21.6kDa.

To identify novel putative binding partners of RpsA not previously observed in fast-growing Gram-negative systems, purified $RpsA^{292}$ was incubated with *M. tuberculosis* H37Ra whole cell lysate. Lysate components with significant binding affinity for RpsA are expected to associate with the peptide during this incubation step. When added to a Ni-NTA matrix, the polyhistidine-tagged $RpsA^{292}$ becomes bound to the matrix along with any associated bound partners, while other lysate components are washed away. Initial pulldown results are presented in Figure 3.2A. Eluents from $RpsA^{292}$ incubated with cell lysate obtained through sonication are shown in lane 6. Because lysate components may bind directly with the Ni-NTA matrix due to native histidine-rich domains or nonspecific binding [53], eluents from lysate incubated with PBS as control are included in lane 7. Notably, five bands of high intensity appear in eluents of lysate incubated with $RpsA^{292}$ that are not observed in eluents of either lysate alone or $RpsA^{292}$ alone (enlarged and annotated in Figure 3.2B) in the size range of approximately 17-22kDa.

Figure 3.1: **Purity of Recombinant RpsA**[292]

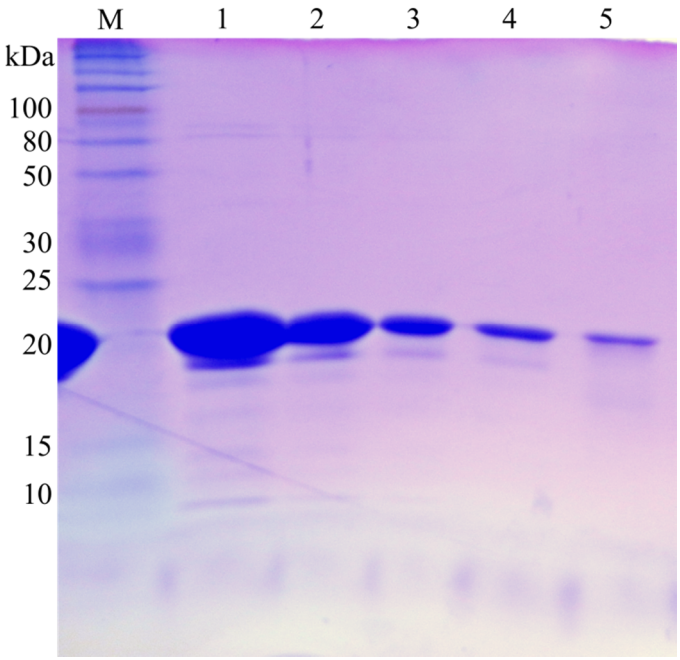

As described in the Methods, a truncated peptide of *M. tuberculosis RpsA* was amplified with an N-terminal polyhistidine affinity tag and cloned into a pET-SUMO vector. Expression was induced by IPTG and cells were lysed via sonication. Lysate supernatants were incubated with Ni-NTA resin and unbound constituents were washed with 20mM imidazole. Lanes 1-5 represent five sequential eluent fractions after wash.

Figure 3.2: RpsA^{292} Cell Lysate Pulldown

Purified RpsA^{292} was incubated with *M. tuberculosis* cell lysate, after which Ni-NTA resin was added to the mixture. The results of the pulldown experiment wash and elution fractions, run on an SDS-PAGE gel, are presented in 3.2A. Lane 1: Lysate alone (before wash); Lane 2: Purified RpsA^{292} alone (before wash); Lane 3: RpsA^{292} with Lysate, wash; Lane 4: Lysate alone, wash; Lane 5: RpsA^{292} alone, eluent; Lane 6: RpsA^{292} plus Lysate, eluent; Lane 7: Lysate alone, eluent. Putative protein binding partners may be identified by comparing bands in the RpsA^{292} alone eluent (Lane 5) and Lysate alone eluent (Lane 7) to those bands with increased intensity in the mixture of RpsA^{292} and Lysate (Lane 6). These lanes are enlarged in 3.2B, and bands which were excised for identification through mass spectrometry are annotated as boxes B through F (Box A indicates the band of RpsA^{292} present in the eluent of both samples).

Figure 3.2: RpsA^{292} Cell Lysate Pulldown

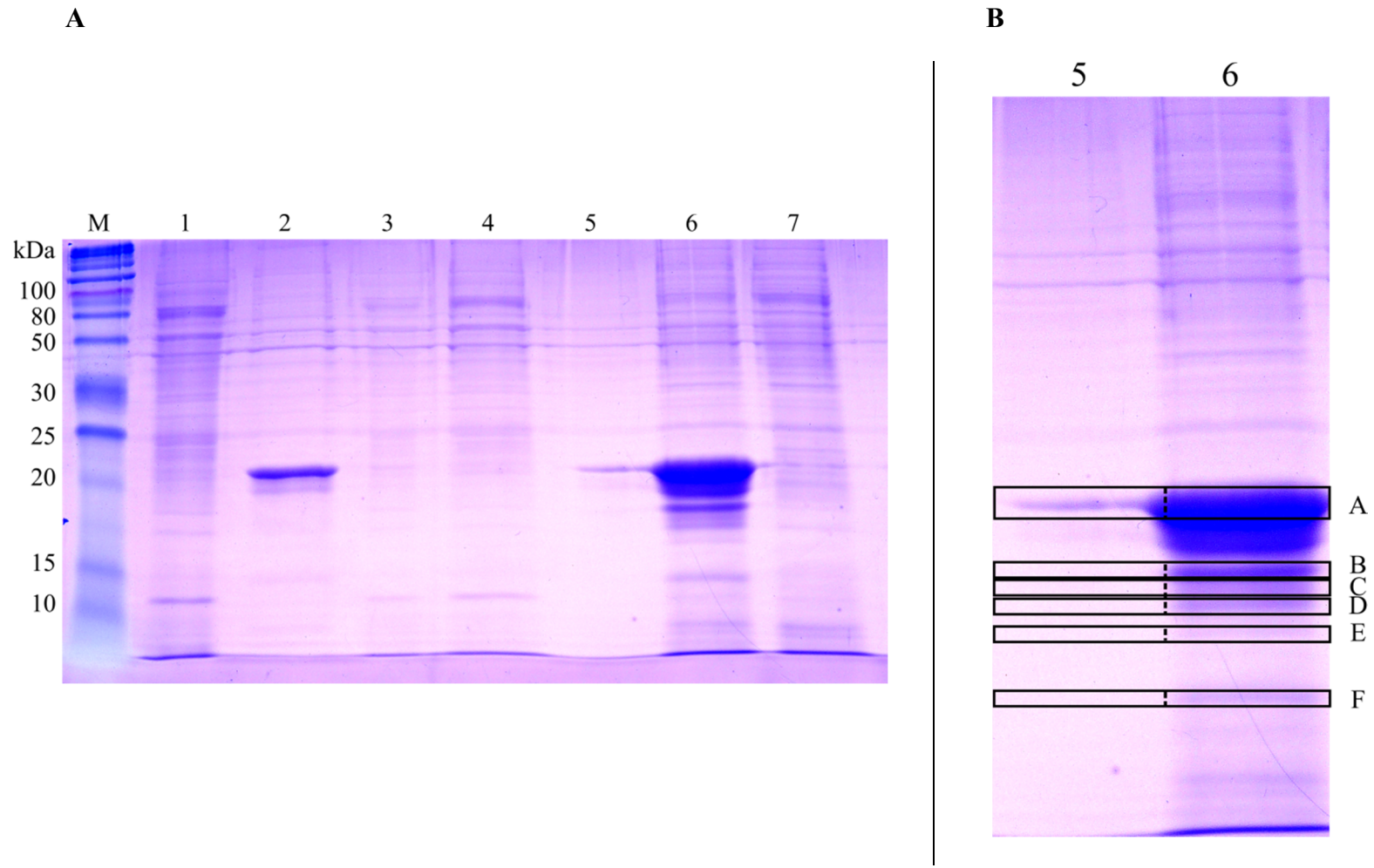

We also tested the binding partners of purified $RpsA^{292}$ in *M. tuberculosis* lysates obtained through French press lysis (Figure 3.3). Rather than observing additional pulldown partners in the French press lysates, we found that the bands of highest intensity found from sonication lysates were not found in French press lysates (lane 3 vs. lane 6). This suggests that this binding partner may itself be a component of a large macromolecular complex which precipitates out of solution when French Press lysates are centrifuged to obtain lysate supernatant.

To definitively identify the putative binding partners of RpsA identified through pulldown, we excised these SDS-PAGE gel bands (Figure 3.2B) and submitted them for analysis via LC-MS/MS by the Johns Hopkins Mass Spectrometry and Proteomics facility. The identities of the highest-likelihood candidate peptides from each band are presented in Table 3.1. Interestingly, the SDS-PAGE band of highest intensity from Figure 3.2 (band B) is consistent with ribosome recycling factor (RRF, Rv2882c), a 185-residue, 20.8kDa protein. Because RRF may play a role in ribosome rescue independent of tmRNA in *E. coli* (discussed below), we sought to test the effects of POA on the putative interactions between RpsA and RRF.

We repeated our pulldown experiment using $RpsA^{292}$ and *M. tuberculosis* lysates obtained from sonication. In this iteration, we also incubated samples with either 300μg/mL POA or DMSO as control (Figure 3.4). While the 21kDa band attributed to RRF appeared to show diminished intensity in the presence of POA (lane 3 vs. lane 5), this may be attributed to variations in the amount of total protein loaded in each lane and is not a definitive finding.

Figure 3.3: Lysis through Sonication or French Press

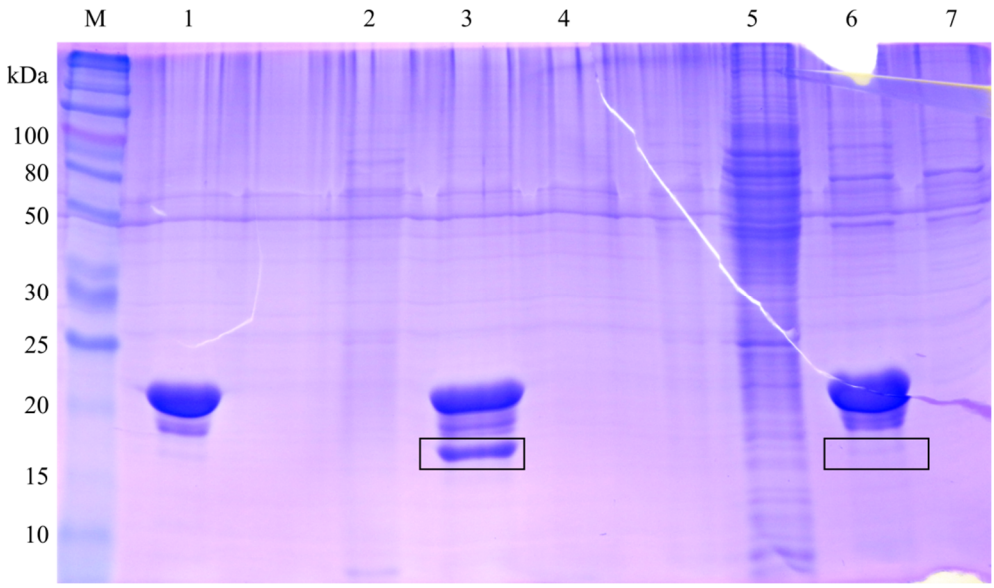

Purified RpsA^{292} was incubated with *M. tuberculosis* cell lysate obtained through either sonication (Lanes 2-4) or French press (Lanes 5-7), and eluents run on an SDS-PAGE gel are presented. Lane 1: RpsA^{292} alone, eluent; Lane 2: Sonication Lysate (before wash); Lane 3: RpsA^{292} plus sonication Lysate, eluent; Lane 4: Sonication Lysate, eluent; Lane 5: French press Lysate (before wash); Lane 6: RpsA^{292} plus French press Lysate, eluent; Lane 7: French press Lysate alone, eluent. Lanes 2-4 represent a replicate of the experiment performed in Figure 3.2. Protein binding partners present in the sonication Lysate but absent in the French press Lysate may be identified by comparing bands of increased intensity in Lane 3 to Lane 6. (Boxes have been added at the same molecular weight position in both lanes for comparison.)

Table 3.1: **Identities of Putative Protein Binding Partners**

Band ID*	Protein Name	Accession Number	Number of Exclusive Unique Spectra	Number of Total Spectra	Peptide Coverage	Molecular Weight (Da)	Protein Identification Probability
B	Ribosome Recycling Factor	gi|148662726	13	22	72%	20,828	>99%
C	Inorganic Pyrophosphatase	gi|494694055	7	16	40%	18,322	>99%
D	50S Ribosomal Protein L6	gi|148660494	17	33	51%	19,359	>99%
E	Hypothetical Protein MRA_0512	gi|148660273	6	11	15%	18,342	>99%
F	Ribose-5-phosphate Isomerase B	gi|148662300	27	99	60%	17,260	>99%

*Band A corresponds to $RpsA^{292}$ present in both samples of Figure 3.2B.

Figure 3.4: Effects of POA on the Binding Partners of RpA^{292}

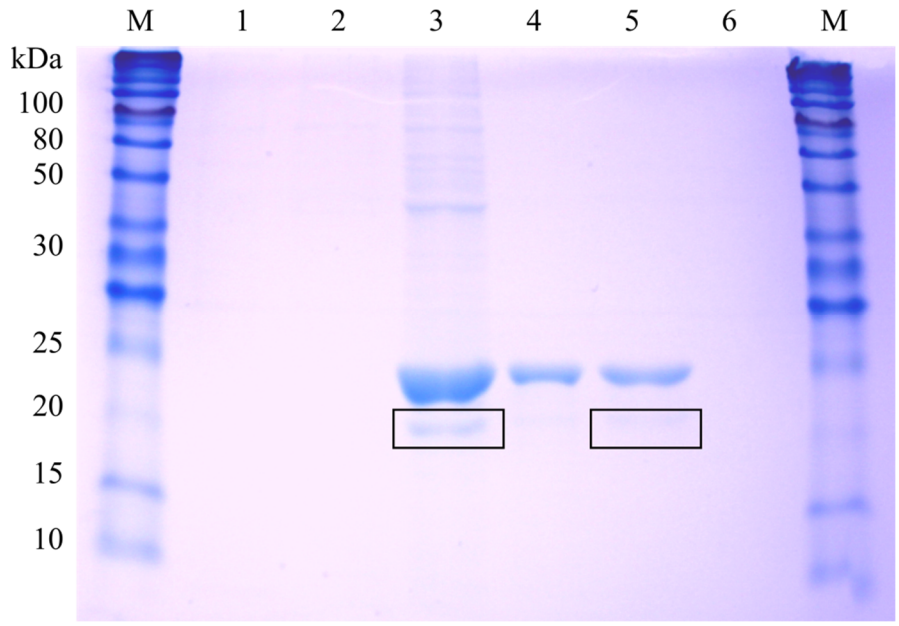

Purified RpsA^{292} was incubated with *M. tuberculosis* cell lysate (obtained through sonication) in the presence of either DMSO (as control, Lanes 2-3) or 300µg/mL POA (Lanes 5-6), and eluents run on an SDS-PAGE gel are presented. Lane 1: Lysate alone (before wash); Lane 2: Lysate alone with DMSO, eluent; Lane 3: RpsA^{292} and Lysate with DMSO, eluent; Lane 4: RpsA^{292} alone (before wash); Lane 5: RpsA^{292} and Lysate with POA, eluent; Lane 6: Lysate alone with POA, eluent. The potential effects of POA on RpsA^{292} binding partners may be assessed by comparing the intensity of bands present in the DMSO sample (Lane 3) with those present in the POA sample (Lane 5). (Boxes have been added at the same molecular weight position in both lanes for comparison.)

To explore physiological and phenotypic changes associated with RRF expression, we cloned wild-type *M. tuberculosis rrf* into a pUV15tetORM vector under control of an ATc-inducible promoter element. (As *rrf* is an essential gene, deletion is infeasible and knockdown or genomic mutation is methodologically problematic in slow-growing mycobacteria.) This vector was transformed into both *M. tuberculosis* H37Ra and H37Rv strains. Overexpression of RRF was induced using increasing concentrations of ATc and colonies were grown on solid media containing increasing concentrations of POA to determine the MIC (Figure 3.5). In both strains of *M. tuberculosis*, no detectable differences were observed in the MIC of POA in any concentration of inducing agent, suggesting that overexpression of RRF does not increase the sensitivity of *M. tuberculosis* to POA.

Figure 3.5: **Effects of RRF Overexpression on POA Sensitivity**

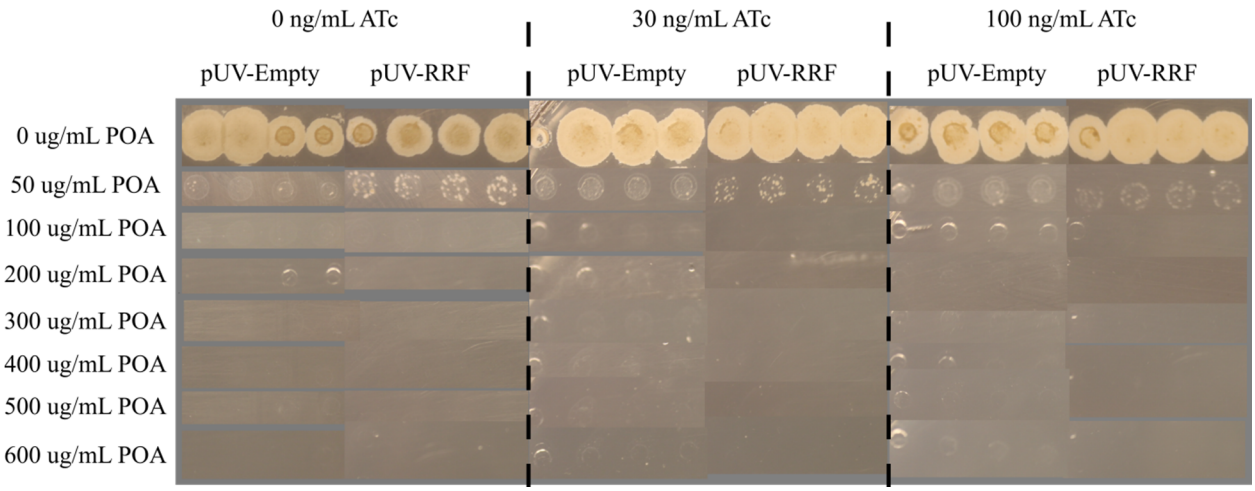

Wild-type *M. tuberculosis* RRF was cloned into a pUV15tetORM vector and transformed into competent *M. tuberculosis* H37Ra cells. Overexpression was induced using either 30ng/mL ATc (middle column) or 100ng/mL ATc (right column), and colonies were plated on Middlebrook 7H11 media containing 50µg/mL hygromycin (as a selective marker for the vector) and between 0 and 600µg/mL POA. The effects of RRF overexpression may be assessed by comparing the MIC of colonies containing the recombinant vector (containing cloned RRF, pUV-RRF) and that of colonies containing the empty vector (pUV-Empty) at each concentration of ATc. In all samples and replicates, no significant differences were noted in MIC between pUV-RRF and pUV-Empty clones.

DISCUSSION

In this study, we investigated the putative binding partners of RpsA in *M. tuberculosis*. We found that purified, truncated $RpsA^{292}$ associated with several cell lysate proteins in a Ni-NTA pulldown. The most significantly enriched protein from sonicated lysates was depleted in French press lysates, indicating that it is possibly associated with large, insoluble complexes intracellularly. By mass spectrometric analysis, the identity of this protein was found to be ribosome recycling factor (RRF), a protein known to bind the ribosomal 50S subunit in bacteria [54]. Incubation of $RpsA^{292}$ and sonicated lysates in the presence of POA did not noticeably inhibit the association of $RpsA^{292}$ with RRF as assessed by pulldown. Overexpression of RRF in *M. tuberculosis* cells did not alter the sensitivity of cells to POA. Cumulatively, these observations suggest that RpsA may bind RRF in bacterial cells – a novel finding – and that this interaction is not likely to be meaningfully impacted by the antibiotic actions of POA.

Ribosome recycling factor plays a core role in translation across bacterial species. Originally termed ribosome releasing factor, RRF was first described in 1970 and soon after its essential role (alongside elongation factor G) in disassembly of the post-termination complex was documented [55,56]. After an mRNA stop codon has entered the ribosomal A-site, release factors 1 and 2 act to hydrolyze the final peptidyl-tRNA ester bond and release the nascent peptide, leaving two uncharged tRNA molecules, the mRNA, and the ribosomal subunits associated as a post-translation complex [57]. Elongation factor G and RRF then act in the P-site to eject the release factors from the occupied A-site, and subsequently dissociate the ribosomal subunits allowing them to be

recycled or degraded [58]. The ribosome/mRNA complex has been co-crystallized with RRF, and on the basis of these structural studies, RRF has been predicted to associate primarily with 50S subunit 23S RNA and possibly proteins L5, L16, and L27 [54,59], but this has not been confirmed *in vivo*. However, due to the flexibility of its C-terminal domain, RpsA is routinely excluded from X-ray crystallographic studies of the ribosome and it is unclear whether it may plausibly interact with the RRF binding position. Our study may present the first evidence of a novel binding partner for RRF in the *M. tuberculosis* post-termination complex. In addition to its traditional role in releasing the post-termination complex, RRF may also play a non-canonical role in ribosome rescue.

In *E. coli*, certain short reading frames have been shown to produce toxic effects when transcribed, and these effects are related to codons cognate for rare tRNAs [60]. As these tRNAs are rapidly depleted, ribosomes stall mid-translation leading to a global halt in protein synthesis [61–64]. Similar to its role in rescuing ribosomes stalled on truncated peptides, overexpression of tmRNA can act to alleviate the toxic effects of ribosomes stalling on these rare codons [65]. Notably, overexpression of RRF demonstrates the same resuscitation phenotype. This observation does not necessarily discount canonical RRF function, as RRF may be recycling ribosomes rescued and terminated through trans-translation. However, when the tmRNA gene is interrupted and rendered nonfunctional, overexpression of RRF still demonstrates a rescue phenotype [65]. This implies that, on a stalled ribosome which cannot be terminated by tmRNA, RRF may still assist in ribosome release even though the peptide chain has not yet been released and the P-site is occupied by peptidyl-tRNA instead of release factors 1 and 2. This non-canonical role for RRF mirrors the phenotypic rescue demonstrated by tmRNA; that this occurs even in the

absence of functional tmRNA suggests that RRF may serve a redundant or complimentary rescue function. Importantly, it suggests that RpsA may play a vital role in interacting with multiple molecules which salvage stalled ribosomes under stress conditions. This would reinforce the existing model that POA's primary mechanism of antibiotic action is to disrupt ribosome rescue [44,66]. Importantly, all such work on RRF-mediated ribosome rescue has been investigated in *E. coli*, and mycobacterial proteins in this pathway may have important functional differences between those in *E. coli* [67,68]. Only further investigation of these pathways in *M. tuberculosis* will confirm or refute this hypothesis.

This experimental methodology is not without its limitations. Our primary finding was detected using a Ni-NTA pulldown and a polyhistidine-tagged bait protein. Such methods of affinity chromatography are subject to several known shortcomings: they are biased to towards interactions with high affinity and slow dissociation; post-translational modifications of RpsA expressed in *E. coli* may not reflect modifications in native *M. tuberculosis*; the binding conditions in buffer are unlikely to reflect intracellular binding conditions; affinities of purified bait proteins (RpsA) may not reflect the binding affinities of proteins in the native cellular niche (i.e., in complex with other ribosomal proteins and nucleotides); and affinity tags may interfere with native protein folding and may disrupt (or enhance) binding affinities [69–71]. It should be noted that these limitations are more likely to reduce the sensitivity of the assay than its specificity, and therefore false positive results are less likely than false negative results (i.e., some true binding partners may not have been captured in our assay, but it is less likely that RRF is a falsely positive binding partner). As discussed above, different cell lysis methods affect

the specific proteins contained in lysate supernatant, and as a result our lysates are unlikely to be fully representative of all potential intracellular binding partners of RpsA. Again, this limitation is more likely to produce false negatives than false positives. For these experiments, we deliberately elected to use a truncation of the full length RpsA as our bait protein, which may not represent all potential binding sites (or obstructions to RRF binding) found in wild-type RpsA. This truncation was selected based on data that POA binding sites occur at residues K307 and later [45], and therefore we were primarily interested in proteins which bound specifically to the C-terminal domain of RpsA. To validate our identification of RRF as a potential binding partner of $RpsA^{292}$, we utilized an overexpression/MIC experimental approach as has been used previously [44]. However, this approach could only confirm if a greater molar concentration of RRF could reduce the sensitivity of *M. tuberculosis* to POA (hypothetically by ensuring excess RRF could access RpsA during ribosomal rescue); negative results (i.e., no change in MIC) cannot distinguish between whether a) RRF binds to RpsA and this interaction is unaffected by POA; or b) RRF does not bind to RpsA regardless of the presence/absence of POA. Additionally, while *M. tuberculosis* cells were confirmed to carry the pUV vector (through selective resistance to hygromycin), we did not confirm that induction with ATc resulted in increased RRF protein levels (e.g., by western blot); as an essential protein used in translation termination, RRF may simply be constitutively expressed at high levels at its genomic locus. Furthermore, studies have demonstrated fundamental flaws in this approach, that overexpression of proteins targeted by antibiotics may counterintuitively lead to a reduction or no change in detectable MIC *in vitro*, depending on the specific kinetics of interactions between pro-drug, activating enzyme, activated

drug, drug target, and drug target binding partners [72]. These limitations suggest that while RpsA may bind RRF under buffered cell-free conditions, they remain inconclusive as to whether this actually occurs in living *M. tuberculosis* cells and to what extent this is inhibited by POA.

Alternative approaches and future experiments may well resolve these outstanding questions. Affinity chromatography (which detects interactions between proteins in cell-free systems) may be validated by an array of additional biochemical assays, such as tandem affinity purification, co-immunoprecipitation, or far western blotting [69–71]. More quantitative information of binding characteristics may be obtained from biochemical and biophysical methods such as isothermal titration calorimetry, surface plasmon resonance, or NMR spectrometry. Just as important as demonstrating a capacity for binding is the demonstration of protein-protein interactions in the intracellular environment. Two hybrid assays, fluorescence resonance energy transfer, and fluorescence co-localization microscopy may be versatile tools to this end. Synthetic lethality and genetic mutagenesis may also be insightful, though recombinant manipulation of genomic RpsA or RRF may be difficult as both are essential genes and may not tolerate significant alteration or disruption. Whether or not RpsA and RRF interact *in vivo*, the clinical relevance of these interactions remains unestablished. Sequencing of RRF from clinical *M. tuberculosis* isolates (particularly PZA-resistant isolates containing no *pncA* mutations and/or containing *RpsA* C-terminal domain mutations) may identify informative mutations to better understand the physiological role of RRF. Again, its function as a conserved, essential gene may make this approach unwieldy, and a search of whole-genome sequences from a library of 498 clinical *M.*

tuberculosis isolates from South Africa and China found no mutations in RRF [73]. Finally, the general hypothesis that POA interferes with one or more aspects of ribosome rescue deserves interrogation using the most powerful and sophisticated techniques available. Transcriptomic sequencing of *M. tuberculosis* cells exposed to POA may reveal changes in transcriptional and regulatory programming in response to antibiotic exposure. Even more powerful, ribosome profiling paired with RNA-seq experiments can reveal a) whether bacterial cells experience increased global ribosomal stalling and arrest when exposed to POA; and b) if specific transcripts experience greater rates of ribosomal stalling which contribute specifically to the antibiotic effects of POA [74,75]. These approaches, individually and in combination, provide exciting opportunities to further interrogate the interactions between RpsA and RRF and what role POA may play in that interaction.

For the purposes of this investigation, we limited our examination of RpsA interactions to the most abundant protein identified by mass spectrometry, RRF. That this protein also possesses functionality analogous to known binding partners of RpsA (e.g., tmRNA) encouraged further characterization of RRF. However, several other candidate proteins were identified by mass spectrometry as putative binding partners of RpsA (see Table 3.1), namely inorganic pyrophosphatase (PPiase, GI: 494694055), 50S ribosomal protein L6 (Rpl6, GI: 148660494), and ribose-5-phosphate isomerase B (Rv2465c, GI: 148662300). The presence of RpsA-RRF interactions does not necessarily preclude the possibility of concomitant interactions between RpsA and one or more of these candidates. While we did not further evaluate putative interactions between these proteins and RpsA, these interactions may offer promising opportunities for future research.

PPiases are ubiquitous proteins that are essential enzymes across bacterial phyla which function to hydrolyze pyrophosphate into inorganic phosphate, a function needed for a variety of metabolic processes including DNA replication, transcription, membrane biosynthesis, etc. [91]. In *M. tuberculosis*, PPiase is constitutively expressed under nutrient rich conditions as well as a variety of stress conditions, making it an attractive target for the development of bactericidal agents [92], and several promising allosteric inhibitors have been identified with activity specific to the PPiase of *M. tuberculosis* [93]. However, PPiase activity is primarily confined to catalysis of pyrophosphate and no interactions with ribosomal subunits or transcriptional substrates or products have been reported in the scientific literature. While this does not preclude the possibility of true interactions with RpsA, a high index of suspicion would be appropriate in follow-up studies.

In contrast with PPiase, Rpl6 is a known ribosomal protein that is likely to be intracellularly co-located with RpsA and may represent more promising interactions. While RRF functions in ribosome disassembly and release, Rpl6 functions in late-stage ribosome assembly and is essential for the functional initiation of translation and is a target for several antibiotics [94,95]. In Gram-positive organisms, mutations of Rpl6 have been associated with the generation of small colony variants, a heterogeneous subpopulation of cells which may tolerate stress conditions and antibiotics [96]. This may offer an alternative explanation of the unique clinical function of PZA (sterilization of small populations of bacteria in acid compartments): inhibition of Rpl6 may deplete a subpopulation of small colony variants which may be induced by acid stress and can tolerate inhibition by other first-line drugs. However, there have been no reports of small

colony variants in the *M. tuberculosis* literature, and most such literature is confined to fast-growing organisms such as *Staphylococcus* and species of Enterobacteriaceae.

Finally, a limited literature of ribose-5-phosphate isomerase B (which catalyzes the reaction of ribulose 5-phosphate and ribose 5-phosphate) exists for the bacterial kingdom. Of those published studies, the function of this protein in *M. tuberculosis* differs from that of *E. coli* [97], but how this may interact with RpsA in *M. tuberculosis* remains unclear. However, as competitive inhibitors of this enzyme have been developed [98,99], it may be relevant to investigate the function of RpsA in the presence of ribose-5-phosphate isomerase B inhibitors. Ultimately, each of these proteins may offer alternative, novel pathways involved in the activity of RpsA and potentially PZA and may merit further research.

In light of our finding that RRF does not increase the sensitivity of *M. tuberculosis* to POA, it may be productive to reexamine the premise that POA functions primarily by binding RpsA and inhibiting trans-translation. As yet, all mechanistic data indicating that POA binds RpsA have been collected in cell-free systems. These data are convincing: affinity chromatography, isothermal titration calorimetry, X-ray crystallography, and NMR spectrometry all indicate a nontrivial binding affinity between POA and RpsA [44,45]. These findings are corroborated by the detection of *RpsA* mutations in clinically PZA-resistant *M. tuberculosis* isolates containing wild-type *pncA* [76,77]. Similar findings that POA inhibits interactions between RpsA and tmRNA have also been observed exclusively in cell-free systems: gel mobility assays and cell-free translation systems [44,45]. However, no *in vivo* system has corroborated these findings.

Recent studies have begun to question the trans-translation model of POA action. An attempt to reproduce earlier findings that RpsA overexpression increased the sensitivity of *M. tuberculosis* to POA could not replicate these results, instead finding that the sensitivity of *M. tuberculosis* to PZA was unchanged [78]. Re-analysis of microarray data from PZA exposure experiments [79] found no change in *RpsA* transcript levels following drug exposure [78]. While binding affinities measured through isothermal titration calorimetry were found to approximate those measured in earlier studies when the pH of RpsA diluent is neutral [44], no energy of dissociation was measured when both solutions (POA and RpsA) were at equal acidic pH [78]. This suggests that the energy of dissociation measured in earlier reports represents proton dissociation as a neutral solution is titrated into an acidic buffer, but does not characterize the affinity of interactions between RpsA and POA. Finally, the POA-associated inhibition of trans-translation in a gel mobility assay and a cell-free system in the presence of POA could not be replicated [78]. In the absence of *in vivo* corroboration of POA-RpsA interactions, these failures to replicate early findings cast doubt over the trans-translation model of POA action.

While, if true, the POA-RpsA model may be informative for novel drug development, evidence suggests it bears little relevance on the detection of clinical drug resistance. Because of its role in activating PZA to POA, upwards of 80% of clinical PZA-resistant isolates have been attributed to mutations in *pncA* [80]. In thirteen publications reporting *RpsA* sequences from clinical isolates, only 33 PZA-resistant isolates (5%) demonstrated non-synonymous *RpsA* mutations out of over 614 PZA-resistant isolates reportedly sequenced with wild-type *pncA* [44,76,81–90]. This indicates

that, at best, *RpsA* mutations may explain only 5% of clinical PZA-resistance not attributable to *pncA*, and incorporating *RpsA* (with or without *panD*) sequencing into molecular PZA-resistance diagnosis algorithms only improves sensitivity 2-5% [82,89]. While any improvement in the detection of antibiotic resistance is important, these modest improvements in sensitivity suggest that still more can be done to understand mutations associated with clinical resistance.

This chapter has endeavored to review the microbiological basis for first-line TB combination therapy and the importance of PZA's sterilizing activity. To that end, it has examined proposed models for the mechanism of action of PZA (including membrane disequilibrium, inhibition of fatty acid synthesis, and inhibition of trans-translation), and discussed experimental evidence for those models. Based on the observation that POA binds and inhibits RpsA, we investigated the putative binding partners of RpsA in *M. tuberculosis*. We found that RpsA may bind RRF *in vitro*, but could not demonstrate that this interaction was inhibited by POA. This is the first report of potential interactions between RpsA and RRF in the scientific literature, and could imply that RpsA may serve a key function in several ribosome rescue pathways. These findings should be validated with further investigation and several such methodologies are proposed here. Finally, this article concludes by critically evaluating the evidence that RpsA may not be an important site of action for PZA's antibiotic effects, both microbiologically and clinically. While PZA remains a critical and indispensable component of first-line TB regimens globally, the mechanism through which it exerts its unique sterilizing effects is still a source of contentious debate. Only through further investigation may we better understand sources

of PZA resistance and develop novel chemotherapeutic agents to enhance or replace pyrazinamide.

REFERENCES

1. Global Tuberculosis Report 2017. Geneva: World Health Organization, **2017**.
2. Tuberculosis Strategy Overview. Seattle: The Bill and Melinda Gates Foundation, **2012**.
3. Fox W, Sutherland I, Daniels M. A five-year assessment of patients in a controlled trial of streptomycin in pulmonary tuberculosis; report to the Tuberculosis Chemotherapy Trials Committee of the Medical Research Council. Q J Med. **1954**; 23(91):347–366.
4. Medical Research Council. Treatment of pulmonary tuberculosis with streptomycin and para-amino-salicylic acid: a Medical Research Council investigation. BMJ. **1950**; 2(4688):1073–1085.
5. Fox W, Ellard GA, Mitchison DA. Studies on the treatment of tuberculosis undertaken by the British Medical Research Council Tuberculosis Units, 1946-1986, with relevant subsequent publications. Int J Tuberc Lung Dis. **1999**; 3(10 Supp 2):S231–S279.
6. Jindani A, Aber VR, Edwards EA, Mitchison DA. The early bactericidal activity of drugs in patients with pulmonary tuberculosis. Am Rev Respir Dis. **1980**; 121(6):939–949.
7. Grosset J, Almeida D, Converse PJ, Tyagi S, Li S, Ammerman NC, et al. Modeling early bactericidal activity in murine tuberculosis provides insights into the activity of isoniazid and pyrazinamide. Proc Natl Acad Sci. **2012**; 109(37):15001–15005.

8. Medical Research Council. Long-term chemotherapy in the treatment of chronic pulmonary tuberculosis with cavitation: a report to the Medical Research Council by their Tuberculosis Chemotherapy Trials Committee. Tubercle. **1962**; 43(3):201–267.

9. Donald PR, Diacon AH. The early bactericidal activity of anti-tuberculosis drugs: a literature review. Tuberculosis. **2008**; 88(Supp 1): S75-S83.

10. WHO Treatment Guidelines for Drug-Resistant Tuberculosis - 2016 Update. Geneva: World Health Organization, **2016**.

11. Treatment of Tuberculosis: Guidelines - 4th edition. Geneva: World Health Organization; **2010**.

12. Ma C, Yang X, Lewis PJ. Bacterial transcription as a target for antibacterial drug development. Microbiol Mol Biol Rev. **2016**; 80(1):139–160.

13. Zhang Y, Shi W, Zhang W, Mitchison D. Mechanisms of pyrazinamide action and resistance. Microbiol Spectr. **2013**; 2(4):1–12.

14. East African/British Medical Research Councils. Controlled clinical trial of five short-course (4-month) chemotherapy regimens in pulmonary tuberculosis: second report of the 4th study. Am Rev Respir Dis. **1981**; 123(2):165–170.

15. Tarshis MS, Weed WA. Lack of significant in vitro sensitivity of *Mycobacterium tuberculosis* to pyrazinamide on three different solid media. Am Rev Tuberc. **1953**; 67(3):391–395.

16. Lanoix JP, Tasneen R, O'Brien P, Sarathy J, Safi H, Pinn M, et al. High systemic exposure of pyrazinoic acid has limited antituberculosis activity in murine and rabbit models of tuberculosis. Antimicrob Agents Chemother. **2016**; 60(7):4197–

4205.

17. Heifets LB, Lindholm-Levy P. Pyrazinamide sterilizing activity in vitro against semidormant *Mycobacterium tuberculosis* bacterial populations. Am Rev Respir Dis. **1992**; 145(5):1223–1225.

18. O'Toole R. Experimental models used to study human tuberculosis. Adv Appl Microbiol. **2010**; 71(10):75–89.

19. Gupta UD, Katoch VM. Animal models of tuberculosis. Tuberculosis. **2005**; 85:277–293.

20. Lanoix J, Lenaerts A, Nuermberger E. Heterogeneous disease progression and treatment response in a C3HeB/FeJ mouse model of tuberculosis. Dis Model Mech. **2015**; 8:603–610.

21. Lanoix J, Betoudji F, Nuermberger E. Sterilizing activity of pyrazinamide in combination with first-line drugs in a C3HeB/FeJ mouse model of tuberculosis. Antimicrob Agents Chemother. **2016**; 60(2):1091–1096.

22. Lanoix JP, Ioerger T, Ormond A, Kaya F, Sacchettini J, Dartois V, et al. Selective inactivity of pyrazinamide against tuberculosis in C3HeB/FeJ mice is best explained by neutral pH of caseum. Antimicrob Agents Chemother. **2016**; 60(2):735–743.

23. Mitchison DA. Basic mechanisms of chemotherapy of. Chest. **1979**; 76(6):771–781.

24. Konno K, Feldmann FM, McDermott W. Pyrazinamide susceptibility and amidase activity of tubercle bacilli. Am Rev Respir Dis. **1967**; 95(3):461–469.

25. Scorpio A, Zhang Y. Mutations in pncA, a gene encoding

pyrazinamidase/nicotinamidase, cause resistance to the antituberculous drug pyrazinamide in tubercle bacillus. Nat Med. **1996**; 2(6):662–667.

26. Ramirez-Busby SM, Valafar F. Systematic Review of mutations in pyrazinamidase associated with pyrazinamide resistance in *Mycobacterium tuberculosis* clinical isolates. Antimicrob Agents Chemother. **2015**; 59(9):5267–5277.

27. Zhang Y, Scorpio A, Nikaido H, Sun Z. Role of acid pH and deficient efflux of pyrazinoic acid in unique susceptibility of *Mycobacterium tuberculosis* to pyrazinamide. J Bacteriol. **1999**; 181(7):2044–2049.

28. Zhang Y, Wade MM, Scorpio A, Zhang H, Sun Z. Mode of action of pyrazinamide: disruption of *Mycobacterium tuberculosis* membrane transport and energetics by pyrazinoic acid. J Antimicrob Chemother. **2003**; 52(5):790–795.

29. Zhang Y, Mitchison D. The curious characteristics of pyrazinamide: a review. Int J Tuberc Lung Dis. **2003**; 7(1):6–21.

30. Peterson ND, Rosen BC, Dillon NA, Baughn AD. Uncoupling environmental pH and intrabacterial acidification from pyrazinamide susceptibility in *Mycobacterium tuberculosis*. Antimicrob Agents Chemother. **2015**; 59(12):7320–7326.

31. Zhang Y, Permar S, Sun Z. Conditions that may affect the results of susceptibility testing of *Mycobacterium tuberculosis* to pyrazinamide. J Med Microbiol. **2002**; 51(1):42–49.

32. Wade MM, Zhang Y. Effects of weak acids, UV and proton motive force inhibitors on pyrazinamide activity against *Mycobacterium tuberculosis* in vitro. J Antimicrob Chemother. **2006**; 58(5):936–941.

33. Zimhony O, Cox JS, Welch JT, Vilchèze C, Jacobs WR. Pyrazinamide inhibits the

eukaryotic-like fatty acid synthetase I (FASI) of *Mycobacterium tuberculosis*. Nat Med. **2000**; 6(9):1043–7.

34. Zimhony O, Vilchèze C, Arai M, Welch JT, Jacobs WR. Pyrazinoic acid and its n-propyl ester inhibit fatty acid synthase type I in replicating tubercle bacilli. Antimicrob Agents Chemother. **2007**; 51(2):752–754.

35. Ngo SC, Zimhony O, Woo JC, Sayahi H, Jacobs WR, Welch JT. Inhibition of isolated *Mycobacterium tuberculosis* fatty acid synthase I by pyrazinamide analogs. Antimicrob Agents Chemother. **2007**; 51(7):2430–2435.

36. Boshoff HI, Mizrahi V, Barry CEI. Effects of pyrazinamide on fatty acid synthesis by whole mycobacterial cells and purifed Fatty Acid Synthase I. J Bacteriol. **2002**; 184(8):2167–2172.

37. Sayahi H, Zimhony O, Jacobs WR, Shekhtman A, Welch JT. Pyrazinamide, but not pyrazinoic acid, is a competitive inhibitor of NADPH binding to *Mycobacterium tuberculosis* Fatty Acid Synthase I. Bioorganic Med Chem Lett. **2011**; 21(16):4804–4807.

38. Zhang S, Chen J, Shi W, Liu W, Zhang W, Zhang Y. Mutations in panD encoding aspartate decarboxylase are associated with pyrazinamide resistance in *Mycobacterium tuberculosis*. Emerg Microbes Infect. **2013**; 2(6):e34.

39. Gopal P, Yee M, Sarathy J, Liang Low J, Sarathy JP, Kaya F, et al. Pyrazinamide resistance is caused by two distinct mechanisms: prevention of coenzyme a depletion and loss of virulence factor synthesis. ACS Infect Dis. **2016**; 2(9):616–626.

40. Rosen BC, Dillon NA, Peterson ND, Minato Y, Baughn AD. Long-chain fatty acyl

Coenzyme A ligase FadD2 mediates intrinsic pyrazinamide resistance in *Mycobacterium tuberculosis*. Antimicrob Agents Chemother. **2017**; 61(2):1–13.

41. Shi W, Chen J, Feng J, Cui P, Zhang S, Weng X, et al. Aspartate decarboxylase (PanD) as a new target of pyrazinamide in *Mycobacterium tuberculosis*. Emerg Microbes Infect. **2014**; 3(8):e58.

42. Dillon NA, Peterson ND, Rosen BC, Baughn AD. Pantothenate and pantetheine antagonize the antitubercular activity of pyrazinamide. Antimicrob Agents Chemother. **2014**; 58(12):7258–7263.

43. Gopal P, Nartey W, Ragunathan P, Sarathy J, Kaya F, Yee M, et al. Pyrazinoic acid inhibits mycobacterial coenzyme A biosynthesis by binding to aspartate decarboxylase PanD. ACS Infect Dis. **2017**; 3(11):807–819.

44. Shi W, Zhang X, Jiang X, Yuan H, Lee JS, Barry CE, et al. Pyrazinamide inhibits trans-translation in *Mycobacterium tuberculosis*. Science. **2011**; 333(6049):1630–1632.

45. Yang J, Liu Y, Bi J, Cai Q, Liao X, Li W, et al. Structural basis for targeting the ribosomal protein S1 of *Mycobacterium tuberculosis* by pyrazinamide. Mol Microbiol. **2014**; 95(5):791–803.

46. Karzai AW, Sauer RT. Protein factors associated with the SsrA-SmpB tagging and ribosome rescue complex. Proc Natl Acad Sci. **2001**; 98(6):3040–4.

47. Keiler KC. Mechanisms of ribosome rescue in bacteria. Nat Rev Microbiol. **2015**; 13(5):285–297.

48. Saguy M, Gillet R, Skorski P, Hermann-Le Denmat S, Felden B. Ribosomal protein S1 influences trans-translation in vitro and in vivo. Nucleic Acids Res.

2007; 35(7):2368–2376.

49. Christensen SK, Pedersen K, Hansen FG, Gerdes K. Toxin-antitoxin loci as stress-response-elements: ChpAK/MazF and ChpBK cleave translated RNAs and are counteracted by tmRNA. J Mol Biol. **2003**; 332(4):809–819.

50. Guerlava P, Izac V, Tholozan JL. Comparison of different methods of cell lysis and protein measurements in *Clostridium perfringens*: application to the cell volume determination. Curr Microbiol. **1998**; 36:131–135.

51. Hajnsdorf E, Boni I V. Multiple activities of RNA-binding proteins S1 and Hfq. Biochimie. **2012**; 94(7):1544–1553.

52. Parish T, Stoker NG. Mycobacteria Protocols. London: Methods Mol. Biol., **2015**.

53. Crowe J, Masone BS, Ribbe J. One-step purification of recombinant proteins with the 6xHis tag and Ni-NTA resin. Mol Biotechnol. **1995**; 4:247–258.

54. Agrawal RK, Sharma MR, Kiel MC, Hirokawa G, Booth TM, Spahn CMT, et al. Visualization of ribosome-recycling factor on the Escherichia coli 70S ribosome: functional implications. Proc Natl Acad Sc. **2004**; 101(24):8900–8905.

55. Hirashima A, Kaji A. Factor dependent breakdown of polysomes. Biochem Biophys Res Commun. **1970**; 41(4):877–83.

56. Hirashima A, Kaji A. Factor-dependent release of ribosomes from messenger RNA: requirement for two heat-stable factors. J Mol Biol. **1972**; 65(1):43–58.

57. Noble CG, Song H. Structural studies of elongation and release factors. Cell Mol Life Sci. **2008**; 65(9):1335–1346.

58. Janosi L, Shimizu I, Kaji A. Ribosome recycling factor (ribosome releasing factor) is essential for bacterial growth. Proc Natl Acad Sci. **1994**; 91(10):4249–53.

59. Weixlbaumer A, Petry S, Dunham CM, Selmer M, Kelley AC, Ramakrishnan V. Crystal structure of the ribosome recycling factor bound to the ribosome. Nat Struct Mol Biol. **2007**; 14(8):733–737.

60. Hernández-Sánchez J, Valadez JG, Herrera J V, Ontiveros C, Guarneros G. lambda bar minigene-mediated inhibition of protein synthesis involves accumulation of peptidyl-tRNA and starvation for tRNA. EMBO J. **1998**; 17(13):3758–65.

61. Delgado-Olivares L, Zamora-Romo E, Guarneros G, Hernandez-Sanchez J. Codon-specific and general inhibition of protein synthesis by the tRNA-sequestering minigenes. Biochimie. **2006**; 88(7):793–800.

62. Cruz-Vera LR, Hernández-Ramón E, Pérez-Zamorano B, Guarneros G. The rate of peptidyl-tRNA dissociation from the ribosome during minigene expression depends on the nature of the last decoding interaction. J Biol Chem. **2003**; 278(28):26065–26070.

63. Heurgué-Hamard V, Dinçbas V, Buckingham RH, Ehrenberg M. Origins of minigene-dependent growth inhibition in bacterial cells. EMBO J. **2000**; 19(11):2701–2709.

64. Cruz-Vera LR, Magos-Castro MA, Zamora-Romo E, Guarneros G. Ribosome stalling and peptidyl-tRNA drop-off during translational delay at AGA codons. Nucleic Acids Res. **2004**; 32(15):4462–4468.

65. Singh NS, Ahmad R, Sangeetha R, Varshney U. Recycling of ribosomal complexes stalled at the step of elongation in Escherichia coli. J Mol Biol. **2008**; 380(3):451–464.

66. Vivanco-Domínguez S, Bueno-Martínez J, León-Avila G, Iwakura N, Kaji A, Kaji H, et al. Protein synthesis factors (RF1, RF2, RF3, RRF, and tmRNA) and peptidyl-tRNA hydrolase rescue stalled ribosomes at sense codons. J Mol Biol. **2012**; 417(5):425–439.

67. Bal NC, Agrawal H, Meher AK, Arora A. Characterization of peptidyl-tRNA hydrolase encoded by open reading frame Rv1014c of *Mycobacterium tuberculosis* H37Rv. Biol Chem. **2007**; 388(5):467–479.

68. Rao a. R, Varshney U. Specific interaction between the ribosome recycling factor and the elongation factor G from *Mycobacterium tuberculosis* mediates peptidyl-tRNA release and ribosome recycling in *Escherichia coli*. EMBO J. **2001**; 20(11):2977–2986.

69. Rao VS, Srinivas K, Sujini GN, Kumar GNS. Protein-protein interaction detection: methods and analysis. Int J Proteomics. **2014**; 2014: 147648.

70. Phizicky EM, Fields S. Protein-protein interactions: methods for detection and analysis. Microbiol Rev. **1995**; 59(1):94–123.

71. Berggård T, Linse S, James P. Methods for the detection and analysis of protein-protein interactions. Proteomics. **2007**; 7(16):2833–2842.

72. Palmer AC, Kishony R. Opposing effects of target overexpression reveal drug mechanisms. Nat Commun. **2014**; 5:1–8.

73. Desjardins CA, Cohen KA, Munsamy V, Abeel T, Maharaj K, Walker BJ, et al. Genomic and functional analyses of Mycobacterium tuberculosis strains implicate ald in D-cycloserine resistance. Nat Genet. **2016**; 48(5):544–551.

74. Ingolia NT. Ribosome profiling: new views of translation, from single codons to

genome scale. Nat Rev Genet. **2014**; 15(3):205–213.

75. Brar GA, Weissman JS. Ribosome profiling reveals the what, when, where and how of protein synthesis. Nat Rev Mol Cell Biol. **2015**; 16(11):651–664.

76. Tan Y, Hu Z, Zhang T, Cai X, Kuang H, Liu Y, et al. Role of pncA and rpsA gene sequencing in detection of pyrazinamide resistance in *Mycobacterium tuberculosis* isolates from southern China. J Clin Microbiol. **2014**; 52(1):291–297.

77. Zhang Y, Mitchison D, Shi W, Zhang W. Mechanisms of pyrazinamide action and resistance. Microbiol Spectr. **2014**; 2(4):1–12.

78. Dillon NA, Peterson ND, Feaga HA, Keiler KC, Baughn AD. Anti-tubercular activity of pyrazinamide is independent of trans-translation and RpsA. Sci Rep. **2017**; 7(1):1–8.

79. Boshoff HIM, Myers TG, Copp BR, McNeil MR, Wilson MA, Barry CE. The transcriptional responses of *Mycobacterium tuberculosis* to inhibitors of metabolism. novel insights into drug mechanisms of action. J Biol Chem. **2004**; 279(38):40174–40184.

80. Chang KC, Yew WW, Zhang Y. Pyrazinamide susceptibility testing in *Mycobacterium tuberculosis*: a systematic review with meta-analyses. Antimicrob Agents Chemother. **2011**; 55(10):4499–4505.

81. Alexander DC, Ma JH, Guthrie JL, Blair J, Chedore P, Jamieson FB. Gene sequencing for routine verification of pyrazinamide resistance in *Mycobacterium tuberculosis*: a role for pncA but not rpsA. J Clin Microbiol. **2012**; 50(11):3726–3728.

82. Simons SO, Mulder A, van Ingen J, Boeree MJ, Soolingen D Van. Role of rpsA

gene sequencing in diagnosis of pyrazinamide resistance. J Clin Microbiol. **2013**; 51(1):382.

83. Bhuju S, Fonseca L de S, Marsico AG, de Oliveira Vieira GB, Sobral LF, Stehr M, et al. *Mycobacterium tuberculosis* isolates from Rio de Janeiro reveal unusually low correlation between pyrazinamide resistance and mutations in the pncA gene. Infect Genet Evol. **2013**; 19:1–6.

84. Akhmetova A, Kozhamkulov U, Bismilda V, Chingissova L, Abildaev T, Dymova M. Mutations in the pnc A and rpsA genes among 77 *Mycobacterium tuberculosis* isolates in Kazakhstan. **2015**; 19(April 2014):179–184.

85. Xia Q, Zhao LL, Li F, Fan YM, Chen YY, Wu BB, et al. Phenotypic and genotypic characterization of pyrazinamide resistance among multidrug-resistant *Mycobacterium tuberculosis* isolates in Zhejiang, China. Antimicrob Agents Chemother. **2015**; 59(3):1690–1695.

86. Maslov DA, Zaĭchikova M V., Chernousova LN, Shur K V., Bekker OB, Smirnova TG, et al. Resistance to pyrazinamide in Russian *Mycobacterium tuberculosis* isolates: pncA sequencing versus Bactec MGIT 960. Tuberculosis. **2015**; 95(5): 608-612.

87. Gu Y, Yu X, Jiang G, Wang X, Ma Y, Li Y, et al. Pyrazinamide resistance among multidrug-resistant tuberculosis clinical isolates in a national referral center of China and its correlations with pncA, rpsA, and panD gene mutations. Diagn Microbiol Infect Dis. **2016**; 84(3):207–211.

88. Werngren J, Alm E, Mansjö M. Non-pncA gene-mutated but pyrazinamide-resistant *Mycobacterium tuberculosis*: why is that? J Clin Microbiol. **2017**;

55(6):1920–1927.

89. Ramirez-Busby SM, Rodwell TC, Fink L, Catanzaro D, Jackson RL, Pettigrove M, et al. A multinational analysis of mutations and heterogeneity in PZase, RpsA, and PanD associated with pyrazinamide resistance in M/XDR *Mycobacterium tuberculosis*. Sci Rep. **2017**; 7(1):1–9.

90. Pang Y, Zhu D, Zheng H, Shen J, Hu Y, Liu J, et al. Prevalence and molecular characterization of pyrazinamide resistance among multidrug-resistant *Mycobacterium tuberculosis* isolates from southern China. BMC Infect Dis. **2017**; 17(1):1–8.

91. Pratt AC, Dewage SW, Pang AH, Biswas T, Barnard-Britson S, et al. Structural and computational dissection of the catalytic mechanism of the inorganic pyrophosphatase from *Mycobacterium tuberculosis.* J Struct Biol 2015; 192(1): 76-87.

92. Triccas JA, Gicquel B. Analysis of stress- and host cell-induced expression of the *Mycobacterium tuberculosis* inorganic pyrophosphatase. BMC Microbiol. 2001; 1:3.

93. Pang AH, Garzan A, Larsen MJ, McQuade TJ, Garneau-Tsodikova S, et al. Discovery of allosteric and Sselective inhibitors of inorganic pyrophosphatase from *Mycobacterium tuberculosis.* ACS Chem Biol. 2016; 11(11): 3084-3092.

94. Shigeno Y, Uchiumi T, Nomura T. Involvement of ribosomal protein L6 in assembly of functional 50S ribosomal subunit in *Escherichia coli* cells. Biochem Biophys Res Commun. 2016; 473(1): 237-242.

95. Davies C, Bussiere DE, Golden BL, Porter SJ, Ramakrishnan V. Ribosomal proteins S5 and L6: high-resolution crystal structures and roles in protein synthesis and antibiotic resistance. J Mol Bio. 1998; 279(4): 873-878.

96. Proctor RA, Kriegeskorte A, Kahl BC, Becker K, Löffler B, et al. *Staphylococcus aureus* Small Colony Variants (SCVs): a road map for the metabolic pathways involved in persistent infections. Front Cell Infect Microbiol. 2014; 99:1-8.

97. Roos AK, Mariano S, Kowalinski E, Salmon L, Mowbray SL. D-ribose-5-phosphate isomerase B from *Escherichia coli* is also a functional D-allose-6-phosphate isomerase, while the *Mycobacterium tuberculosis* enzyme is not. J Mol Bio. 2008; 382(3): 667-679.

98. Roos AK, Burgos E, Ericsson DJ, Salmon L, Mowbray SL. Competitive inhibitors of *Mycobacterium tuberculosis* ribose-5-phosphate isomerase B reveal new information about the reaction mechanism. J Biol Chem. 2005; 280(8): 6416-6422.

99. Mariano S, Roos AK, Mowbray SL, Salmon L. Competitive inhibitors of type B ribose 5-phosphate isomerases: design, synthesis and kinetic evaluation of new D-allose and D-allulose 6-phosphate derivatives. Carbohydr Res. 2009; 344(7): 869-880.

CHAPTER IV

PROJECTING EPIDEMIC TRAJECTORIES OF TUBERCULOSIS: HOW THE TRANSMISSION EFFICIENCY OF DRUG RESISTANCE IMPACTS LONG-TERM TRENDS IN MDR-TB

Phillip P. Salvatore[1], Emily A. Kendall[2,3], David W. Dowdy[3,4,5]

1. Department of Molecular Microbiology and Immunology, The Johns Hopkins Bloomberg School of Public Health, Baltimore, MD, USA
2. Division of Infectious Diseases, The Johns Hopkins University School of Medicine, Baltimore, MD, USA
3. The Center for Tuberculosis Research, The Johns Hopkins University School of Medicine, Baltimore, MD, USA
4. Department of Epidemiology, The Johns Hopkins Bloomberg School of Public Health, Baltimore, MD, USA
5. Department of International Health, The Johns Hopkins Bloomberg School of Public Health, Baltimore, MD, USA

ABSTRACT

Background: The extent to which MDR-TB can transmit infection relative to drug sensitive TB is unclear. We assessed the impacts of competing assumptions about the transmission efficiency of MDR-TB on long-term trends in MDR-TB epidemics in South Africa and Vietnam.

Methods: We formulated a deterministic mathematical model of DS-TB and MDR-TB. Using this structure, we compared three scenarios with different assumptions about the efficiency with which MDR-TB transmits: MDR-TB transmits less efficiently than DS-TB; it transmits equally as efficiently as DS-TB; or it initially transmits at a deficit which gradually shrinks over time. We calibrated these scenarios with data from national drug resistance surveys and projected epidemic trends to 2040.

Results: Long-term trends in MDR-TB epidemiology are highly dependent on its transmission efficiency. Current trends in MDR-TB are consistent with MDR-TB incidence rates in South Africa increasing by either 5% (assuming a constant efficiency deficit) or by 226% (assuming a shrinking efficiency deficit) by 2040, and by either 84% or 465% (respectively) in Vietnam. The most significant determinants of long-term MDR-TB incidence were the transmission efficiency of MDR-TB, and the rate with which deficits in MDR-TB transmission may be reduced over time.

Conclusions: Whether MDR-TB remains a small proportion of global TB cases will depend on the transmission efficiency of MDR-TB relative to that of DS-TB. A better understanding of these characteristics is necessary to more precisely predict long-term TB trends.

INTRODUCTION

The global epidemic of multidrug resistant tuberculosis (MDR-TB) represents a significant challenge to worldwide TB control efforts. In 2016, an estimated 490,000 cases of MDR-TB occurred, representing 4% of new TB cases and 19% of previously-treated TB cases globally [1]. While significant efforts have been made to improve the accurate and timely detection of patients suffering from drug resistant TB and to provide these patients with effective second-line therapies, the global burden of MDR-TB has not abated [1]. In the face of myriad challenges posed by TB epidemics, the World Health Organization has adopted the END TB strategy to reduce global TB incidence by 90% (to less than 10 per 100,000 annually) and TB deaths by 95% between 2015 and 2035 [2]. In light of the poor clinical outcomes, economic burden, and human cost associated with detecting and treating patients suffering from MDR-TB, the success of efforts to reach these goals will likely depend to an important extent on the future trajectory of MDR-TB epidemics around the world. However, predicting the trajectory of these epidemics remains a challenge. Mathematical epidemic models may assist in understanding these trends and predicting the effects of TB interventions.

Strategies to control MDR-TB often emphasize the prevention of drug resistance through detection and effective treatment of drug sensitive TB (DS-TB), assuming that MDR-TB fails to spread efficiently [3]. Early microbiological studies found that highly isoniazid (INH) resistant isolates of *Mycobacterium tuberculosis* were associated with reduced virulence in animal models of TB [4,5], suggesting that resistance-conferring mutations carry with them a physiological fitness cost in the absence of antimicrobial

pressure. According to this classical dogma that MDR-TB suffers a fitness cost compared to DS-TB, the appropriate management of DS-TB cases should be sufficient to contain epidemics of MDR-TB [3,6]. Therefore, several leading public health organizations have made effective management of DS-TB the cornerstone of MDR-TB control [2,7,8].

The extent to which trends in MDR-TB incidence may be reversed through effective control of DS-TB is likely to depend significantly on the ability of MDR-TB cases to transmit infection and generate secondary cases [9]. In contrast with early studies of INH-resistant *M. tuberculosis*, more recent *in vitro* and *in vivo* studies have cast doubt over the consistency of the fitness cost hypothesis [10,11]. Further studies have demonstrated that drug resistant mutants with reduced physiological fitness may be restored to full virulence over time through secondary compensatory mutations and evolutionary selection [12,13]. While it is unclear to what extent *in vitro* fitness and compensatory evolution relates to the relative efficiency of MDR-TB transmission at the population level, epidemiological time-series studies indicate that the prevalence of MDR-TB isolates carrying these low-cost or compensatory mutations has increased over time in several settings [14,15]. Simultaneously, evidence has accumulated that modern MDR-TB epidemics are driven primarily by transmission rather than by the acquisition of drug resistance during treatment [16,17]. Therefore, the future trajectory of MDR-TB epidemics (and the long-term success of control efforts which prioritize DS-TB control) is likely to depend significantly on the relative efficiency with which MDR-TB cases transmit infection to others and cause disease in the secondary host.

In light of the varied approaches used to model MDR-TB transmission efficiency and given the complexity of empirical evidence about MDR-TB dynamics, we sought to

compare the impacts of different assumptions about MDR-TB transmission efficiency on projections of long-term MDR-TB incidence. We used a mathematical model of DS-TB and MDR-TB in two high burden settings to project future trajectories of MDR-TB epidemics under three competing assumptions about the relative transmission efficiency of MDR-TB. Within this framework, we demonstrate the ability of different modeling scenarios to recapitulate empirical epidemic characteristics with varying degrees of success. We further show that such scenarios forecast highly divergent trajectories of MDR-TB epidemics.

METHODS

TB Dynamics and Natural History

To explore the evolutionary impact of differential transmissibility, we formulated a deterministic compartmental model of adult TB transmission [18] in two high burden settings: South Africa and Vietnam. Our model represents the natural history of DS-TB and MDR-TB as follows (Figure 4.1A): susceptible populations who become infected with either DS-TB or MDR-TB may develop latent TB infection (followed by a slow rate of progression to active TB disease) or rapidly progress to active TB. Regardless of whether populations progress rapidly or slowly, all experience a subclinical (and less infectious) period of disease before developing clinically detectable (and fully infectious) TB. The emergence of MDR-TB occurs initially through the natural selection of spontaneous mutations during first-line treatment of DS-TB but subsequently spreads through person-to-person transmission (see Supplemental Methods for a detailed description of modeling methods and ordinary differential equations).

Our model incorporates a simplified interaction of HIV and TB co-epidemics (Figure 4.1B) without explicitly incorporating HIV transmission, but rather with the annual incidence of HIV fitted to setting-specific UNAIDS estimates [19] of adult HIV incidence (independent of TB status; see Supplemental Methods for full details). Populations living with HIV are classified into three states: High CD4 (representative of populations with $CD4^+$ T cell levels above approximately 250 cells/mL), Low CD4 (representative of populations with CD4 levels below approximately 250 cells/mL), and Receiving antiretroviral therapy (ART; representative of a weighted population average

of CD4 levels among those receiving ART). An individual's HIV status may then influence rates of TB mortality, infectiousness, rapid progression, reactivation, diagnosis, etc.

Diagnosis & Treatment

Upon diagnosis, TB patients initiate either effective therapy or ineffective therapy. Those receiving effective therapy demonstrate a rapid cessation of infectiousness [20], a reduction in mortality, and – upon treatment completion – long-term cure or eventual relapse. Those receiving ineffective therapy experience continued infectiousness and TB-associated mortality. Patients with MDR-TB receive drug susceptibility testing (DST) at a rate determined by setting-specific national estimates of DST coverage over time (since 2006; see Supplemental Methods for full details) [1,21,22]. Those who do not receive DST may only initiate ineffective first-line therapy (6 months in duration), while those who receive DST may initiate effective or ineffective second-line therapy (20 months in duration). Additionally, patients may default from any treatment regimen (correlated with the length of each regimen, see Table 1) and MDR-TB patients may fail to initiate treatment following DST. Rates of ART initiation are calculated from setting- and time-dependent data on ART coverage and, to reflect the integration of TB and HIV care in these settings, co-infected patients in whom either disease is detected experience increased rates of treatment initiation for their coinfections.

Figure 4.1: Model Structure

States of TB infection and possible transitions between them are represented in panel A. Upon initial infection, populations develop latent infection or incipient (preclinical) disease. After developing fully infectious active TB, populations initiate treatment at a specified rate, and treatment may be effective (eventually achieving sputum conversion) or ineffective. For those who complete an effective treatment course, they may either achieve durable cure or are rendered temporarily non-infectious but with future relapse anticipated. Those receiving an ineffective first-line regimen may re-initiate treatment after failure. MDR-TB may be acquired during first-line treatment (without cure) or as a result of transmission. Populations with MDR-TB may initiate ineffective first-line treatment or, following DST, effective or ineffective second-line treatments. Compartment colors correspond to the respective infectiousnes and TB-associated mortality of each state (see Methods and Supplementary Methods for more details). In addition to TB natural history, populations are also classified by treatment history (treatment-naïve or previously-treated, not shown), and HIV status (represented in panel B). Following HIV infection, populations transition through states of increasing immunosuppression or to antiretroviral therapy (ART) at defined rates.

Figure 4.1: Model Structure

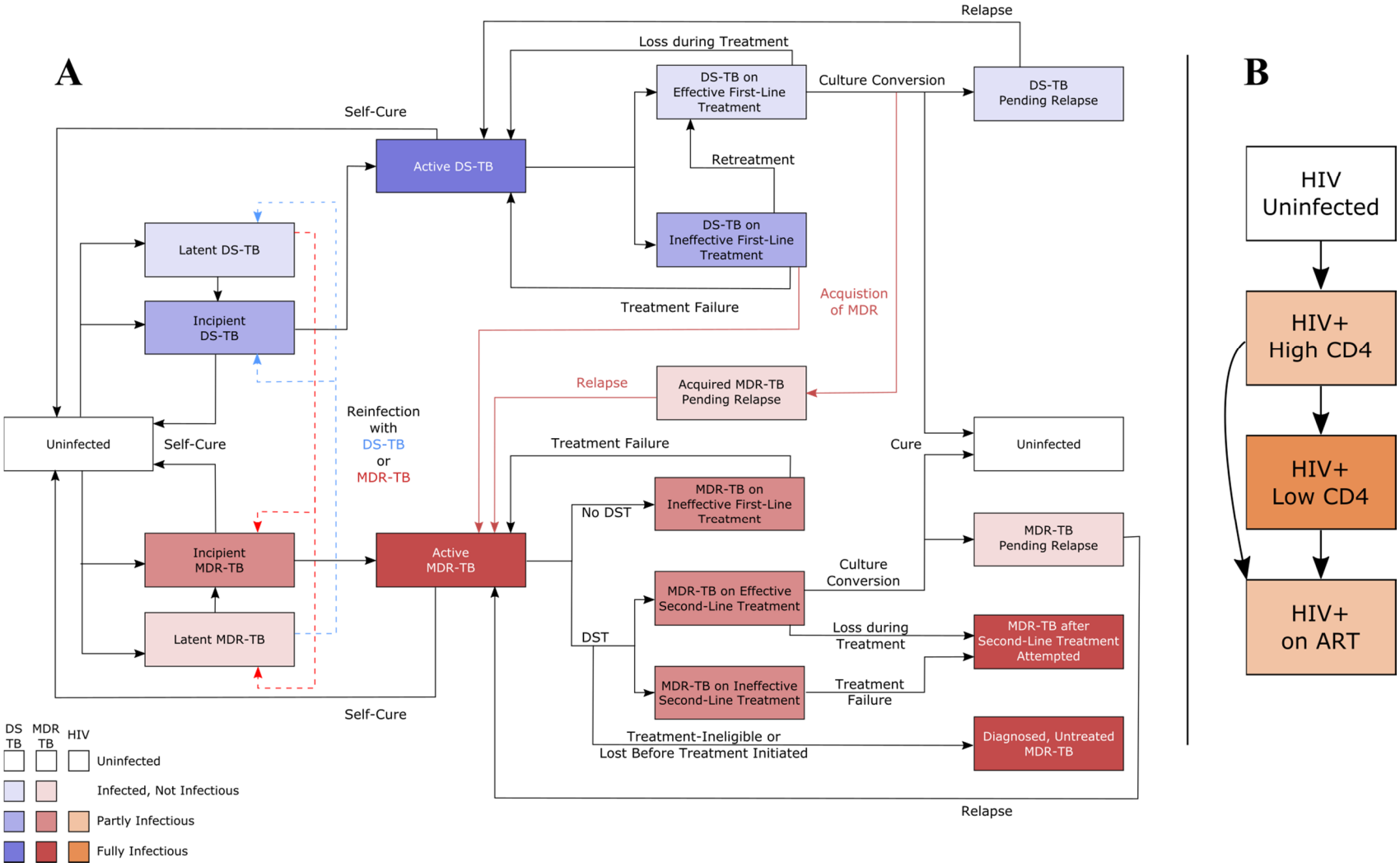

Approach to TB Transmission

We investigated the impact of transmission-related differences between DS-TB and MDR-TB by varying initial assumptions about the transmission efficiency of each strain over time. We define the coefficient of transmission efficiency as the number of new TB infections that result from each infectious person-year of active TB. Transmission efficiency captures the biological processes of TB transmission (aerosol production, infectious doses, bacterial virulence, etc.) as well as non-biological processes that influence transmission (contact rates, population mixing, etc.). Therefore, the transmission efficiency of either DS- or MDR-TB strain may be increased through changes in underlying biology (e.g., compensatory mutation) or through population-level influences (e.g., hospital housing of MDR-TB patients). In all cases, we assume the transmission efficiency of DS-TB declines slowly after 2000 to capture the roughly 2% annual decline in overall TB incidence (due to various secular trends in improved health status, living conditions, etc., and unrelated to improvements in MDR-TB case management) [1].

To reflect divergent hypotheses concerning the transmission of MDR-TB relative to DS-TB, we constructed three scenarios regarding the transmission efficiency of MDR-TB over time (Figure 4.2). In the first scenario ("Constant Efficiency Deficit"), we assume that MDR-TB emerges historically with a deficit in transmission efficiency (relative to that of DS-TB) which remains constant through the present and into the future (i.e., with no opportunity for compensatory mutations, increased cohorting of MDR-TB patients in congregate settings, or other processes to increase the transmission efficiency of MDR-TB over time). While the transmission efficiency of DS-TB declines slowly

over time in this scenario, we conservatively assume that the transmission efficiency of MDR-TB remains constant. In the second scenario ("Shrinking Efficiency Deficit"), we assume that MDR-TB emerges with a deficit in transmission efficiency which gradually shrinks until the efficiency of MDR-TB equals that of DS-TB (through, for example, compensatory evolution, natural selection of "high fitness" MDR-TB strains, or social processes such as recurrent imprisonment that concentrate MDR-TB in high-transmission settings). In the third scenario ("No Efficiency Deficit"), we assume that MDR-TB emerges historically with a transmission efficiency equal to that of DS-TB. In all scenarios, the transmission efficiency of MDR-TB is modeled independently from that of DS-TB, such that declines in DS-TB transmission do not necessarily cause declines in MDR-TB, although the efficiency of MDR-TB may never exceed that of DS-TB.

As described below, a range of possible values was defined for parameters related to MDR-TB transmission, and calibration was used to identify those values most consistent with empirical MDR-TB epidemic observations. The emergence of modern MDR-TB was allowed to range from 1971 to 1996 (see Supplementary Table 1). The initial transmission efficiency of MDR-TB relative to that of was allowed to range from 39-94% in the Constant Deficit and Shrinking Deficit scenarios (and was fixed at 1.0 for the No Deficit scenario). In the Shrinking Deficit scenario, the annual rate of reduction in the MDR-TB transmission efficiency deficit was allowed to range from 0 to 1.5% per year. (Further details on the parameterization of each scenario may be found in the Supplementary Methods.)

Figure 4.2: Transmission Efficiency Scenarios

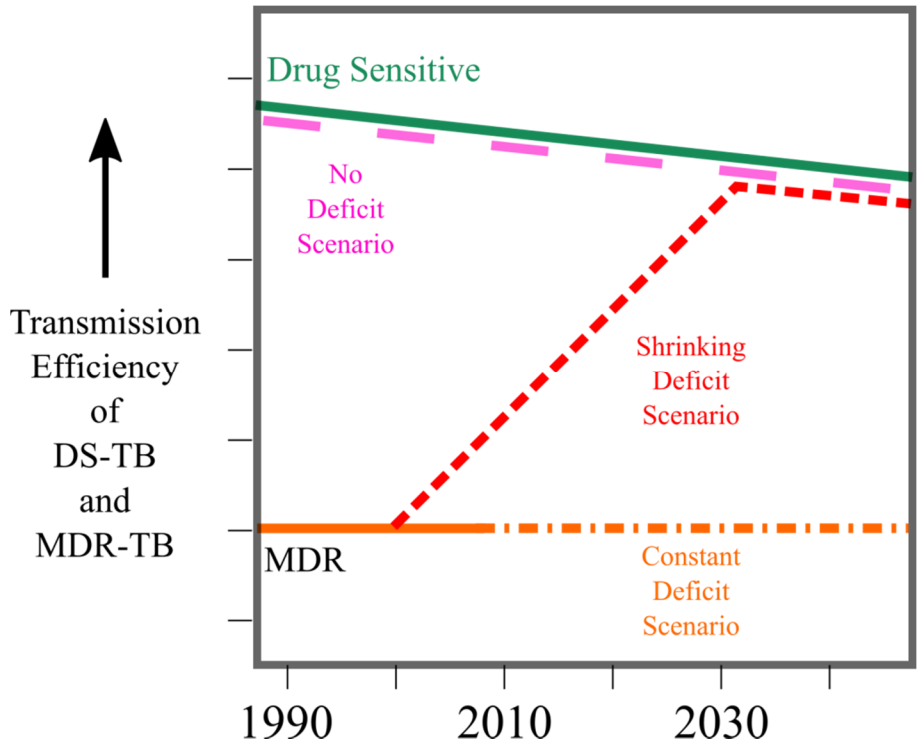

The assumed transmission efficiency (transmission events per 1,000 infectious person-years) of DS-TB over time is drawn in green; the downward slope recapitulates reductions in TB transmission efficiency due to secular trends unrelated to MDR-TB diagnosis and treatment (for example, reductions in crowding, improved socioeconomic conditions, etc.). In our three model scenarios, we assume either that the transmission efficiency of MDR-TB is at a perpetual defict compared to that of DS-TB (Constant Deficit Scenario, drawn in orange); that the transmission efficiency of MDR-TB is consistently the same as that of DS-TB (No Deficit Scenario, drawn in magenta); or that MDR-TB has lower transmission efficiency than DS-TB initially but gradually converges towards that of DS-TB over time (Shrinking Deficit Scenario, drawn in red). Years are shown for illustrative purposes; dates of MDR-TB emergence and rates of increase/decrease in transmission efficiency are sampled from defined ranges; see Sampling & Calibration for further details.

Sampling & Calibration

For each input parameter used in the formation of our model, we defined a range of plausible values based on the scientific literature (Table 4.1 and Supplementary Table S2.1). These ranges were parameterized as lognormal (for continuous ranges bounded at 0), logit-normal (for continuous ranges bounded between 0 and 1), or uniform probability distributions (for parameters on continuous ranges with sparse support in empirical literature). To capture the uncertainty in these parameter values, we utilized a two-stage, semi-Bayesian Sampling/Importance Resampling algorithm [23] to simulate epidemics consistent with empirical data.

Using Latin hypercube sampling [24], we generated 135,000 sets of initial parameters, each set composed of one value for each parameter related to DS-TB drawn from the probability density defined in Table 1. Each parameter set was then used to simulate a DS-TB epidemic to 1990 followed by a DS-TB/HIV epidemic to 2016. In the first stage of calibration, these simulations were fitted to the WHO estimates of total TB incidence in each setting and setting-specific estimates of the proportion of HIV-positive patients among incident TB cases (using national survey data in South Africa and WHO estimates in Vietnam) [1,25]. Each calibration point was defined as a bounded beta distribution and a pseudo-likelihood weight for each initial parameter set was defined as the joint probability density of the set's simulated DS-TB epidemic incidence and proportion of HIV-positive patients.

In the second stage of sampling, 135,000 DS-TB/HIV parameter sets were resampled (with replacement) according to their pseudo-likelihood weights (as described above) and accompanying values for MDR-TB parameters in each set were drawn from

their defined distributions (Table 4.1), again using Latin hypercube sampling. These parameter sets were used to simulate new DS-TB/HIV/MDR-TB epidemics from the date of the emergence of MDR-TB (itself a sampled parameter value) until 2016. In the second stage of calibration, these simulations were fitted to the proportion of MDR-TB among recently-diagnosed TB in new and – separately – in previously-treated patients (as measured in national drug resistance surveys) [26–28]. Each calibration point (proportion MDR among recently-diagnosed new and previously-treated TB cases) was defined as an independent normal distribution and a new pseudo-likelihood weight for each parameter set was calculated from the MDR-TB calibration targets. These pseudo-likelihood weights were used to resample those DS-TB/HIV/MDR-TB parameter sets most consistent with historical MDR-TB epidemics before projecting outcomes into the future.

Outcomes and Statistical Analysis

Our primary outcomes in each setting were the absolute incidence of MDR-TB in 2040; the incidence of MDR-TB relative to all incident TB in 2040; and the fold change in absolute and relative MDR-TB incidence between 2016 and 2040. For projections of these primary outcomes we report median values as well as Uncertainty Ranges (UR), defined by the 5^{th} and 95^{th} percentiles of posterior distributions. The three scenarios related to MDR-TB transmission efficiency were compared in terms of fit to the observed epidemiological data by calculating Bayes Factors. (A Bayes Factor (BF) is calculated as the ratio of the cumulative posterior probabilities of two models, and can be interpreted as the calibration data's support for one model over another [46].) Unless otherwise stated in the text, Bayes Factors were calculated in support of the Constant Deficit scenario over other models. We investigated the sensitivity of the primary outcomes to

individual input parameters by comparing the primary outcome in those simulations sampling within the lowest quintile of each input parameter's (posterior) range against those simulations sampling within the highest quintile. Nonparametric partial rank correlation coefficients are also presented in the Supplementary Results.

Replication of Previous Findings

A recently-published mathematical model of MDR-TB in several countries implemented an approach to MDR-TB transmission conceptually comparable to our No Deficit scenario [17]. Despite the similar approach utilized, our results demonstrate qualitatively different trends in MDR-TB incidence (see below). Therefore, we sought to replicate the findings of this previous study by altering assumptions about a small number of key input parameters (see Supplementary Methods for further details).

Table 4.1: Selected* Parameter Values

Description	Median	Sampling Range†	Distribution	References
Probability of rapid progression after initial tuberculosis infection	0.14	0.08-0.25	Logit-normal	[29]
Reactivation rate from latent to incipient (preclinical) active tuberculosis, per year	0.001	0.0005-0.002	Lognormal	[30–33]
Rate of tuberculosis diagnosis and treatment initiation, per year	1.0	0.7-1.5	Lognormal	[1,34,35]
Proportion failing to initiate treatment for multidrug-resistant tuberculosis after diagnosis (in excess of loss to follow-up of patients with drug-susceptible tuberculosis)	0.05	0.02-0.10	Logit-normal	[1,35]
Proportion of treated patients who have an apparent treatment response				
Newly diagnosed patients with drug-susceptible tuberculosis, first-line therapy	0.98	0.96-0.99	Logit-normal	[1,36–38]
Patients with multidrug-resistant tuberculosis, longer therapy	0.77	0.66-0.85	Logit-normal	[39–41]
Proportion who relapse, among those with apparent treatment response				
Newly diagnosed patients with drug-susceptible tuberculosis, first-line therapy	0.04	0.026-0.06	Logit-normal	[41,42]
Patients with multidrug-resistant tuberculosis, longer therapy	0.04	0.015-0.10	Logit-normal	[42,43]
Probability of loss to follow-up during therapy				
First-line therapy	0.06	0.03-0.10	Logit-normal	[1]
Longer therapy for multidrug-resistant tuberculosis	0.11	0.04-0.25	Logit-normal	[44,45]
Risk of acquiring multidrug resistance during first-line therapy	0.004	0.0015-0.01	Logit-normal	[40]

*See the Supplementary Methods for a full listing of all parameters, sampling distributions, and references. †Sampling ranges represent the 2.5th to 97.5th percentiles of unbounded distributions and lower to upper bounds of uniform distributions.

RESULTS

Calibration and Model Fit

After calibration, we compared the ability of each of our MDR-TB transmission models to accurately reproduce empirical observations of MDR-TB prevalence among treatment-naïve and previously-treated patients in South Africa and Vietnam. In South Africa, while Constant Deficit and Shrinking Deficit models were similarly supported by the data (BF=2.6), the No Deficit model was supported far more poorly relative to either model ($BF<10^{-8}$) (Figure 4.3A).

Similar findings were obtained from Constant Deficit and Shrinking Deficit models in Vietnam (BF=2.1, Figure 4.3B). In this setting, where the MDR-TB epidemic has been growing faster than in South Africa, the No Deficit model was better supported by empirical data but was nonetheless less supported than either of the other models ($BF<10^{-3}$). Due to the poor performance of the No Deficit model in both settings, we only considered Constant Deficit and Shrinking Deficit models in our primary results (see Supplementary Results for further details).

These results differ importantly from those of a recent publication implementing an approach similar to our No Deficit scenario [17]. We were able to successfully reproduce the findings of that publication by altering several assumptions about TB natural history and treatment availability (see Supplemental Results for more details).

Figure 4.3: Calibration Performance

Simulated epidemics are weighted according to how well each reproduced empirical calibration targets (historical estimates of MDR in new and previously-treated TB cases). Recent TB diagnoses were used (instead of incident TB cases) to better represent the sampling methodologies used in national drug resistant surveys which were used for calibration. Recent diagnoses are defined as any populations transitioning from active, untreated TB into any diagnosis/treatment state. Red points represent median and 95% confidence intervals for calibration targets drawn from national survey data. (The 1996 prevalence survey in Vietnam measured the proportion MDR in new cases only.) IQR represents 25th to 75th percentiles and the 90% range represents the 5th to 95th percentiles of posterior simulations.

Figure 4.3: Calibration Performance

A – South Africa

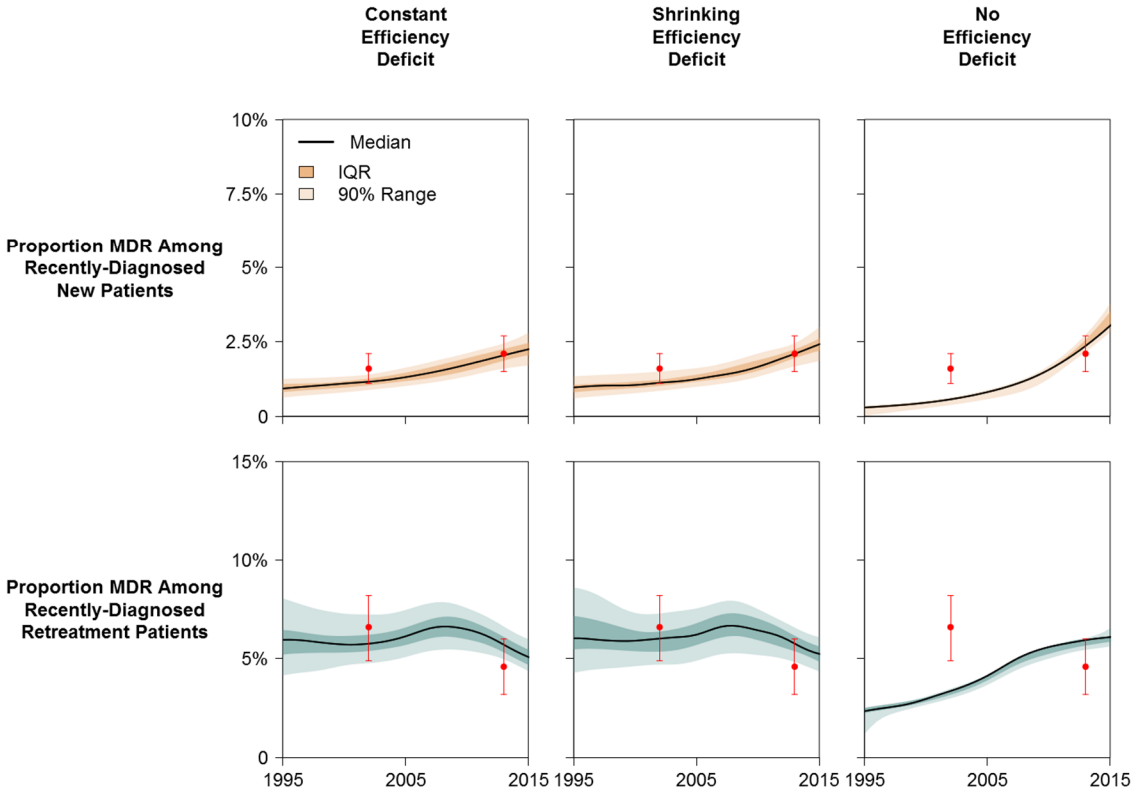

B – Vietnam

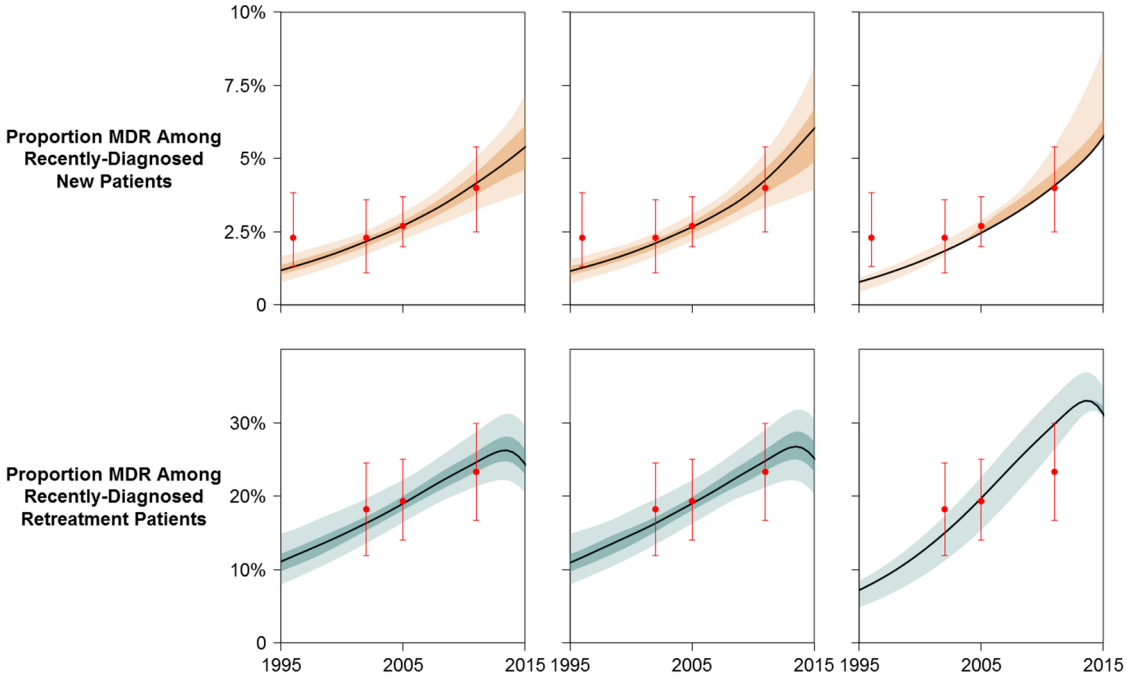

Projections of MDR-TB Burden

When projecting these simulations to 2040, the potential epidemics predicted by the Constant Deficit and Shrinking Deficit models diverge significantly. In South Africa (Figure 4.4), the Constant Deficit scenario predicts the incidence of MDR-TB at 26 cases per 100,000 (IQR: 17-41), comprising 5% (IQR: 4-9%) of all incident TB by 2040. These results indicate a median 2.0-fold increase in the relative incidence of MDR-TB from 2016 to 2040. Projections from the Shrinking Deficit scenario predict much higher potential increases in MDR-TB, reaching a median of 69 cases per 100,000 (IQR: 38-131) by 2040 and accounting for 15% of incident TB (IQR: 8-27%) by that time: a median 5.1-fold increase in relative incidence from 2016 to 2040 (IQR 2.8-fold to 7.7-fold). Similar trends were predicted in Vietnam (Figure 4.5), where the Constant Deficit scenario predicts a 2.2-fold increase (IQR: 1.6-3.6-fold) over 2016 and the Shrinking Deficit scenario predicts a 5.4-fold increase (IQR: 3.6-7.4-fold) in the relative incidence of MDR-TB.

Figure 4.4: Projections of the MDR-TB Burden in South Africa

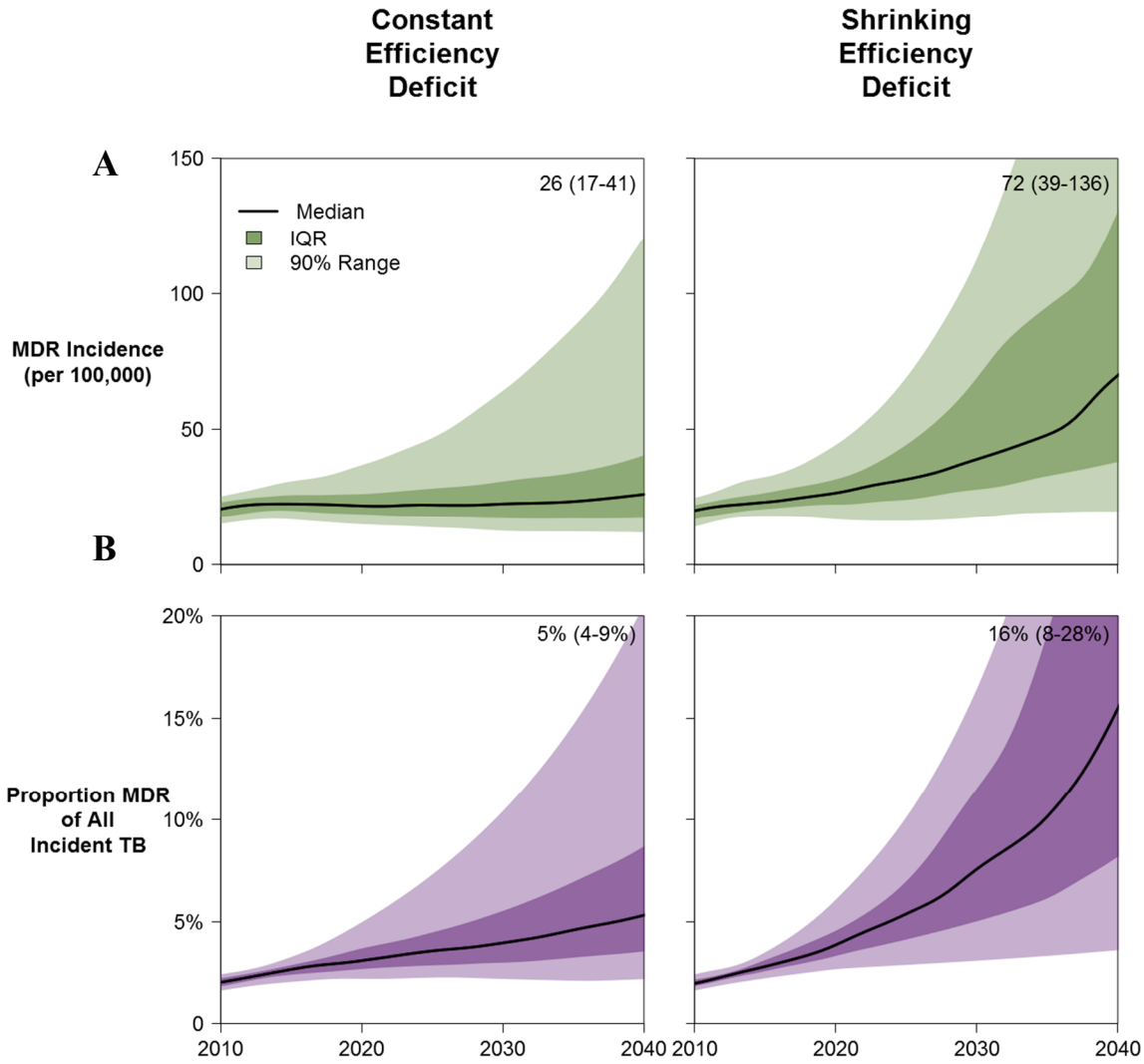

Simulated MDR-TB epidemics in South Africa were and projected from 2010 to 2040. Row A illustrates the projected absolute MDR-TB incidence in each scenario, while Row B illustrates MDR-TB as a proportion of all incident TB. The 2040 projected median (IQR) values are included in the upper right of each panel. IQR represents 25th to 75th percentiles and the 90% range represents the 5th to 95th percentiles of posterior simulations.

Figure 4.5: Projections of the MDR-TB Burden in Vietnam

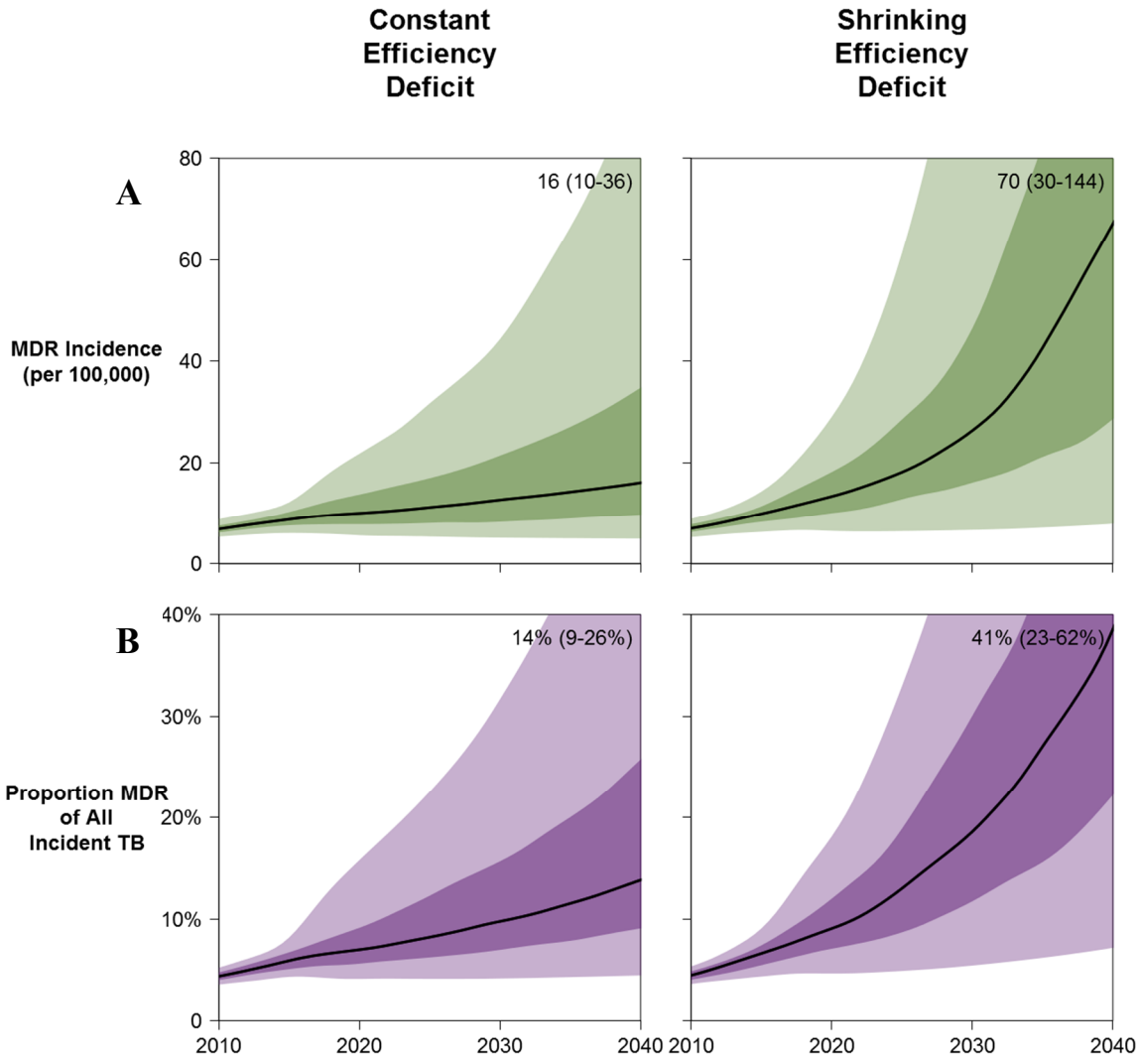

Simulated MDR-TB epidemics in Vietnam were and projected from 2010 to 2040. Row A illustrates the projected absolute MDR-TB incidence in each scenario, while Row B illustrates MDR-TB as a proportion of all incident TB. The 2040 projected median (IQR) values are included in the upper right of each panel. IQR represents 25th to 75th percentiles and the 90% range represents the 5th to 95th percentiles of posterior simulations.

Sensitivity Analyses

The variability in these MDR-TB outcomes was influenced most strongly by parameters determining the transmission and mortality of MDR-TB. The distributions of 2040 MDR-TB incidence projections in South Africa, separated by parameter quintile values, are presented in Figure 4.6. More influential parameters demonstrate a greater separation of outcome distributions between the upper and lower quintiles of their values. (Similar results were observed for the relative increase in MDR-TB incidence and for outcomes in Vietnam, presented in the Supplementary Results). In the Shrinking Deficit model, the rate of reduction in the MDR-TB transmission efficiency deficit remained highly correlated with 2040 incidence (upper vs. lower quintile medians: 117 vs. 38 per 100,000). Similar correlations were observed for rates of TB mortality and loss during first-line treatment (which determine infectious MDR-TB person-time in the absence of second-line therapy). In the Constant Deficit model, the efficiency of MDR-TB transmission remained correlated with future incidence (upper vs. lower quintile medians, 32 vs. 19 per 100,000), as were rates of TB mortality and loss during first-line treatment. Outcomes in both models were similarly influenced by parameters related to TB natural history, diagnosis and treatment, and HIV interactions (see Supplementary Results). Additional parametric and nonparametric sensitivities analyses for projections in South Africa and Vietnam are included in the Supplementary Results.

Figure 4.6: Sensitivity Analysis – Influence of Key Model Parameters on Projections of MDR-TB Incidence in South Africa

Each boxplot represents the distribution of values for the primary outcome (the incidence of MDR-TB in 2040) within a given set of simulations. Pairs of boxplots represent groups of simulations categorized by values of a single input parameter: red boxplots represent the outcomes of those simulations with parameter values in the upper 20% of all simulations; blue boxplots represent the outcomes of those simulations with parameter values in the lower 20% of all simulations. More influential parameters demonstrate a greater separation of the distributions of outcome between simulations in the upper quintile and simulations in the lower quintile of parameter values. To the left of each panel are included the input parameter values corresponding to the accompanying quintile. In black is represented the overall distribution of the outcome across all simulations and the median estimate is drawn as a vertical dotted line. Boxes represent the median, 25th, and 75th percentiles of the distribution of outcomes; whiskers represent the 5th and 95th percentiles of the distribution of outcomes. In the Constant Deficit model, parameters involving the reduction in MDR-TB transmission efficiency deficit are excluded.

Figure 4.6: Sensitivity Analysis – Influence of Key Model Parameters on Projections of MDR-TB Incidence in Vietnam

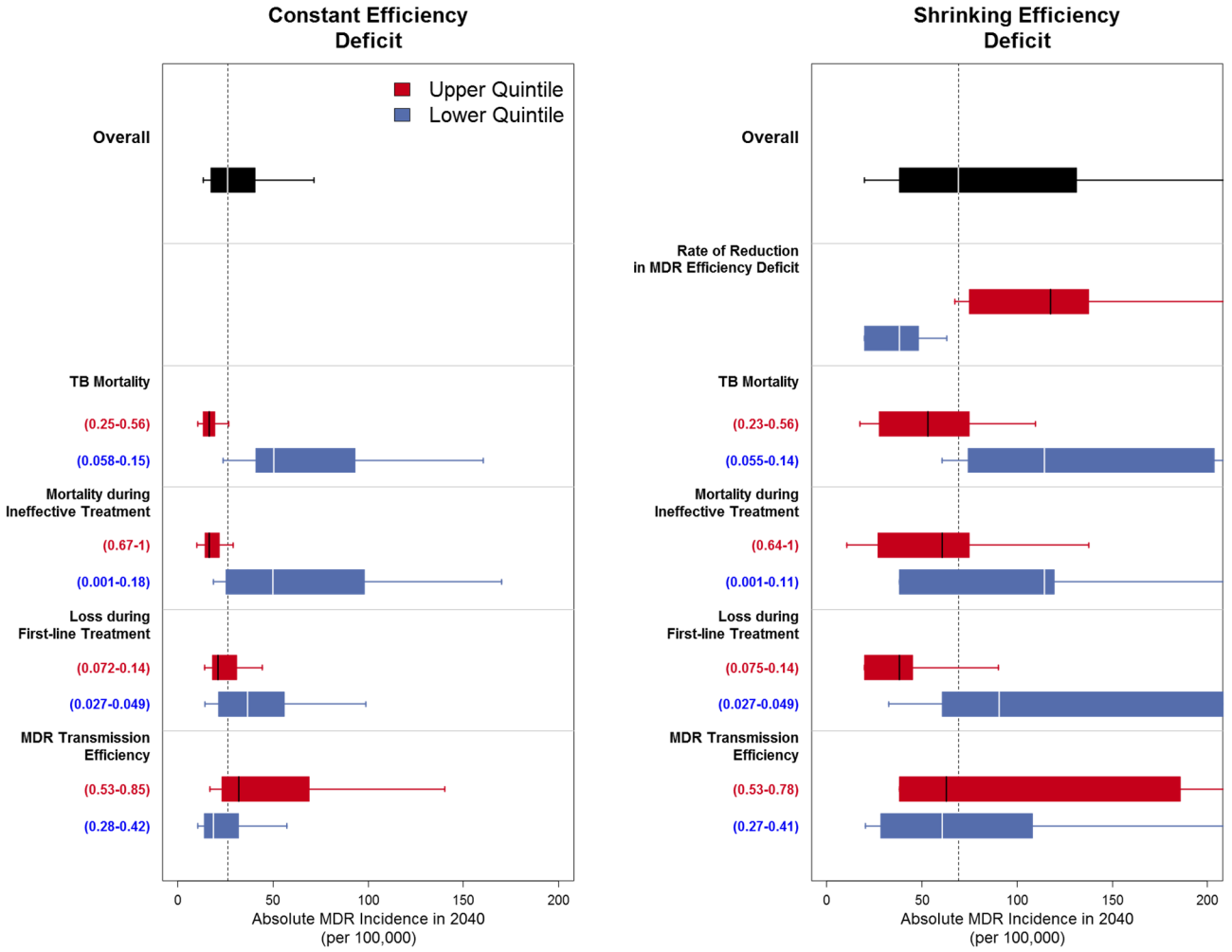

DISCUSSION

This analysis illustrates that the future trajectory of MDR-TB in South Africa and Vietnam remains highly uncertain, with the absolute incidence of MDR-TB increasing by either 5% or 226% in South Africa by 2040 and by either 85% or 465% in Vietnam, depending on the transmission efficiency of MDR-TB. A major determinant of this uncertainty reflects our current lack of knowledge as to whether any deficit in transmission efficiency of MDR-TB relative to DS-TB currently exists, and whether such a deficit is likely to be reduced into the future. If one assumes that the transmission efficiency of MDR-TB is unlikely to change over time, we project that the relative incidence of MDR-TB will increase over time with median projected increases of 98% in South Africa and 120% in Vietnam by 2040. However, if one assumes that the transmission efficiency of MDR-TB may increase over time, we project that the relative incidence of MDR-TB may increase dramatically, with median increases of 410% in South Africa (ranging upwards of 670%) and 437% in Vietnam (ranging up to 636%). This raises the critical question: what evidence exists to suggest that the transmission efficiency of MDR-TB may increase over time, and how quickly may this occur?

Unfortunately, clear evidence of the potential for increases in the transmission efficiency of MDR-TB remains sparse. Much of the scientific literature examining the fitness costs and compensatory evolution of drug resistant *M. tuberculosis* originates from laboratory studies which are imperfect models of human transmission. Initial studies demonstrated that mutations in the promoter of *ahpC* may improve *in vitro* peroxide tolerance of INH resistance-conferring *katG* mutations [12,47]. Such *ahpC* mutations,

however, are uncommon in clinical INH-resistant *M. tuberculosis* isolates, raising questions of the clinical relevance of such adaptations [48]. Similar laboratory observations have been noted in the associations of ethambutol resistance and secondary mutations in *Rv3792* [49], while the ability of *rpoA* and *rpoC* mutations to compensate rifampin resistance-conferring mutations have been documented *in vivo* and in human populations [13,50].

Biological compensatory evolution only partially represents epidemiological transmission efficiency and experimental assays used to study compensatory evolution are prone to methodologically overestimating the benefit of compensatory mutations [51]. For the purposes of projecting future trends in MDR-TB epidemics, more important than laboratory measures of physiological fitness are estimates of what we have termed transmission efficiency; by this we mean the capacity of a case of TB to transmit infection and propagate disease in secondary hosts, best represented by the number of new TB infections that result from an infectious-person year of active disease. No reasonable laboratory systems are capable of quantifying transmission efficiency, and therefore we must rely primarily on studies of incident and prevalent TB in human populations [52]. Epidemiological studies examining household contacts of DS-TB and MDR-TB patients have suggested that fewer secondary cases arise from index MDR-TB patients than from DS-TB patients when adjusted for infectious person-time of exposure, though the risk of secondary infection (rather than secondary disease) from MDR-TB may actually be higher than from DS-TB [53,54]. Importantly, while physiological fitness and adaptation of MDR-TB may increase transmission efficiency, the transmission efficiency of MDR-TB may also increase as a result of changes in contact

rates, mixing patterns, contact susceptibility, and other population-level characteristics which influence TB transmission. For example, the clustering of MDR-TB in incarcerated populations – where cases and contacts are confined in close quarters with inadequate ventilation or access to MDR-TB diagnosis and second-line treatment – is well documented [55]. Both MDR-TB and extensively drug resistant TB have also demonstrated dramatic clustering in hospital settings, where infectious source cases are concentrated and typical contacts – hospitalized patients, often living with HIV or other immunosuppressive conditions – are more susceptible to TB infection [56,57]. How these heterogeneous mixing and contact patterns influence the transmission efficiency of MDR-TB across a large population (and in relation to DS-TB transmission) remains an unsettled question. Outside institutional settings, the transmission efficiency of MDR-TB may also increase in communities as the result of increasing urbanization which can mimic the same risk factors as cohorting in hospitals or prisons [58]. Increased population density and rural-to-urban migration have been identified as significant risk factors for MDR-TB transmission in cities across Asia and Africa [59,60]. That the urban populations of Asia and Africa are expected to double and triple, respectively, by 2050 [61] suggests that the transmission efficiency of MDR-TB may potentially increase (or continue increasing) in countries already hardest hit by DS-TB epidemics.

Considering the importance of changes in the transmission efficiency of MDR-TB in influencing long-term trends in MDR-TB incidence, the scientific community must better understand these characteristics at the population level. Some existing study designs have laid the foundations for understanding MDR-TB transmission efficiency. Molecular clustering studies have been used for a number of years to characterize how

phenotypic and genetic traits of pathogen and hosts associate with the transmission of TB [62]. Such studies, however, require costly molecular surveillance programs and at least two years of follow-up, and are subject to a number of biases in sampling and inference [63–65]. More recent phylogenetic approaches utilizing the high resolution afforded by whole genome sequencing of *M. tuberculosis* isolates have also been utilized to reconstruct chains of transmission influenced by putative high- or low-fitness mutations [66]. The utility of such studies to draw inferences regarding the transmission efficiency of MDR-TB relative to DS-TB may be limited, as transmission chains may not be directly or quantitatively compared. Nested case-control studies may improve sampling efficiency and shorten surveillance duration over traditional cluster analyses [67]. Cross-sectional designs combined with whole genome sequencing may offer unique insight in characterizing the transmission of MDR-TB in vulnerable patient populations [68]. Ultimately, the most important sources of data will be the continuation and expansion of repeated national drug resistance surveys [26–28].

Each of the study designs described above has improved our understanding of MDR-TB transmission relative to DS-TB transmission. Despite the utility of these studies, none have fully characterized population-level relative transmission efficiency (specifically examining exposure time-adjusted transmission and secondary case generation). An idealized design to accomplish this might be described in the following manner: a large, population-representative cohort of MDR-TB and DS-TB patients enrolled, for whom the time of onset of infectiousness could be identified with precision, whose secondary contacts (confirmed to be previously TB-uninfected) are exhaustively investigated for the new acquisition of infection. With such a study, the denominator of

transmission efficiency – total infectious person-time – could be quantified and well-defined, and the numerator – the number of new infections which result – could be measured with little error. Further, such a study would need to be conducted repeatedly to assess whether the transmission efficiency of MDR-TB is changing over time (a critical determinant of long-term MDR-TB epidemiology).

Such an idealized design is unrealistic and infeasible for a number of reasons: MDR-TB would be a relatively rare event in a population-representative sample (currently less than 10% of all TB cases in South Africa) [1,27]; it is difficult to ascertain the time of onset of infectiousness; exposed secondary contacts may not be identified or may not consent to study participation; confirmation of previous infection history is difficult to ascertain; and biological diagnosis of new infection is imperfect [69,70]. However, existing study designs and novel epidemiological tools may assist in assessing different components of the idealized study design described. Cross-sectional survey designs can characterize which demographic groups would compose a representative population of TB patients and/or contacts. Novel biomarkers and diagnostic assays may help determine the onset of infectiousness (and its trajectory over the course of disease [71,72]) as well as newly acquired infections [73,74], while genotypic surveillance and cluster studies can link index cases with secondary contacts. Combining several of these strategies (e.g., nesting genotypic or biomarker studies within larger cohorts or clinical trials [75]) may further improve our ability to inform the existing gaps in our understanding of the complex characteristics of MDR-TB transmission efficiency. Until such studies provide a more clear understanding of current trends in TB transmission

efficiency, our results indicate that the future of MDR-TB epidemics will remain, necessarily, uncertain.

Our approach in this analysis was intended to demonstrate the importance of assumptions about the transmission efficiency of MDR-TB in projecting the long-term burden of drug resistant TB in two high burden settings. In South Africa, where the burden of MDR-TB remained relatively stable between 2002 and 2013, we found little support for a model in which the transmission efficiency of MDR-TB has historically equaled that of DS-TB. In Vietnam, where the relative incidence of MDR-TB has risen significantly between 1996 and 2011, possibly suggesting a greater role for the transmission of MDR-TB, there was somewhat better support for the highly transmission-driven MDR-TB epidemics necessitated in the No Deficit model. Nevertheless, in both settings, this was the most poorly-supported model examined.

Our results offer an important complement to MDR-TB modeling projections published previously. Our previous studies have projected that acquired drug resistance accounted for less than 10% of MDR-TB cases in 2013, consistent with the results presented here (see Supplementary Results for further details) [16]. Estimates of MDR-TB incidence using our Constant Deficit and Shrinking Deficit models are comparable to those estimated by Blower and colleagues, though our calibration methodology leads to significantly less variance in these estimates [76]. Importantly, we found our No Deficit model was poorly supported by empirical data in South Africa and projected greater increases in the burden of MDR-TB than was recently reported by Sharma and colleagues using a similar approach [17]. We were able to reproduce the findings of that report by implementing a more slowly-developing TB epidemic than used in our primary analysis

and a delay of many years between the onset of infectiousness and treatment initiation, as was assumed in that study (see Supplementary Methods and Supplementary Results).

Our methodology is not without its limitations. South Africa and Vietnam are countries with unique DS-TB, MDR-TB, and HIV epidemics that are not generalizeable to all settings but were chosen based on the availability of repeated national drug resistance survey data. Uncertainty in our projections may reflect uncertainty in the underlying data (e.g., only two national MDR-TB surveys in South Africa) and uncertainty in underlying natural history parameters. Our sensitivity analyses suggest that, while our results were largely robust to uncertainty in these parameters, our estimates were importantly influenced by parameters determining the infectious person-time of untreated MDR-TB cases (TB mortality and loss during first-line treatment). More complete consensus around these estimates would likely reduce the variance of long term projections, while significant future improvements in MDR-TB detection (particularly in Vietnam, where DST remains unavailable to more than 80% of new TB cases [1]) or treatment of MDR-TB (e.g., access to effective short-course second-line regimens) are not captured in our projections and could possibly curtail long term increases in MDR-TB incidence. Finally, in the absence of unambiguous empirical data describing changes in MDR-TB transmission efficiency, we used a simple model of a linear increase over time (see Shrinking Deficit Scenario in Figure 4.2) with rates of change (i.e., the range of possible slopes in Figure 4.2, from very slow to rapid increases) sampled from a broad uniform distribution. Therefore, estimating the future of MDR-TB critically depends on better understanding the transmission efficiency of MDR-TB and

both the magnitude and shape by which that transmission efficiency may change over time.

Global efforts to control TB are likely to hinge on the future trajectory of MDR-TB epidemics. While MDR-TB is often described as carrying a fitness cost associated with drug resistance, this characterization may be inaccurate. Alternative arguments suggest that the transmission efficiency of MDR-TB may equal that of DS-TB already or in the future. We investigated the importance of these assumptions in influencing mathematical projections of MDR-TB epidemics. We found that while there was little empirical support for models in which there is No Deficit in transmission efficiency between MDR-TB and DS-TB, there was roughly comparable support for models in which MDR-TB emerges with limited transmission efficiency with or without a subsequent increase in transmission efficiency over time. Our results indicate that the future of MDR-TB epidemics depends significantly on whether the transmission efficiency of MDR-TB may increase over time. A better understanding of these dynamics in human populations will improve our ability to predict (and possibly prevent) increases in the burden of MDR-TB into the future.

REFERENCES

1. Global Tuberculosis Report 2017. Geneva: World Health Organization, **2017**.
2. Global strategy and targets for tuberculosis prevention , care and control after 2015. Geneva: Secretariat of the World Health Organization, **2013**.
3. Dye C, Williams BG. Criteria for the control of drug-resistant tuberculosis. Proc Natl Acad Sci. **2000**; 97(14):8180–8185.
4. Barnett M, Busby SR, Mitchison DA. Tubercle bacilli resistant to isoniazid: virulence and response to treatment with isoniazid in guinea-pigs and mice. Br J Exp Pathol. **1953**; 34(5):568–81.
5. Middlebrook G, Cohn M. Some observations on the pathogenicity of isoniazid-resistant variants of tubercle bacilli. Science. **1953**; 118(3063):297–299.
6. Dye C, Espinal MA. Will tuberculosis become resistant to all antibiotics? Proc Biol Sci. **2001**; 268(1462):45–52.
7. The Bill and Melinda Gates Foundation. Tuberculosis strategy overview. **2012**.
8. The Centers for Disease Control and Prevention (CDC), NCHHSTP. Strategic Plan through 2020. **2015**.
9. Cohen T, Murray M. Modeling epidemics of multidrug-resistant *M. tuberculosis* of heterogeneous fitness. Nat Med. **2004**; 10(10):1117–21.
10. Gagneux S, Long CD, Small PM, Van T, Schoolnik GK, Bohannan BJM. The competitive cost of antibiotic resistance in *Mycobacterium tuberculosis*. Science. **2006**; 312(5782):1944–6.
11. Borrell S, Gagneux S. Infectiousness, reproductive fitness and evolution of drug-

resistant *Mycobacterium tuberculosis*. Int J Tuberc Lung Dis. **2009**; 13(12):1456–1466.

12. Sherman D, Mdluli K, Hickey M, Arain T. Compensatory ahpC gene expression in isoniazid-resistant Mycobacterium tuberculosis. Science. **1996**; 272(5268):1641–1643.

13. de Vos M, Müller B, Borrell S, Black P, van Helden PD, Warren RM, et al. Putative compensatory mutations in the rpoC gene of rifampin-resistant *Mycobacterium tuberculosis* are associated with ongoing transmission. Antimicrob Agents Chemother. **2013**; 57(2):827–32.

14. Cohen KA, Abeel T, Manson McGuire A, Desjardins CA, Munsamy V, Shea TP, et al. Evolution of extensively drug-resistant tuberculosis over four decades: whole genome sequencing and dating analysis of *Mycobacterium tuberculosis* isolates from KwaZulu-Natal. PLoS Med. **2015**; 12(9):1–22.

15. Huo F, Luo J, Shi J, Zong Z, Jing W, Dong W, et al. Increasing prevalence of rifampicin-resistant *Mycobacterium tuberculosis* is associated with the rransmission of strains harboring compensatory mutations in China: a 10-year comparative analysis. Antimicrob Agents Chemother. **2018**; (97): 02303-17.

16. Kendall EA, Fofana MO, Dowdy DW. Burden of transmitted multidrug resistance in epidemics of tuberculosis: A transmission modelling analysis. Lancet Respir Med. **2015**; 3(12):963–972.

17. Sharma A, Hill A, Kurbatova E, van der Walt M, Kvasnovsky C, Tupasi TE, et al. Estimating the future burden of multidrug-resistant and extensively drug-resistant tuberculosis in India, the Philippines, Russia, and South Africa: a mathematical

modelling study. Lancet Infect Dis. **2017**; 17(7):707–715.

18. Kendall EA, Fojo AT, Dowdy DW. Expected effects of adopting a 9 month regimen for multidrug-resistant tuberculosis: a population modelling analysis. Lancet Respir Med. **2017**; 5(3):191–199.
19. UNAIDS. Ending Aids Progress Towards the 90-90-90 Targets. Glob. Aids Updat. 2017.
20. Dharmadhikari AS, Mphahlele M, Venter K, Stoltz A, Mathebula R, Masotla T, et al. Rapid impact of effective treatment on transmission of multidrug-resistant tuberculosis. Int J Tuberc Lung Dis. **2014**; 18(9):1019–1025.
21. Global Tuberculosis Report 2012. Geneva: World Health Organization, **2012**.
22. Global Tuberculosis Report 2014. Geneva: World Health Organization, **2014**.
23. Smith AFM, Gelfand AE. Bayesian statistics without tears: a sampling-resampling perspective. Am Stat. **1992**; 46(2):84–88.
24. Stein M. Large sample properties of simulations using Latin hypercube sampling. Technometrics. **1987**; 29(2):143–151.
25. Shisana O, Rehle T, Simbayi LC, Zuma K, Jooste S, Zungu N, et al. South African National HIV Prevalence, Incidence and Behaviour Survey, 2012. HSRC Press. **2014**; :194.
26. Weyer K, Brand J, Lancaster J, Levin J, van der Walt M. Determinants of multidrug-resistant tuberculosis in South Africa : results from a national survey. South African Med J. **2007**; 97(11):1120–1128.
27. National Institute for Communicable Diseases (NICD). South African Tuberculosis Drug Resistance Survey 2012–14. 2016.

28. Nhung N V., Hoa NB, Sy DN, Hennig CM, Dean AS. The fourth national anti-tuberculosis drug resistance survey in Viet Nam. Int J Tuberc Lung Dis. **2015**; 19(6):670–5.

29. Vynnycky E, Fine PE. The natural history of tuberculosis: the implications of age-dependent risks of disease and the role of reinfection. Epidemiol Infect. **1997**; 119(2):183–201.

30. Andrews JR, Noubary F, Walensky RP, Cerda R, Losina E, Horsburgh CR. Risk of progression to active tuberculosis following reinfection with *Mycobacterium tuberculosis*. Clin Infect Dis. **2012**; 54(6):784–791.

31. Fox GJ, Barry SE, Britton WJ, Marks GB. Contact investigation for tuberculosis: a systematic review and meta-analysis. Eur Respir J. **2013**; 41(1):140–156.

32. Sloot R, Schim Van Der Loeff MF, Kouw PM, Borgdorff MW. Risk of tuberculosis after recent exposure: a 10-year follow-up study of contacts in Amsterdam. Am J Respir Crit Care Med. **2014**; 190(9):1044–1052.

33. Horsburgh CR, O'Donnell M, Chamblee S, Moreland JL, Johnson J, Marsh BJ, et al. Revisiting rates of reactivation tuberculosis: a population-based approach. Am J Respir Crit Care Med. **2010**; 182(3):420–425.

34. Onozaki I, Law I, Sismanidis C, Zignol M, Glaziou P, Floyd K. National tuberculosis prevalence surveys in Asia, 1990-2012: an overview of results and lessons learned. Trop Med Int Heal. **2015**; 20(9):1128–1145.

35. MacPherson P, Houben RM, Glynn JR, Corbett EL, Kranzer K. Pre-treatment loss to follow-up in tuberculosis patients in low- and lower-middle-income countries and high-burden countries: a systematic review and meta-analysis. Bull World

Health Organ. **2014**; 92(2):126–138.

36. Gillespie SH, Crook AM, McHugh TD, Mendel CM, Meredith SK, Murray SR, et al. Four-month moxifloxacin-based regimens for drug-sensitive tuberculosis. N Engl J Med. **2014**; 371(17):1577–1587.

37. Merle CS, Fielding K, Sow OB, Gninafon M, Lo MB, Mthiyane T, et al. A four-month gatifloxacin-containing regimen for treating tuberculosis. N Engl J Med. **2014**; 371(17):1588–1598.

38. Jindani A, Harrison TS, Nunn AJ, Phillips PPJ, Churchyard GJ, Charalambous S, et al. High-dose rifapentine with moxifloxacin for pulmonary tuberculosis. N Engl J Med. **2014**; 371(17):1599–1608.

39. Holtz TH, Sternberg M, Kammerer S, Laserson KF, Riekstina V, Zarovska E, et al. Time to sputum culture conversion in multidrug-resistant tuberculosis: predictors and relationship to treatment outcome. Ann Intern Med. **2006**; 144(9):650–659.

40. Ahuja SD, Ashkin D, Avendano M, Banerjee R, Bauer M, Bayona JN, et al. Multidrug resistant pulmonary tuberculosis treatment regimens and patient outcomes: an individual patient data meta-analysis of 9,153 Patients. PLoS Med. **2012**; 9(8).

41. Marx FM, Dunbar R, Enarson DA, Williams BG, Warren RM, Spuy GD Van Der, et al. The temporal dynamics of relapse and reinfection tuberculosis after successful treatment: a retrospective cohort study. Clin Infect Dis. **2014**; 58(12):1676–1683.

42. Menzies D, Benedetti A, Paydar A, Martin I, Royce S, Pai M, et al. Effect of duration and intermittency of rifampin on tuberculosis treatment outcomes: a

systematic review and meta-analysis. PLoS Med. **2009**; 6(9):1–18.

43. Ahmad Khan F, Gelmanova IY, Franke MF, Atwood S, Zemlyanaya NA, Unakova IA, et al. Aggressive regimens reduce risk of recurrence after successful treatment of MDR-TB. Clin Infect Dis. **2016**; 63(2):214–220.

44. Johnston JC, Shahidi NC, Sadatsafavi M, Fitzgerald JM. Treatment outcomes of multidrug-resistant tuberculosis: a systematic review and meta-analysis. PLoS One. **2009**; 4(9).

45. Toczek A, Cox H, Cros P Du, Cooke G, Ford N. Strategies for reducing treatment default in drug-resistant tuberculosis: systematic review and meta-analysis. Int J Tuberc Lung Dis. **2013**; 17(3):299–307.

46. Marin J-M, Robert CP. Importance sampling methods for Bayesian discrimination between embedded models. Front Stat Decis Mak Bayesian Anal. **2010**; 513–527.

47. Sherman D, Mdluli K, Hickey M, Barry CI, Stover C. AhpC, oxidative stress and drug resistance in *Mycobacterium tuberculosis*. Biofactors. **1999**; 10:211–217.

48. Gagneux S, Burgos M V, DeRiemer K, Encisco A, Muñoz S, Hopewell PC, et al. Impact of bacterial genetics on the transmission of isoniazid-resistant *Mycobacterium tuberculosis*. PLoS Pathog. **2006**; 2(6):e61.

49. Safi H, Lingaraju S, Amin A, Kim S, Jones M, Holmes M, et al. Evolution of high-level ethambutol-resistant tuberculosis through interacting mutations in decaprenylphosphoryl-β-D-Arabinose biosynthetic and utilization pathway genes. Nat Genet. **2013**; 45(10):1190–1197.

50. Comas I, Borrell S, Roetzer A, Rose G, Malla B, Kato-Maeda M, et al. Whole-genome sequenceing of rifampicin-resistant *M. tuberculosis* strains identifies

compensatory mutations in RNA polymerase. Nat Genet. **2011**; 44(1):106–110.

51. MacLean RC, Vogwill T. Limits to compensatory adaptation and the persistence of antibiotic resistance in pathogenic bacteria. Evol Med Public Heal. **2015**; 2015(1):4–12.

52. van Leth F, van der Werf MJ, Borgdorff MW. Prevalence of tuberculous infection and incidence of tuberculosis; a re-assessment of the Styblo rule. Bull World Health Organ. **2008**; 86(1):20–26.

53. Grandjean L, Gilman RH, Martin L, Soto E, Castro B, Lopez S, et al. Transmission of multidrug-resistant and drug-susceptible tuberculosis within households: a prospective cohort study. PLoS Med. **2015**; 12(6):1–22.

54. Golla V, Snow K, Mandalakas AM, Schaaf SH, Preez K Du, Hesseling AC, et al. The impact of drug resistance on the risk of tuberculosis infection and disease in child household contacts: a cross sectional study. BMC Infect Dis. **2017**; 17(1):1–10.

55. Droznin M, Johnson A, Johnson AM. Multidrug resistant tuberculosis in prisons located in former Soviet countries: a systematic review. PLoS One. **2017**; 12(3):1–13.

56. Gandhi NR, Moll A, Sturm AW, Pawinski R, Govender T, Lalloo U, et al. Extensively drug-resistant tuberculosis as a cause of death in patients co-infected with tuberculosis and HIV in a rural area of South Africa. Lancet. **2006**; 368(9547):1575–1580.

57. Shenoi S V., Escombe AR, Friedland G. Transmission of drug-susceptible and drug-resistant tuberculosis and the critical importance of airborne infection control

in the era of HIV infection and highly active antiretroviral therapy rollouts. Clin Infect Dis. **2010**; 50(S3):S231–S237.

58. Hasan R. Drug resistant tuberculosis: Challenges of urbanization. Int J Mycobacteriology. **2014**; 3(2):79–81.

59. Alene KA, Viney K, McBryde ES, Clements ACA. Spatial patterns of multidrug resistant tuberculosis and relationships to socioeconomic, demographic and household factors in northwest Ethiopia. PLoS One. **2017**; 12(2):1–14.

60. Wang W, Wang J, Zhao Q, Darling ND, Yu M, Zhou B, et al. Contribution of rural-to-urban migration in the prevalence of drug resistant tuberculosis in China. Eur J Clin Microbiol Infect Dis. **2011**; 30(4):581–586.

61. Alirol E, Getaz L, Stoll B, Chappuis F, Loutan L. Urbanization and infectious diseases in a globalised world. Lancet Infect Dis. **2011**; 11(2):131–41.

62. van Doorn HR, Haas PEW de, Kremer K, Vandenbroucke-Grauls CMJE, Borgdorff MW, van Soolingen D. Public health impact of isoniazid-resistant *Mycobacterium tuberculosis* strains with a mutation at amino-acid position 315 of katG: a decade of experience in The Netherlands. Clin Microbiol Infect. **2006**; 12(8):769–75.

63. van Soolingen D. Molecular epidemiology of tuberculosis and other mycobacterial infections: main methodologies and achievements. J Intern Med. **2001**; 249(1):1–26.

64. Glynn JR, Vynnycky E, Fine PEM. Influence of sampling on estimates of clustering and recent transmission of *Mycobacterium tuberculosis* derived from DNA fingerprinting techniques. Am J Epidemiol. **1999**; 149(4):366–371.

65. Murray M, Alland D. Methodological problems in the molecular epidemiology of tuberculosis. Am J Epidemiol. **2002**; 155(6):565–571.

66. Casali N, Nikolayevskyy V, Balabanova Y, Harris SR, Ignatyeva O, Kontsevaya I, et al. Evolution and transmission of drug-resistant tuberculosis in a Russian population. Nat Genet. **2014**; 46(3):279–86.

67. Salvatore PP, Becerra MC, Wiesch PA zur, Hinkley T, Kaur D, Sloutsky A, et al. Fitness costs of drug-resistance mutations in multidrug resistant *M. tuberculosis*: a household-based case-control study. J Infect Dis. **2016**; 213(1):149-55.

68. Ssengooba W, Lukoye D, Meehan CJ, Kateete DP, Joloba ML, Jong BC de, et al. Tuberculosis resistance-conferring mutations with fitness cost among HIV-positive individuals in Uganda. Int J Tuberc Lung Dis. **2017**; 21(5):531–536.

69. Lu P, Chen X, Zhu L, Yang H. Interferon-gamma release assays for the diagnosis of tuberculosis: A systematic review and meta-analysis. Lung. **2016**; 194(3):447–458.

70. Pai M, Behr M. Latent *Mycobacterium tuberculosis* infection and interferon-gamma release assays. Microbiol Spectr. **2016**; 4(5).

71. Dowdy DW, Basu S, Andrews JR. Is passive diagnosis enough? The impact of subclinical disease on diagnostic strategies for tuberculosis. Am J Respir Crit Care Med. **2013**; 187(5):543–551.

72. Salvatore PP, Proaño A, Kendall EA, Gilman RH, Dowdy DW. Linking individual natural history to population outcomes in tuberculosis. J Infect Dis. **2017**; 217(1):112–121.

73. Pai M, P NM, Boehme CC. Tuberculosis diagnostics: state of the art and future

directions. Microbiol Spectr. **2016**; 4(5).

74. Fennelly KP, Jones-López EC, Ayakaka I, Kim S, Menyha H, Kirenga B, et al. Variability of infectious aerosols produced during coughing by patients with pulmonary tuberculosis. Am J Respir Crit Care Med. **2012**; 186(5):450–457.

75. Hamilton CD, Swaminathan S, Christopher DJ, Ellner J, Gupta A, Sterling TR, et al. RePORT International: advancing tuberculosis biomarker research through global collaboration. Clin Infect Dis. **2015**; 61(S3):S155–S159.

76. Blower SM, Chou T. Modeling the emergence of the "hot zones": tuberculosis and the amplification dynamics of drug resistance. Nat Med. **2004**; 10(10):1111–6.

CHAPTER V

DISCUSSION

SYNOPSIS

This dissertation represents a series of investigations of tuberculosis (TB) through a variety of methodological and substantive lenses: microbiological, epidemiological, and theoretical. While much has been accomplished in recent years to improve the diagnosis, treatment, and prevention of TB, the disease remains one of the most significant causes of disease morbidity and mortality worldwide. To ensure these improvements continue and accelerate in coming decades, control of the global TB epidemic will require the optimal use of currently available public health tools today, as well as the development of new tools for tomorrow. As scientific training becomes increasingly specialized, so too may expertise become increasingly segmented and insular. Advances in TB control efforts into the future are unlikely to be accomplished by isolated disciplines, but will require the interface of scientific experts and public health professionals with a variety of backgrounds and areas of expertise. The studies described here offer a unique approach of multidisciplinary training and research in public health science. Such a cross-fertilization of scientific fields may offer a new avenue to generate or hasten new insights into infectious disease control. In this section, we contextualize the findings of these studies, offer a critical evaluation of their strengths, and propose several avenues for future investigation.

SUMMARY OF RESULTS

The translation of laboratory findings – particularly from animal models – is a complex dilemma facing many fields of biomedicine [1]. We recognize this issue in the TB field and, in Chapter II, offer a new perspective. We introduce a novel theoretical framework for linking observations of individual-level pathogenesis, disease progression, and recovery with population-level clinical outcomes in humans. Our analysis demonstrates that TB progression in humans is decisively slower than is predicted by animal models. We also successfully implemented this approach to provide evidence – based on individual-level disease progression – that improved TB detection and treatment alone may not effectively improve population-level morbidity, as has been observed with the rollout of the DOTS strategy as well as Xpert® MTB/RIF [2,3].

In Chapter III, we investigate the bacterium *M. tuberculosis* and the intracellular mechanisms underlying drug action and the detection of drug resistance, key elements in epidemic multidrug resistant TB (MDR-TB). Based on previous findings that the first-line drug pyrazinamide (PZA) interacts with the bacterial protein RpsA [4], we sought to characterize the protein binding partners of RpsA which may be involved in this interaction. We identified the essential protein Ribosome Recycling Factor (RRF) as a high-affinity binding partner through affinity chromatography amongst a handful of other proteins, presenting the first evidence of RpsA-RRF interactions. While laboratory findings are critical in the study of TB, in some cases it is difficult to draw clear conclusions of their impacts on the TB epidemic. We discuss the contradictory laboratory and epidemiological evidence for fitness costs associated with drug resistance.

Experimental evidence has accumulated for several decades strengthening the hypothesis that mutations which confer drug resistance also carry physiological and evolutionary tradeoffs in the absence of drug pressure. More recent molecular studies have demonstrated the potential of compensatory evolution and genetic epistasis to overcome these tradeoffs. Yet, how these principles translate to the transmission and epidemic spread of MDR-TB remains unclear. In Chapter IV, we explore how these molecular and evolutionary principles may influence the global TB epidemic in the coming decades. We compare competing assumptions about the efficiency with which MDR-TB transmits infection, whether with a persistent deficit in efficiency, with a deficit that is gradually eliminated, or with no deficit at all. Our findings demonstrate that long-term trends in MDR-TB incidence vary dramatically depending on the assumptions made about biological fitness and transmission efficiency. Additionally, we effectively reproduced the contradictory findings of a recently published analysis [5] and were able to demonstrate that the discrepancies in our results are attributable to questionable assumptions contained in that study. Our analyses provide important context for any attempt to predict long-term trends in the MDR-TB epidemic, and highlight important characteristics of the TB epidemic about which there remains much uncertainty.

STRENGTHS AND LIMITATIONS

These findings offer novel insights into the biology and epidemiology of TB. Our individual-level model uses a mathematical and theoretical framework to translate studies of individual-level disease progression with large-scale population impacts. This framework can accurately recapitulate key characteristics of human TB and can robustly predict the population-level impacts of individual interventions (e.g., passive case detection and improved diagnostic sensitivity). In this study, we intentionally adopted a modeling framework as simple as possible at the individual-level while accurately recapitulating human clinical TB. As a result, in its current form, this model cannot capture complex pathophysiology and mechanistic interactions which underlie clinical progression. However, the simplicity of this framework may serve as a useful platform for the community of TB researchers to build upon in complexity and application.

Our molecular findings, that RpsA may interact with RRF in *M. tuberculosis*, present important clues to better understanding the role of PZA in sterilizing infection during first-line treatment. However, these findings were not confirmed *in vivo*. Nevertheless, the chromatography methods utilized are prone to lower sensitivity than specificity, and this observed interaction was unlikely falsely-positive or an experimental artefact. While RpsA and RRF may indeed interact biochemically, overexpression of *rrf* did not affect the sensitivity of *M. tuberculosis* to pyrazinoic acid, and therefore this interaction may not be relevant in the mechanism of PZA action. Furthermore, recent studies have raised critical questions about the role of RpsA in mediating the effects of PZA [6], and the prospects of this field remains in flux.

Our projections of the MDR-TB epidemic illustrate the importance of carefully translating experimental findings to human populations, as they can dramatically influence estimates of long-term epidemic trends. While our results differ importantly from those of a recent publication [5], we were able to accurately replicate those findings and demonstrate the methodological nature of these discrepancies. Nonetheless, our findings are intended to compare a series of competing assumptions about the transmission efficiency of MDR-TB, and cannot be interpreted as rigorous predictions of national or global TB epidemics. Furthermore, as a modeling exercise, our model makes many simplifying assumptions about the complex nature of ongoing TB epidemics around the world. Our sensitivity analyses demonstrate that these findings are largely robust to model parameterization, though it is possible that our model structure or parameter selection do not fully capture some critical details of TB transmission and treatment.

Despite the above limitations, these investigations represent important, novel, and robust approaches to the epidemiological analysis and microbiological study of TB.

OPPORTUNITIES FOR FUTURE STUDY

As with many scientific endeavors, these studies are not self-contained and may lay the foundations for further research which can enhance, elaborate, confirm, or even contradict the findings presented here.

Our theoretical framework for linking individual-level and population-level outcomes is intended as a novel tool for the TB research community. Several studies have already built detailed within-host models of TB immunology and pathogenesis [7,8], but these models are restricted to the study and prediction of TB pathology in animal models. Populating our framework's simplified Markov probabilities with a detailed within-host model may elucidate key differences in the dynamics of *M. tuberculosis* infection in animal models and humans. Additionally, our framework may prove useful for improving population-level epidemic models which often make simplifying assumptions about the course of TB pathology and the inter-person heterogeneity of disease. For example, compartmental models assume that populations transition from being asymptomatic to being fully infectious and detectable. Yet, ignoring preclinical/incipient disease is likely to greatly overestimate the impact of interventions on TB incidence [9]. Our framework may provide an important tool to study and simulate this period of disease (which is inherently difficult to characterize empirically). Incorporating these dynamics may assist us in predicting the outcomes of interventions which influence individual-level dynamics (such as time-to-diagnosis, etc.) or in understanding how the transmission dynamics of TB change over time (e.g., when individuals become more infectious as their course of disease progresses) [10,9].

The molecular findings we describe – a novel role for RRF in RpsA activity – offer several promising routes for future research. Previous studies indicate that PZA acts by inhibiting the tmRNA-mediated trans-translation response of *M. tuberculosis* [4,11]. Studies in *Escherichia coli* have demonstrated that RRF may play a non-canonical role in ribosome rescue, supplementary to and independent of the role of tmRNA [12–15]. These observations, in combination with our findings, suggest an exciting hypothesis that PZA may act by inhibiting several ribosome stress-response pathways (i.e., mediated by tmRNA and RRF). Confirmation of this hypothesis will require an in-depth evaluation of the cellular (and ribosomal) function of RRF in mycobacterial species, an area of limited previous research.

Finally, our projections of MDR-TB epidemics recommend both short-term methodological responses and long-term research priorities. Our study demonstrates that building mathematical epidemic models of drug resistance upon assumptions of fitness costs (or the absence thereof) can critically alter long-term outcomes; in the absence of strong empirical data about the transmission efficiency of MDR-TB, modelling studies must address this uncertainty in their initial assumptions and in the sensitivity of their results to changes in transmission efficiency. More fundamentally, future trends in the MDR-TB epidemic will depend highly on the transmission efficiency of MDR-TB relative to DS-TB and whether it may change over time. This critical quantity remains highly uncertain, and characterizing transmission efficiency will require integrating several epidemiological approaches as we have described.

Cumulatively, our work presents exciting opportunities (as well as fundamental challenges) for furthering our understanding of *M. tuberculosis* biology and TB

epidemiology at large, which may – directly or indirectly – contribute to control of the global TB epidemic.

CONCLUSION

Despite the heavy losses of life and health that can be attributed to tuberculosis throughout history, today, TB is on the decline. Global incidence of TB has fallen continuously since the turn of the millennium, despite alarming increases in some high burden settings [16]. Mortality due to TB has dropped even faster, falling by 37% in this period. This progress, while encouraging, is too slow for the many millions who die or fall ill with TB each year. It will not be sufficient to achieve the current global targets for TB control (reducing incidence by 90% between 2015 and 2035) without more rapid declines [16].

The future of TB control remains a challenge both daunting and promising. To face this challenge effectively, the public health community will need new tools and new techniques drawn from myriad sources of scientific inquiry and public health practice. It is our hope that multidisciplinary approaches like those presented here will improve public health science and fortify efforts to control the heavy burden and human cost of infectious diseases now and in the future.

REFERENCES

1. Seok J, Warren HS, Cuenca AG, Mindrinos MN, Baker H V, Xu W, et al. Genomic responses in mouse models poorly mimic human inflammatory diseases. Proc Natl Acad Sci. **2013**; 110(9):3507–12.
2. Dowdy DW, Chaisson RE. The persistence of tuberculosis in the age of DOTS: reassessing the effect of case detection. Bull World Health Organ. **2009**; 87(4):296–304.
3. Menzies NA, Cohen T, Lin HH, Murray M, Salomon JA. Population health impact and cost-effectiveness of tuberculosis diagnosis with Xpert MTB/RIF: a dynamic simulation and economic evaluation. PLoS Med. **2012**; 9(11):e1001347.
4. Shi W, Zhang X, Jiang X, Yuan H, Lee JS, Barry CE, et al. Pyrazinamide inhibits trans-translation in *Mycobacterium tuberculosis*. Science. **2011**; 333(6049):1630–1632.
5. Sharma A, Hill A, Kurbatova E, Walt M van der, Kvasnovsky C, Tupasi TE, et al. Estimating the future burden of multidrug-resistant and extensively drug-resistant tuberculosis in India, the Philippines, Russia, and South Africa: a mathematical modelling study. Lancet Infect Dis. **2017**; 17(7):707–715.
6. Dillon NA, Peterson ND, Feaga HA, Keiler KC, Baughn AD. Anti-tubercular activity of pyrazinamide is independent of trans-translation and RpsA. Sci Rep. **2017**; 7(1):1–8.
7. Gong C, Linderman J, Kirschner D. A population model capturing dynamics of tuberculosis granulomas predicts host infection outcomes. Math Biosci Eng. **2015**;

12(3):625–642.

8. Sud D, Bigbee C, Flynn JL, Kirschner DE. Contribution of CD8+ T cells to control of *Mycobacterium tuberculosis* infection. J Immunol. **2006**; 176(7):4296–314.

9. Dowdy DW, Basu S, Andrews JR. Is passive diagnosis enough? The impact of subclinical disease on diagnostic strategies for tuberculosis. Am J Respir Crit Care Med. **2013**; 187(5):543–551.

10. Proaño A, Bravard MA, López JW, Lee GO, Bui D, Datta S, et al. Dynamics of cough frequency in adults undergoing treatment for pulmonary tuberculosis. Clin Infect Dis. **2017**; 64(9):1174–1181.

11. Yang J, Liu Y, Bi J, Cai Q, Liao X, Li W, et al. Structural basis for targeting the ribosomal protein S1 of *Mycobacterium tuberculosis* by pyrazinamide. Mol Microbiol. **2014**; 95(5):791–803.

12. Delgado-Olivares L, Zamora-Romo E, Guarneros G, Hernandez-Sanchez J. Codon-specific and general inhibition of protein synthesis by the tRNA-sequestering minigenes. Biochimie. **2006**; 88(7):793–800.

13. Cruz-Vera LR, Hernández-Ramón E, Pérez-Zamorano B, Guarneros G. The rate of peptidyl-tRNA dissociation from the ribosome during minigene expression depends on the nature of the last decoding interaction. J Biol Chem. **2003**; 278(28):26065–26070.

14. Singh NS, Ahmad R, Sangeetha R, Varshney U. Recycling of ribosomal complexes stalled at the step of elongation in *Escherichia coli*. J Mol Biol. **2008**; 380(3):451–464.

15. Vivanco-Domínguez S, Bueno-Martínez J, León-Avila G, Iwakura N, Kaji A, Kaji H, et al. Protein synthesis factors (RF1, RF2, RF3, RRF, and tmRNA) and peptidyl-tRNA hydrolase rescue stalled ribosomes at sense codons. J Mol Biol. **2012**; 417(5):425–439.

16. Global Tuberculosis Report 2017. Geneva: World Health Organization, **2017**.

APPENDIX A:

SUPPLEMENTARY INFORMATION FOR CHAPTER 2

SUPPLEMENTARY METHODS

This modeling strategy utilizes an agent-based, stochastic approach to simulate the clinical progression of symptomatic TB in individual patients over a course of infection. The clinical progression of disease is parameterized as the simulated disease burden of the infected patient. The individual-level dynamics through which this model functions are conceived as the consequence of two components: a sequence of states of infection, and the progression or recovery of disease during each element of the sequence.

The Sequence of Infection States

In clinical populations, a qualitative dichotomy is often observed between TB patients who are experiencing decompensation and concomitant worsening of symptoms and prognosis versus patients who are experiencing improvement in symptom resolution and prognosis whether due to successful treatment or spontaneous self-resolution [1]. Additionally, individual patients may experience one or both of these trends over the course of infection. While these general trends are the manifestations of complex immunological and pathophysiological processes, the trends themselves hold important prognostic information about the likely outcome of the patient.

To quantitatively capture these prognostic qualitative phases, a simplifying assumption is made that, at each discrete time step during the course of a single infection, the disease burden of a patient exists in one of two mutually exclusive states . $^{(t)} \in \{progression, recovery\}$. Between any two time steps $\{S^{(t)}, S^{(t+1)}\}$, the infection can

freely transition between these states. The probability of transition in any time step is dependent only on the current state of infection:

$$S^{(t)}, S^{(t+1)} \sim \text{i.i.d. Pr}\left(S^{(t+1)} \middle| S^{(t)}\right) \quad (1)$$

Therefore, the sequence of states that composes any individual infection $\{S^{(0)}, \cdots, S^{(n)}\}$ has the properties of a simple Markov Chain.

Infection Growth and Decay

One of the most significant prognostic determinants of TB mortality is pulmonary bacillary burden [2–4]. While experimentally unfeasible to measure in TB patients, bacillary burden is commonly measured in time course studies of infection in animals. Empirical data of changes in bacillary burden has been successfully modeled according to exponential dynamics of bacterial populations, consistent with the underlying biology of bacterial replication [5,6]. Therefore, this within-host model assumes that patient "disease burden" is analogous to, though an indirect instrument of, bacillary burden size.

During any single time step Δt, the disease burden of a patient is assumed to follow the properties of a simple exponentially reproducing population: $N_{t+1} = N_t e^{r_{S^{(t)}}\Delta t}$ where N_t represents the disease burden at time t and $r_{S^{(t)}}$represents the exponential rate constant during the interval $\Delta t = [t, t+1)$ in which the infection exists in state $S^{(t)}$. Therefore, when $r_{S^{(t)}} > 0$, the disease burden is increasing exponentially; when $r_{S^{(t)}} < 0$, the disease burden is decaying exponentially. When $r_{S^{(t)}} = 0$, the disease burden is stationary during the interval Δt and $N_{t+1} = N_t$. The cumulative dynamics of the bacillary burden of any infection can then be summarized as:

$$N_n = N_0 \prod_{t=1}^{n} e^{r_{S^{(t)}}\Delta t} \; for \; S = \{S^{(0)}, \cdots, S^{(n)}\} \quad (2)$$

Between-Host Variability

It is notable that, in clinical populations, certain patients are particularly vulnerable to progression once infected while other patients are particularly resilient. This between-host heterogeneity may result from the specific interactions between each human host, the quality of his or her immune response, and the genetic and epigenetic characteristics of the inciting strain/genotype of *M. tuberculosis* [3,7,8]. While recognizing the significant between-host heterogeneity that exists in a population of TB patients, the population as a whole exhibits characteristic trends in disease progression and resolution. For example, relatively few patients progress from symptom onset to death in less than 10 weeks or more than 10 years; the average duration of disease in TB patients has been estimated at 3 years [9]. These population-level characteristics can be used to inform the likely amount of between-host variability in the population.

This between-host variability is captured mathematically as the distribution of exponential rate constants of infections in the population. For each possible state $S^{(t)} \in \{progression, recovery\}$, the corresponding rate constant $r_{S^{(t)}}$ is modeled as a beta distribution with parameters $\beta(\omega_{S^{(t)}}, \kappa = 20)$ transformed over the interval $[\alpha_{S^{(t)}}, \zeta_{S^{(t)}}]$ where $\omega_{S^{(t)}}$ represents the mode of exponential rate constants in the population of infections in state $S^{(t)}$, κ represents the beta distribution concentration parameter, $\alpha_{S^{(t)}}$ represents the minimum allowable exponential rate constant in state $S^{(t)}$, and $\zeta_{S^{(t)}}$ represents the maximum allowable exponential rate constant in state $S^{(t)}$. This concentration value was chosen to maintain a clear central tendency in any simulated

population, with a standard deviation less than 11% the sampling range ($\max(\sigma_\beta) = \sqrt{\frac{(0.5\kappa)^2}{\kappa(\kappa+1)}}$). For any individual infection in the population:

$$r_{progression} \sim i.i.d.\beta(\omega_{progression}, \kappa = 20, \alpha_{progression}, \zeta_{progression}) \quad (3)$$

and

$$r_{recovery} \sim i.i.d.\beta(\omega_{recovery}, \kappa = 20, \alpha_{recovery}, \zeta_{recovery}). \quad (4)$$

Clinical Characteristics

For the purposes of this model, population outcomes of infection simulations are calibrated to empirical estimates of the clinical characteristics of TB patients in the pre-chemotherapy era [9],notably the case fatality ratio, disease duration, and proportion of cases resolved amongst symptomatic TB patients. To parameterize the disease burden for calibration, conceptual thresholds are imposed on the disease burden to define the onset/resolution of symptoms and the point of death. Such thresholds have been used in other within-host mathematical models as instruments for analyzing the transition from subclinical to detectable disease in ovarian cancer [10]. The mathematical "symptom threshold", σ, is defined as the disease burden above which the patient is considered to experience severe enough symptoms for clinical presentation and diagnosis and below which the patient experiences a clinically inapparent infection and/or a resolution of symptoms. The mathematical "death threshold", δ, is defined as the disease burden above which the patient expires. For any individual infection, the duration of disease (specifically, the duration of symptomatic disease) can then be calculated as:

$$D(p) = [\,(\min(t|t \in \mathbb{N}\,, N_t \geq \delta)) \vee (\min(t|t \in \mathbb{N}\,, N_{t-1} \geq \sigma\,, N_t < \sigma\,))] - [\min(t|t \in \mathbb{N}\,, N_t \geq \sigma)] \quad (5)$$

For a population $\mathbb{P} \in \{1, \cdots, P\}$, each member with a disease burden $N_t(p)$, the case-fatality ratio can be calculated as:

$$M(\mathbb{P}) = \frac{|\{\mathbb{P}|max(N_t(p))>\delta\}|}{|\{\mathbb{P}|max(N_t(p))>\sigma\}|} \quad (6)$$

and the proportion of cases which self-resolve can be calculated as:

$$R(\mathbb{P}) = \frac{|\{\mathbb{P}|\, N_t(p)>\sigma, N_{t+\mathbb{N}}(p)\leq\sigma\}|}{|\{\mathbb{P}|max(N_t(p))>\sigma\}|} \quad (7)$$

Parameterization and Sampling

Ranges of values for each parameter that were deemed plausible on an a-priori basis are detailed in Table 1. The probability of transition from progression to recovery $\left(\Pr\left(S^{(t+1)} = recovery \middle| S^{(t)} = progression\right)\right)$ was defined by the limits of 0.1%-29.29% per week. The lower bound of this range, equivalent to a 5% probability that individuals transition in the first year of progression, was used considering that roughly 45% of patients survive the first five years of disease [9]; therefore, we speculated at least 10% of those survivors would begin to recover within the first year. The upper bound of this range, equivalent to a 75% probability that individuals transition in the first month of progression, was used considering that patients delay seeking treatment for an average of 25-32 days after symptom onset [11] and that clinical diagnostic criteria of pulmonary TB include a history of cough for 2-3 weeks [12,13]; therefore we speculated that at least one quarter of TB patients experience a continuous worsening of disease over the first month of symptoms. The probability of transition from recovery to progression $\left(\Pr\left(S^{(t+1)} = progression \middle| S^{(t)} = recovery\right)\right)$, analogous to the reactivation of latent TB infection, was defined by the limits of 0.001% to 0.00001% per week, equivalent to

the benchmarks that minimum of 0.05% and a maximum of 5% of patients transition in the first year of recovery . These limits were defined with consideration that the yearly probability of reactivation latent TB infection has been estimated as 0.084% per year in asymptomatic individuals [14]. In light of these estimates, we assumed that the probability of symptomatic (recovering) patients experiencing symptom recrudescence would not be substantially less than the probability of reactivation from latency in immunocompetent adults but could be as high as two orders of magnitude greater.

The "death threshold" (δ) was allowed to vary from 10^7 to 10^{10} units, using an analogous reference frame estimated from the maximum measured bacillary burdens of non-human primates suffering from asymptomatic and fulminant TB disease [15]. To ensure there is always a plausible separation between the "death threshold" and the "symptom threshold" (σ), the latter was defined by the log-difference $\log_{10}(\delta) - \log_{10}(\gamma)$, a "window width" parameter which defined the extent of disease progression between the onset of symptoms and death. The "window width" was allowed to vary between benchmarks of 10^4 to 10^7 units informed by the typical variations between bacillary burdens of asymptomatic/latent and symptomatic non-human primates. Therefore, deriving the "symptom threshold" from this log-difference allowed the "symptom threshold" to vary between 1 to 10^6 units [15–18].

The bounds of the distribution of exponential rate constants in the progression phase ($[\alpha_{progression}, \zeta_{progression}]$) were defined according to the benchmarks that no patient in the progression phase would progress from asymptomatic/subclinical disease to death in less than 90 days – informed by the slow pathophysiology of clinical TB and early studies which found overall mortality in the first year of disease to be no greater

than 30% [19]. We define the partition of "progression" and "recovery" phases according to the boundary of their exponential rate constants such that any patient who remains continuously in the progression phase would die in a maximum of 5 years of symptomatic disease. Therefore, for any patient $\frac{\log\left(\frac{\delta}{\sigma}\right)}{90} \leq r_{progression} \leq \frac{\log\left(\frac{\delta}{\sigma}\right)}{260\times7}$ and thus $[\alpha_{progression}, \zeta_{progression}] = \left[\frac{\log\left(\frac{\delta}{\sigma}\right)}{90}, \frac{\log\left(\frac{\delta}{\sigma}\right)}{260\times7}\right]$. Assuming a reasonable value of $\frac{\delta}{\sigma} = 10^4$, the limits of the distribution of exponential rate constants in the progression phase were specified as 0.005 and 0.102 per day, equivalent to population doubling times in the of 137 days to 6 days, respectively.

The upper bound of the recovery phase exponential rate constant $\left(\zeta_{recovery}\right)$ was similarly defined according to the above definition such that any patient continuously progressing would die in a maximum of 5 years; consequentially, we define that, if any patient continuously in the recovery phase were to die, it would occur after no less than 5 years of symptomatic disease. The lower bound of the recovery phase exponential rate constant ($\alpha_{recovery}$) – the fastest allowable rate of spontaneous recovery – was informed by data on the average rate of recovery with the assistance of bactericidal therapies. It has been estimated that a patient receiving effective drug therapy will experience sputum conversion no sooner than an average of 35 days after initiation [20]. If one assumes that a symptomatic (spontaneously recovering) patient receiving no drug therapy will recover no faster than ¼ the rate of a patient receiving drug therapy, then for any patient $\frac{log\left(\frac{\sigma}{\delta}\right)}{35\times4} \leq r_{recovery} \leq \frac{log\left(\frac{\delta}{\sigma}\right)}{365\times5+1}$ and thus $\left[\alpha_{recovery}, \zeta_{recovery}\right] = \left[\frac{log\left(\frac{\sigma}{\delta}\right)}{35\times4}, \frac{log\left(\frac{\delta}{\sigma}\right)}{365\times5+1}\right]$. Assuming a reasonable value of $\frac{\delta}{\sigma} = 10^4$, the limits of the distribution of exponential rate constants in

the recovery phase were specified as -0.066 and 0.005 per day, equivalent to a population half-life of 11 days and a population doubling time in the range of 137 days, respectively.

Modes of the population distributions of these exponential rate constants $(\omega_{progression}, \omega_{recovery})$ were allowed to vary across the full range of allowable values for each respective phase.

For each of the 2,000,000 simulations of the individual-level model, Latin hypercube sampling was used to draw one value from the specified ranges of each parameter to create 2,000,000 six-parameter sets. Transition probabilities from progression to recovery and vice versa were conceptualized as characteristics of the cohort (i.e., one value per cohort), with each individual patient trajectory comprised as stochastic realizations of these probabilities. Additionally, symptom and death thresholds were conceptualized as reference frames with which to compare individuals' progression, and were therefore fixed for all patients (i.e., one value each per cohort). Parameter values for these transition probabilities and thresholds were uniformly sampled on $\log_{10}$-transformed scales. By contrast, rate constants of progression and recovery were conceptualized as distributional values – the mode was selected for a given cohort, and each individual's personal rate of progression and recovery was drawn from a beta distribution around that mode. As the exponential rate constants ranged across both positive and negative values, the modal (cohort-level) values were sampled on the log-modulus-transformed scale [21], defined here as $T(r) = \frac{|r|}{r} \times \log(100 \times |r| + 1)$.

Importance Resampling

Following initial Latin hypercube sampling [22], importance resampling [23] was used to generate Bayesian posteriors for each parameter as described below. A joint likelihood function was generated to describe probable values of the clinical characteristics of a cohort of TB cases from the pre-chemotherapy era [9]. The case-fatality ratio likelihood was modeled as a binomial distribution with p=0.55 and parameters $\left(k = \left|\{\mathbb{P}\middle|max\left(N_t(p)\right) > \delta\}\right|, n = \left|\{\mathbb{P}\middle|max\left(N_t(p)\right) > \sigma\}\right|\right)$ populated from values of each realized simulation. The likelihood for the median disease duration of a cohort was modeled as a symmetric beta distribution $\beta(\omega = 0.5, \kappa = 8)$ scaled to a range [1 , 5] years (modal equivalent of 3 years). This concentration value was used to define a broad likelihood function around the median duration (standard deviation of 8 months). The likelihood of the proportion of cases which self-resolve was modeled as a uniform distribution on the interval [0.1, 1.0]. Each parameter set was weighted according to the quotient of the set's joint likelihood, $L(\theta_i ; x)$, and the marginal likelihood of all sets:

$$q_i = \frac{L(\theta_i;x)}{\sum_{j=1}^{n} L(\theta_j;x)} \tag{8}$$

Each parameter value was then resampled from the Latin hypercube according to its weight to construct its posterior distribution.

Diagnosis and Treatment

To simulate the potential impact of diagnosis and treatment on the cumulative disease burden and time spent symptomatic among patients in a cohort, we compare various scenarios using the maximum likelihood parameter set identified above. Diagnosis and treatment is conceptualized as a weekly probability of detection,

dependent upon disease burden. If a patient initiates treatment at time *t* (D_t=1), she is removed from the infectious cohort before time *t*+1. The weekly probability of initiating treatment, $Pr(D_t=1 \mid N_t)$, is set equal to zero at any disease burden below the symptom threshold. This probability increases logarithmically to a maximum p_{max} (defined as $Pr(D_t=1|N_t=\delta)$) when the disease burden equals the death threshold such that:

$$\Pr(D_t = 1|N_t) = \frac{\log_{10} N_t - \log_{10} \sigma}{\log_{10} \delta - \log_{10} \sigma} \times p_{max} \quad (9)$$

This disease-dependent probability of detection ensures that patients with nearly asymptomatic disease are unlikely to be diagnosed while patients near death are most likely to be diagnosed.

When the cohort is simulated with the introduction of diagnosis and treatment (each patient with a possibility of being detected and starting on treatment [$Pr(D_t(p)=1)$] at each time *t*), the case detection proportion (commonly called the "case detection rate", or CDR) of the entire cohort can be defined as the proportion of symptomatic patients detected prior to death or self-resolution:

$$CDR(\mathbb{P}) = \frac{|\{\mathbb{P}|\ max(D_t(p))=1\}|}{|\{\mathbb{P}|max(N_t(p))>\sigma\}|} \quad (10)$$

Values for p_{max} (weekly probability of initiating treatment at the time of maximum symptom burden) were sampled randomly from a uniform distribution on the log10 scale from 10-5 to 1.0 (median: 1.0% probability of detection per week), and one cohort of 1,000 patients each was simulated for each of the 1,000 p_{max} values sampled (holding all other parameters constant at their maximum likelihood values). The pseudo-likelihood associated with each value for p_{max} was calculated using the estimated 2015 global CDR

of 59% [95% CI: 50-70%] [24]. The pseudo-likelihood function was parameterized as a normal distribution with a mean of 59% and a standard deviation of 5.1%.

The potential impact of treatment initiation was then estimated by comparing the cumulative burden-time of the cohort with and without detection and treatment. For each patient, the total burden-time is defined as the area under the curve of (disease burden above the symptom threshold) versus time (see Figure S1.4 for a graphical representation). If the time of symptom onset for a given patient p is a=[min($t|t\in$N ,$N_t\geq\sigma$)] and the time of exit from the cohort (due to death, cure, detection, or end of follow-up) is b, then the patient's total burden-time is:

$$\mathbb{B}(p) = \int_{\mathrm{a}}^{b} N_t \, dt - \int_{a}^{b} \sigma \, dt \tag{11}$$

The cumulative burden-time for a population of P symptomatic patients can then be calculated as $\sum_1^P \mathbb{B}(p)$.

SUPPLEMENTARY RESULTS

Of the 2,000,000 simulated patient cohorts (each containing 1,000 patients), 76,544 (3.8%) had no TB patients who progressed to symptomatic disease within 5 years of infection. In an additional 34,596 cohorts (1.7%), all symptomatic TB cases suffered symptoms for at least five years before death or resolution; these cohorts were excluded from further analysis. Of the remaining cohorts, the epidemiological characteristics of TB were highly varied with case fatality ratios ranging from 0%-100% [Interquartile range (IQR): 7.5%, 80%] and median durations ranging from 1 week to 5 years [IQR:0.48 years, 1.3 years]. After applying the joint likelihood function to differentially weight plausibly realistic cohorts from discernibly unrealistic cohorts, 551,100 cohorts (28% of the total) had results consistent with historical estimates of the natural history of TB (joint likelihoods greater than zero). Amongst these plausible cohorts, the median case fatality ratio was 42.5% [IQR: 18%, 67%] and the median duration of disease for the 50^{th} percentile of cohorts was 1.5 years [IQR:1.2 years, 1.9 years]; however, amongst those cohorts accounting for 90% of total likelihood mass (n=20,770), the median duration of disease was substantially longer at 2.3 years [IQR:1.9 years, 2.7 years]. Notably, these results indicate a closer recapitulation of historical case fatality ratio estimates (target: 55%; posterior IQR: 54-56%) than disease duration estimates (target: 3.0 years; posterior IQR: 2.1-2.8 years). This suggests that, in the simplified modeling approach used here, cohorts with case fatality proportions that are most similar to the reported values (i.e., highest likelihood cohorts) have mean disease durations that are somewhat shorter than those reported. In other words, a disease process that results in 55% case fatality in our

simplified model generally progresses more rapidly than would be expected if the mean disease duration were actually 3.0 years. Further work is justified to discern whether this discrepancy is more likely a reflection of the simplified modeling framework utilized here (e.g., if addition of further model complexity would result in less of a discrepancy) or whether this apparent discrepancy may suggest actual measurement error in pre-chemotherapy studies that relied largely on reported symptoms for their estimates of disease duration.

Of the 1,000 cohorts simulated with detection and treatment initiation, 6.2% demonstrated case detection proportions consistent with global estimates (median: 59%; 95% CI: 50-70%). After importance resampling, the median posterior CDR in these simulated cohorts was 57.2% (95% UR: 47.9-69.8%). In the absence of detection and treatment, mortality using the maximum likelihood parameter set identified above was 53.2%. When the maximum likelihood estimate of the weekly detection probability (1.4% per week) was applied, mortality in this cohort dropped to 17.2% (omitting possible deaths during treatment). Although mortality was not calibrated to data from patients receiving treatment, this estimate was nevertheless very similar to the reported 2015 global mortality rate of 17.3% [24].

Figure S1.1: Values of the Symptom Window Width Consistent with Observed Cohort Data.

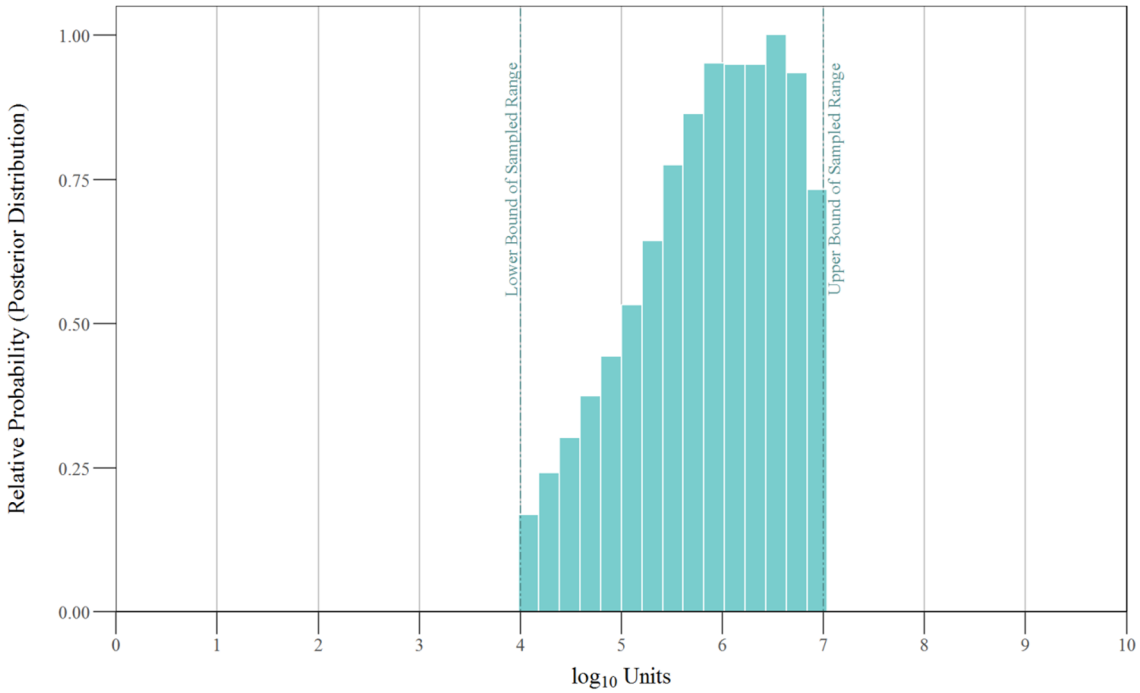

The symptom width window was used to define the symptom threshold by determining the difference between the death threshold (δ) and the symptom threshold (σ). Model input values (prior distributions) were sampled uniformly on the log-transformed scale between reasonable bounds selected on an a priori basis (denoted by vertical dashed lines). Histogram densities show the proportion of 2 million weighted parameter values that were most consistent with observed cohort data from the pre-chemotherapy era (posterior distributions).

Figure S1.2: Values of Threshold Parameters Consistent with Observed Cohort Data.

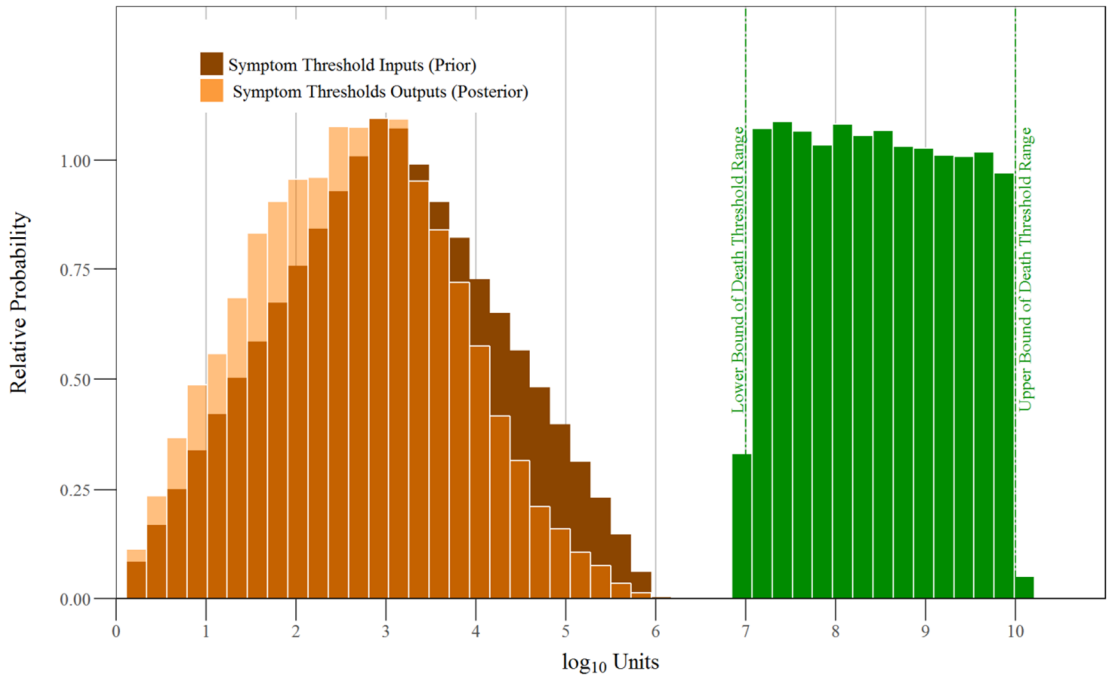

The symptom threshold parameter was derived as the difference between the log-transformed death threshold and symptom window width. Therefore, the model input values (prior distribution) for the symptom threshold parameter was not uniformly sampled, but was derived from two uniformly sampled parameters (the death threshold and the symptom window width). Input values for the symptom threshold are depicted in darker shades behind the weighted values most consistent with observed data (depicted in lighter transparent shades). Input values for the death threshold were sampled uniformly on the log-transformed scale between the displayed bounds, and weighted values most consistent with observed cohort are depicted in green.

Figure S1.3: Values of the Probability of Transition to Progression Consistent with Observed Cohort Data.

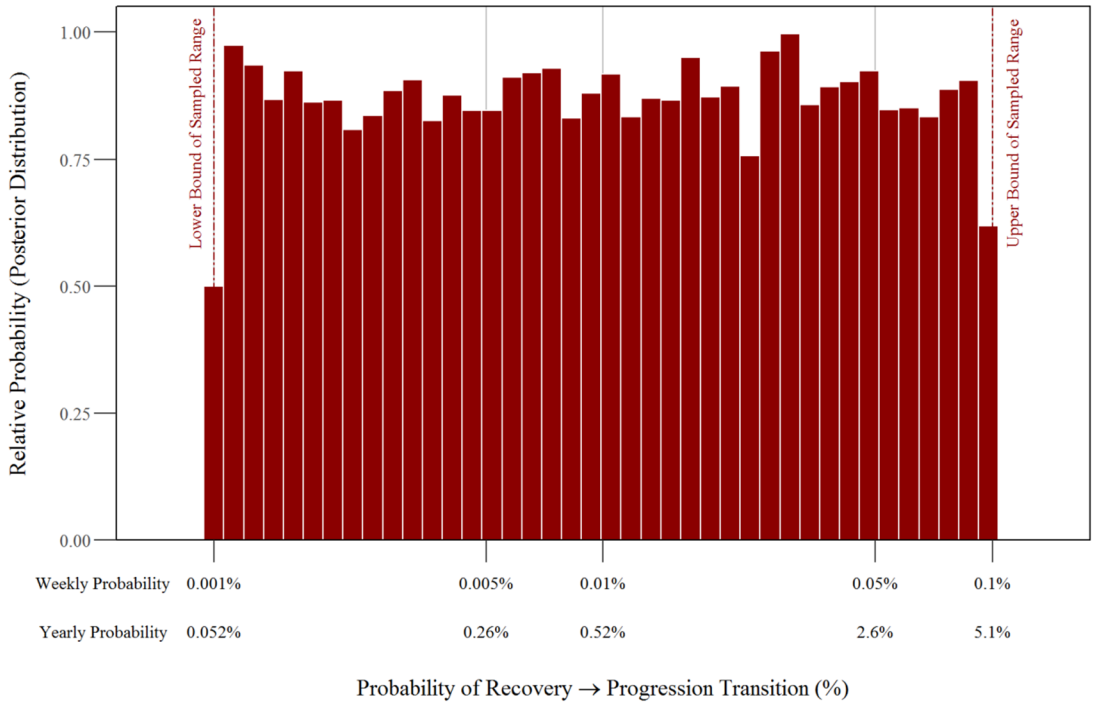

Model input values (prior distributions) were sampled uniformly on the log-transfomred scale between the defined bounds (depicted as vertical dashed lines). Histogram densities depict the proportion of 2 million weighted parameter values most consistent with observed cohort data from the pre-chemotherapy era (posterior distribution). Probabilities of transition from the recovery phase to the progression phase are depicted on weekly and annualized scales.

Without diagnosis and treatment initiation, the cohort's cumulative burden-time was 11.0 log(unit-weeks). When the maximum likelihood probability of detection and treatment initiation was applied (from above), the burden-time was reduced to 10.5 log(unit-weeks), a 4.5% reduction in cumulative burden time (on the $\log_{10}$ scale). We then explored the potential impact of improved diagnosis using Xpert® MTB/RIF over sputum microscopy (assuming that the probability of diagnosis and treatment is proportional to the sensitivity of the assay used). When the probability of weekly detection was increased 1.4-fold (to represent the improved sensitivity of Xpert® MTB/RIF over sputum microscopy [25,26]), the log burden-time was further reduced to 10.3 log(unit-weeks). This reduction represents a 6.3% reduction in cumulative burden-time compared with no detection and treatment but only a 1.9% reduction in burden-time compared with detection and treatment based on the existing standard of care. To the extent that cumulative burden-time also reflects cumulative transmission potential (especially if expressed on the log scale as in our model), these results may illustrate why improvements in detection and treatment can yield important reductions in mortality without dramatically impacting incidence – as has been seen both with the scale-up of DOTS in the 1990s and more recently projected for the scale-up of Xpert® MTB/RIF over the past five years [27,28].

Figure S1.4: Evaluating the Impact of Detection and Treatment on TB Morbidity

The impact of detection and treatment was evaluated by comparing a cohort's cumulative burden-time in the absence or presence of an intervention. (A) A representative cohort in which no patients are detected and treated, as described in the Methods and Figure 2.2. Emphasized are the disease trajectories of three patients (labeled 1-3). (B) The results of the same cohort when each patient has a weekly probability of detection and treatment, dependent on his or her disease burden in each week. Patients who are detected and treated before surpassing the death threshold (or self-resolution or the end of follow-up) are depicted in violet, with the times of detection/treatment overlaid as purple points. (C) Comparison of the trajectories of Patients 1-3 in the absence and presence of detection and treatment. Patient 1 does not receive treatment before surpassing the death threshold. Patients 2-3 are detected and treated and are removed from the infectious cohort at the time of detection and treatment. (D) Cumulative burden-time is calculated as the sum of the areas under each patient's disease burden curve (above the symptom threshold). Shaded areas (of any color) denote this cumulative burden-time for each patient in the absence of detection and treatment. Red shaded areas represent each patient's burden-time prior to the point of detection and treatment. Green shaded areas represent the burden-time averted through detection and treatment.

Figure S1.4: Evaluating the Impact of Detection and Treatment on TB Morbidity

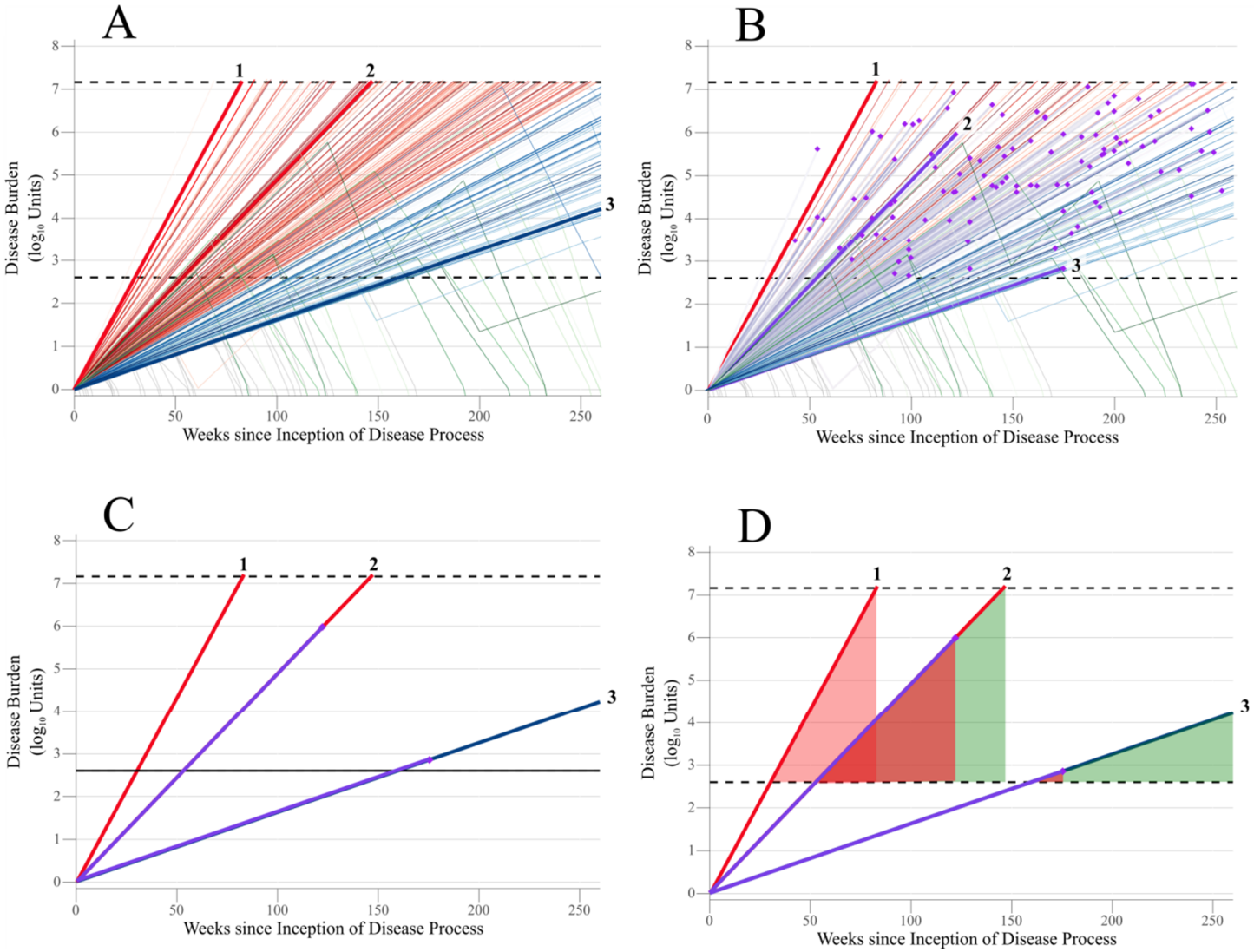

REFERENCES

1. Waitt CJ, Squire SB. A systematic review of risk factors for death in adults during and after tuberculosis treatment. Int J Tuberc Lung Dis. **2011**; 15(7):871–885.
2. Lopez B, Aguilar A, Orozco H, Burger M, Espitias C, Ritacco V, et al. A marked difference in pathogenesis and immune response induced by different *Mycobacterium tuberculosis* genotypes. Clin Exp Immunol. **2003**; 133:30–37.
3. Dormans J, Burger M, Aguilar D, Hernandez-Pando R, Kremer R, Roholl P, et al. Correlation of virulence , lung pathology , bacterial load and delayed type hypersensitivity responses after infection with different *Mycobacterium tuberculosis* genotypes in a BALB/c mouse model. Clin Exp Immunol. **2004**; 137:460–468.
4. Marquina-Castillo B, Garcia-Garcia L, Ponce-de-Leon P, Jimenez-Corona M, Bobadilla-del-Valle M, Cano-Arellano B, et al. Virulence , immunopathology and transmissibility of selected strains of *Mycobacterium tuberculosis* in a murine model. Immunology. **2009**; 128(1):123–133.
5. Gill WP, Harik NS, Whiddon MR, Liao RP, Mittler JE, Sherman DR. A replication clock for Mycobacterium tuberculosis. Nat Med. **2009**; 15(2):211–214.
6. McDaniel MM, Krishna N, Handagama WG, Eda S, Ganusov V. Quantifying limits on replication, death, and quiescence of *Mycobacterium tuberculosis* in mice. Front Microbiol. **2016**; 7:862.
7. Salie M, Merwe L van der, Möller M, Daya M, Spuy GD van der, Helden PD Van, et al. Associations between human leukocyte antigen class i variants and the *Mycobacterium tuberculosis* subtypes causing disease. J Infect Dis. **2014**;

209:216–223.

8. Caws M, Thwaites G, Dunstan S, Hawn TR, Lan N, Thuong N, et al. The influence of host and bacterial genotype on the development of disseminated disease with *Mycobacterium tuberculosis*. PLoS Pathog. **2008**; 4(3):e1000034.
9. Tiemersma EW, Werf MJ van der, Borgdorff MW, Williams BG, Nagelkerke NJD. Natural history of tuberculosis: duration and fatality of untreated pulmonary tuberculosis in HIV negative patients: A systematic review. PLoS One. **2011**; 6(4):e17601.
10. Botesteanu D, Lee J, Levy D. Modeling the dynamics of high-grade serous ovarian cancer progression for transvaginal ultrasound-based screening and early detection. PLoS One. **2016**; 11(6):e0156661.
11. Sreeramareddy CT, Panduru K V, Menten J, Ende J Van den. Time delays in diagnosis of pulmonary tuberculosis: a systematic review of literature. BMC Infect Dis. **2009**; 9:91.
12. The Centers for Disease Control and Prevention (CDC). Core curriculum on tuberculosis : what the clinician should know. 6th Ed. Centers Dis. Control Prev. Natl. Cent. HIV/AIDS, Viral Hepatitis, STD, TB Prev. Div. Tuberc. Elimin. Atlanta; 2013.
13. World Health Organization (WHO), International Union Against Tuberculosis and Lung Disease (IUATLD), Royal Netherlands Tuberculosis Association (KNCV). Revised international definitions in tuberculosis control. Int J Tuberc Lung Dis. **2001**; 5(3):213–215.
14. Shea KM, Kammerer JS, Winston CA, Navin TR, Horsburgh CR. Estimated rate

of reactivation of latent tuberculosis infection in the United States, overall and by population subgroup. Am J Epidemiol. **2014**; 179(2):216–225.

15. Lin PL, Rodgers M, Smith L, Bigbee M, Myers A, Bigbee C, et al. Quantitative comparison of active and latent tuberculosis in the cynomolgus macaque model. Infect Immun. **2009**; 77(10):4631–4642.
16. Capuano SV 3rd, Croix DA, Pawar S, Zinovik A, Myers A, Lin PL, et al. Experimental *Mycobacterium tuberculosis* infection of cynomolgus macaques closely resembles the various manifestations of human M. tuberculosis infection. Infect Immun. **2003**; 71(10):5831–5844.
17. Lin PL, Coleman T, Carney JPJ, Lopresti BJ, Tomko J, Fillmore D, et al. Radiologic responses in cynomolgus macaques for assessing tuberculosis chemotherapy regimens. Antimicrob Agents Chemother. **2013**; 57(9):4237–4244.
18. Lin PL, Ford CB, Coleman MT, Myers AJ, Gawande R, Ioerger T, et al. Sterilization of granulomas is common in active and latent tuberculosis despite within-host variability in bacterial killing. Nat Med. Nature Publishing Group; **2014**; 20(1):75–79.
19. Berg A. The prognosis of open pulmonary tuberculosis. A clinical-statistical study. Acta Tuberc Scand. **1939**; Supplement:1–206.
20. Kanda R, Nagao T, Tho N Van, Ogawa E, Murakami Y, Osawa M, et al. Factors affecting time to sputum culture conversion in adults with pulmonary tuberculosis: a historical cohort study without censored cases. PLoS One. **2015**; 10(11):e0142607.
21. John J, Draper N. An alternative family of transformations. Appl Stat. **1980**;

29(2):190–197.

22. Stein M. Large sample properties of simulations using Latin hypercube sampling. Technometrics. **1987**; 29(2):143–151.

23. Smith AFM, Gelfand AE. Bayesian statistics without tears: a sampling-resampling perspective. Am Stat. **1992**; 46(2):84–88.

24. World Health Organization (WHO). Global tuberculosis report 2016. Geneva; 2016.

25. Davis JL, Cattamanchi A, Cuevas LE, Hopewell PC, Steingart KR. Diagnostic accuracy of same-day microscopy versus standard microscopy for pulmonary tuberculosis: a systematic review and meta-analysis. Lancet Infect Dis. Elsevier Ltd; **2013**; 13(2):147–154.

26. Steingart KR, Schiller I, Horne DJ, Pai M, Boehme CC, Dendukuri N. Xpert ® MTB / RIF assay for pulmonary tuberculosis and rifampicin resistance in adults. Cochrane Database Syst Rev. **2014**; Jan 21(1):CD009593.

27. Dowdy DW, Chaisson RE. The persistence of tuberculosis in the age of DOTS: reassessing the effect of case detection. Bull World Health Organ. **2009**; 87(4):296–304.

28. Menzies NA, Cohen T, Lin HH, Murray M, Salomon JA. Population health impact and cost-effectiveness of tuberculosis diagnosis with Xpert MTB/RIF: a dynamic simulation and economic evaluation. PLoS Med. **2012**; 9(11):e1001347.

APPENDIX B:

SUPPLEMENTARY INFORMATION FOR CHAPTER 4

SUPPLEMENTARY METHODS

Model Summary

TB Natural History

Populations in our model are categorized and described by core states of TB infection and substates of resistance status (DS-TB or MDR-TB), TB treatment history (new or previously-treated), and HIV status (Figure 4.1).

TB infection results from a density-dependent transmission process. Upon initial infection, populations may progress rapidly to incipient/preclinical/asymptomatic TB (hereafter referred to as early-active TB) or may develop latent infection; those latently infected may reactivate to early-active TB at a constant rate. Individuals in states of early-active TB, symptomatic active TB, ineffectively treated TB, or diagnosed-untreated TB contribute infectious person-time to transmission (with reduced infectiousness and mortality associated with early-active or ineffectively treated TB). Self-cure (with return to the susceptible state) may occur at a constant rate during early-active or active TB.

When TB patients develop fully symptomatic active TB, they may initiate first-line or (in cases of MDR-TB) second-line treatment. Upon initiating treatment, TB patients are separated into states of effective or ineffective treatment; those who complete effective treatment regimens experience culture conversion by the end of the treatment duration. (In the absence of DST, MDR-TB patients can only initiate ineffective first-line treatment). After effective treatment, TB patients may either achieve durable cure (becoming susceptible again) or may eventually relapse; after ineffective treatment,

patients may either immediately re-initiate treatment or return to symptomatic active TB. During any TB treatment state, patients may be lost to follow-up; all those lost from ineffective treatment return to active TB, while those lost from effective treatment may return to active TB or (having received a sufficiently curative treatment before default) may achieve durable cure.

MDR-TB infections may result from transmission of MDR-TB or from acquisition of drug resistance during treatment of DS-TB. MDR-TB may develop from transmission in populations who are susceptible to TB or (as a superinfection) in populations who are latently infected with DS-TB. (Similarly, populations latently infected with MDR-TB may be subsequently superinfected with DS-TB.) MDR-TB may be acquired during first-line treatment (including ineffective treatment, as well as effective treatment with future relapse).

TB treatment history influences several of the dynamics described above. TB patients with a history of first-line treatment have an increased probability of acquiring MDR-TB upon retreatment. Similarly, they have a reduced probability of receiving effective first-line treatment and a reduced probability of durable cure following effective first-line treatment. Among patients with MDR-TB who have received DST and initiated second-line therapy, those who are treated with second-line therapy unsuccessfully become treatment-ineligible (as we assume that an attempted second-line treatment may include changes in drug regimen if treatment fails to resolve symptoms).

HIV status also affects a variety of the dynamics of TB infection. HIV infected populations have higher rates of TB-independent mortality, and those with low CD4 status concurrent with active (untreated) TB experience an additional mortality associated

with HIV/TB interactions. The probability of rapid TB progression upon initial infection is increased in HIV-infected populations, while the probability of TB self-cure is reduced. In populations latently infected with TB, HIV co-infection increases the rate of TB reactivation and reduces the degree of protection against a rapidly progressing superinfection. The infectiousness of each TB disease state is somewhat lower in populations with HIV co-infection than in their HIV-uninfected counterparts. Finally, due to more rapid disease progression and more frequent encounters with the health system, active TB reaches diagnosis and treatment initiation more quickly for HIV-infected populations.

TB Transmission

TB transmission occurs as a function of time-varying transmission efficiency coefficients and the size of the infectious TB population. As previously described, we define the transmission efficiency of each strain (DS-TB vs. MDR-TB) as the number of new infections which would develop in a susceptible population from each infectious person-year contributed by prevalent infectious DS-TB or prevalent infectious MDR-TB, respectively. An initial coefficient β_S^0 is used to define the equilibrium transmission efficiency of DS-TB cases. Due to secular trends in overall TB incidence in recent years, we allow for the overall transmission of DS-TB $\beta_S(t)$ to decline at an annual geometric rate d_S after the year t_S. In Vietnam, we define t_S as the first year with data used to calibrate our epidemics ($t_S = 1996$). In South Africa, due to the HIV/TB co-epidemic over 1995-2010, we felt there was insufficient evidence for secular declines in DS-TB transmission in HIV-uninfected populations starting in the first year of survey data

(2001). Instead, we assumed any such declines would not occur until 2010 ($t_S = 2010$). Therefore, we define the transmission efficiency of DS-TB as follows:

$$\beta_S(t) = \beta_S^0 \times \begin{cases} 1 & \text{if } t < t_S \\ (1 + d_S)^{t - t_S} & \text{if } t \geq t_S \end{cases} \quad (1)$$

In all MDR-TB scenarios we examined, the transmission efficiency of MDR-TB, $\beta_R(t)$, is initialized at the start of the modern MDR-TB epidemic (in the year t_R^0) with an initial value determined by the initial transmission efficiency of DS-TB β_S^0 and a relative efficiency term E_R. In the Shrinking Efficiency Deficit scenario, the transmission efficiency of MDR-TB is allowed to increase annually (through an annual percentage increase d_R in the relative efficiency coefficient) beginning in the year t_R. (The rate of increase term d_R is set equal to zero in both the No Efficiency Deficit and Constant Efficiency Deficit scenarios, and the relative efficiency term E_R is set equal to one in the No Efficiency Deficit scenario.) Therefore, the transmission efficiency of MDR-TB is defined as:

$$\beta_R(t) = \beta_S^0 \times \begin{cases} 0 & \text{if } t < t_R^0 \\ E_R & \text{if } t_R^0 \leq t < t_R \\ E_R + (t - t_R) d_R & \text{if } t \geq t_R \end{cases} \quad (2)$$

In this way, any declines in DS-TB secular transmission efficiency (after time t_S) are not necessarily mirrored by MDR-TB, as trends in the transmission efficiency of DS-TB and MDR-TB are likely to occur through different processes (though $\beta_R(t)$ is never permitted to exceed $\beta_S(t)$).

Drug Sensitivity Testing and Second-line Treatment

The probability of MDR-TB cases receiving DST and initiating second-line therapy, *DST*(*t*), is defined as a country-specific time-varying quantity that depends on

the availability of DST and individualized second-line regimens. We assume that DST is not widely available prior to 2006. We then separately define the probability of receiving DST during two time intervals: from 2006 to the time of Xpert® MTB/RIF adoption by national TB programs t_{Xpert} (modeled as 2011 in South Africa and 2013 in Vietnam); and from t_{Xpert} to 2016. At t_{Xpert}, we use WHO estimates of each country's provision of DST among all TB cases (data was not yet stratified by new and retreatment cases) and the proportion of detected MDR-TB cases that initiated treatment to estimate DST coverage, $\widehat{DST}(t_{Xpert})$. We modeled the availability of DST and the initiation of second-line treatment as a linear increase in $DST(t)$from $DST(2006)=0$ to the value of $\widehat{DST}(t_{Xpert})$ that we estimated from WHO data. We similarly used WHO estimates of each country's DST provision (stratified by new and retreatment cases) and treatment initiation of detected MDR-TB cases to estimate $\widehat{DST}(2016)$. Again, we modeled the availability of DST as a linear increase from the estimated $\widehat{DST}(t_{Xpert})$ to $\widehat{DST}_N(2016)$ and $\widehat{DST}(2016)$. We then assumed the linear trends of DST availability will each continue into the future beyond 2016 until eventually reaching 100% coverage. These trends are plotted graphically in Figure S2.2.1 below, and are summarized as follows:

$$DST_N(t) = \begin{cases} 0 & \text{if } t < 2006 \\ \frac{\widehat{DST}(t_{Xpert})}{t_{Xpert}-2006}(t-2006) & \text{if } 2006 \le t < t_{Xpert} \\ \min[\,100\%\,, & \text{if } t \ge t_{Xpert} \\ \frac{\widehat{DST}_N(2016)-\widehat{DST}(t_{Xpert})}{2016-t_{Xpert}}(t-t_{Xpert}) + \widehat{DST}(t_{Xpert})] & \end{cases} \quad (3)$$

$$DST_P(t) = \begin{cases} DST_N(t) & \text{if } t < t_{Xpert} \\ \min[100\%, & \text{if } t \geq t_{Xpert} \\ \frac{\widehat{DST}_P(2016) - \widehat{DST}(t_{Xpert})}{2016 - t_{Xpert}}(t - t_{Xpert}) + \widehat{DST}(t_{Xpert})] & \end{cases} \quad (4)$$

Figure S2.1: Modeled Trends in the Availability of Drug Sensitivity Testing and Second-line Treatment

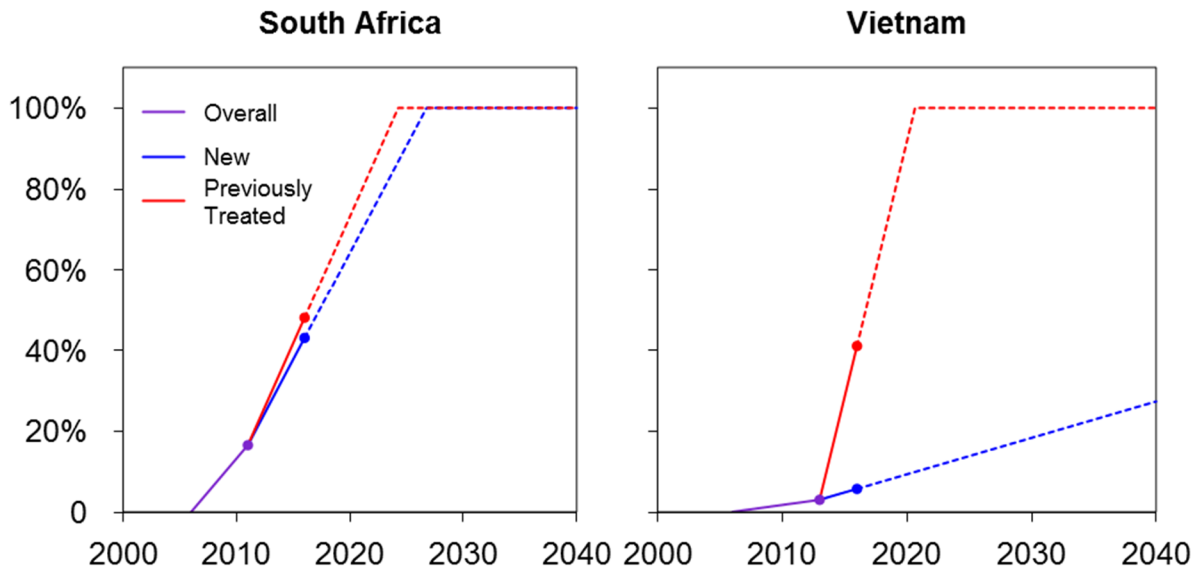

Each line represents the time-varying probability of DST for MDR-TB cases after TB diagnosis. Points represent country-specific estimates in DST availability over time drawn from WHO reports. From 2006 to 2011 in South Africa and 2013 in Vietnam, estimates of only overall (cumulative) DST were reported and therefore used for both new and previously-treated cases. Dashed lines represent current trends in DST extrapolated into the future until reaching 100% coverage.

Births and Deaths

We make a simplifying assumption of a steady-state population size. "Births" (entry of new 15-year olds into the population) are forced to equal cumulative deaths due to TB, HIV, and background mortality. New adults are added to treatment-naïve susceptible or latently infected states. The proportions of new adults which enter into latent TB states are determined by the cumulative TB forces of infection over the preceding 15 years (approximated by an exponential distribution using the transmission efficiencies of TB at the midpoint 7.5 years prior and the current prevalence of infection; see differential equations below). These new latently-infected adults are divided between DS-TB and MDR-TB infections according to the ratio of each strain's approximate force of infection over the preceding 15 years.

HIV Infection and ART Initiation

Our model does not attempt to replicate the complex dynamics and partner networks which characterize transmission in HIV epidemics. To capture macro trends in the HIV epidemics of South Africa and Vietnam, we fitted our model to reported UNAIDS estimates of the prevalence of HIV among adults in yearly intervals from 1990 to 2016 (Figure S2.2.2A below) in the following manner. At any time t_1, the prevalence of HIV infections in our fixed population of 100,000 is calculated as the sum of individuals in any HIV-infected substate *V(t)* divided by the total population size:

$$P_{HIV}(t_1) = \frac{\sum V(t_1)}{N} \quad (5)$$

After a time interval from $[t_1,t_2)$, the prevalence of HIV survivors (without new incident infections) $P^0_{HIV}(t_2)$ would equal the prevalence at t_1 minus the number of deaths

(based on the state-specific cumulative mortality rates μ_{All}^{V}) from all HIV-infected states during the time interval:

$$P_{HIV}^{0}(t_2) = P_{HIV}(t_1) - \frac{\sum V(t_1)\mu_{All}^{V}}{N} \tag{6}$$

For reference, we use UNAIDS country-specific estimates of the prevalence of HIV among adults 15 years and older $\widehat{P_{HIV}}(Y)$ for the discrete time points $Y \in \{1990, 1991, \ldots, 2016\}$. The expected HIV prevalence at time t_2 is then calculated by linear interpolation between the two time points nearest in time to t_2 (the maximum Y less than t_2 and the minimum Y greater than t_2):

$$\begin{aligned} \widehat{P_{HIV}}(t_2) &= \widehat{P_{HIV}}(max(Y|Y \le t_2)) \\ &+ \left[\frac{\widehat{P_{HIV}}(min(Y|Y \ge t_2)) - \widehat{P_{HIV}}(max(Y|Y \le t_2))}{(min(Y|Y \ge t_2)) - (max(Y|Y \le t_2))} \times (t_2 - (max(Y|Y \le t_2)))\right] \end{aligned} \tag{7}$$

To reach the necessary $P_{HIV}(t_2)$ between $[t_1,t_2)$, the number of new HIV infections in this interval $I_{HIV}(t_1, t_2)$ must therefore equal the expected prevalence minus the prevalence of surviving HIV infections multiplied by the population size:

$$I_{HIV}(t_1, t_2) = (\widehat{P_{HIV}}(t_2) - P_{HIV}^{0}(t_2)) \times N \tag{8}$$

The rate of new HIV infections during the interval is determined by the number of new HIV infections needed and the size of currently HIV-uninfected populations in states X^{U}:

$$FOI_{HIV}(t_1, t_2) = \frac{I_{HIV}(t_1,t_2)}{\sum X^{U}(t_1)} \tag{9}$$

All incident HIV infections are modeled as transitions from an HIV-uninfected state to a state of HIV infection with a High CD4 count. After 2016, the expected rate of change in HIV prevalence is assumed to equal that of 2015-2016. At no time is the rate of new HIV infections allowed to become negative.

Prior to 2004, we assume that antiretroviral therapy (ART) is not widely available. Between 1990 and 2004, individuals in High CD4 substates gradually progress

to Low CD4 substates where they remain until death. Between 2004 and 2010, we assume that ART is available only to those with Low CD4 counts. During this time, the time-varying rate of ART initiation is derived such that the proportion of HIV-infected patients receiving ART are consistent with UNAIDS estimates (Figure S2.2B below).

The rate of ART initiation is fitted to UNAIDS estimates in a similar manner used to fit HIV prevalence. We define the proportion of HIV-infected individuals receiving ART at any time *A(t)* as equal to the cumulative size of ART substates X^A divided by the cumulative size of all HIV-infected substates *V*:

$$A(t) = \frac{\sum X^A(t)}{\sum V(t)} \quad (10)$$

After a time interval from $[t_1, t_2)$, the number of survivors *continuing* to receive ART $X^{A,0}(t_2)$ would equal the number receiving ART at t_1 minus the number of deaths (based on the state-specific cumulative mortality rates μ_{All}^{A}) from all ART substates during the time interval:

$$\sum X^{A,0}(t_2) = \sum X^A(t_1)(1 - \mu_{All}^{A}) \quad (11)$$

The total ART coverage (continued and newly initiated) expected at time t_2 is again fitted to UNAIDS estimates. Based on the shape of UNAIDS estimates of this quantity (Figure S2.2B), we used nonlinear (weighted) least squares regression to fit a sigmoid function (assuming ART coverage approaches a future asymptote A_{max} at 60%) of the form:

$$\hat{A}(t) = \frac{A_{max}}{1+e^{-bt-c}} \quad (12)$$

To reach this new level of ART coverage, the number of new ART initiations during the interval $I_{ART}(t_1, t_2)$ can be calculated as the number of total individuals receiving ART at t_2 minus the number *continuing* to receive ART:

$$I_{ART}(t_1, t_2) = \left(\hat{A}(t_2)\sum V(t_2)\right) - \sum X^{A,0}(t_2) \quad (13)$$

The time-varying rate of ART initiation $\Omega(t_1, t_2)$ is derived according to the number of required new patients initiating ART $I_{ART}(t_1, t_2)$ and the population eligible to receive ART at time t_2. Between 2004 and 2010, all new ART initiation is restricted to Low CD4 populations X^L. After 2010, we allow for ART initiation to occur in both Low CD4 and High CD4 populations X^H to reflect improved access to HIV care and changing national guidelines for ART provision. However, ART initiation in High CD4 populations occurs at a lower rate than initiation in Low CD4 populations, according to an initiation coefficient k_H (that is, for every one High CD4 patient, there are only k_H High CD4 patients *eligible* for ART). Therefore, the time-varying rate of ART initiation is defined as follows:

$$\Omega(t_1, t_2) = \begin{cases} 0 & \text{if } t_2 \leq 2006 \\ \frac{I_{ART}(t_1,t_2)}{\sum X^L(t_2)} & \text{if } 2006 < t_2 \leq 2010 \\ \frac{I_{ART}(t_1,t_2)}{\sum (X^L(t_2)+k_H X^H(t_2))} & \text{if } t_2 > 2010 \end{cases} \quad (14)$$

Finally, among HIV-infected patients receiving TB treatment, this rate of ART initiation is increased by a factor k_{tb} to reflect increased HIV screening in patients diagnosed with TB. Therefore, the total rate of ART initiation in TB treatment states equals $k_{tb}\Omega(t_1, t_1)$.

Figure S2.2: Modeled Trends in HIV Incidence and ART Coverage

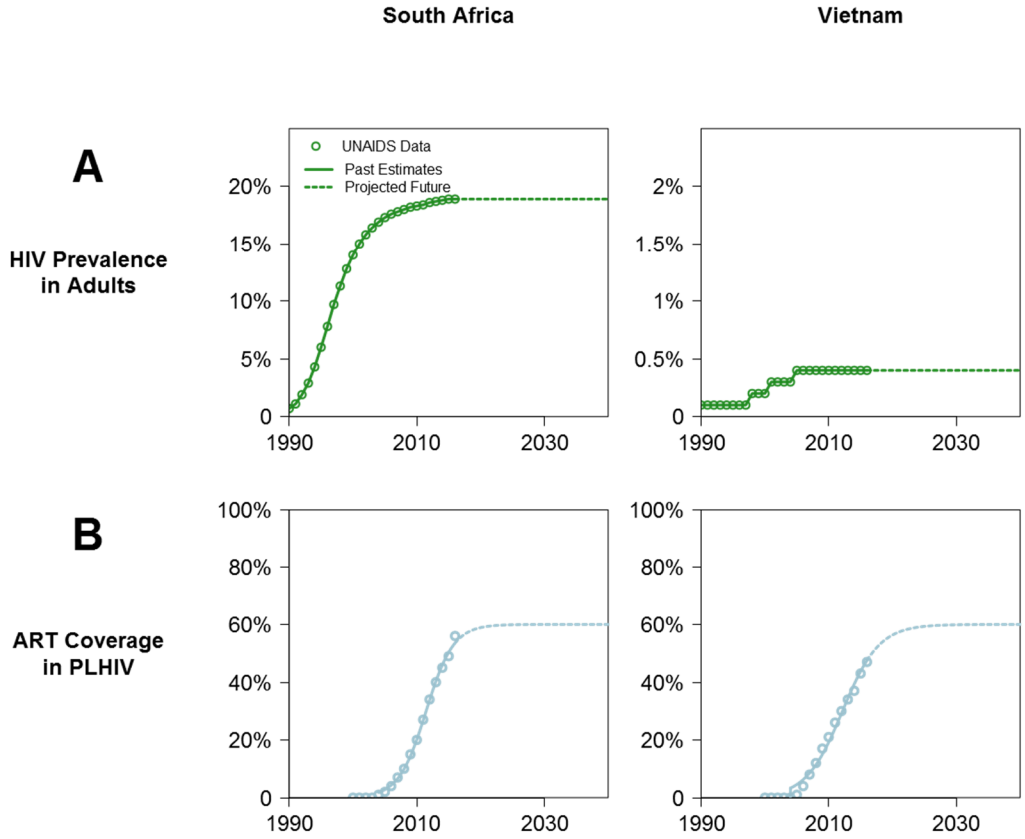

Plots present country-specific trends in HIV prevalence or ART coverage. (A) The prevalence of HIV among adults 15 years and older. Points represent UNAIDS estimates of prevalence at yearly intervals, while lines represent our interpolation/extrapolation of incidence rates from those data. (B) The proportion of persons living with HIV currently receiving ART. Points represent ART coverage from UNAIDS estimates. These estimates were used to fit sigmoid functions with ART coverage approaching a maximum of 60%. Lines represent the fitted functions which were used to model ART coverage. Dashed lines represent current trends extrapolated into the future.

Differential Equations

Notation and Conventions

Core TB states are defined according to the following abbreviations:

S = susceptible

L = latently infected

E = early-active TB (incipient TB, not yet seeking care)

A = symptomatic active TB

B_{1e} = on effective first-line treatment (leading to culture conversion)

B_{1i} = on ineffective first-line treatment (remaining infectious)

W = post-treatment, will relapse

B_{2e1} = on effective second-line treatment (the initial six months of MDR-TB treatment, remaining partially infectious)

B_{2e2} = on effective second-line treatment (the continuation phase of MDR-TB treatment, leading to culture conversion after 14 months)

B_{2i} = on ineffective second-line treatment (remaining infectious)

Z = post second-line treatment, will relapse

F = post second-line treatment, active MDR-TB

C = diagnosed untreated MDR-TB

X = any state above

I = any infectious state above $\{E, A, B_{1i}, B_{2e1}, B_{2i}, F, C\}$

G = any diagnosis/treatment state above $\{B_{1e}, B_{1i}, B_{2e1}, B_{2e2}, B_{2i}, C\}$

Populations in any of the above core TB states are additionally categorized using the following subscripts and superscripts (some combinations may be null):

T = treatment status (a value of N indicates TB treatment-naïve; a value of P indicates previously-treated for TB)

D = drug sensitivity status (a value of S indicates DS-TB infections; a value of R indicates MDR-TB infections)

V = HIV status (a value of U indicates HIV-uninfected; a value of H indicates HIV-infected with High CD4 counts; a value of L indicates a HIV-infected with Low CD4 counts; a value of A indicates HIV-infected and receiving ART)

As described above, several rates and probabilities of core TB states are modified by TB treatment history and HIV status. Unless otherwise noted, parameter values with a superscript of naught ("0") represent the rate/probability in HIV-negative, treatment-naïve patients; values with a superscript of $V \in \{U, H, L, A\}$ reflect the multiplicative factor associated with each respective HIV substate; and values with a superscript of $T \in \{N, P\}$ reflect the multiplicative factor associated with each respective category of TB treatment history. Thus, if ρ^0 represents the probability of rapid progression in HIV-uninfected populations, then $\rho^0\rho^{\mathrm{H}}$ represents the probability of rapid progression in HIV-infected populations with a High CD4 count. (Multiplicative factors with superscripts of U or N are set equal to one; thus $\rho^0\rho^{\mathrm{U}} = \rho^0$.)

Populations Susceptible to TB Infection

The total population is initiated at a size of 100,000 and forced to remain at steady-state. The size of newly added populations is forced to equal the number of deaths in the population at any time, defined by the rates of background mortality (μ^0), HIV-associated mortality (μ^V), and active-TB associated mortality (μ_{tb} , reduced by factors i_X associated with early/incompletely treated active TB):

$$M(t) = \sum_{V\in\{U,H,L,A\}}\left[\sum_{X^V\in I_D^V}\left(X^V(t)(\mu^0+\mu^V+\mu_{tb})\right)+\sum_{X^V\notin I_D^V}\left(X^V(t)(\mu^0+\mu^V)\right)\right] \quad (15)$$

All newly added populations are divided between susceptible and latently infected states (described above). We define the forces of infection applied to individuals before entering the population at age 15 as using the approximate forces of infection distributed over the preceding 7.5 years:

$$\hat{FOI}_D\,(t-7.5) = \sum_{V\in\{U,H,L,A\}}\left[i^V\sum_{X^V\in\{I_D^V\}}(X^V(t)i_X\beta_D(t-7.5))\right] \quad (16)$$

These approximate forces of infection are used to determine the number of new 15-year olds entering the population as susceptible to TB infection. Newly added susceptible populations S_N occur to replace deaths (excluding those latently infected) and those who self-cure (according to the rate of self-cure (ν^0)) without treatment. Transitions from the susceptible state occur due to new infection (dependent on the time-varying forces of infection ($FOI_D(t)$), described below) and death:

$$\frac{dS_N^U}{dt} = M(t)e^{-\sum_{D\in\{S,R\}}\left(\hat{FOI}_D(t-7.5)\right)}+\nu^0\left(\sum_{D\in\{S,R\}}E_{ND}^U(t)+A_{ND}^U(t)\right)-S_N^U(t)\left(\mu^0+\sum_{D\in\{S,R\}}FOI_D(t)\right) \quad (17)$$

All newly susceptible 15-year olds are modeled as initially HIV-uninfected (ignoring contributions from perinatal infection). In HIV-infected populations, new susceptible populations occur only through TB self-cure:

$$\text{For V} \in \{H, L, A\}:$$
$$\frac{dS_N^V}{dt} = \nu^0 \nu^V \left(\sum_{D \in \{S,R\}} E_{ND}^V(t) + A_{ND}^V(t) \right) - S_N^V(t) \left(\mu^0 + \mu^V + \sum_{D \in \{S,R\}} FOI_D(t) \right) \quad (18)$$

Transitions into the previously-treated susceptible state S_P occur as the result of self-cure ($\nu^0 \nu^V$) of previously-treated patients with early-active E_P (due to new infection after previous cure) or active TB A_P (after failed treatment or new infection after previous cure).

Effective first-line treatment B1eS can result in also durable cure (returning to the susceptible state S_P) after treatment has been completed (duration $\tau_{t1} = 6$ months) without the acquisition of MDR during treatment (based on the probability of MDR acquisition during treatment $\alpha^0 \alpha^T$) in two ways: a) treatment is completed without loss to follow-up (based on the probability of loss during first-line treatment δ_1) and without subsequent relapse (based on the probability of relapse among those with DS-TB who complete first-line treatment $\omega_1^0 \omega_1^T$); or b) treatment is not completed due to loss to follow-up but after a sufficiently curative treatment has been received (based on the proportion of those lost during first-line treatment who remain culture positive at the time of loss η_1). Durable cure can also be achieved after the continuation phase of effective second-line B_{2e2} treatment (duration $\tau_{22} = 14$ months) if relapse does not occur (probability $1 - \omega_2^0$). Transitions out of the previously-treated susceptible state occur due to death or new infection.

$$\begin{aligned}\frac{dS_P^V}{dt} &= \nu^0\nu^V\left(\sum_{D\in\{S,R\}} E_{PD}^V(t) + A_{PD}^V(t)\right)\\ &+\sum^{T\in\{S,P\}}\left[B_{1eST}^V(t)\frac{1-\alpha^0\alpha^T}{\tau_{t1}}((1-\delta_1)(1-\omega_1^0\omega_1^T)+\delta_1(1-\eta_1))\right]\\ &+B_{2e2}^V(t)(1-\omega_2)/\tau_{22} - S_P^V(t)\left(\mu^0+\mu^V+\sum_{D\in\{S,R\}} FOI_D(t)\right)\end{aligned} \quad (19)$$

Transmission of TB Infection

New latently infected populations L_N may result from the addition of previously-infected 15-year olds (all assumed to be HIV-uninfected), new infections, or superinfection of already latently-infected populations. The total number of new 15-year olds is equal to the number of deaths *M(t)* as above, and the proportion that enters with a previous latent infection is determined by an exponential distribution of the cumulative estimated force of infection over 15 years ($\sum_{D\in\{S,R\}}(\hat{FOI}_D\ (t-7.5))$); these latent infections are divided between DS-TB and MDR-TB weighted by the strain-specific force of infection during this period ($\hat{FOI}_D\ (t-7.5)$).

New infections from susceptible states S occur based on the current force of infection $FOI_D(t)$ and the probability that new infections do not progress rapidly to early-active TB ($1-\rho^0$). The time-varying force of infection for a given TB strain $FOI_D(t)$ describes the cumulative, state-adjusted infectious person-time contributed by all TB cases. For a given infectious state I_D^V, the population size of $I_D^V(t)$ is reduced by the relative infectiousness of the core TB state ix (associated with early-active disease or incomplete/ineffective treatment) and the relative infectiousness of the HIV substate i^V, and multiplied by the transmission efficiency $\beta_D(t)$ (defined above).

$$FOI_D(t) = \sum_{V\in\{U,H,L,A\}}\left[i^V\sum_{X^V\in\{I_D^V\}}(X^V(t)i_X\beta_D(t))\right] \quad (20)$$

Transitions between MDR-TB and DS-TB latent states (e.g., L_{NS} to L_{NR}) occur due to exogenous superinfections which do not progress rapidly ($1-\rho^0$). Additional protection against rapid infection is afforded by an existing latent infection (based on the reduced probability of rapid progression in latently infected populations $1-\lambda^0$). The proportions of superinfections which change state (e.g., latent DS-TB to latent MDR-TB) are weighted by the strain-specific transmission efficiencies such that, if $\beta_S(t)=\beta_R(t)$, then half of reinfected latent DS-TB patients will transition to latent MDR-TB patient and vice versa.

Transitions out of the new, latently infected state occur due to background mortality, reactivation to early-active TB (based on the constant rate of reactivation (r^0)), or reinfection followed by rapid progression (despite the protection afforded by an existing latent infection ($(1-\lambda^0)\rho^0$)).

$$\begin{aligned}\frac{dL_{ND}^U(t)}{dt} &= M(t)\frac{\hat{FOI}_D(t-7.5)}{\sum_{D\in\{S,R\}}(\hat{FOI}_D(t-7.5))}\left(1-e^{-\sum_{D\in\{S,R\}}(\hat{FOI}_D(t-7.5))}\right)\\ &+S_N^U(1-\rho^0)FOI_D(t)\\ &+(1-\rho^0(1-\lambda^0))\left[\frac{\beta_D(t)}{\beta_D(t)+\beta_{\overline{D}}(t)}FOI_D(t)L_{N\overline{D}}^U(t)-\frac{\beta_{\overline{D}}(t)}{\beta_D(t)+\beta_{\overline{D}}(t)}FOI_{\overline{D}}(t)L_{ND}^U(t)\right]\\ &-L_{ND}^U(t)(r^0+\mu^0)-(1-\lambda^0)\rho^0FOI_D(t)\sum_{D\in\{S,R\}}(L_{ND}^U(t))\end{aligned} \quad (21)$$

As described above, all new 15-year olds are assumed to be initially uninfected. Therefore, new additions to HIV-infected latent states occur due to new infections of susceptible populations and superinfections of latent populations. Losses occur in the same manner as HIV-uninfected latent populations.

$$\begin{aligned}&\text{For V}\in\{H,L,A\}:\\ \frac{dL_{ND}^V}{dt} &= S_N^V(1-\rho^0\rho^V)FOI_D(t)\\ &+(1-\rho^0\rho^V(1-\lambda^0\lambda^V))\left[\frac{\beta_D(t)}{\beta_D(t)+\beta_{\overline{D}}(t)}FOI_D(t)L_{N\overline{D}}^V(t)-\frac{\beta_{\overline{D}}(t)}{\beta_D(t)+\beta_{\overline{D}}(t)}FOI_{\overline{D}}(t)L_{ND}^V(t)\right]\\ &-L_{ND}^V(t)(r^0r^V+\mu^0+\mu^V)-(1-\lambda^0\lambda^V)\rho^0\rho^VFOI_D(t)\sum_{D\in\{S,R\}}(L_{ND}^V(t))\end{aligned} \quad (22)$$

Among previously-treated populations, latent infections L_P result from new infections of previously-treated TB susceptible populations and superinfections of previously-treated, latently infected populations in the same manner as above. (Newly added 15-year olds are assumed to have negligible previous TB treatment history and are excluded from these populations upon initial entry.)

$$\begin{aligned}\frac{dL_{PD}^{V}(t)}{dt} &= S_P^V(1-\rho^0\rho^V)FOI_D(t) \\ &+(1-\rho^0\rho^V(1-\lambda^0\lambda^V))\left[\frac{\beta_D(t)}{\beta_D(t)+\beta_{\overline{D}}(t)}FOI_D(t)L_{P\overline{D}}^{V}(t)-\frac{\beta_{\overline{D}}(t)}{\beta_D(t)+\beta_{\overline{D}}(t)}FOI_{\overline{D}}(t)L_{PD}^{V}(t)\right] \\ &-L_{PD}^{V}(t)(r^0r^V+\mu^0+\mu^V)-(1-\lambda^0\lambda^V)\rho^0\rho^VFOI_D(t)\textstyle\sum_{D\in\{S,R\}}(L_{PD}^{V}(t))\end{aligned} \quad (23)$$

Progression into early-active states E occur from a) a susceptible state S according to the force of infection and the proportion of infections which progress rapidly ($\rho^0\rho^V$); b) from a latent state L due to reactivation of endogenous infection according to the rate of reactivation (r^0r^V); or c) from rapid progression of a recent, exogenous superinfection according to the proportion of infections which progress rapidly, reduced by the protection afforded by an existing latent infection ($(1-\lambda^0\lambda^V)\rho^0\rho^V$). Transitions from the early-active state occur due to death, spontaneous resolution, or progression to active TB.

$$\begin{aligned}\frac{dE_{TD}^{V}}{dt} &= S_T^V(t)\rho^0\rho^VFOI_D(t)+L_{TD}^{V}r^0r^V+(1-\lambda^0\lambda^V)\rho^0\rho^VFOI_D(t)\textstyle\sum_{D\in\{S,R\}}(L_{TD}^{V}) \\ &-E_{TD}^{V}(t)(1/a+\nu^0\nu^V+\mu^0+\mu^V+i_E\mu_{tb})\end{aligned} \quad (24)$$

Active TB

Transitions into the symptomatic, active TB states A occur from the progression of early-active TB E according to the duration of early-active TB a. Transitions from the active disease state occur due to death, spontaneous resolution, or treatment initiation.

$$\frac{dA_{ND}^{V}}{dt}=aE_{ND}^{V}(t)-A_{ND}^{V}\left(\frac{1}{x^0x^V}+\nu^0\nu^V+\mu^0+\mu^V+\mu_{tb}\right) \quad (25)$$

In those previously treated, active disease A_P may additionally result from: a) relapse among those who will relapse W after the mean time to relapse (τ_ω); b) loss to follow-up (δ_1) during ineffective first-line treatment B_{1i} ; c) loss to follow-up during effective treatment B_{1e} provided that culture conversion has not yet occurred ($\delta_1\eta_1$); or d) failing ineffective first-line therapy provided that treatment has been completed without loss to follow-up $(1-\delta_1)$ after treatment duration $\tau_{t1} = 6$ months and that care is not immediately reinitiated $(1-\gamma)$.

$$\begin{aligned}\frac{dA_{PS}^V}{dt} &= aE_{PS}^V(t) + W_S^V(t)(1/\tau_\omega) \\ &+\frac{1}{\tau_{t1}}\sum_{T\in\{N,P\}}\left[(1-\alpha^0\alpha^T)\left(B_{1eST}^V(t)\delta_1\eta_1 + B_{1iST}^V(t)(\delta_1+(1-\delta_1)(1-\gamma))\right)\right] \\ &-A_{PS}^V(t)\left(\frac{1}{x^0x^V}+\nu^0\nu^V+\mu^0+\mu^V+\mu_{tb}\right)\end{aligned} \quad (26)$$

In those with MDR-TB, active disease A_{PR} may also result from the new acquisition of drug resistance during ineffective first-line therapy B_{1iS} based on the probability of MDR acquisition during first-line treatment $\alpha^0\alpha^T$. (Patients with preexisting MDR-TB only initiate ineffective first-line treatment B_{1iR}, described below.)

$$\begin{aligned}\frac{dA_{PR}^V}{dt} &= aE_{PR}^V + W_R^V(t)(1/\tau_\omega) \\ &+\frac{1}{\tau_{t1}}\sum_{T\in\{N,P\}}\left(\alpha^0\alpha^T B_{1iST}^V + B_{1iTR}^V(t)\right)(\delta_1+(1-\delta_1)(1-\gamma)) \\ &-A_{PR}^V(t)\left(\frac{1}{x^0x^V}+\nu^0\nu^V+\mu^0+\mu^V+\mu_{tb}\right)\end{aligned} \quad (27)$$

Among those with MDR-TB who have been diagnosed and received DST, some may be lost before linkage to appropriate second-line therapy while others may not receive second-line therapy based on the specific drug resistance pattern (e.g., extensively drug resistant TB) and available drug regimens. These patients enter in the diagnosed active but untreated MDR-TB state *C*. These patients must first receive DST (with probability $DST_T(t)$, described above) at the time of diagnosis or re-evaluation (after a delay in diagnosis – duration x^0x^V – or at the completion of a failed first-line regimen –

duration $\tau_{t1} = 6$ months). MDR-TB patients eligible to receive DST are those with active, untreated TB A_R; those with pre-existing MDR-TB at the completion of an ineffective first-line regimen; or those with DS-TB who acquire MDR-TB during first-line therapy B_{1eS} with (probability $\alpha^0\alpha^T$). Those receiving a first-line therapy are eligible for a DST re-evaluation provided they complete the first-line regimen without loss to follow-up $(1-\delta_1)$ and reinitiate care immediately upon completion (γ). After receiving DST, these patients are lost/declined second-line treatment with probability *b*. Losses from C occur due to death.

$$\begin{aligned}\frac{dC_R^V}{dt} &= b\sum_{T\in\{N,P\}}\left[DST_T(t)\left(\frac{1}{x^0x^V}A_{RT}^V(t)+\frac{\gamma(1-\delta_1)}{\tau_{t1}}\left(B_{1iRT}^V(t)+\alpha^0\alpha^T B_{1eST}^V(t)\right)\right)\right] \\ &\quad -C_R^V(t)(\mu^0+\mu^V+\mu_{tb})\end{aligned} \tag{28}$$

MDR-TB patients who have initiated second-line treatment without successful completion enter the failed second-line therapy state *F*. These transitions include those who initiate successful treatment B_{2el} but are subsequently lost to follow-up with probability δ_2; those who experience treatment failure B_{2i} (due to ineffective second-line therapy after duration $\tau_{t21} = 6$ months); or those complete treatment but subsequently relapse Z_R (after a mean time to relapse τ_ω). Losses from *F* occur due to death.

$$\frac{dF_R^V}{dt} = \delta_2 B_{2e1}^V(t)+\frac{1}{\tau_{t21}}B_{2i}(t)+\frac{1}{\tau_\omega}Z_R^V(t)-F_R^V(t)(\mu^0+\mu^V+\mu_{tb}) \tag{29}$$

TB Treatment

Upon the initiation of treatment, TB patients are separated between effective and ineffective TB treatment states based on the probability of culture conversion among those who complete treatment ($\sigma_1^0\sigma_1^T$ for first-line therapy and σ_2 for second-line therapy).

Transitions into the effective first-line therapy B_{1e} occur from the symptomatic active TB states A according after a mean delay before diagnosis (duration x^0x^V). Transitions out of B_{1e} occur due to death or ending treatment.

$$\frac{dB^V_{1eNS}}{dt} = A^V_{NS}(t)\frac{\sigma_1^0\sigma_1^N}{x^0x^V} - B^V_{1eNS}(t)(\mu^0 + \mu^V + 1/\tau_{t1}) \tag{30}$$

Among those previously treated, effective first-line therapy B_{1eP} may also be initiated following the failure of a previous first-line treatment regimen B_{1i}. This only occurs provided the previous regimen was completed (after duration $\tau_{t1} = 6$ months) without loss to follow-up $(1 - \delta_1)$, that retreatment is started immediately upon completion of the previous regiment (γ), and that MDR-TB was not acquired during the previous regimen $(1 - \alpha^0\alpha^T)$).

$$\begin{aligned}\frac{dB^V_{ePS}}{dt} &= \sigma_1^0\sigma_1^P\left[\frac{1}{x^0x^V}A^V_{PS}(t) + \frac{1}{\tau_{t1}}\sum_{T\in\{N,P\}}\left(B^V_{1iST}(t)(1-\alpha^0\alpha^T)(1-\delta_1)\gamma\right)\right] \\ &\quad -B^V_{1ePS}(t)(\mu^0 + \mu^V + 1/\tau_{t1})\end{aligned} \tag{31}$$

Among DS-TB patients, transitions into the state of ineffective first-line therapy B_{1iS} occur from the same sources of effective first-line therapy above (according to the probability that treatment will not be successful $1 - \sigma_1^0\sigma_1^N$).

$$\frac{dB^V_{1iNS}}{dt} = A^V_{NS}(t)\frac{1-\sigma_1^0\sigma_1^N}{x^0x^V} - B^V_{1iNS}(t)(\mu^0 + \mu^v + 1/\tau_{t1}) \tag{32}$$

$$\begin{aligned}\frac{dB^V_{iPS}}{dt} &= (1-\sigma_1^0\sigma_1^P)\left[\frac{1}{x^0x^V}A^V_{PS}(t) + \frac{1}{\tau_{t1}}\sum_{T\in\{N,P\}}\left(B^V_{1iST}(t)(1-\alpha^0\alpha^T)(1-\delta_1)\gamma\right)\right] \\ &\quad -B^V_{1ePS}(t)(\mu^0 + \mu^V + 1/\tau_{t1})\end{aligned} \tag{33}$$

In those with MDR-TB, all first-line therapy is ineffective. Transitions into B_{1iR} occur from treatment initiation or re-initiation based on the proportion of cases which do not receive DST $(1 - DST_T(t))$.

$$\frac{dB^V_{1iNR}}{dt} = A^V_{NR}(t)\frac{1-DST_N}{x^0x^V} - B^V_{1iNR}(t)(\mu^0 + \mu^v + 1/\tau_{t1}) \tag{34}$$

$$\frac{dB_{iPR}^{V}}{dt} = A_{PR}^{V}(t)\frac{1-DST_P(t)}{x^0x^V} + \frac{1}{\tau_{t1}}\sum_{T\in\{N,P\}}\left(B_{1iRT}^{V}(t)(1-DST_T(t))(1-\alpha^0\alpha^T)(1-\delta_1)\gamma\right) - B_{1iPR}^{V}(t)(\mu^0+\mu^V+1/\tau_{t1}) \quad (35)$$

As with first-line therapy, TB patients initiating second-line therapy are separated between effective and ineffective TB treatment states based on the probability of culture conversion among those who complete treatment (σ_2). Those who enter the effective second-line treatment state begin with the initiation phase B_{2e1} (duration $\tau_{t21} = 6$ months) followed by the continuation phase B_{2e2} (duration $\tau_{t21} = 14$ months) upon completion of the initiation phase. Those who enter the ineffective second-line treatment state B_{2i} will only receive treatment for a duration of τ_{t21} before treatment is withdrawn.

Transitions into the initiation phase of effective second-line therapy B_{2e1} occur as the result of: a) symptomatic active MDR-TB which, after a delay (duration x^0x^V) before diagnosis, has received DST and was not lost before treatment initiation ((DST_T) $(1-b)$); b) failure of ineffective first-line treatment for pre-existing MDR-TB B_{1iR} or DS-TB (B_{1iS}) which subsequently acquired MDR-TB (with probability $\alpha^0\alpha^T$). In the case of failure, patients must have completed treatment (duration $\tau_{t1} = 6$ months) without loss to follow-up followed by immediate retreatment$(1-\delta_1)\gamma$. Transitions from B_{2e1} occur due to death or finishing the initiation phase.

$$\frac{dB_{2e1}^{V}}{dt} = \sigma_2(1-b)\sum_{T\in\{N,P\}}\left(\frac{DST_T(t)}{x^0x^V}A_{TR}^{V}(t) + \frac{DST_T(t)}{\tau_{t1}}(1-\delta_1)\gamma(\alpha^0\alpha^T B_{1iST}^{V}(t) + B_{1iRT}^{v}(t))\right) - B_{2e1}^{V}(t)(\mu^0+\mu^V+i_{B_{2e1}}\mu_{tb}+1/\tau_{t21}) \quad (36)$$

Transitions into ineffective second-line therapy for MDR-TB B_{2i} occur from the same states as above.

$$\frac{dB_{2i}^{V}}{dt} = (1-\sigma_2)(1-b)\sum^{T\in\{N,P\}}\left(\frac{DST_T(t)}{x^0x^V}A_{TR}^{V}(t) + \frac{DST_T(t)}{\tau_{t1}}(1-\delta_1)\gamma(\alpha^0\alpha^T B_{1iST}^{V}(t) + B_{1iRT}^{v}(t))\right) - B_{2i}^{V}(t)(\mu^0+\mu^V+i_{B_{2i}}\mu_{tb}+1/\tau_{t21}) \quad (37)$$

Transitions into the continuation phase of effective second-line therapy for MDR-TB B_{2e2} occur only after completion of the initiation phase B_{2e1} (duration $\tau_{t21} = 6$ months), provided patients were not lost to follow-up $(1 - \delta_2)$. Transitions from this state occur due to death or finishing treatment (duration τ_{t22}= 14 months).

$$\frac{dB_{2e2}^V}{dt} = B_{2e1}^V(t)\frac{1-\delta_2}{\tau_{t21}} - B_{2e2}^V(t)(\mu^0 + \mu^V + i_{B_{2e2}}\mu_{tb} + 1/\tau_{t22}) \quad (38)$$

After Treatment

Among those who complete effective first-line therapy B_{1e} (culture negative at the end of treatment), a proportion ω_2 will eventually relapse to active TB *A*. Between the completion of first-line treatment and the time of relapse, these populations occupy an asymptomatic state *W* for a mean duration of τ_ω. Transitions into *W* occur following completion of effective first-line therapy (after duration τ_{t1}) with or without the acquisition of MDR during treatment (based on the probability of acquisition $\alpha^0\alpha^T$) leading to eventual relapse with DS-TB (W_S) or MDR-TB (W_R), respectively. Losses from these states occur due to death or relapse.

$$\frac{dW_S^V}{dt} = \sum_{T\in\{N,P\}}\left(\frac{\omega_T}{\tau_{t1}}(1 - \alpha^0\alpha^T)B_{1eST}^V(t)\right) - W_S^V(t)(\mu^0 + \mu^V + 1/\tau_\omega) \quad (39)$$

$$\frac{dW_R^V}{dt} = \sum^{T\in\{N,P\}}\left(\frac{\omega_T}{\tau_{t1}}\alpha^0\alpha^T B_{1eST}^V(t)\right) - W_R^V(t)(\mu^0 + \mu^V + 1/\tau_\omega) \quad (40)$$

Among those who complete effective second-line therapy B_{2e2} (culture negative at the end of treatment), a proportion ω_2 will eventually relapse to chronic (untreated) MDR-TB *C*. Between the completion of second-line treatment and the time of relapse, these populations occupy an asymptomatic state *Z* for a mean duration of τ_ω. This population differs from that of W_R through a history of attempted second-line therapy;

afterwards, those who relapse from Z will be ineligible for retreatment with second-line therapy. Losses from this state occur due to death or relapse.

$$\frac{dZ_R^V}{dt} = \frac{\omega_2}{\tau_{t22}} B_{2e2}^V(t) - Z_R^V(t)(\mu^0 + \mu^V + 1/\tau_\omega) \quad (41)$$

HIV Infection

In addition to the rates of change across states of TB infection (and births/deaths) described above, transitions between HIV substates occur due to initial HIV infection (Uninfected to High CD4), gradual immunosuppression (High CD4 to Low CD4), or ART initiation. Interactions between TB state and HIV substate influence HIV mortality (excess mortality rates in Low CD4 patients with active, untreated TB; see Table S2.1) and the rate of ART initiation (HIV patients receiving TB treatment initiate ART at an increased rate).

New High CD4 infections X^H occur based on the fitted HIV force of infection (described above); prior to 2010, transitions from the High CD4 substate occur only due to immunosuppression or death. (In our notating convention, HIV-associated mortality is presented in differential equations of TB transitions above and is therefore not duplicated here.) After 2010, transitions from the High CD4 substate may occur due to death or ART initiation.

New Low CD4 infections X^L occur solely due to immunosuppression based on the rate of CD4 decline, with an approximate duration of $1/\phi_H$ between initial infection and decline below 250 CD4 cells/mL. Prior to 2006, transitions from the Low CD4 substate occur solely due to death; after 2006, transitions from the Low CD4 substate may occur due to death or ART initiation.

HIV-infected populations are assumed to be unable to access ART before at least 2006. After 2006, Low CD4 populations become eligible for ART at a time-varying rate $\Omega(t)$ described in detail above. After 2010, High CD4 populations also become eligible for ART at a rate lower than that among Low CD4 populations (determined by the relative proportion of new ART initiations from patients with High CD4 counts k_H). For populations in any TB treatment state G, ART initiation occurs at an amplified rate ($k_{tb}\Omega(t)$). These dynamics are summarized as follows:

$$\text{For X } \notin G: \quad \frac{dX^H}{dt} = \begin{cases} FOI_{HIV}(t)X^U(t) - X^H(t)\phi_H & \text{if } t < 2010 \\ FOI_{HIV}(t)X^U(t) - X^H(t)(k_H\Omega(t) + \phi_H) & \text{if } t \geq 2010 \end{cases}$$

$$\frac{dX^L}{dt} = \begin{cases} X^H(t)\phi_H & \text{if } t < 2006 \\ X^H(t)\phi_H - X^L(t)\,\Omega(t) & \text{if } t \geq 2006 \end{cases} \tag{42}$$

$$\text{For X } \in G: \frac{dX^H}{dt} = \begin{cases} FOI_{HIV}(t)X^U(t) - X^H(t)\phi_H & \text{if } t < 2010 \\ FOI_{HIV}(t)X^U(t) - X^H(t)(k_{tb}k_H\Omega(t) + \phi_H) & \text{if } t \geq 2010 \end{cases}$$

$$\frac{dX^L}{dt} = \begin{cases} X^H(t)\phi_H & \text{if } t < 2006 \\ X^H(t)\phi_H - X^L(t)(k_{tb}\Omega(t)) & \text{if } t \geq 2006 \end{cases} \tag{43}$$

$$\frac{dX^A}{dt} = \begin{cases} 0 & \text{if } t < 2006 \\ \Omega(t)\left[\sum_{X\notin G}(X^L(t)) + k_{tb}\sum_{X\in G}(X^L(t))\right] & \text{if } 2006 \leq t < 2010 \\ \Omega(t)\left[\sum_{X\notin G}(X^L(t) + k_H X^H(t)) + k_t b\sum_{X\in G}(X^L(t) + k_H X^H(t))\right] & \text{if } t \geq 2010 \end{cases} \tag{44}$$

Sampling & Calibration

To enrich our projections using simulated TB epidemics which were most consistent with empirical estimates of TB epidemics in South Africa and Vietnam, we implemented a two-stage semi-Bayesian Sampling/Importance-Resampling algorithm [1]. In the first stage of calibration, parameter sets were composed of a single value for

each DS-TB or HIV parameter (drawn using Latin hypercube sampling [2], Tables S2.1-2.2 below) while values for MDR-TB parameters (Table S2.3) were set to zero. Each parameter set was then assigned a likelihood value based on the DS-TB/HIV epidemic the set produced. Joint likelihoods were defined by the each epidemic's pseudo-likelihood of absolute TB incidence (per 100,000) in 2005, 2010, and 2015 (from WHO country estimates [3]) as well as the proportion of incident TB cases infected with HIV. Targets for HIV calibration were taken from a 2012 national TB drug resistance survey in South Africa [4]; comparable data from surveys in Vietnam were unavailable, thus the most recent WHO estimate of incident HIV-infected TB cases (in 2015) was used. Targets were modeled as independent beta distributions with bounds set equal to the 95% confidence limits of estimated TB incidence; bounds were set equal to 85% and 115% of the HIV point estimate. (All calibration targets are presented in Table S2.4 below.) The product of each simulation's pseudo-likelihoods was used as the joint likelihood of the corresponding DS-TB parameter set. Each parameter set was weighted then weighted according to the quotient of the set's joint likelihood $L(\theta_i ; y)$ and the cumulative likelihood of all sets:

$$q_i = \frac{L(\theta_i;y)}{\sum_{j=1}^{n} L(\theta_j;y)} \tag{45}$$

DS-TB parameter sets were then resampled (with replacement) proportional to the weights assigned above. In the second stage of calibration, each resampled DS-TB parameter set was paired with a new MDR-TB parameter set (again drawn using Latin hypercube sampling, Table S2.3 below). Each new parameter set was then used to simulate a DS-TB epidemic to a time equal to the value of the MDR-TB parameter t_R^0. After this time, MDR-TB epidemics were simulated forward to 2040. Each epidemic was

then assigned a new joint likelihood defined by the epidemics pseudo-likelihood of the proportion of recent TB diagnoses with MDR-TB among new and previously-treated cases.

Table S2.1: TB Natural History Parameter Prior Distributions

	Description	Median	Sampling Range[†]	Distribution	References
μ^0	Baseline mortality rate for ages 15+ (per year)	0.017	(0.015-0.018)	Lognormal	[5]
μ_{tb}	Added mortality rate of untreated symptomatic TB in HIV- populations (per year)	0.15	(0.07-0.3)	Lognormal	[3,6]
ρ^0	Probability of rapid progression after initial TB infection in HIV- populations	0.14	(0.07-0.25)	Logit-normal	[7]
λ^0	Protection by latent infection: reduction in rapid progression after second infection event in HIV- populations	0.5	(0.1-0.9)	Logit-normal	[7,8]
r^0	Reactivation rate, latent to early (asymptomatic) active TB in HIV- populations (per year)	0.001	(0.0005-0.002)	Lognormal	[8–11]
a	Duration of asymptomatic (preclinical) TB if no death or spontaneous resolution (years)	0.6	(0.36-1.0)	Lognormal	[12,13]
i_E	Infectiousness and mortality of asymptomatic (preclinical) TB, relative to symptomatic TB in HIV- populations	0.22	(0.1-0.4)	Logit-normal	[14,15]
ν^0	Rate of spontaneous resolution of untreated active TB in HIV-populations (per year)	0.13	(0.08-0.2)	Lognormal	[6]
x^0	Time to TB diagnosis and treatment initiation (with pretreatment loss to follow up incorporated for DS-TB) in HIV- populations (years)	1	(0.67-1.5)	Lognormal	[3,12,16]
$\sigma_1{}^0$	First-line treatment success (fraction of new DS-TB patients who will successfully complete treatment if adherent; includes those who may relapse with or without acquired resistance)	0.98	(0.96-0.99)	Logit-normal	[3,17–19]
$\sigma_1{}^P$	Reduction in first-line treatment success for previously treated DS-TB patients (multiplicative factor)	0.95	(0.9-1.0)	Uniform	[3,20]

[†]Sampling ranges represent the 2.5th to 97.5th percentiles of unbounded distributions and lower to upper bounds of uniform distributions.

Table S2.1 (Continued): TB Natural History Parameter Prior Distributions

ω_1^0	Relapse risk after first-line therapy (if no acquired drug resistance), new DS-TB patients	0.04	(0.026-0.06)	Logit-normal	[21,22]
ω_1^P	Increase in relapse risk after first-line therapy, retreatment DS-TB patients (multiplicative factor)	2	(1-3)	Uniform	[20,21]
τ_ω	Median time to relapse, among patients who will relapse (years)	1.5	(0.9-2.5)	Lognormal	[21]
δ_1	Probability of loss to follow up during first-line therapy	0.06	(0.035-0.10)	Logit-normal	[3]
η_1	Probability of returning to active TB after loss to follow-up during effective first-line treatment of DS-TB	0.4	(0.16-0.7)	Logit-normal	[23,24]
Γ	Probability of immediate retreatment after DS-TB treatment failure	0.92	(0.85-1.0)	Uniform	Model Assumption
i_A	Infectiousness and mortality of TB on ineffective treatment, relative to untreated active TB	0.5	(0-1)	Uniform	Model Assumption
β_S^0	TB transmission coefficient until t_s	6.5	(6.0-7.0)	Uniform	Calibrated to Target Incidence
d_S	Rate of decline in TB transmission coefficient, starting in 2000	-0.0125	(-0.025 - 0)	Uniform	Calibrated to Target Incidence

Table S2.2: HIV and TB/HIV Parameter Prior Distributions

	Description	Median	Sampling Range	Distribution	References
μ^H	Added mortality rate of HIV+, High CD4 populations (per year)	0.05	(0.03-0.07)	Lognormal	[25]
μ^L	Added mortality rate of HIV+, Low CD4 populations (per year)	0.27	(0.23-0.33)	Lognormal	[25]
μ^A	Added mortality rate of HIV+, receiving ART populations (per year)	0.01	(0.008-0.013)	Lognormal	[26]
μ_{tb}^L	Excess added mortality rate of HIV+, Low CD4 individuals infected with untreated active TB (per year)	0.8	(0.5-1.3)	Lognormal	[27]
φ_H	Rate of transition from HIV+, High CD4 to HIV+, Low CD4 (per year)	0.2	(0.15-0.26)	Lognormal	[28,29]
k_H	Reduced probability of initiating ART for HIV+, High CD4 populations relative HIV+, Low CD4 populations (after 2006 only)	0.33	(0.11-1.0)	Logit-normal	[30]
ρ^H	Relative increase in the probability of rapid progression of TB in HIV+, High CD4 populations	2.9	(1.8-4.7)	Lognormal	[27]
ρ^L	Relative increase in the probability of rapid progression of TB in HIV+, Low CD4 populations	8	(6.3-10.1)	Lognormal	[27]
ρ^A	Relative increase in the probability of rapid progression of TB in HIV+, on ART populations	2.9	(1.8-4.7)	Lognormal	[27]
λ^H	Relative reduction in the probability of protection against rapid progression upon reinfection in HIV+, High CD4 populations	0.25	(0-0.5)	Uniform	[31]
λ^L	Relative reduction in the probability of protection against rapid progression upon reinfection in HIV+, Low CD4 populations	0.25	(0-0.5)	Uniform	[31]
λ^A	Relative reduction in the probability of protection against rapid progression upon reinfection in HIV+, on ART populations	0.25	(0-0.5)	Uniform	[31]
r^H	Relative increase in the rate of reactivation in HIV+, High CD4 populations	34	(20-60)	Lognormal	[32,33]

[†]Sampling ranges represent the 2.5th to 97.5th percentiles of unbounded distributions and lower to upper bounds of uniform distributions.

Table S2.2 (Continued): HIV and TB/HIV Parameter Prior Distributions

r^L	Relative increase in the rate of reactivation in HIV+, Low CD4 populations	67	(31-158)	Lognormal	[32,33]
r^A	Relative increase in the rate of reactivation in HIV+, on ART populations	34	(20-60)	Lognormal	[32,33]
ν^H	Relative reduction in the rate of spontaneous resolution in HIV+, High CD4 populations	0.5	(0-1)	Uniform	Model Assumption
ν^L	Relative reduction in the rate of spontaneous resolution in HIV+, Low CD4 populations	0.25	(0-0.5)	Uniform	Model Assumption
ν^A	Relative reduction in the rate of spontaneous resolution in HIV+, on ART populations	0.5	(0-1)	Uniform	Model Assumption
i^H	Relative reduction in the infectiousness of HIV+, High CD4 populations	0.89	(0.53-0.98)	Logit-normal	[34,35]
i^L	Relative reduction in the infectiousness of HIV+, Low CD4 populations	0.5	(0.12-0.88)	Logit-normal	[34]
i^A	Relative reduction in the infectiousness of HIV+, on ART populations	0.89	(0.53-0.98)	Logit-normal	[34,35]
k_{tb}	Relative increase in the rate of ART initiation in HIV+ TB patients receiving any form of TB treatment	2.4	(1.0-5.6)	Lognormal	[36]
x^A	Relative reduction in the duration before TB treatment initiation in HIV+ TB patients receiving ART	0.43	(0.3-0.6)	Lognormal	[37]

Table S2.3: MDR-TB Parameter Prior Distributions

	Description	Median	Sampling Range	Distribution	References
t_R^0	Time since emergence of modern MDR-TB strains (years)	30	(20-45)	Lognormal	[38,39]
α^0	Risk of acquired multidrug-resistance during first-line therapy, new DS-TB patients	0.004	(0.0015-0.01)	Logit-normal	[22]
α^P	Increase in risk of acquired multidrug resistance, retreatment DS-TB patients (multiplicative factor)	2	(1-3)	Uniform	[20,40]
b	Pre-treatment loss to follow up after MDR-TB diagnosis	0.05	(0.025-0.10)	Logit-normal	[3,16]
σ_2	MDR-TB treatment success (fraction of MDR-TB patients who successfully complete treatment if adherent; includes those who may relapse)	0.77	(0.66-0.85)	Logit-normal	[41–43]
i_2	Infectiousness during the first six months of effective MDR-TB therapy, relative to untreated active TB	0.1	(0-0.2)	Uniform	[42,44]
δ_1	Probability of loss to follow up during MDR-TB therapy	0.11	(0.04-0.25)	Logit-normal	[41,45]
ω_2	Relapse risk after successful completion of conventional MDR-TB treatment	0.04	(0.015-0.1)	Logit-normal	[42,46]
E_R	Transmissibility of drug-resistant strain, relative to drug-susceptible strain at the time of MDR emergence	0.6	(0.38-0.94)	Lognormal	[47–49]
d_R	Annual rate of increase in MDR-TB Transmission coefficient (in the Shrinking Deficit scenario)	0.0075	(0-0.015)	Uniform	Model Assumption
t_R	Year of start of increase in MDR-TB Transmission coefficient (as a percentile of [t_R^0, 2016]	0.5	(0-1)	Uniform	Model Assumption

[†]Sampling ranges represent the 2.5th to 97.5th percentiles of unbounded distributions and lower to upper bounds of uniform distributions.

Table S2.4: Calibration Targets

	Total TB Incidence[a,b] (per 100,000)		HIV-Infected Incident TB[b,c] (%)		MDR-TB[d] in New Cases (%)		MDR-TB[d] in Previously-Treated Cases (%)	
	Year	Median (Range)	Year	Median (Range)	Year	Mean (Range)	Year	Mean (Range)
South Africa	2005	932 (603-1331)	2012	63.2 (62.2-64.2)	2002	1.6 (1.1-2.1)	2002	6.6 (4.9-8.2)
	2010	948 (710-1219)			2013	2.1 (1.5-2.7)	2013	4.6 (3.2-6.0)
	2015	834 (539-1190)						
Vietnam	2005	176 (114-252)	2015	4.3 (4.0-4.6)	1996	2.3 (1.3-3.8)	1996	18.2 (11.9-24.5)
	2010	155 (114-202)			2002	2.3 (1.1-3.6)	2002	19.3 (14.0-25.0)
	2015	137 (110-166)			2005	2.7 (2.0-3.7)	2005	23.3 (16.7-29.9)
					2011	4.0 (2.5-5.4)	2011	18.2 (11.9-24.5)

[a]Incidence estimates were taken from WHO country reports (as published with the 2016 Global TB Report) [3].

[b]These estimates were modeled as independent beta distributions with bounds defined by the estimated 95% confidence intervals.

[c]HIV targets represent the proportion of HIV-infected populations among all incident TB cases. Estimates were taken from the 2012 TB drug resistance survey in South Africa [4] and the 2016 WHO estimate in Vietnam. [d]MDR-TB targets represent the proportion of MDR-TB cases among all recent TB diagnoses (defined as any population transitioning from a state of active, untreated TB to a state of TB diagnosis/treatment). Estimates were taken from national drug resistance surveys in South Africa [4,50] and Vietnam [51]. These estimates were modeled as independent normal distributions with two standard deviations set equal to half the widths of the estimated 95% confidence intervals.

Recent TB diagnoses were used (instead of incident TB cases) to recapitulate the sampling methodologies used in national drug resistant surveys: a representative sampling of prevalent TB cases who have recently submitted sputum specimens to public health facilities at the time of the survey. (Not all incident TB cases may be captured by survey methods; for example, due to delays between the onset of symptomatic TB and the time of presentation at a clinical center.) In our model, we define recent diagnoses as any populations transitioning from a state of active, untreated TB A into any treatment state G, regardless of whether appropriate/effective treatment is initiated afterwards.

Targets for MDR-TB diagnoses were drawn from national drug resistance survey data in each country. To date, results from two such surveys in South Africa have been published (2002 and 2013) [4,50] while results from one such survey in Vietnam has been published (2011) [51]. Results from three additional surveys (1996, 2002, and 2005) have been provided to us by Dr. Nguyen Binh Hoa of the Vietnam National TB Program. (The 1996 survey only assessed MDR-TB in new TB patients.) Each MDR-TB calibration target was modeled as an independent normal distribution with means set equal to survey point estimates and standard deviations set equal to half the estimated 95% confidence interval divided by Z=1.96. Joint likelihoods were calculated as the product of pseudo-likelihoods for each simulated epidemic, and weights were assigned in the same manner as above. Simulated MDR-TB epidemics were resampled (with replacement) proportional to these weights to create posterior distributions of epidemics in each scenario and in each setting.

Bayesian Model Comparison

To compare the performance of our model scenarios, we calculated a Bayes Factor for each pair of scenarios in each country. A Bayes Factor is traditionally defined as the posterior odds to prior odds ratio [52]. For posterior distributions from any two models $p(\theta_1|y)$ and $p(\theta_2|y)$ and data *y* (our empirical calibration targets), a Bayes Factor can be defined as:

$$BF = \frac{p(\theta_1|y)/p(\theta_1)}{p(\theta_2|y)/p(\theta_2)} \quad (46)$$

(In this notation, $p(\theta_1)$ and $p(\theta_2)$ represent the prior distributions of each model.) As with common Monte Carlo approximations to Bayesian inference, if independent samples are drawn from $p(\theta_1)$ and $p(\theta_2)$, the BF may be consistently estimated by [52]:

$$\frac{n_2 \sum_{j=1}^{n_1} L(\theta_{j_1};y)}{n_1 \sum_{j=1}^{n_2} L(\theta_{j_2};y)} \quad (47)$$

In our approach, the number of independent simulations run in each scenario's prior distribution was equal ($n_1 = n_2$). Therefore, the BF is approximated by the ratio of the sums of likelihood values for the *n* prior simulations (before resampling) in each scenario ($\sum_{j=1}^{n} L(\theta_j; y)$). When presented in the text, the Constant Deficit scenario is used as the denominator model $p(\theta_2|y)$ in calculating a BF unless noted otherwise.

Replication of Previous Findings

After review of our primary results, we noted important discrepancies in our projections of the MDR-TB epidemic in South Africa under the No Deficit scenario and those published in a similar study by Sharma and colleagues in which the transmission efficiency of DS-TB and MDR-TB were assumed to be identical [53]. Notably, their work projected the relative incidence of MDR-TB in South Africa to be 5.7% (95% UR:

3.0-7.6%) by 2040, significantly lower and with less variance than our estimates. In an attempt to reconcile these projections, we undertook to identify the source(s) of these discrepancies in our approach.

In reviewing the methodology of the previously published study, we identified several parameters with comparable surrogates in our model where our values diverged. Whereas our colleagues parameterized the 5-year probability of latent TB reactivation with a median of 2.9%, we parameterized the rate of TB reactivation r^0 with a median of 0.1 per 100 person-years (equivalent to a 5-year probability of 0.5%). Additionally, they parameterized the median probabilities of acquiring active TB and latent TB from an infectious index case as 3.3% and 51%, respectively. It follows that, among those who acquire a new TB infection, approximately 6% would bypass the latent state (3.3/(51+3.3). We parameterized the comparable median probability of rapid progression upon acquiring a new TB infection ρ^0 as 14%. Finally, our colleagues' approach to the rate of treatment initiation used a case detection rate of 75% with a wide prior distribution (3-98%) for the probability that TB patients will initiate effective treatment following detection. The posterior of this distribution is significantly narrower (6-26%) with a low median value (11.3%). This implies that only 8% of DS-TB patients would initiate effective TB treatment in South Africa; equivalently, the mean time between TB onset and treatment initiation would be 11 years. By comparison, we parameterized the mean delay between TB onset and treatment initiation as 12 months.

To replicate these previously published results, we altered our parameter priors in a stepwise manner. First, in our Slower Epidemic scenario, we decreased the prior probability of rapid progression ρ^0 upon new infection from 14% (95% range: 7-25%) to

4% (95% range: 1-15%) and increased the range for the rate of latent TB reactivation r^0 from 0.05-0.2 per 100 person-years to 0.01-1.0 per 100 person-years and executed our No Deficit scenario as before. Afterwards, in our Delayed Treatment scenario, we additionally increased the prior duration of time between TB onset and treatment initiation from 12 months (95% range: 8-18 months) to 10 years (95% range: 7.5-12.5 years). To assess model performance, we calculated Bayes Factors comparing these two new scenarios with our No Deficit scenario and our Constant Deficit scenario.

Sensitivity Analyses

We implemented two strategies in our sensitivity analyses. For each parameter in each scenario, we calculated the partial rank correlation coefficient (PRCC) between the parameter's posterior values and two primary outcomes of interest generated from simulations with those values: the absolute 2040 MDR-TB incidence and the fold change in the relative MDR-TB incidence (as a proportion of all TB) between 2016 and 2040. This multivariate analysis evaluates the strength of rank correlation between a parameter input value and the associated outcome value, adjusting for all other parameters. Additionally, in a univariate approach, we stratified outcome values across quintiles of parameter values. Briefly, for each parameter in each scenario, posterior simulations were ordered by parameter value (least to greatest). The bottom 20% of simulations (those with the lowest parameter values) and the top 20% of simulations (those with the highest parameter values) were identified and outcomes of simulations in each quintile were plotted. In cases where a parameter is highly influential on an outcome, a clear separation is expected between the distributions of the outcome in the lowest and highest quintiles of

the parameter's value. In cases where a parameter is not influential, the distribution of outcomes is not expected to differ significantly between quintiles of the parameter's value.

Sensitivity to Conditions at Initiation

All simulations were initiated under the same initial conditions: in a population of 100,000 members, 49.5% were latently infected (in state L_{NS}^{U}), 0.3% were in a state of early-active TB (state E_{NS}^{U}), 0.2% were in a state of active TB (state A_{NS}^{U}), and the remaining 50% were uninfected (state S_{N}^{U}). Simulations were initiated 150 years before the present and run without interruption until the introduction of MDR-TB (sampled between 1971 and 1996) or the introduction of HIV (1990 in all simulations). To evaluate the behavior of the ODE system under different initial conditions, the parameter set producing the maximum likelihood DS-TB simulation under these initial conditions was subsequently used to simulate epidemics following a variety of alternative initial conditions. For these alternative conditions, the prevalence of active DS-TB cases was varied between 0.001% and 90% and the prevalence of latent TB infection among those without active TB was varied between 0% and 99%; these simulations were again initiated 150 years before the present and run without interruption until the introduction of MDR-TB or HIV.

SUPPLEMENTARY RESULTS

Calibration

As described in the Methods, our scenarios were calibrated in a two-stage semi-Bayesian algorithm. The results of the second stage of calibration – using empirical estimates of MDR-TB incidence – are presented in Chapter IV (Figure 4.3). The results of the first stage of calibration – using estimates of absolute TB incidence and HIV among incident TB cases – are presented in Figure S2.3. All Bayes Factors calculated between the three primary scenarios examined are presented in Table S2.5. Posterior distributions of parameter values resampled during calibration in the Constant Deficit and Shrinking Deficit scenarios are compared with the prior distributions used for Latin hypercube sampling in Figures S4-S6 (South Africa) and in Figures S7-S9 (Vietnam).

Figure S2.3: TB and HIV Incidence Calibration Results

A – South Africa

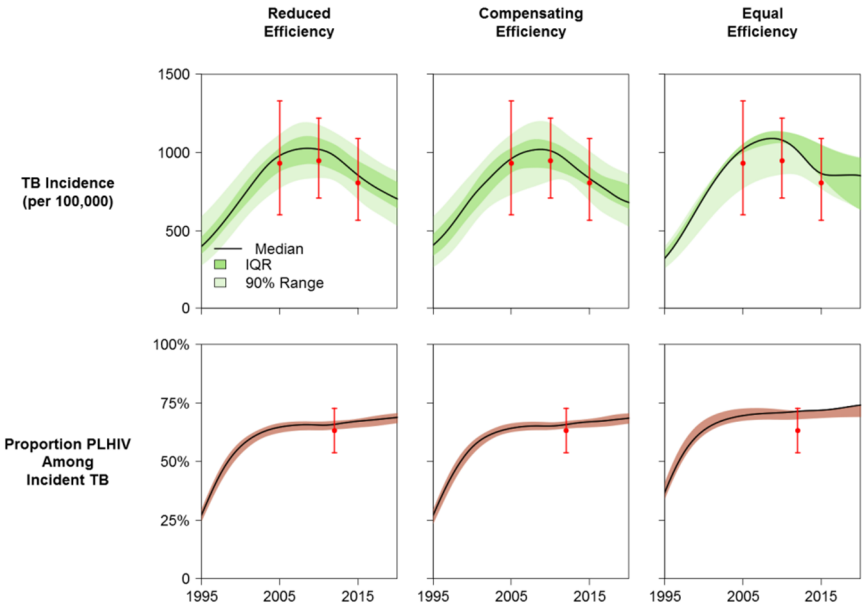

B – Vietnam

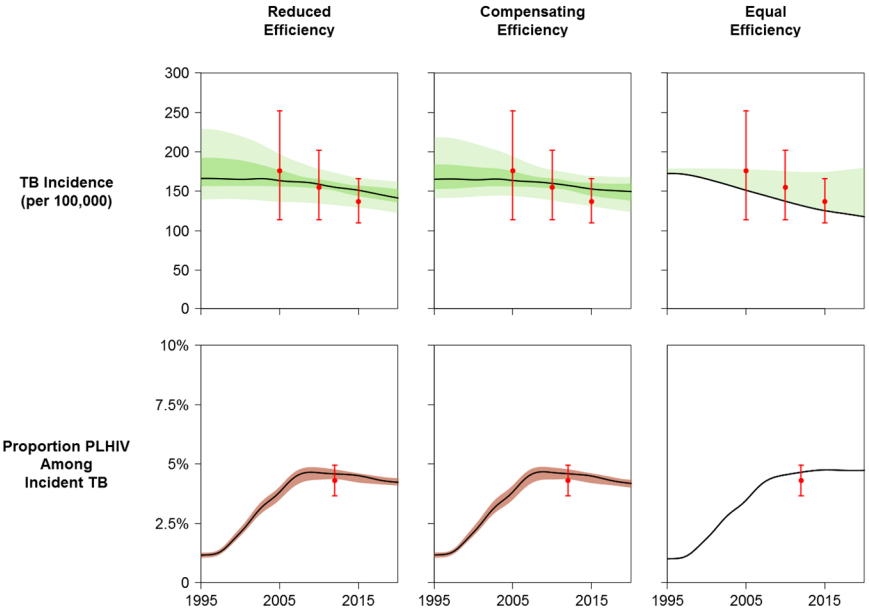

Simulated epidemics are weighted according to how well each reproduced empirical calibration targets (historical estimates of absolute TB incidence and the proportion of incident TB cases infected with HIV). Red points represent median values and bounds for calibration targets drawn from WHO estimates and national survey data. IQR represents 25th to 75th percentiles and the 90% range represents the 5th to 95th percentiles of posterior simulations.

Table S2.5: Model Comparison with Bayes Factors

BF Numerator Scenario[a]	BF Denominator Scenario[b]	South Africa BF[c]	Vietnam BF[d]
Constant Efficiency Deficit	No Efficiency Deficit	67,380,983	3354
Constant Efficiency Deficit	Shrinking Efficiency Deficit	2.6	2.1
Shrinking Efficiency Deficit	No Efficiency Deficit	25,868,566	1607

[a]The model used in the numerator of the calculation of the Bayes Factor (i.e., $p(\theta_1|y)$ in Equation 47 above).

[b]The model used in the denominator of the calculation of the BF (i.e., $p(\theta_2|y)$ in Equation 47 above).

[c]The BF corresponding to the performance of the numerator model relative to the denominator model in South Africa.

[d]The BF corresponding to the performance of the numerator model relative to the denominator model in Vietnam

Figure S2.4: TB Natural History Parameter Distributions – South Africa

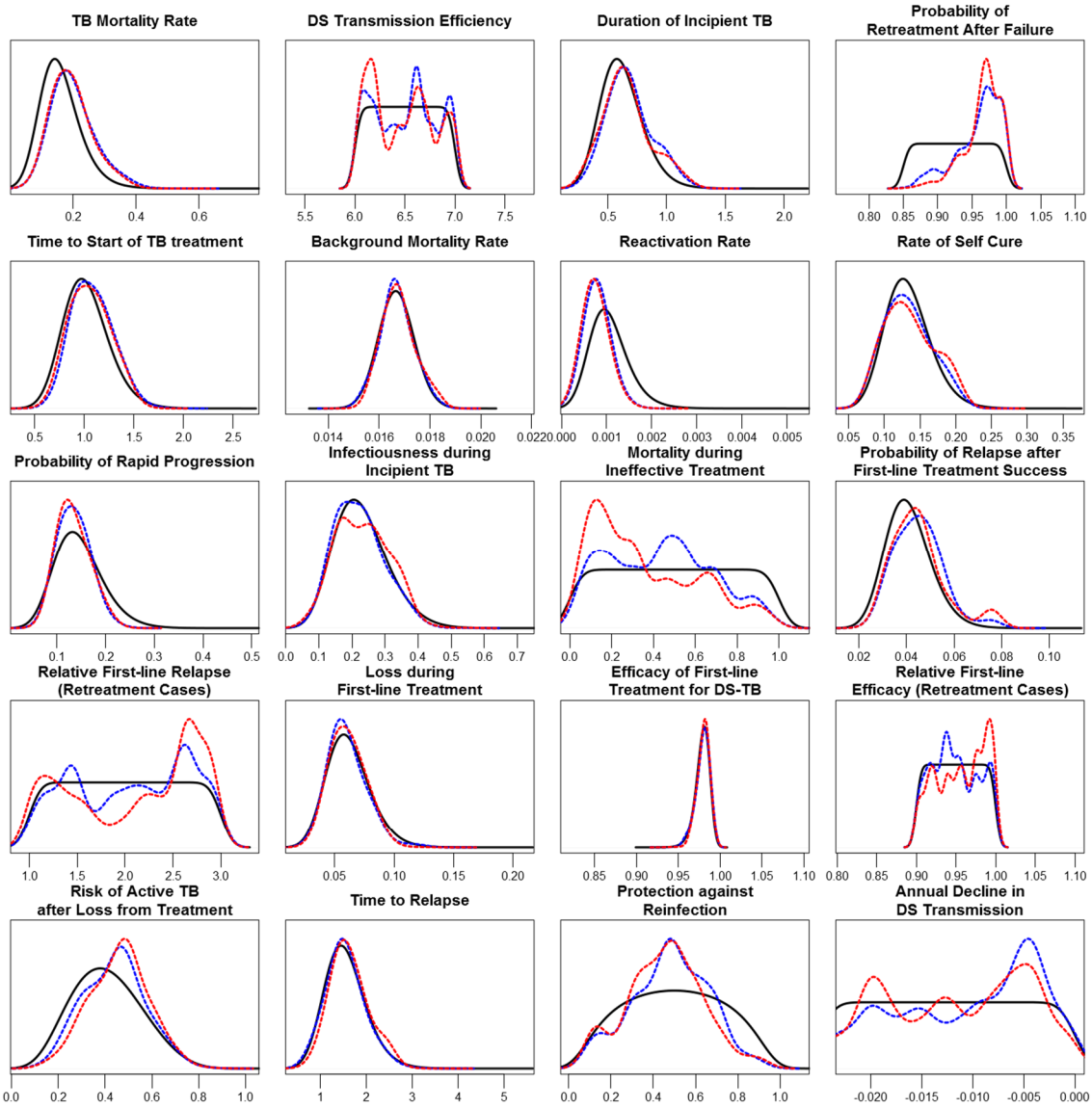

The probability distribution function used to sample initial values for each parameter (the prior distribution) is illustrated in **Black** in each plot. (Identical prior distributions were used to sample parameter values in both Constant Deficit and Shrinking Deficit scenarios.) The distribution of values for each parameter after resampling in the Constant Deficit scenario is illustrated in **Blue** in each plot. The distribution of values for each parameter after resampling in the Shrinking Deficit scenario is illustrated in **Red** in each plot. See Table S2.1 for full descriptions, sampling ranges, and references for each parameter and prior distribution.

Figure S2.5: HIV and TB/HIV Parameter Distributions – South Africa

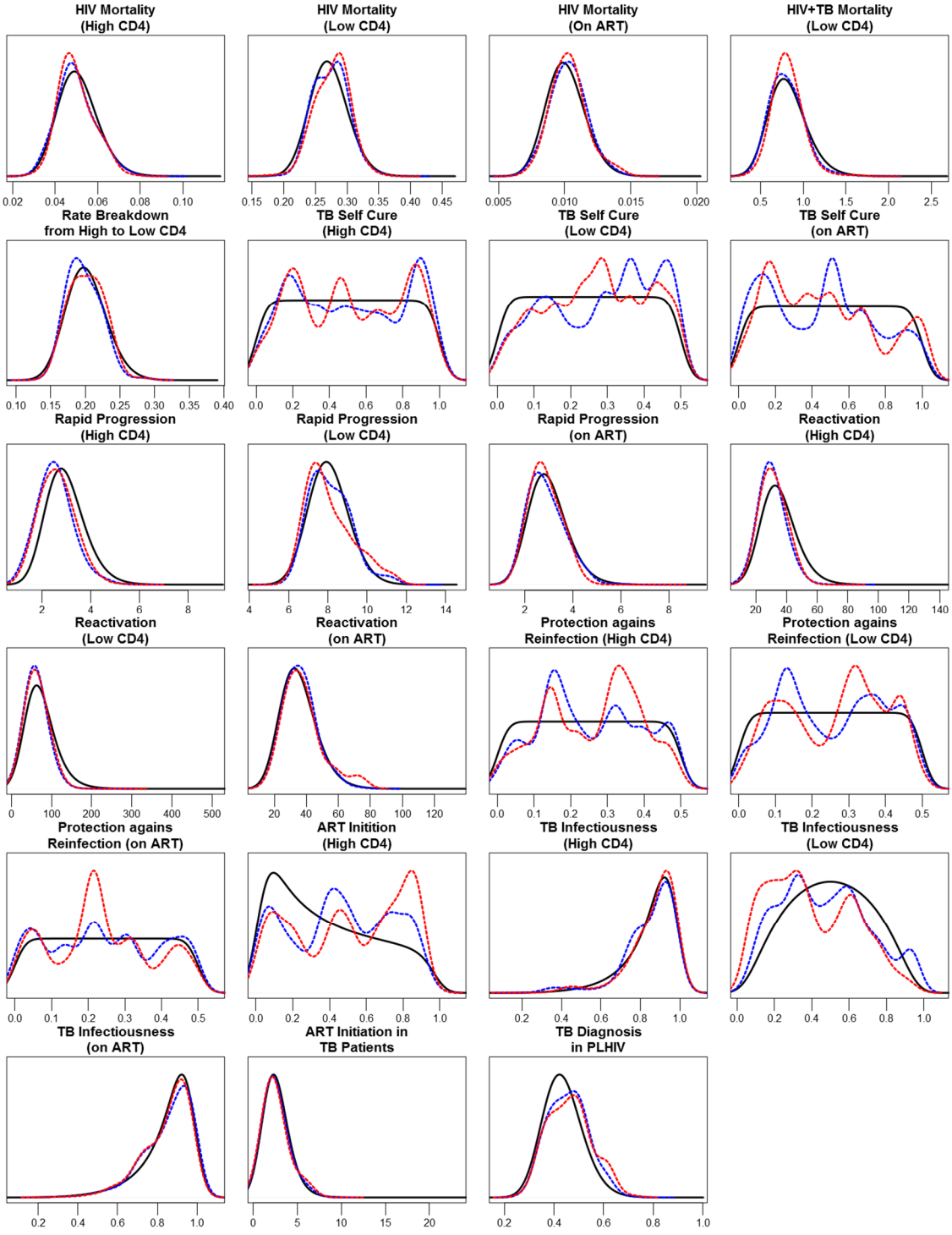

Figure S2.6: MDR-TB Parameter Distributions – South Africa

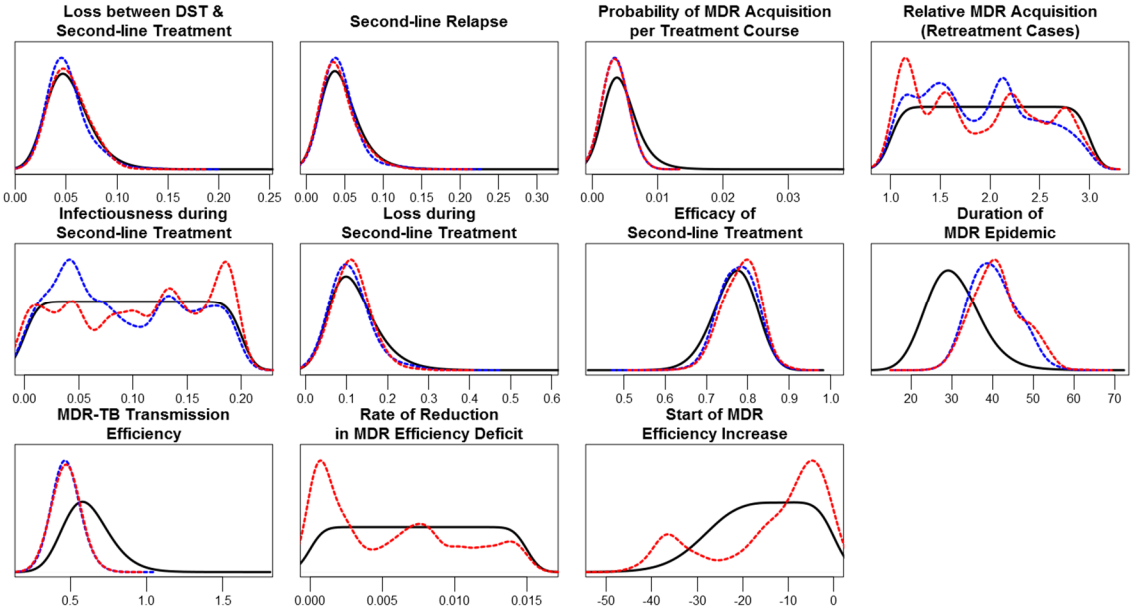

Figure S2.7: TB Natural History Parameter Distributions – Vietnam

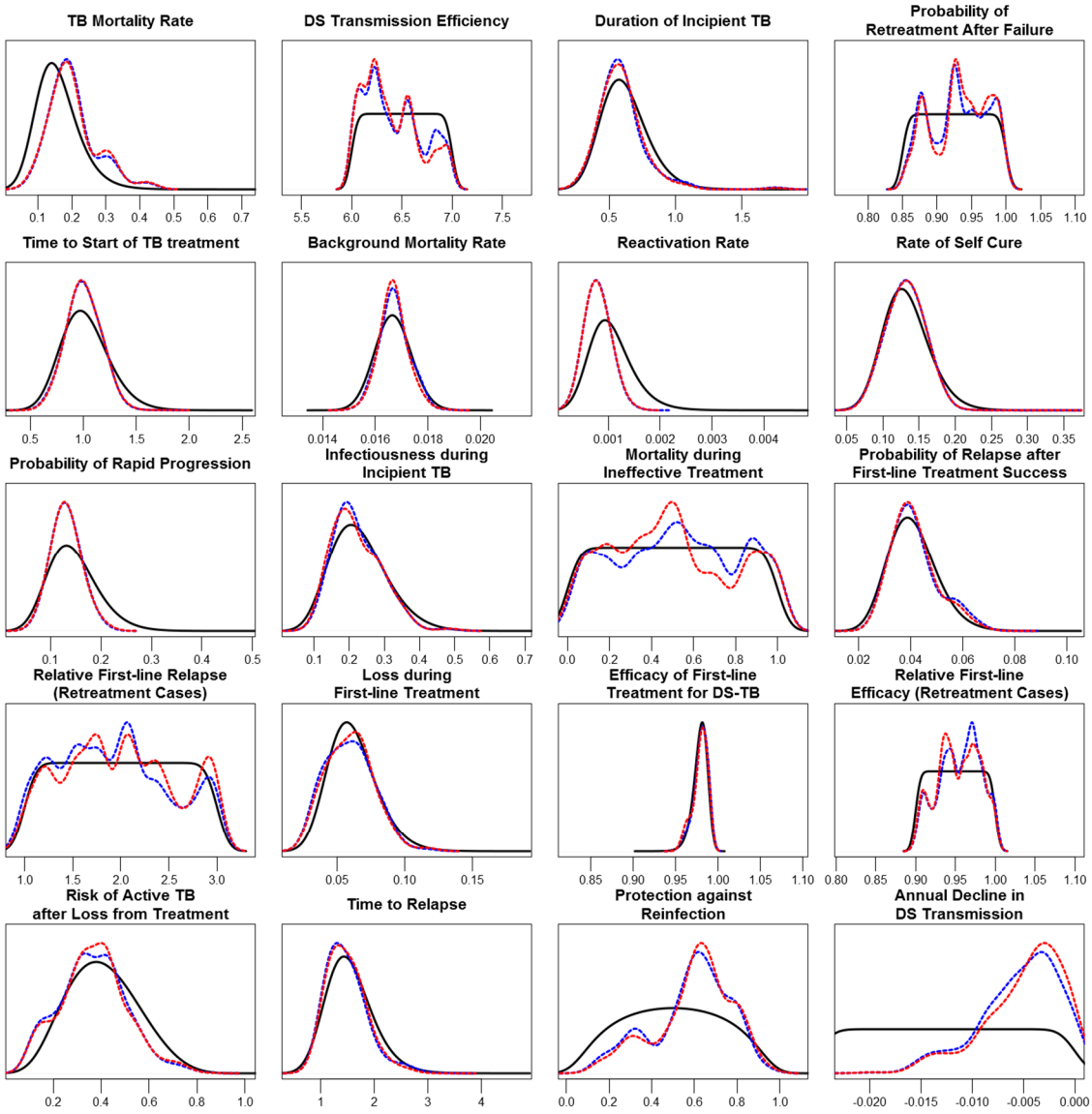

The probability distribution function used to sample initial values for each parameter (the prior distribution) is illustrated in **Black** in each plot. (Identical prior distributions were used to sample parameter values in both Constant Deficit and Shrinking Deficit scenarios.) The distribution of values for each parameter after resampling in the Constant Deficit scenario is illustrated in **Blue** in each plot. The distribution of values for each parameter after resampling in the Shrinking Deficit scenario is illustrated in **Red** in each plot. See Table S2.1 for full descriptions, sampling ranges, and references for each parameter and prior distribution.

Figure S2.8: HIV and TB/HIV Parameter Distributions – Vietnam

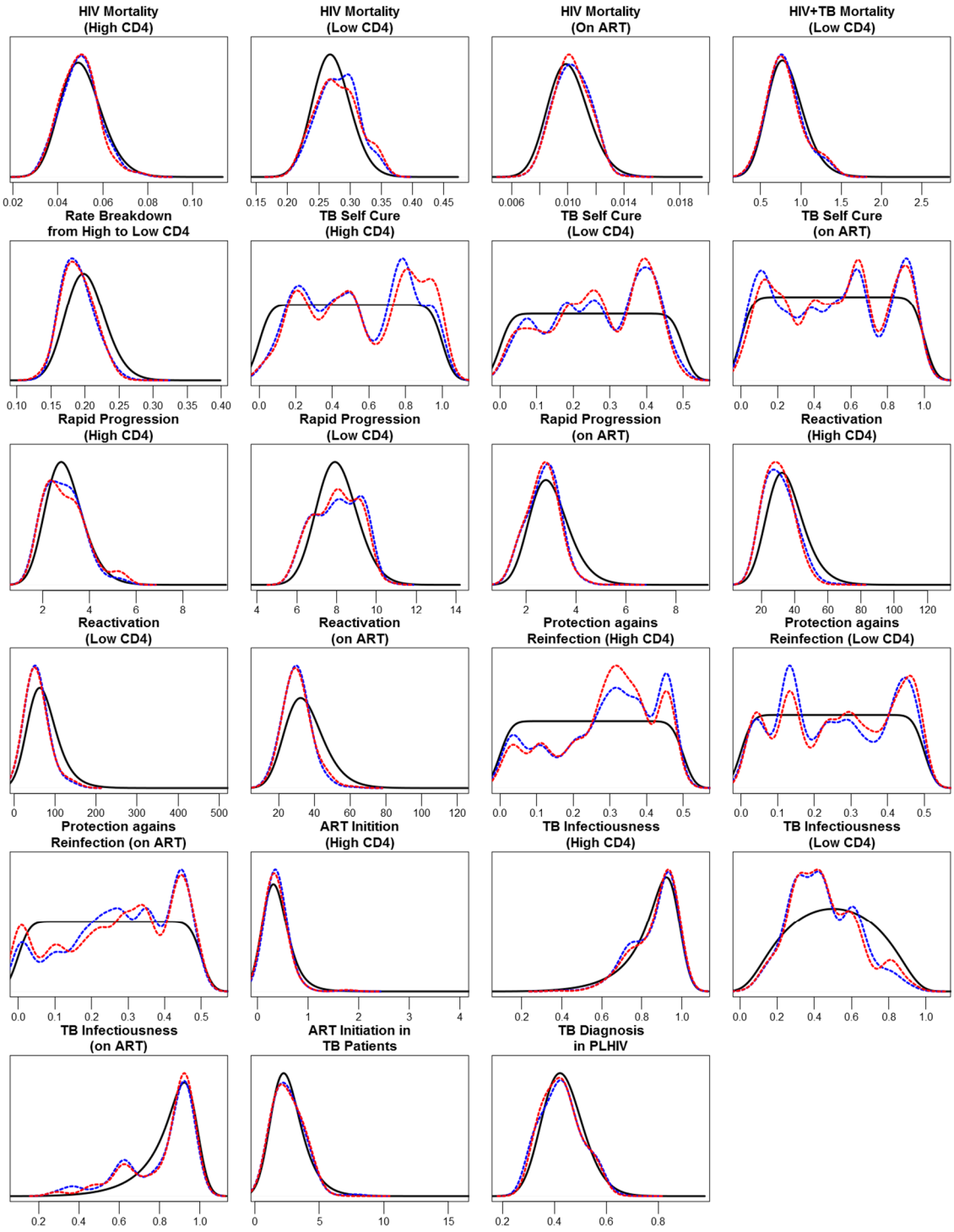

Figure S2.9: MDR-TB Parameter Distributions – Vietnam

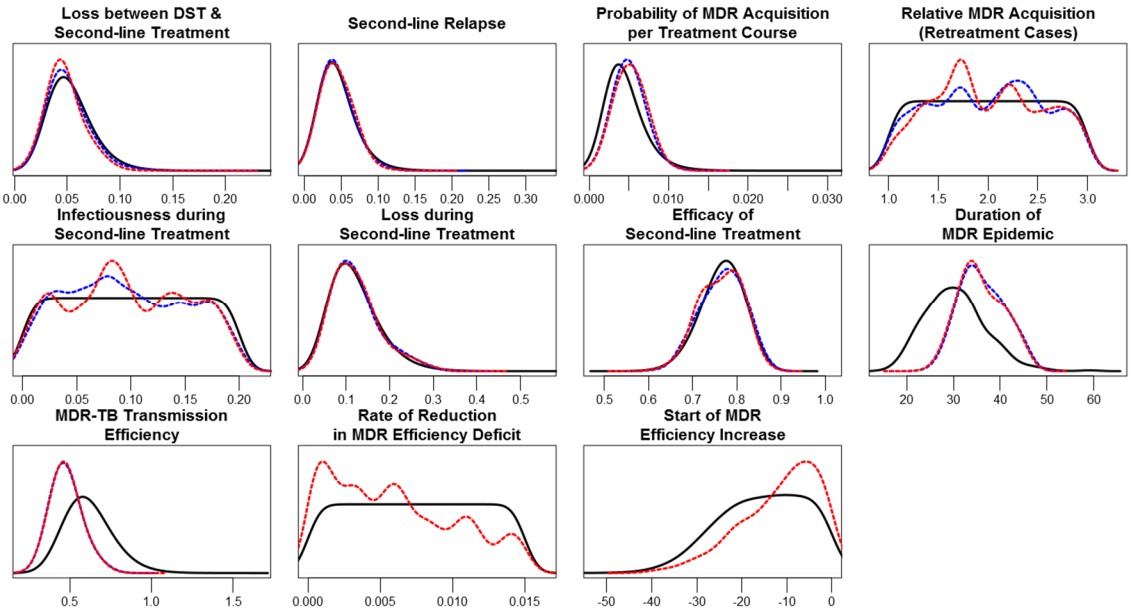

Model Projections

The primary outcomes of interest in our study were the projected changes absolute and relative incidences of MDR-TB over time. Results of these outcomes in the Constant Deficit and Shrinking Deficit scenarios are presented in Chapter IV. Here, we present results of these outcomes in the No Deficit scenario in Figure S2.10.

Additionally, we investigated several secondary outcomes of interest in all scenarios. Projections of the absolute TB incidence (used to calculate the relative MDR-TB incidence presented in Chapter IV) are illustrated in Figure S2.11. The proportion of incident MDR acquired during recent first-line therapy is presented in Figure S2.12.

Figure S2.10: Projections of the MDR-TB Burden in the No Deficit Scenario

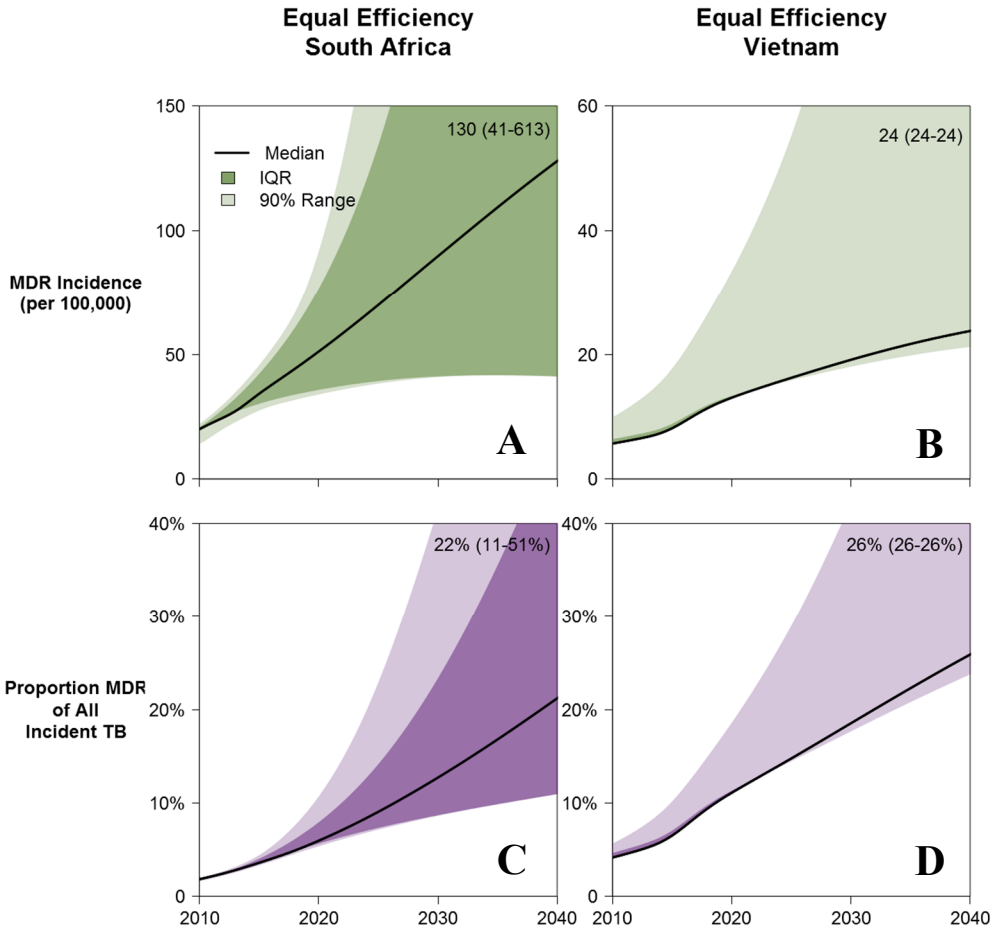

Simulated MDR-TB epidemics were projected from 2010 to 2040. Panels A and B demonstrate the projected absolute MDR-TB incidence in each country, while Panels C and D demonstrate MDR-TB as a proportion of all incident TB. The 2040 projected median (IQR) values are included in the upper right of each panel. IQR represents 25th to 75th percentiles and the 90% range represents the 5th to 95th percentiles of posterior simulations.

Figure S2.11: Projections of the Absolute Burden of TB

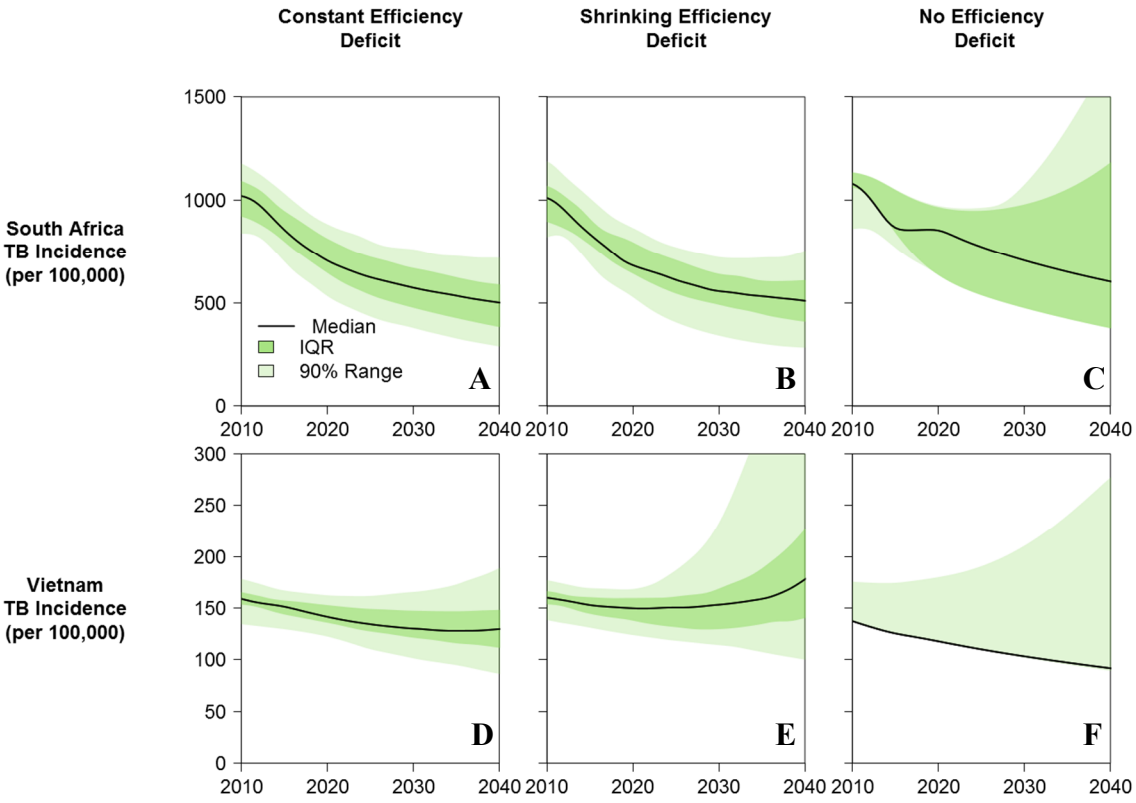

Simulated MDR-TB epidemics were projected from 2010 to 2040, and the absolute incidence of all forms of TB (DS-TB and MDR-TB) are illustrated. Panels A and D represent projections in the Constant Deficit scenario in each country; panels B and E represent projections in the Shrinking Deficit scenario; panels C and F represent projections in the "Equal Transmission Efficency" scenario. The 2040 projected median (IQR) values are included in the upper right of each panel. IQR represents 25th to 75th percentiles and the 90% range represents the 5th to 95th percentiles of posterior simulations.

Figure S2.12: Projections of Acquired Drug Resistance

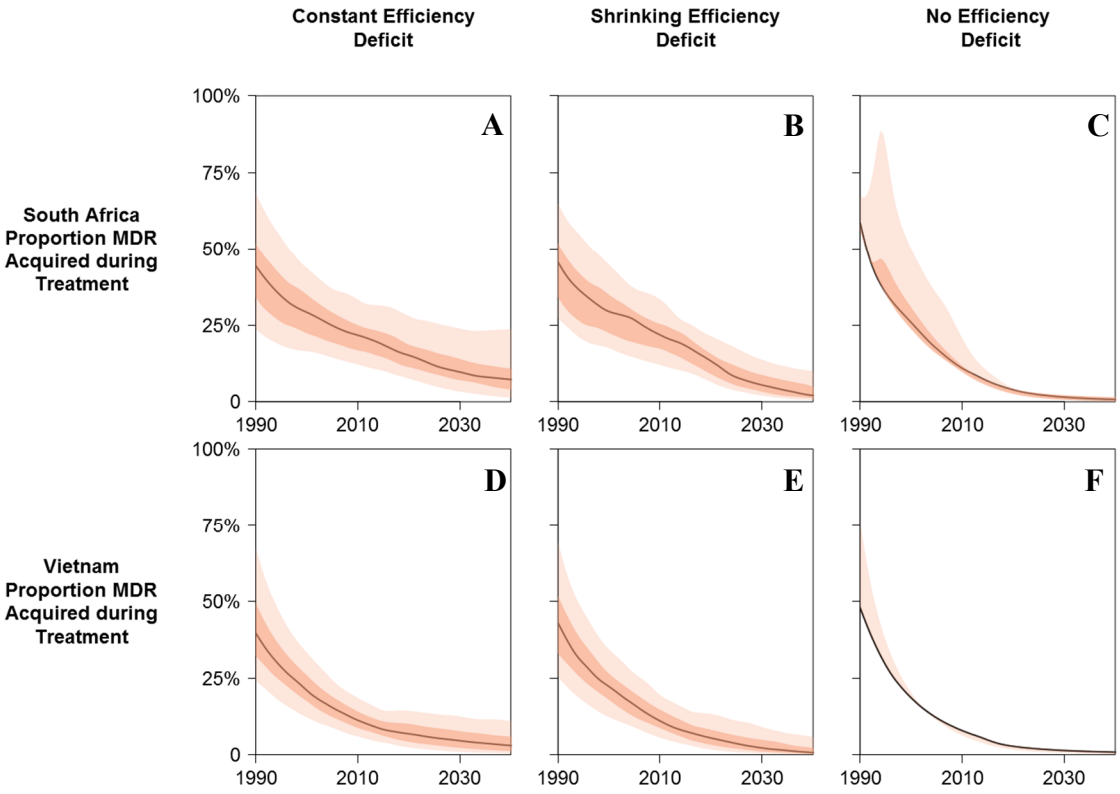

In our model, the acquisition of drug resistance (ADR) is defined as occurring at the time any population exits a DS-TB treatment state (B_{1eS} or B_{1iS}) and enters a state of symptomatic MDR-TB, will relapse with symptomatic MDR-TB, or initiates MDR-TB treatment (A_{PR} , B_{1iPR}, W_R, B_{2e1}, B_{2i}, or C_R). The transmission of drug resistance (in the calculation of proportion ADR) is defined as occurring at the time any asymptomatic, treatment-naïve population experiences the first onset of detectable MDR-TB (from S or L_R to E_R). The projected proportion of all recent-onset MDR-TB due to ADR is illustrated above. Panels A and D represent projections in the Constant Deficit scenario in each country; panels B and E represent projections in the Shrinking Deficit scenario; panels C and F represent projections in the No Deficit scenario. The 2040 projected median (IQR) values are included in the upper right of each panel. IQR represents 25th to 75th percentiles and the 90% range represents the 5th to 95th percentiles of posterior simulations.

Replication of Previous Findings

In our modeling approach, posterior simulations in the No Deficit scenario were poorly supported by empirical data and projections of the relative incidence of MDR-TB in South Africa estimated that MDR-TB would composed 22% (IQR: 11-51%; Figure S2.10 above) by 2040, significantly higher than the estimate of 5.7% (95% UR: 3.0-7.6%) published by Sharma and colleagues using a comparable model [53]. In our attempt to replicate their results using our No Deficit scenario, we first altered prior distributions for two parameters – the probability of rapid progression upon initial TB infection and the rate of reactivation upon latent infection – such that simulated TB epidemics were driven less by rapidly progressing TB and driven more by the reactivation of latent TB, leading to a more slowly developing TB epidemic. The calibration results of this Slower Epidemic scenario are presented in Figure S2.13, in comparison with the results of our Constant Deficit and No Deficit scenarios. This Slower Epidemic scenario was supported even less by empirical data relative to our No Deficit scenario (BF=24). As the Slower Epidemic becomes driven by reactivation, a high proportion of incident TB cases are among those living with HIV; this higher than expected proportion of HIV in TB cases performs poorly to our calibration of HIV/TB coinfection targets. In the Slower Epidemic scenario, we project MDR-TB will account for 17% of all incident TB by 2040 (see Figure S2.14).

Figure S2.13: Calibration Results of a Slower Epidemic Scenario in South Africa

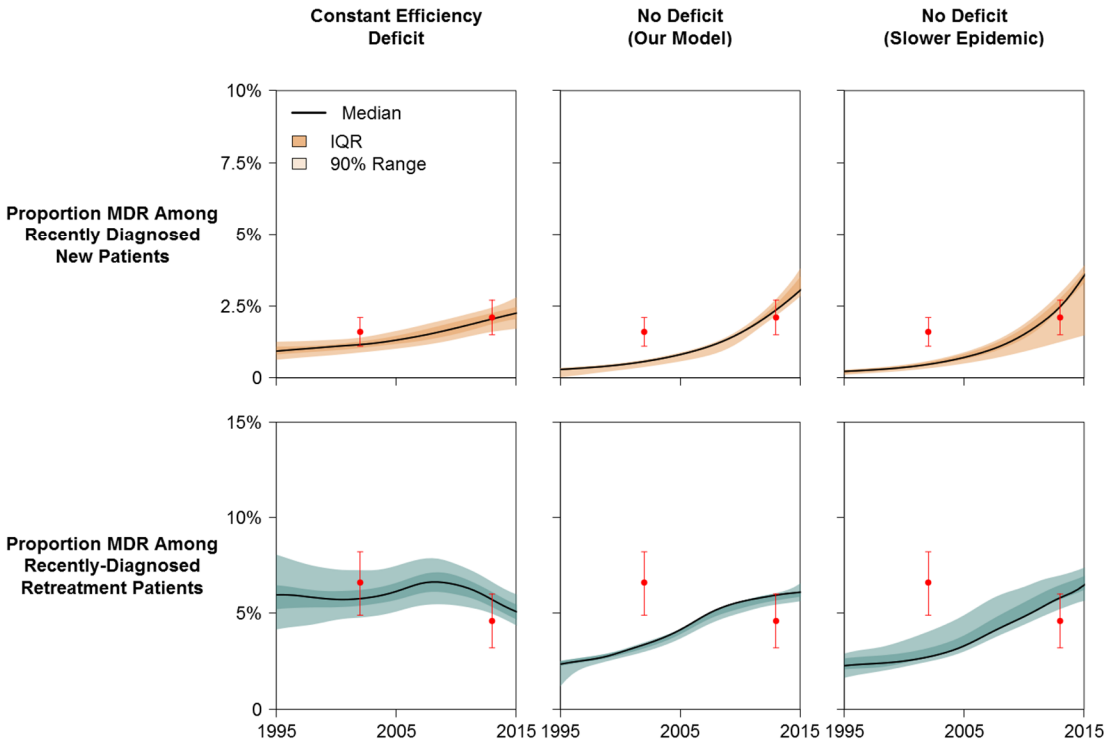

Simulated epidemics are weighted according to how well each reproduced empirical calibration targets. Red points represent median and 95% confidence intervals for calibration targets drawn from national survey data. For comparison, results from the Constant Deficit scenario and the No Deficit scenario (Figure 4.3) are reproduced here. IQR represents 25th to 75th percentiles and the 90% range represents the 5th to 95th percentiles of posterior simulations.

Figure S2.14: Projections of MDR-TB Burden in a Slower Epidemic

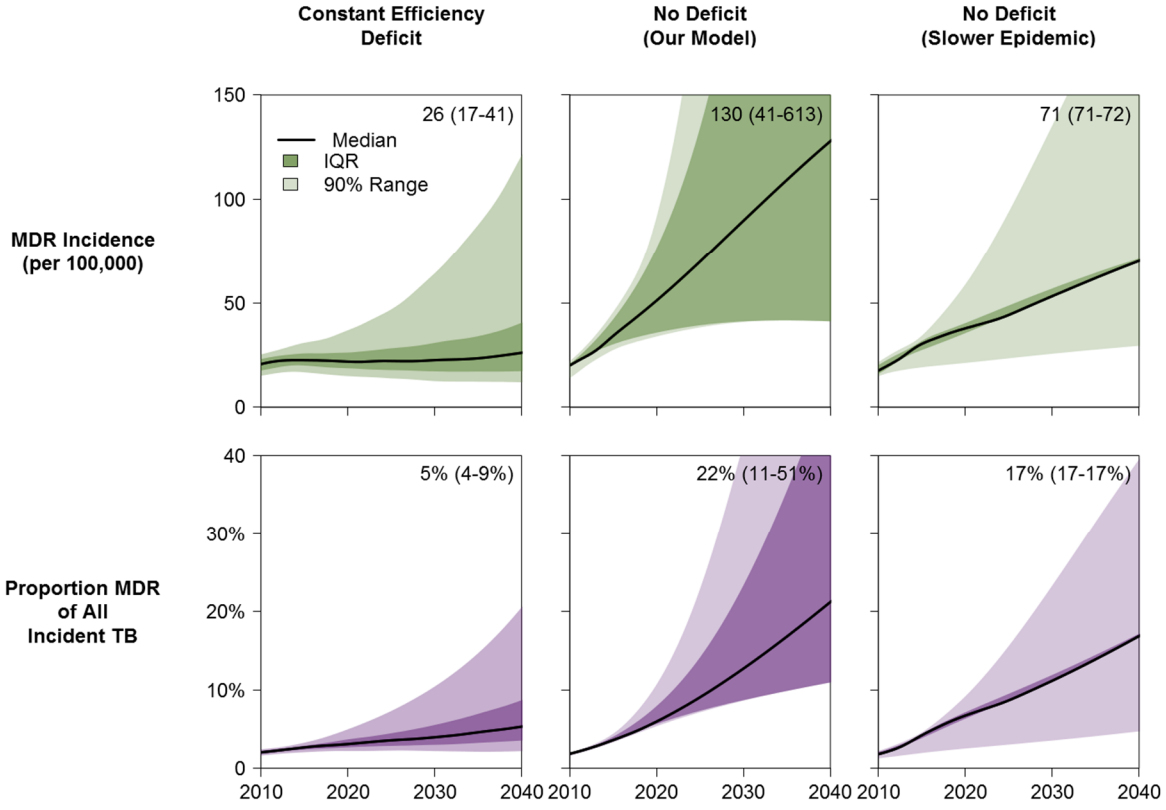

Simulated MDR-TB epidemics in South Africa were projected from 2010 to 2040. Panels in the top row illustrate the projected absolute MDR-TB incidence, while panels in the lower row illustrate MDR-TB as a proportion of all incident TB. For comparison, results from the Constant Deficit scenario (Figure 4.4) and the No Deficit scenario (Figure S2.10 above) are reproduced here. The 2040 projected median (IQR) values are included in the upper right of each panel. IQR represents 25th to 75th percentiles and the 90% range represents the 5th to 95th percentiles of posterior simulations.

These results were still meaningfully higher than the estimates published by Sharma and colleagues. We therefore adjusted this scenario further by increasing the prior distribution of the duration of delay between the onset of TB and the initiation of care from a median of 12 months to a median of 10 years, comparable to the posterior probability of effective DS-TB treatment initiation published by Sharma and colleagues. In this Delayed Treatment scenario, few TB patients (DS-TB or MDR-TB) receive treatment of any kind, having died of TB or self-cured before treatment begins. As a result, MDR-TB exerts little competitive advantage over DS-TB (through lower probabilities of cure and longer durations of symptomatic, infectious disease). With this additional adjustment, the Delayed Treatment scenario was better supported by empirical data than the Slower Epidemic scenario ($BF>10^6$) but still more poorly supported relative to our Constant Deficit scenario (BF=0.08); calibration results of this model are presented in Figure S2.15.

Figure S2.15: Calibration Results of a Delayed Treatment Scenario

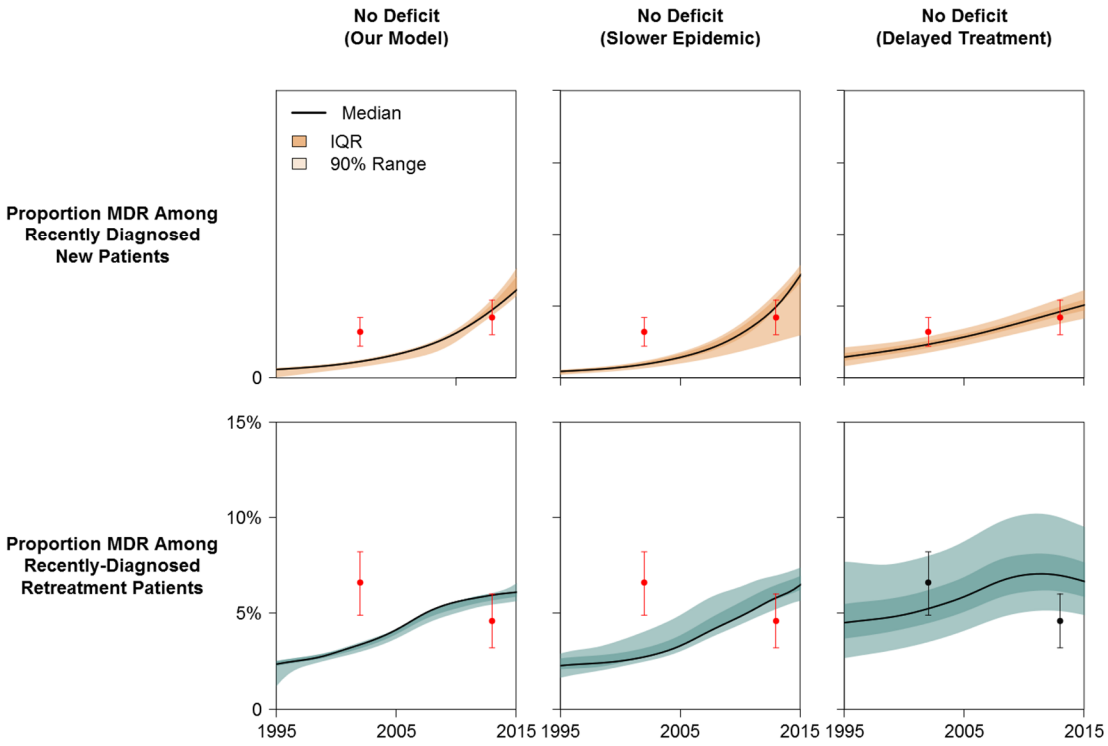

Simulated epidemics are weighted according to how well each reproduced empirical calibration targets. Red points represent median and 95% confidence intervals for calibration targets drawn from national survey data. For comparison, results from the No Deficit scenario (Figure 4.3) and the Slower Epidemic scenario (Figure S2.13 above) are reproduced here. IQR represents 25th to 75th percentiles and the 90% range represents the 5th to 95th percentiles of posterior simulations.

In the Delayed Treatment scenario, we project that MDR-TB will account for 6% (IQR: 5-7%) of incident TB in South Africa by 2040 (see Figure S2.16), comparable to the estimate published by Sharma and colleagues. This implies that the discrepancies between our primary results and those previously published may not be due to fundamental differences in model structures or statistical approaches but can be explained largely by differences in the selection of parameter priors. Parameter selection is a delicate task and even minor differences in prior distributions may affect long-term projections [54]. A number of epidemiological studies have examined primary progressive TB and TB reactivation, with some variation in estimates between studies and between demographic groups within studies [7,9,8,10,11]. These estimates may be parameterized in several ways, and the values used in our Slower Epidemic scenario may be consistent with this body of literature.

More uncertainty exists around the probabilities and timing of care seeking, diagnosis, referral, and treatment initiation in South Africa, and parameterizing these processes is complex. Nonetheless, WHO estimates of treatment initiation indicate that 54% (95% confidence interval: 40-78%) of incident TB cases in South Africa were diagnosed in 2016 [3], and measured total delays in Africa before treatment initiation may be 1-2 orders of magnitude shorter than our modified median prior value of 10 years [55–57]. Therefore, while our Delayed Treatment scenario may perform well statistically, it is unlikely to be an accurate or informative representation of the current MDR-TB epidemic in South Africa.

Figure S2.16: Projections of MDR-TB Burden in a Delayed Treatment Scenario

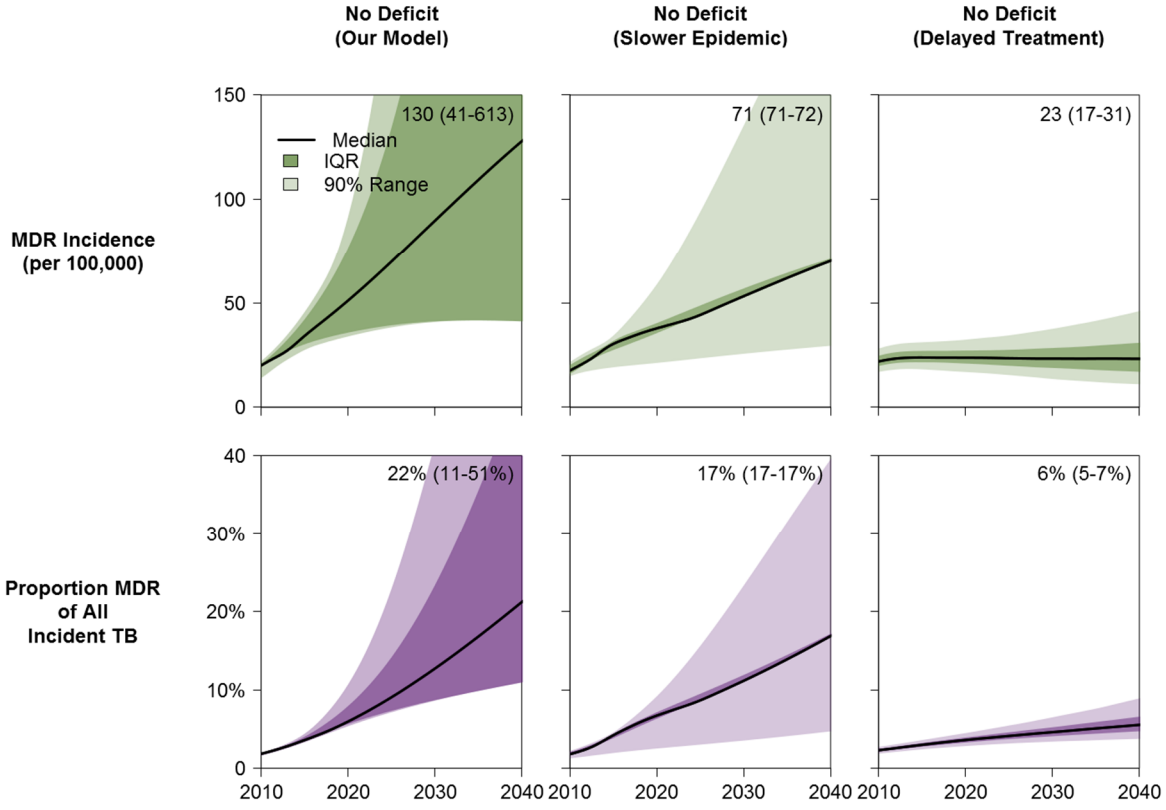

Simulated MDR-TB epidemics in South Africa were projected from 2010 to 2040. Panels in the top row illustrate the projected absolute MDR-TB incidence, while panels in the lower row illustrate MDR-TB as a proportion of all incident TB. For comparison, results from the No Deficit scenario and the Slower Epidemic scenario (Figure S2.14 above) are reproduced here. The 2040 projected median (IQR) values are included in the upper right of each panel. IQR represents 25th to 75th percentiles and the 90% range represents the 5th to 95th percentiles of posterior simulations.

Sensitivity Analyses

As described in the Supplementary Methods, we performed multivariate sensitivity analyses using PRCCs and univariate sensitivity analyses using parameter quintiles associated with two primary outcomes: the absolute incidence of MDR-TB in 2040 and the fold change in the relative incidence of MDR-TB between 2016 and 2040. Results of sensitivity analyses around the absolute MDR-TB incidence in 2040 for all parameters in South Africa are presented in Figures S2.17-S2.22, and results of analyses around the fold change in relative incidence are presented in Figures S2.22-S2.28. Results of sensitivity analyses around the absolute MDR-TB incidence in 2040 in Vietnam are presented in Figures S2.29-S2.34, and results of analyses around the fold change in relative incidence are presented in Figures S2.35-S2.40.

Figure S2.17: Sensitivity Analysis – PRCCs of TB Natural History Parameters and Absolute MDR-TB Incidence – South Africa

Each bar represents the partial rank correlation coefficient of the association between each model parameter and the the primary outcome (the incidence of MDR-TB in 2040), adjusting for all other parameters in the model. Beneath each parameter label is the sampling range from which parameter values were sampled.

Figure S2.18: Sensitivity Analysis – Absolute MDR-TB Incidence by TB Natural History Parameter Quintiles – South Africa

Each boxplot represents the distribution of values for the primary outcome (the incidence of MDR-TB in 2040) within a given set of simulations. Pairs of boxplots represent groups of simulations categorized by values of a single input parameter: red boxplots represent the outcomes of those simulations with parameter values in the upper 20% of all simulations; blue boxplots represent the outcomes of those simulations with parameter values in the lower 20% of all simulations. More influential parameters demonstrate a greater separation of the distributions of outcome between simulations in the upper quintile and simulations in the lower quintile of parameter values. To the left of each panel are included the input parameter values corresponding to the accompanying quintile. In black is represented the overall distribution of the outcome across all simulations and the median estimate is drawn as a vertical dotted line. Boxes represent the median, 25th, and 75th percentiles of the distribution of outcomes; whiskers represent the 5th and 95th percentiles of the distribution of outcomes. In the Constant Deficit model, parameters involving the increase in MDR-TB transmission efficiency are excluded.

Figure S2.17: Sensitivity Analysis – PRCCs of TB Natural History Parameters and Absolute MDR-TB Incidence – South Africa

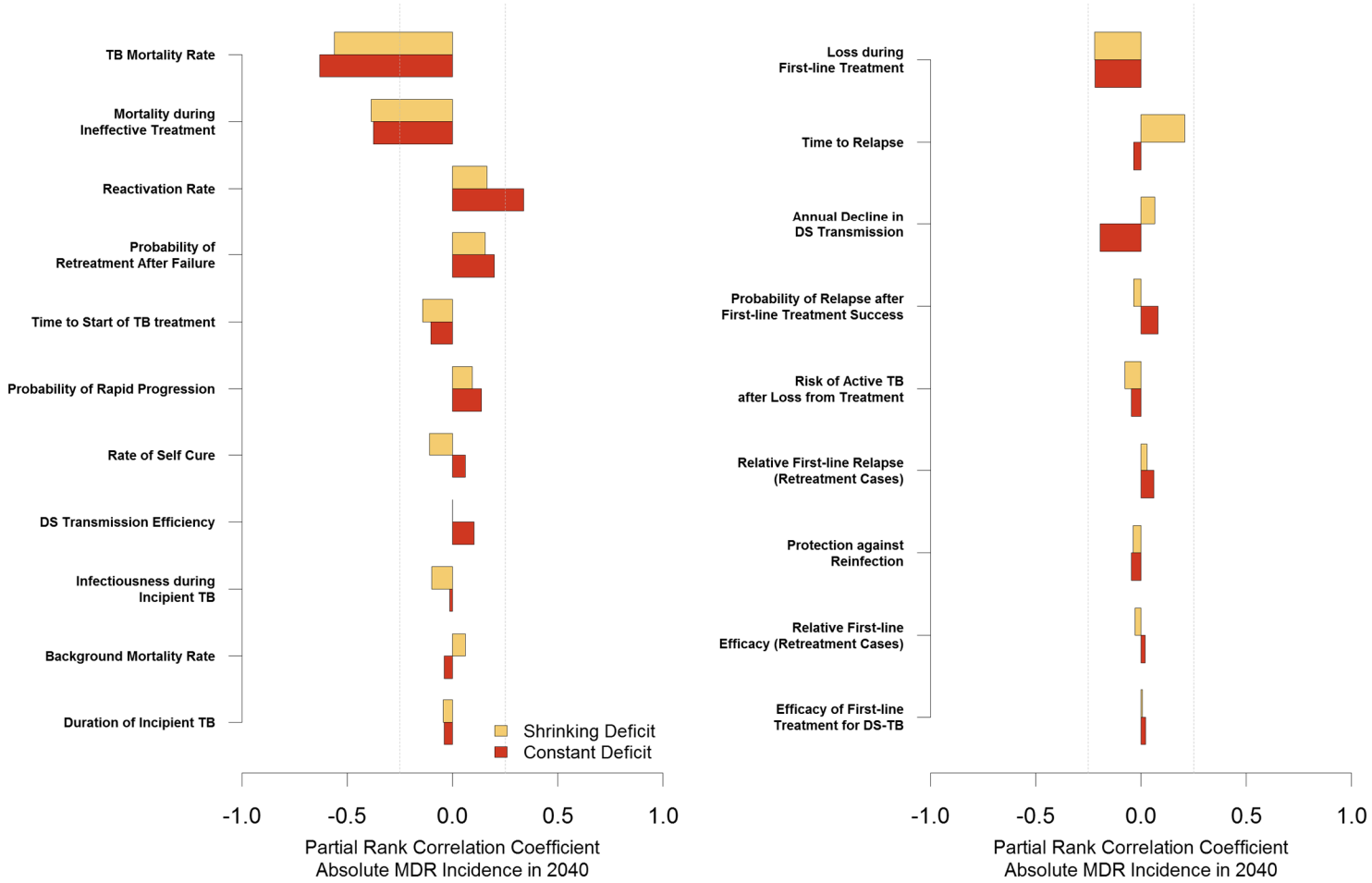

Figure S2.18: Sensitivity Analysis – Absolute MDR-TB Incidence by TB Natural History Parameter Quintiles – South Africa

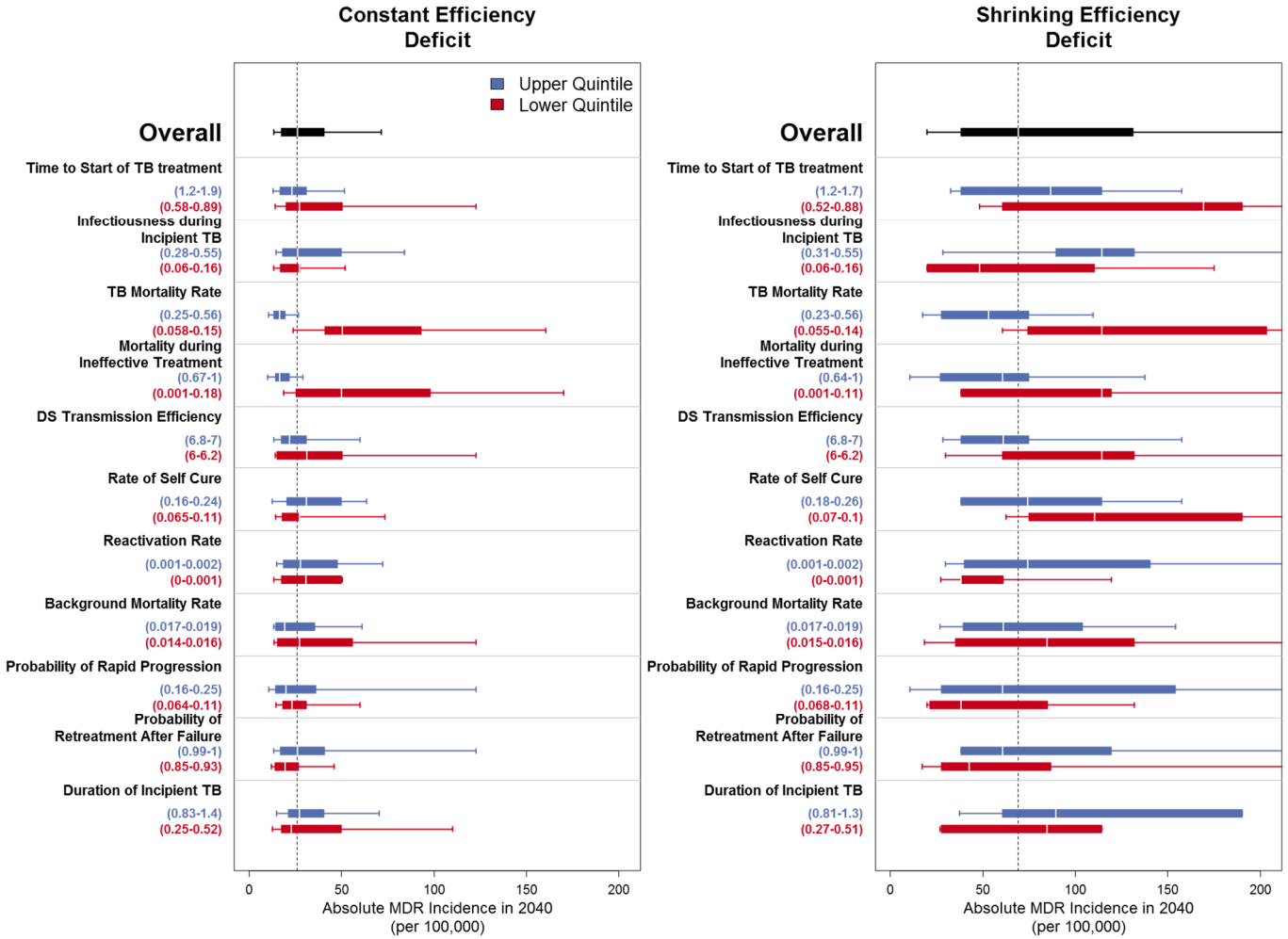

Figure S2.18 (Continued): Sensitivity Analysis – Absolute MDR-TB Incidence by TB Natural History Parameter Quintiles – South Africa

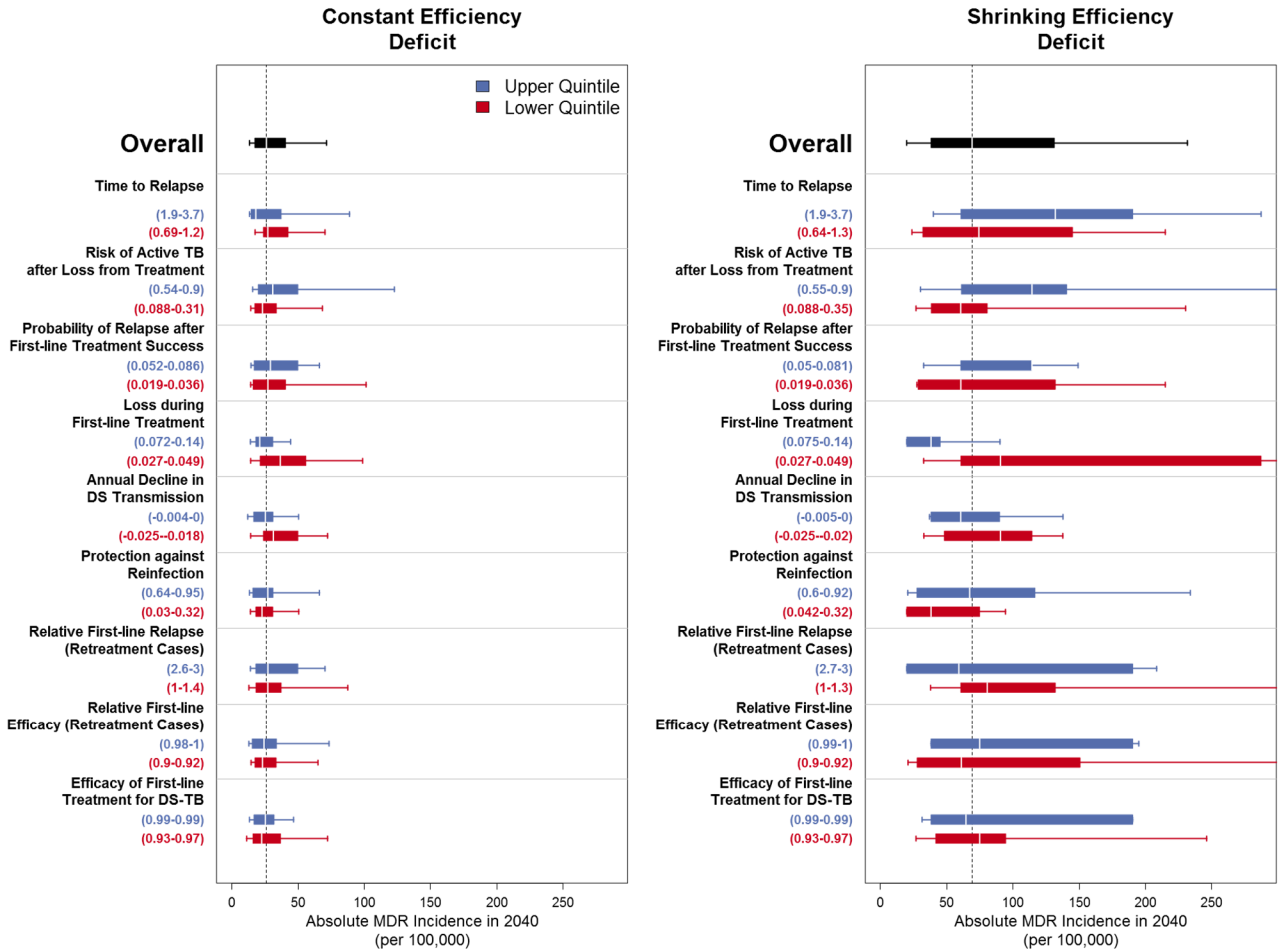

Figure S2.19: Sensitivity Analysis – PRCCs of HIV and HIV/TB Parameter and Absolute MDR-TB Incidence – South Africa

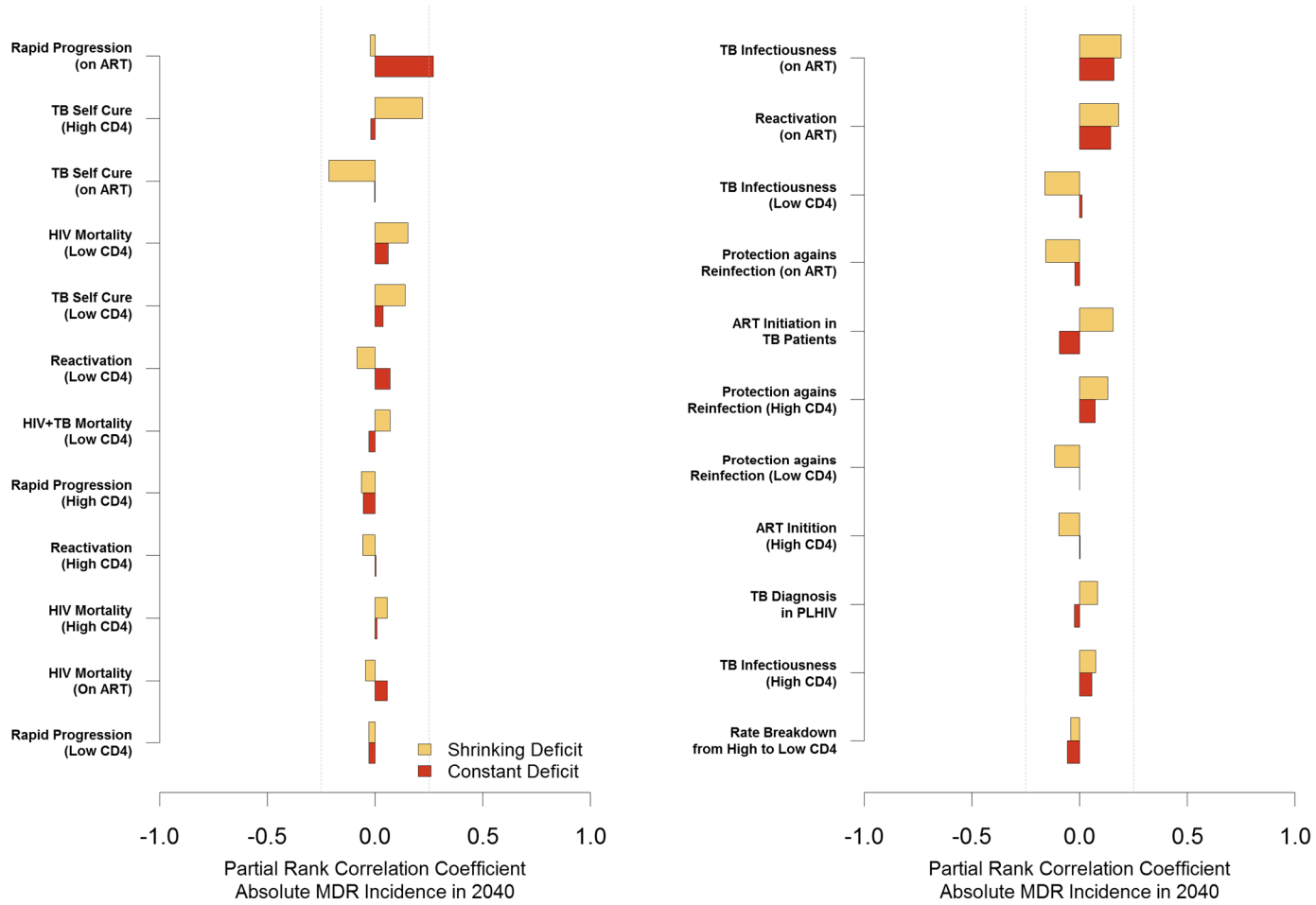

Figure S2.20: Sensitivity Analysis – Absolute MDR-TB Incidence by HIV and HIV/TB Parameter Quintiles – South Africa

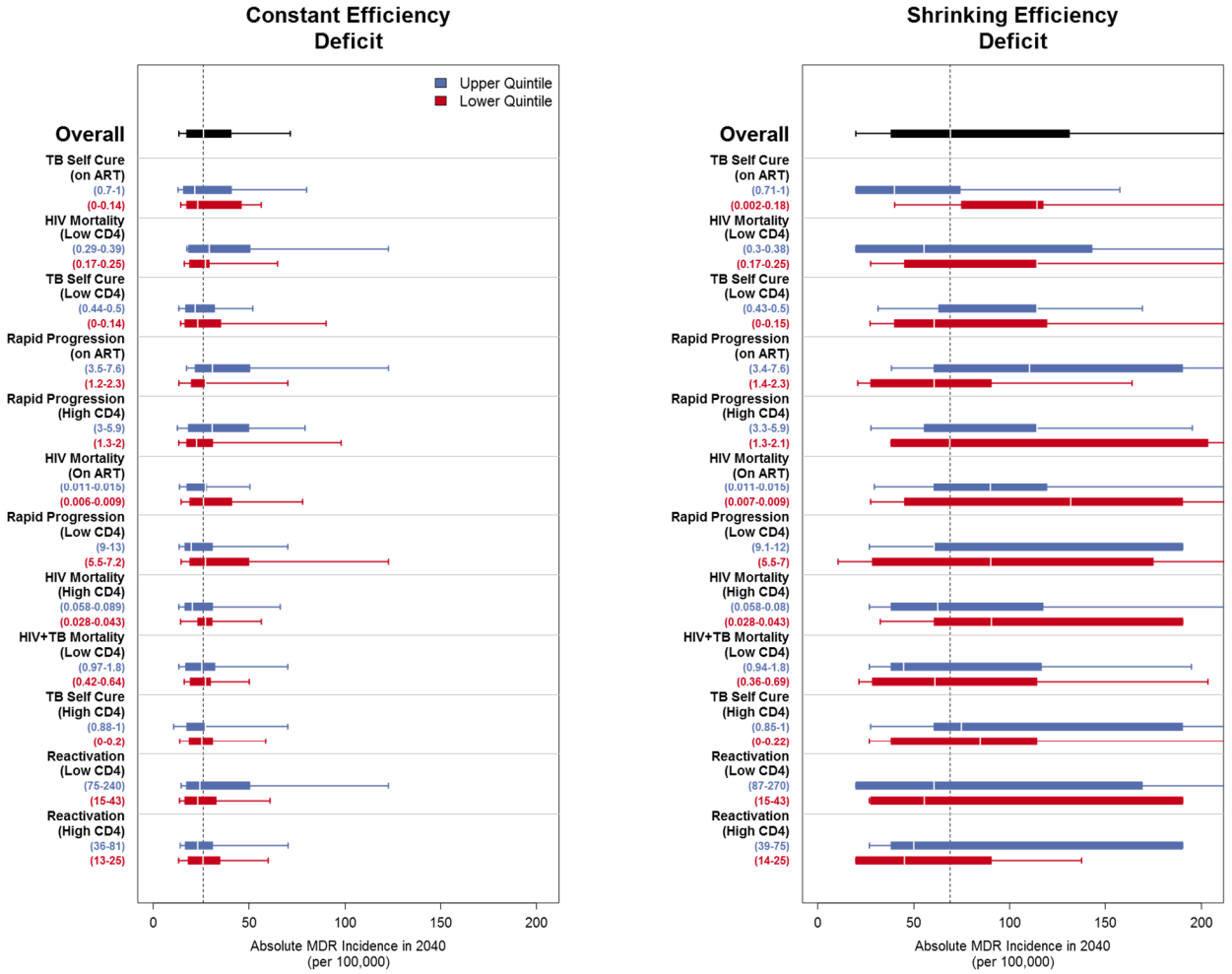

Figure S2.20 (Continued): Sensitivity Analysis – Absolute MDR-TB Incidence by HIV and HIV/TB Parameter Quintiles – South Africa

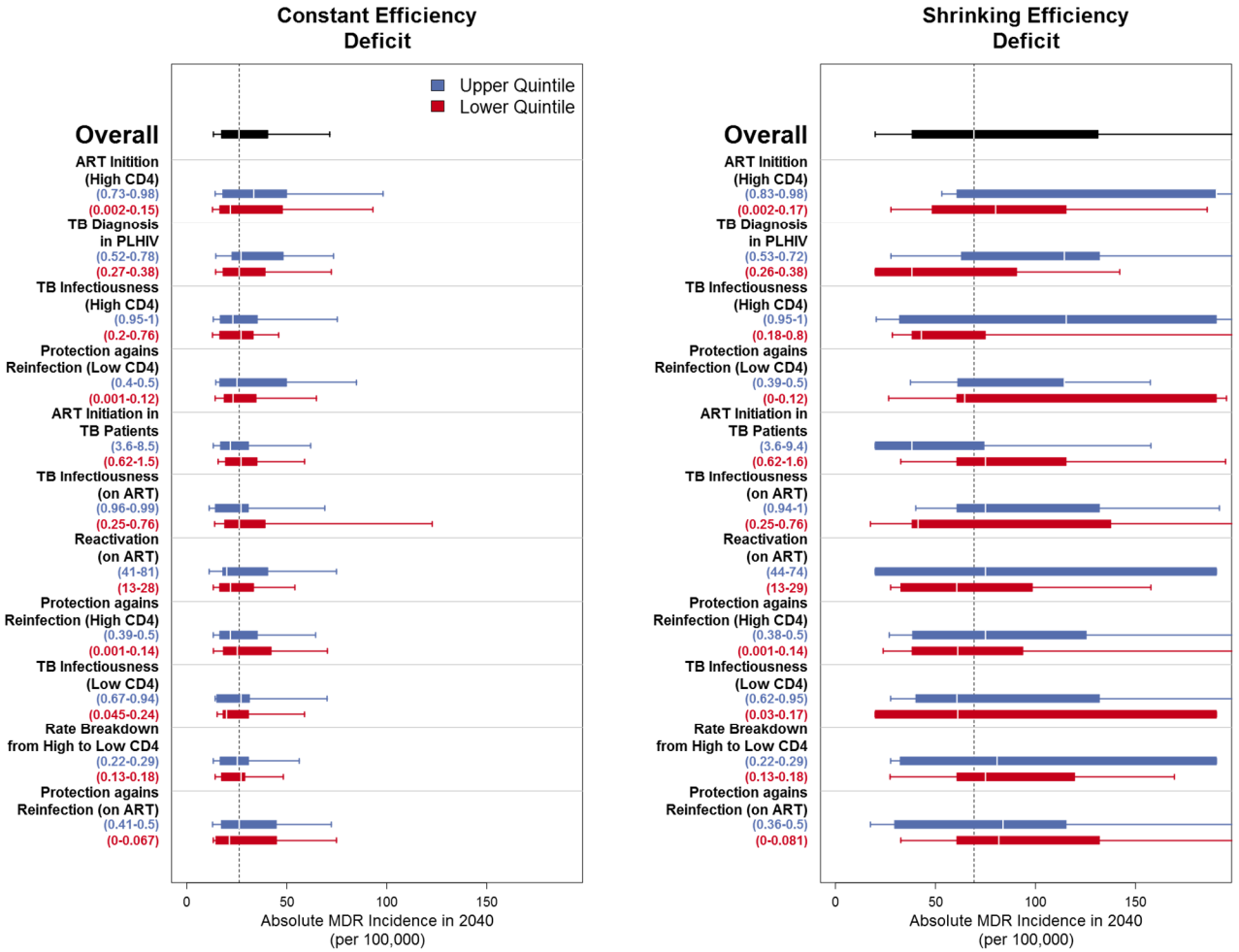

Figure S2.21: Sensitivity Analysis – PRCCs of MDR-TB Parameters and Absolute MDR-TB Incidence – South Africa

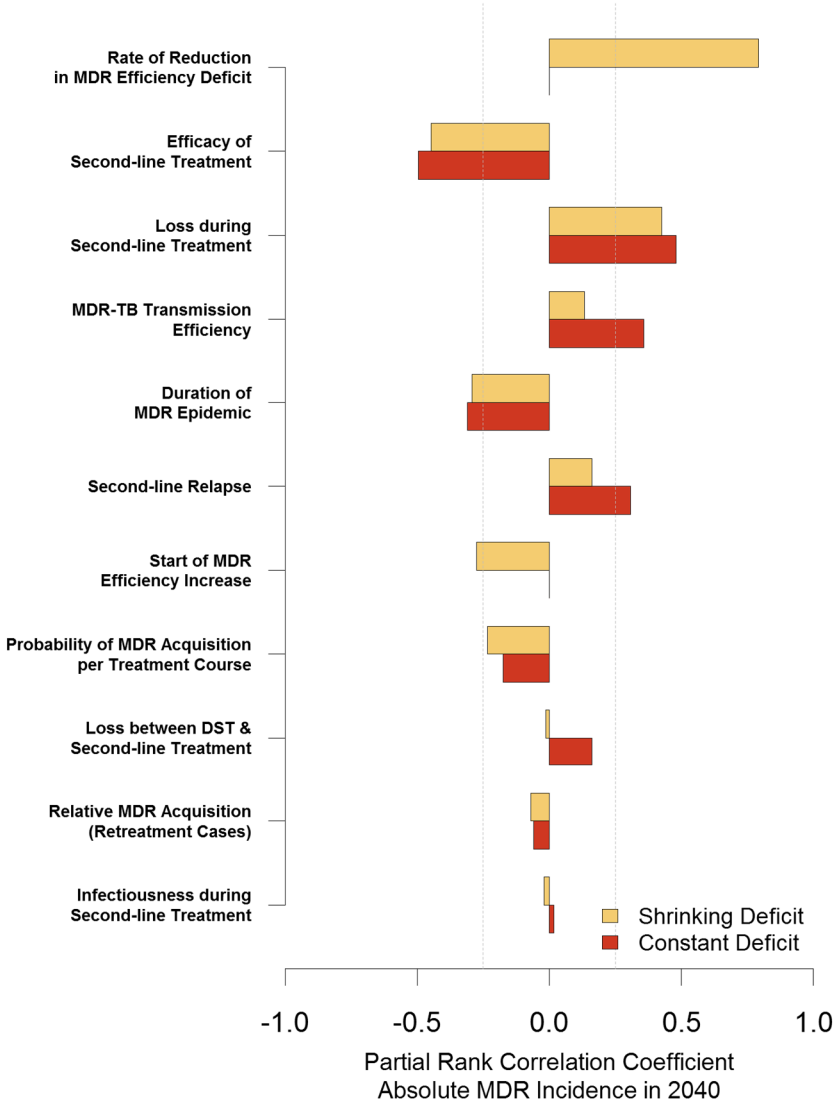

Figure S2.22: Sensitivity Analysis – Absolute MDR-TB Incidence by MDR-TB Parameter Quintiles – South Africa

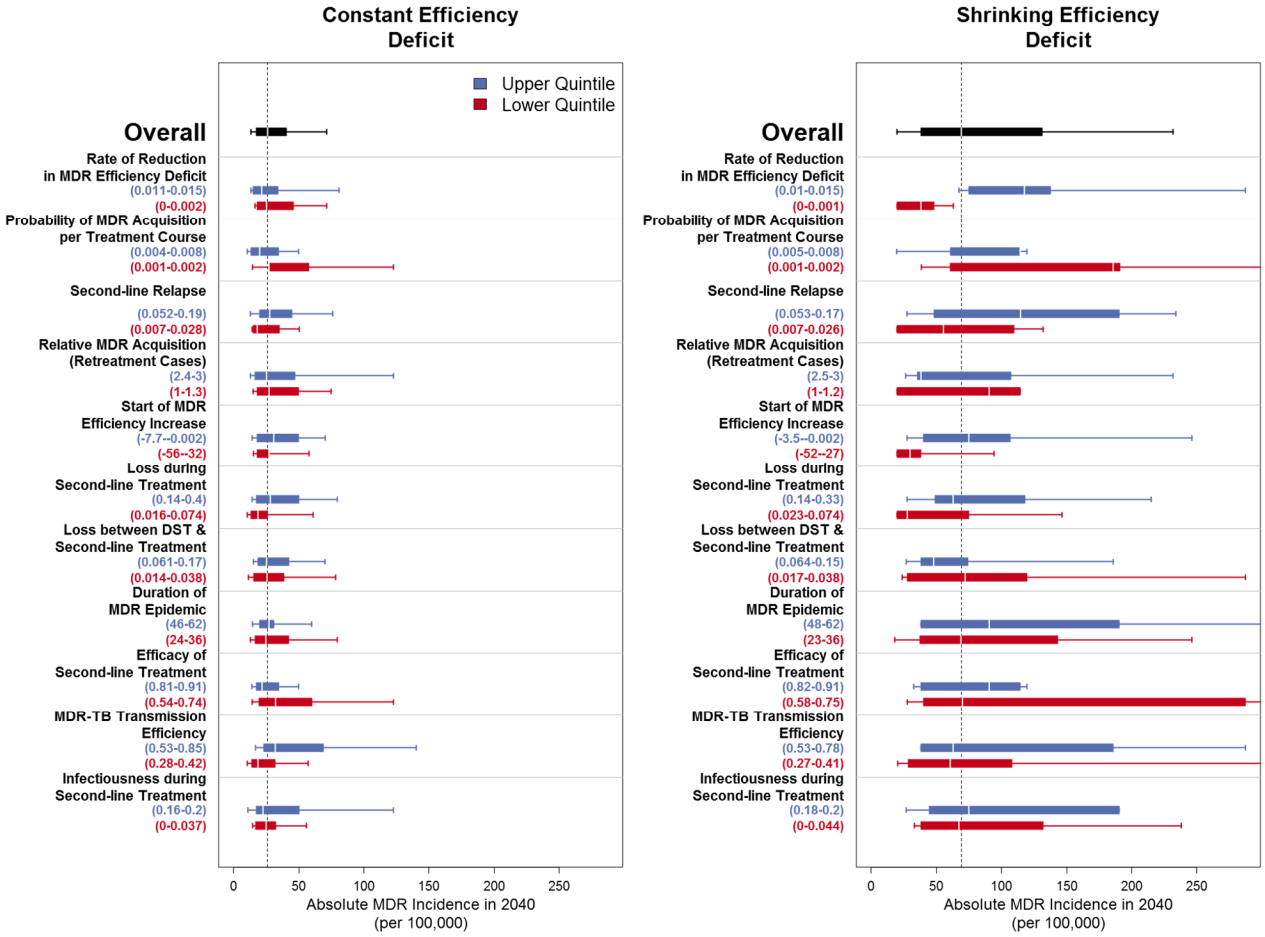

Figure S2.23: Sensitivity Analysis – PRCCs of TB Natural History Parameters and Change in Relative MDR-TB Incidence – South Africa

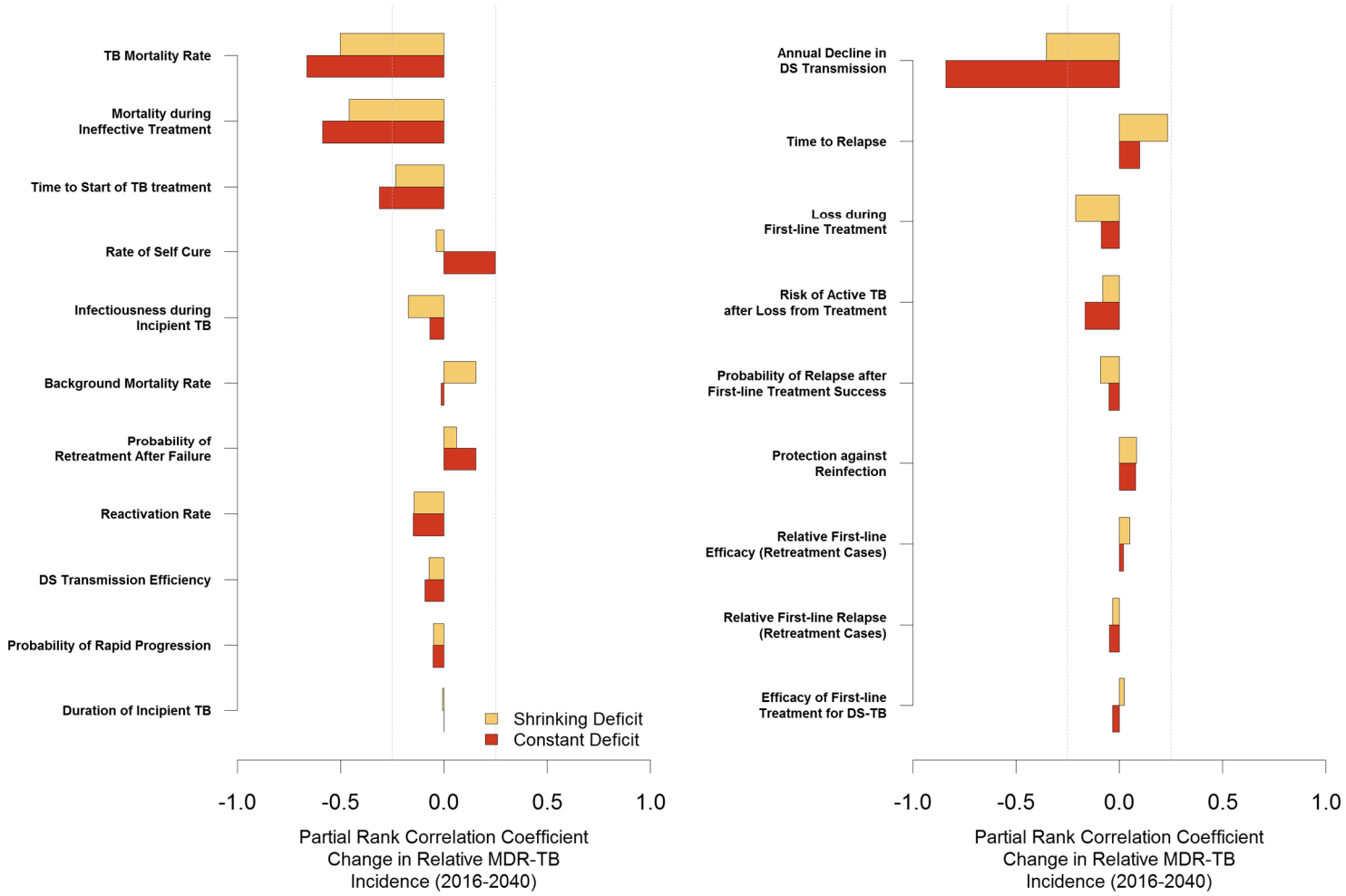

Figure S2.24: Sensitivity Analysis – Change in Relative MDR-TB Incidence by TB Natural History Parameter Quintiles – South Africa

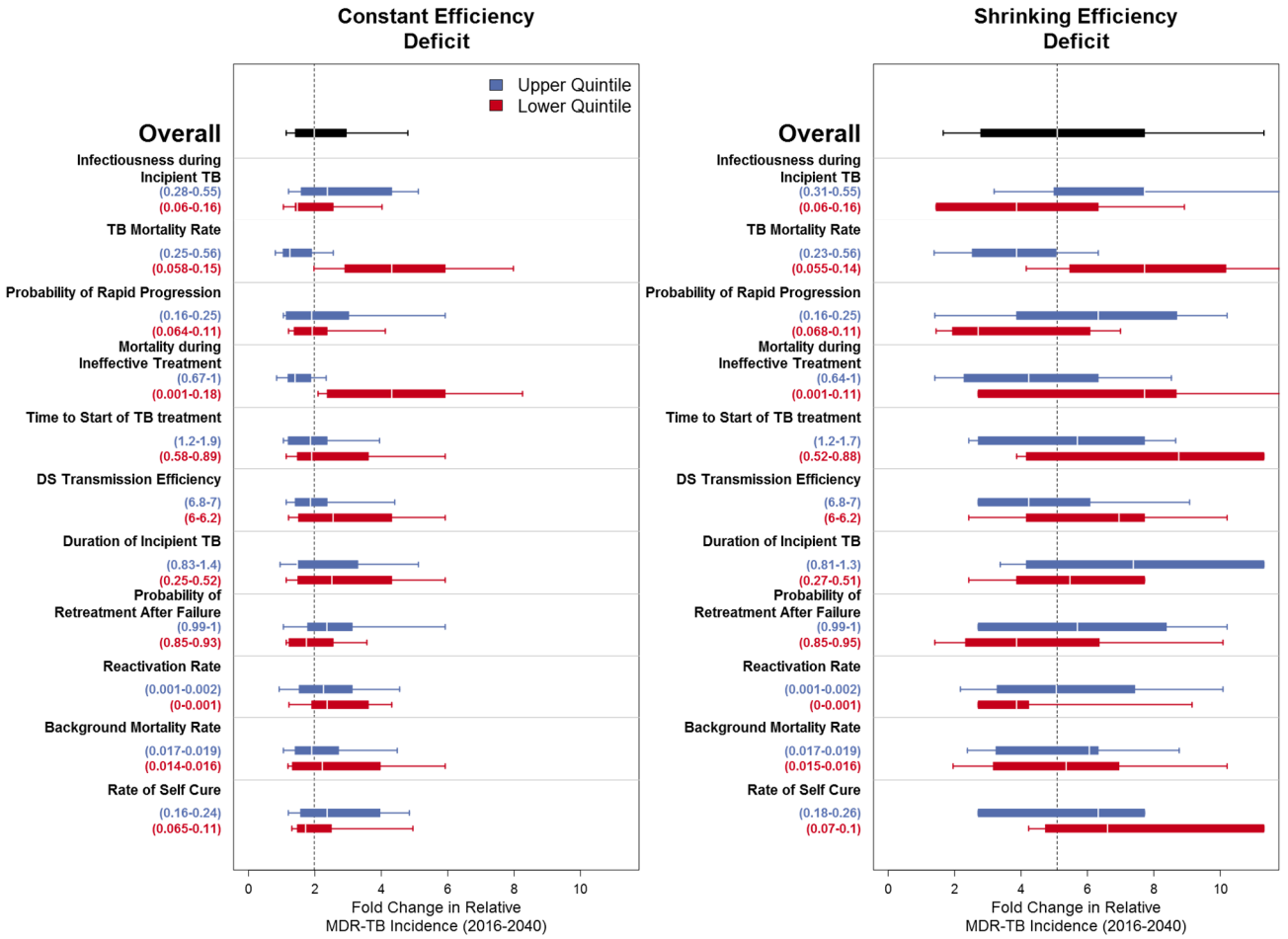

Figure S2.24 (Continued): Sensitivity Analysis – Change in Relative MDR-TB Incidence by TB Natural History Parameter Quintiles – South Africa

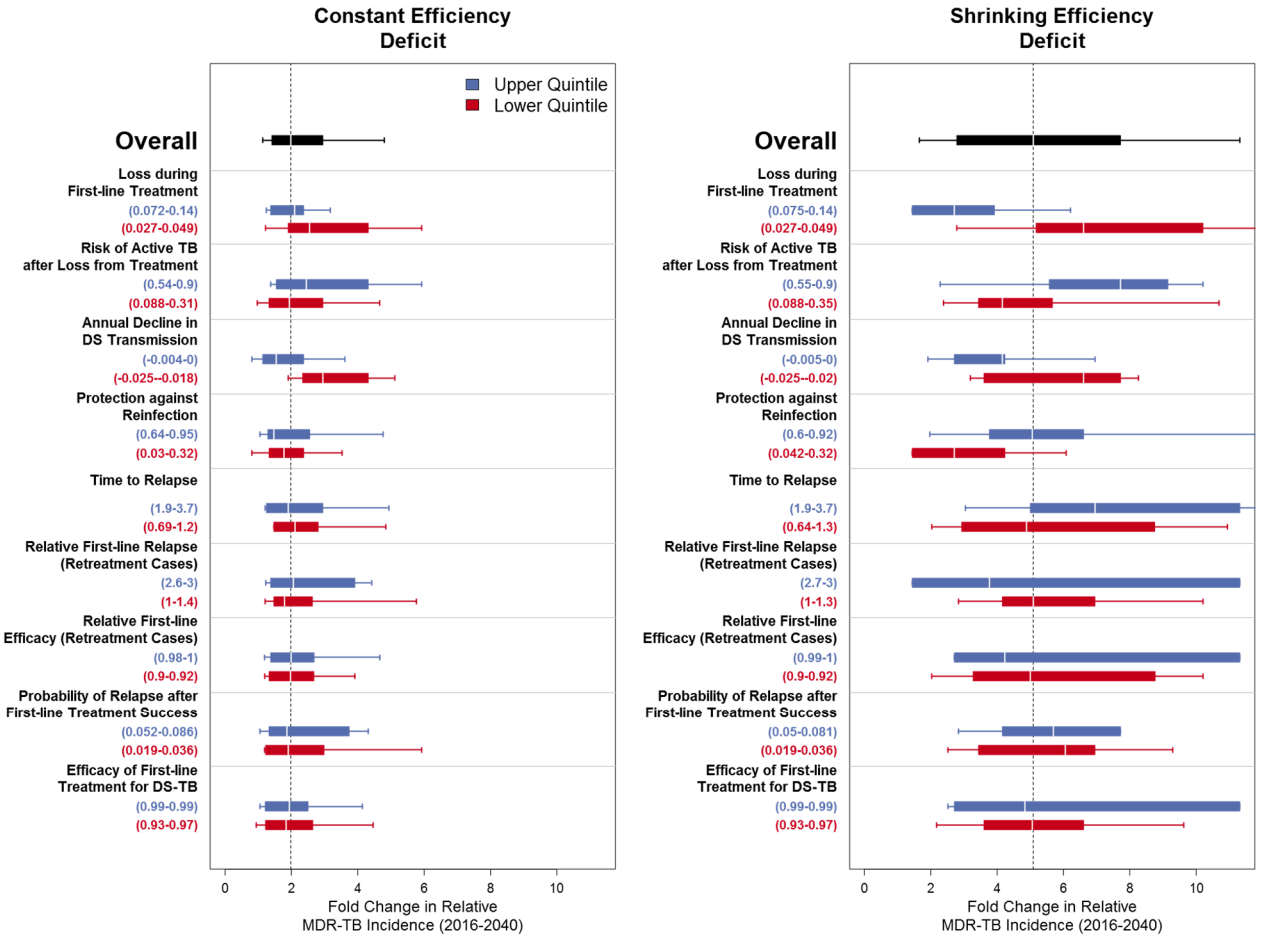

Figure S2.25: Sensitivity Analysis – PRCCs of HIV and HIV/TB Parameter and Change in Relative MDR-TB Incidence – South Africa

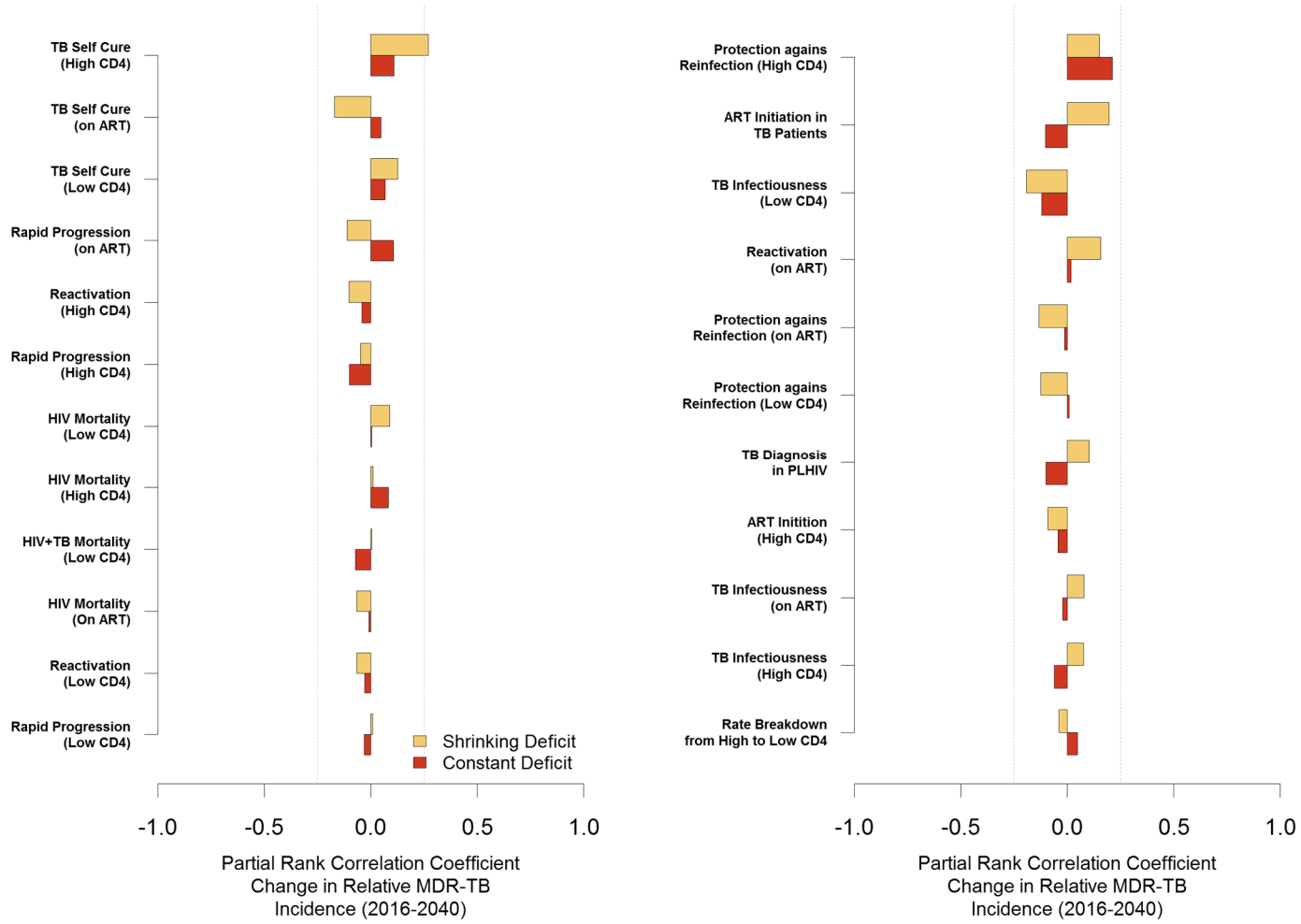

Figure S2.26: Sensitivity Analysis – Change in Relative MDR-TB Incidence by HIV and HIV/TB Parameter Quintiles – South Africa

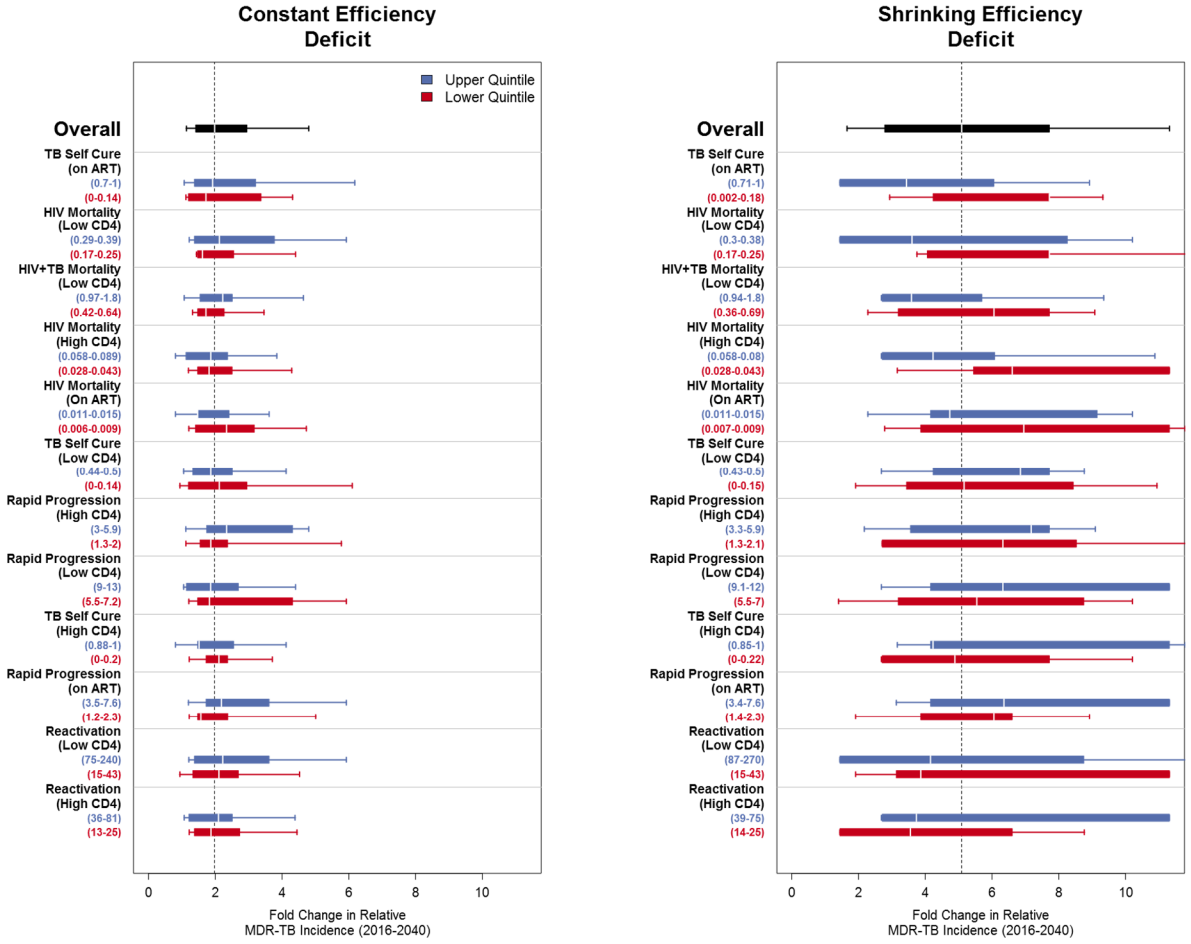

Figure S2.26 (Continued): Sensitivity Analysis – Change in Relative MDR-TB Incidence by HIV and HIV/TB Parameter Quintiles – South Africa

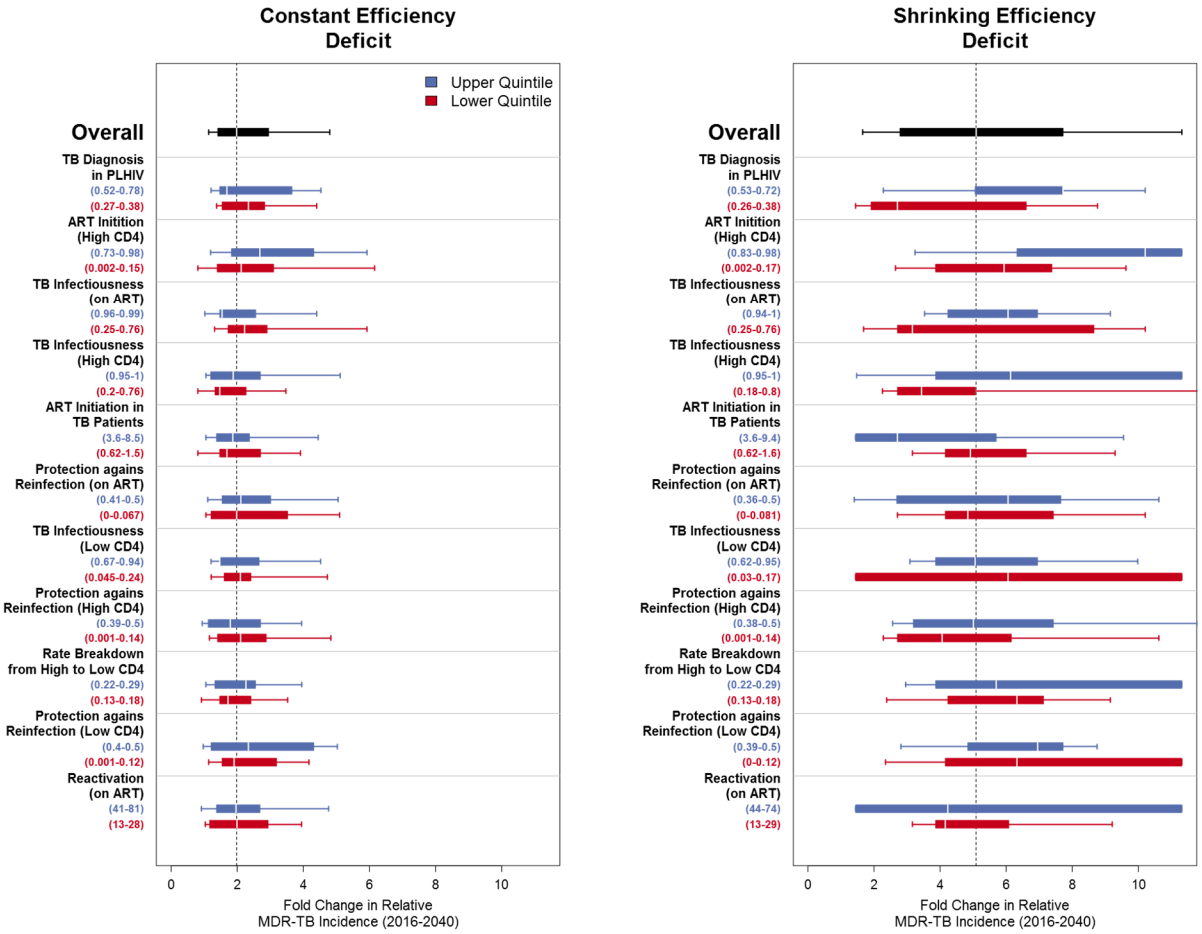

Figure S2.27: Sensitivity Analysis – PRCCs of MDR-TB Parameters and Change in Relative MDR-TB Incidence – South Africa

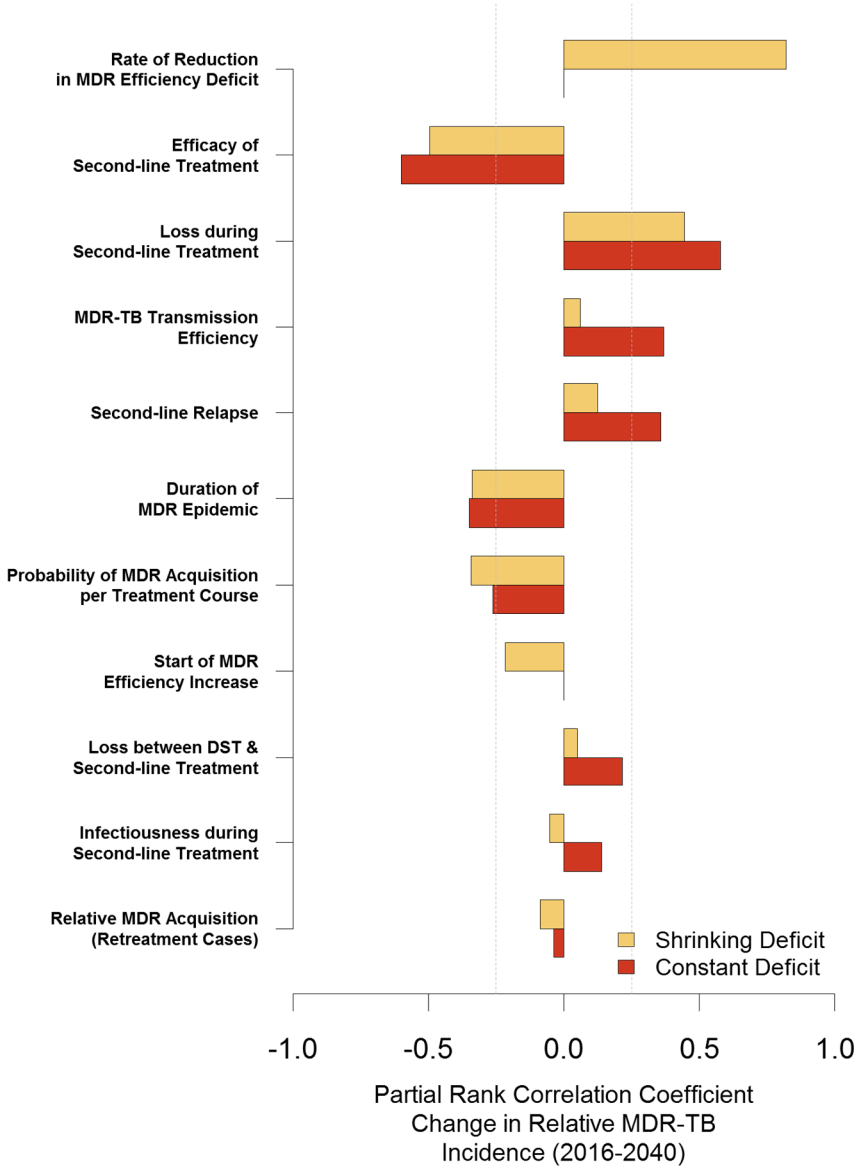

Figure S2.28: Sensitivity Analysis – Change in Relative MDR-TB Incidence by MDR-TB Parameter Quintiles – South Africa

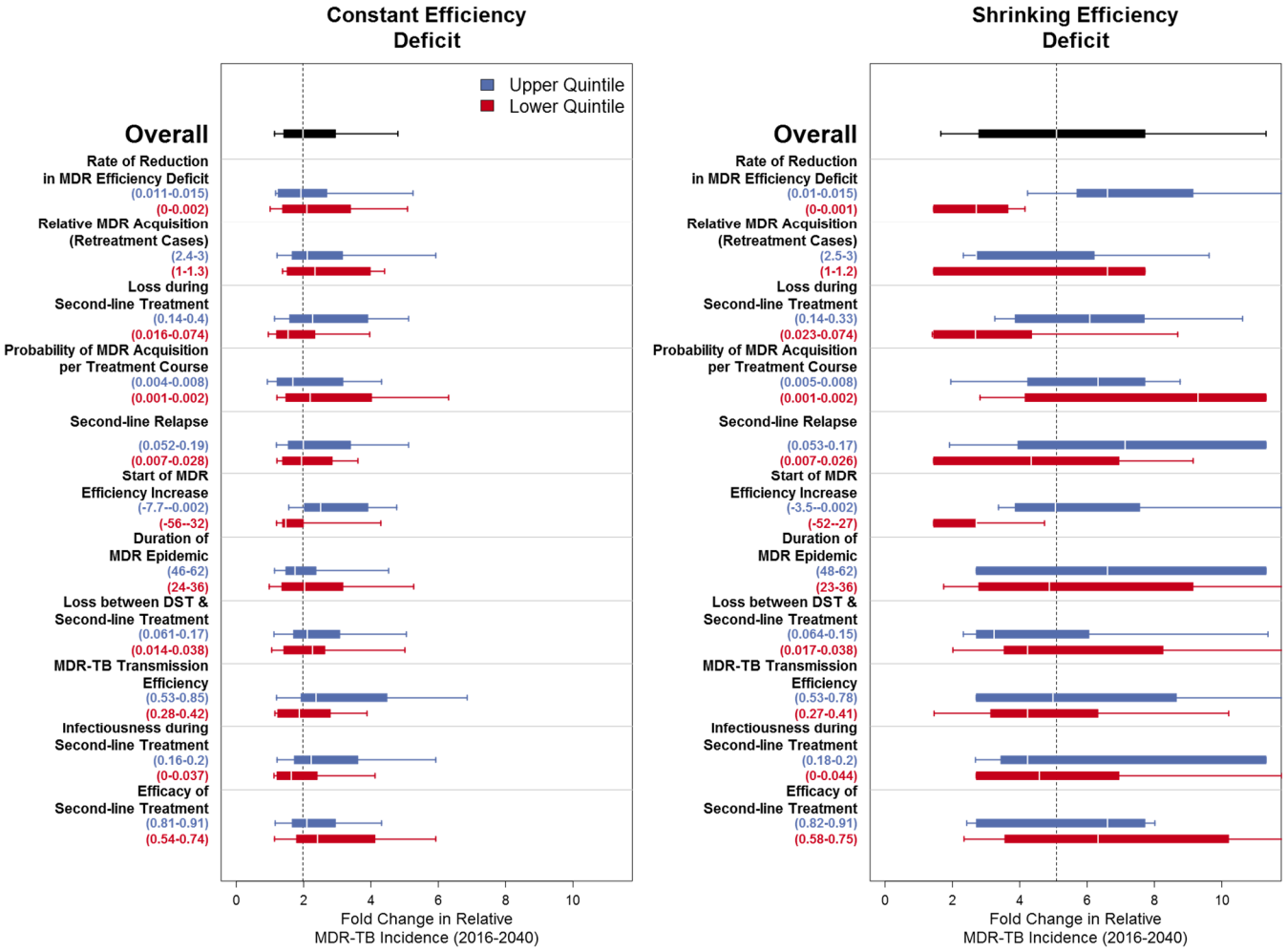

Figure S2.29: Sensitivity Analysis – PRCCs of TB Natural History Parameters and Absolute MDR-TB Incidence – Vietnam

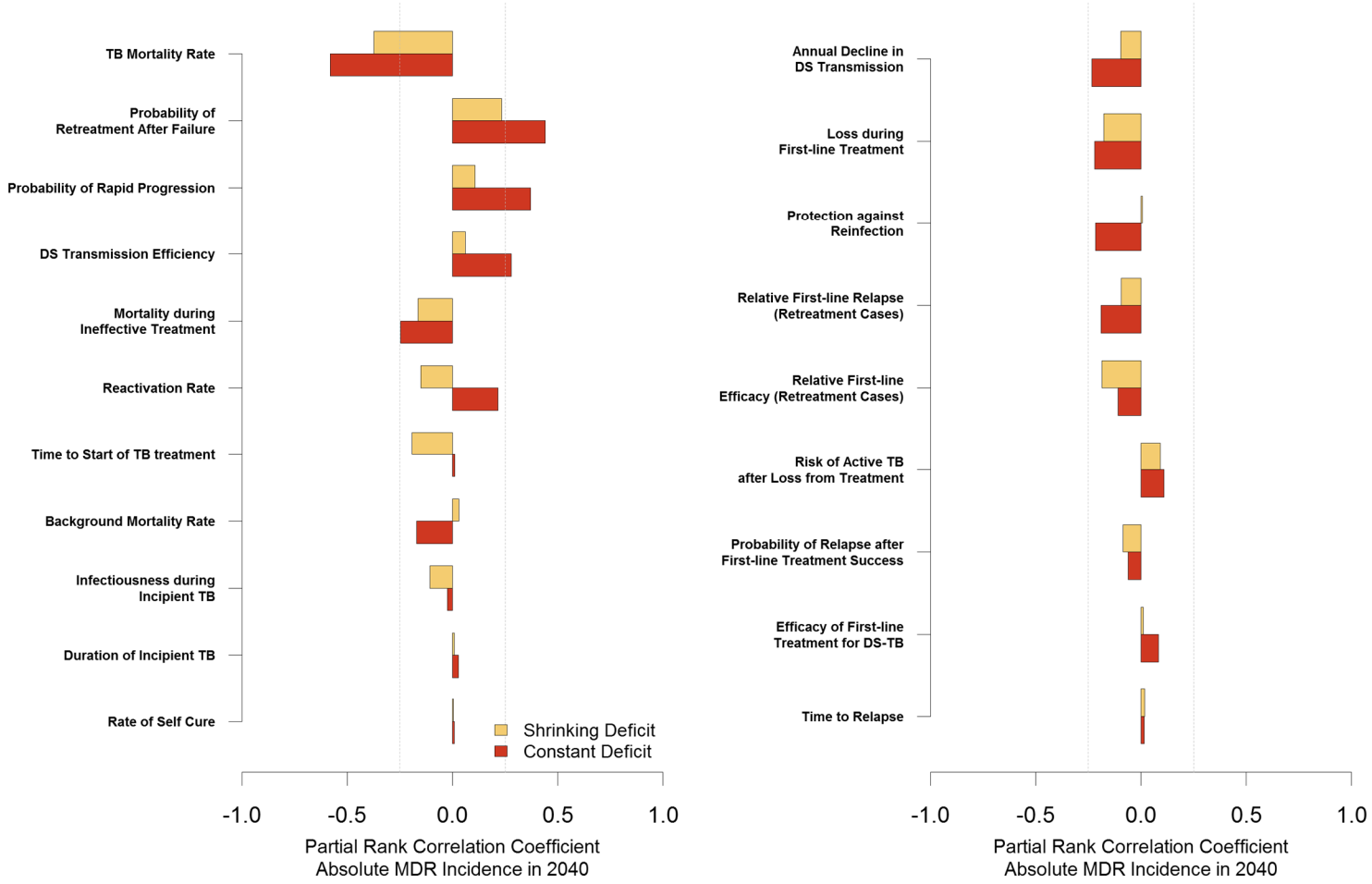

Figure S2.30: Sensitivity Analysis – Absolute MDR-TB Incidence by TB Natural History Parameter Quintiles – Vietnam

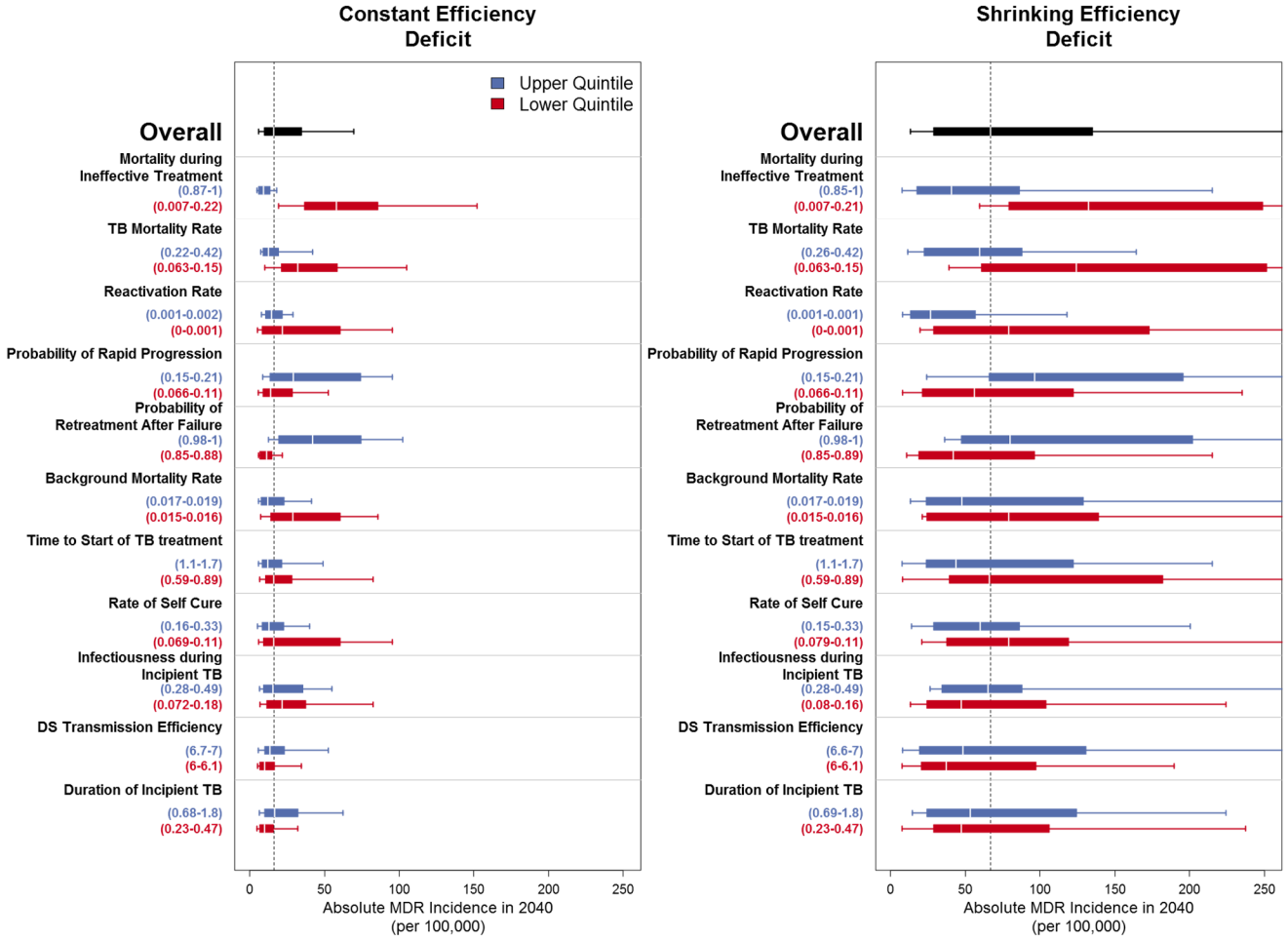

Figure S2.30 (Continued): Sensitivity Analysis – Absolute MDR-TB Incidence by TB Natural History Parameter Quintiles – Vietnam

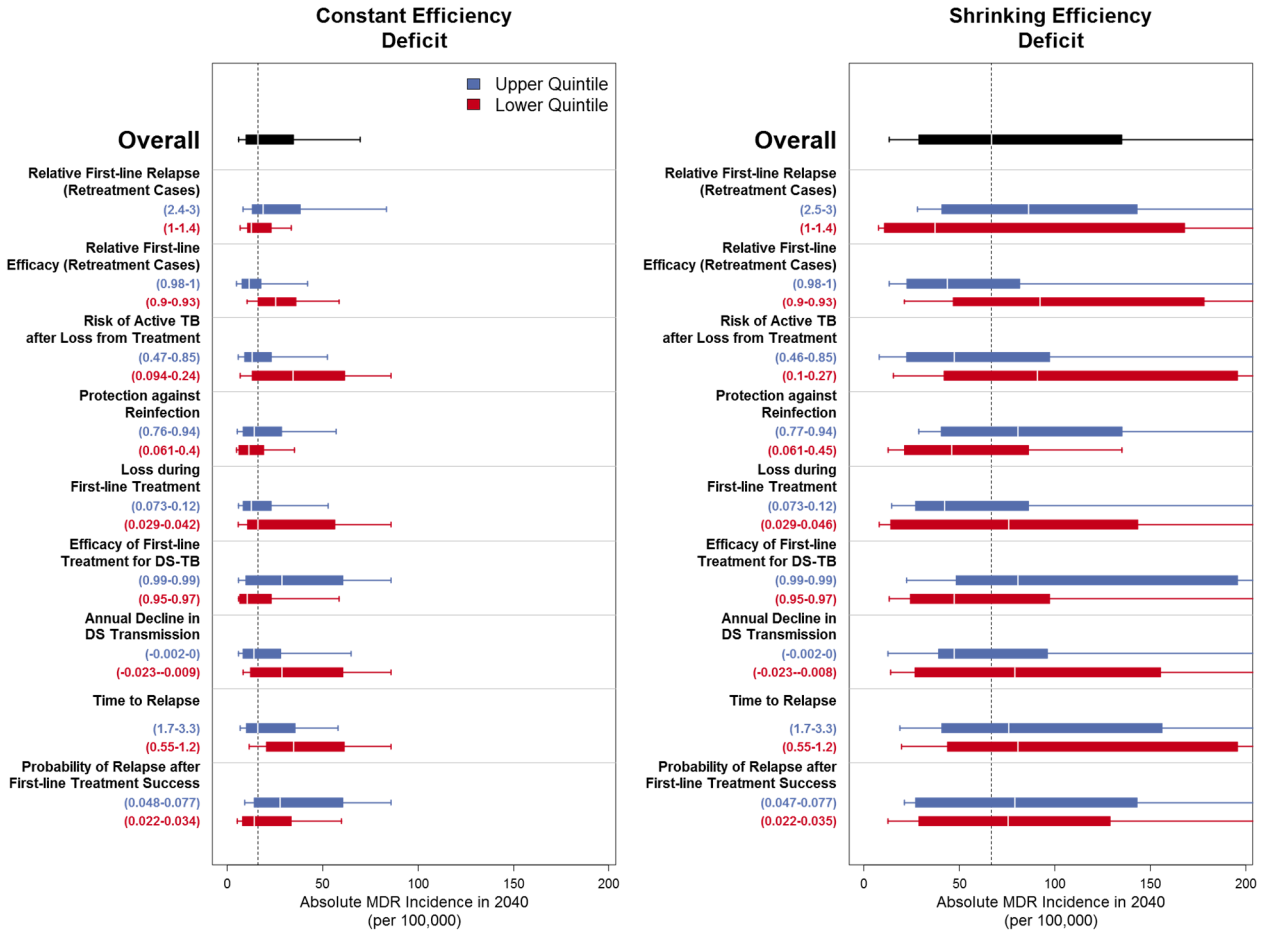

Figure S2.31: Sensitivity Analysis – PRCCs of HIV and HIV/TB Parameter and Absolute MDR-TB Incidence – Vietnam

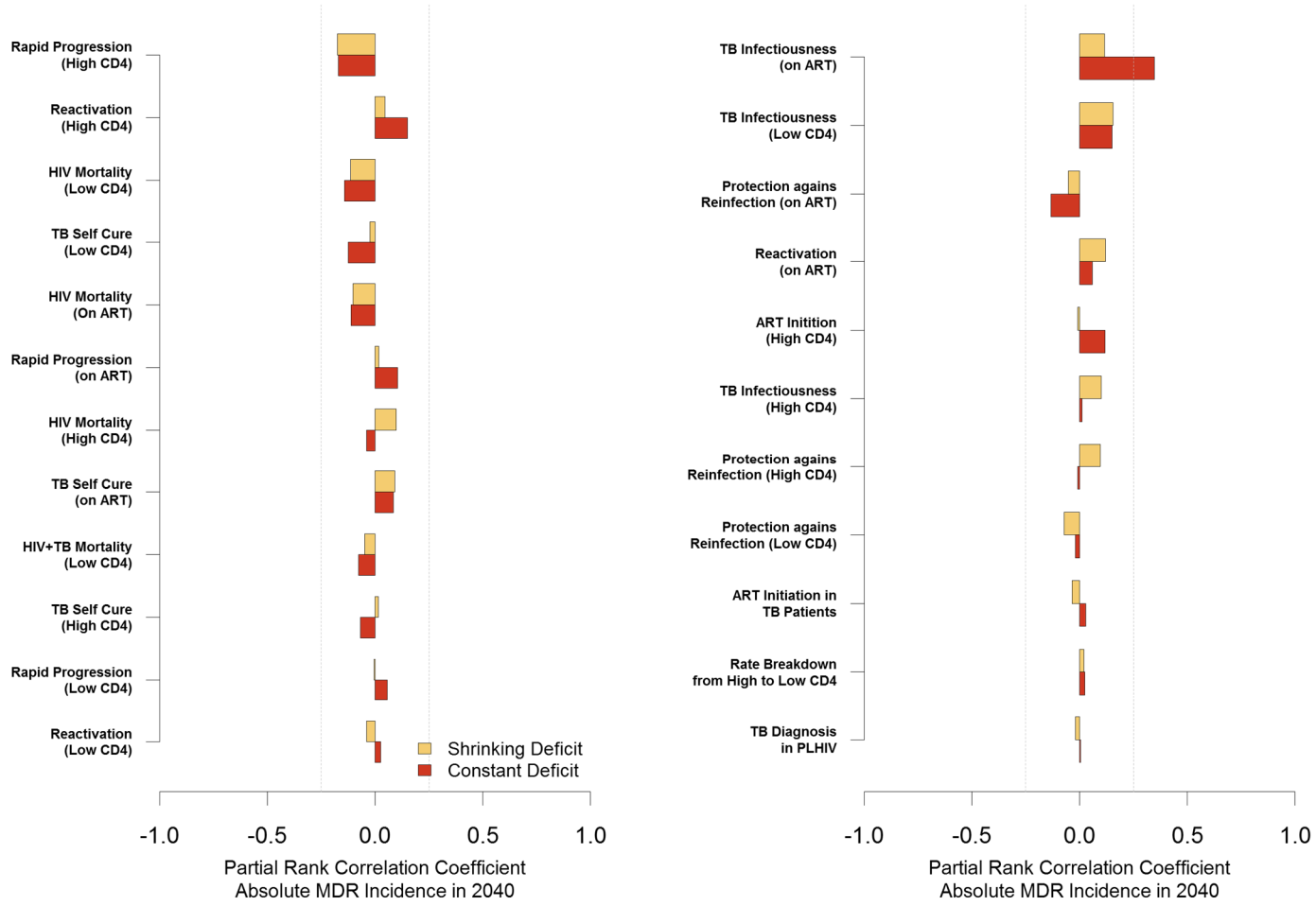

Figure S2.32: Sensitivity Analysis – Absolute MDR-TB Incidence by HIV and HIV/TB Parameter Quintiles – Vietnam

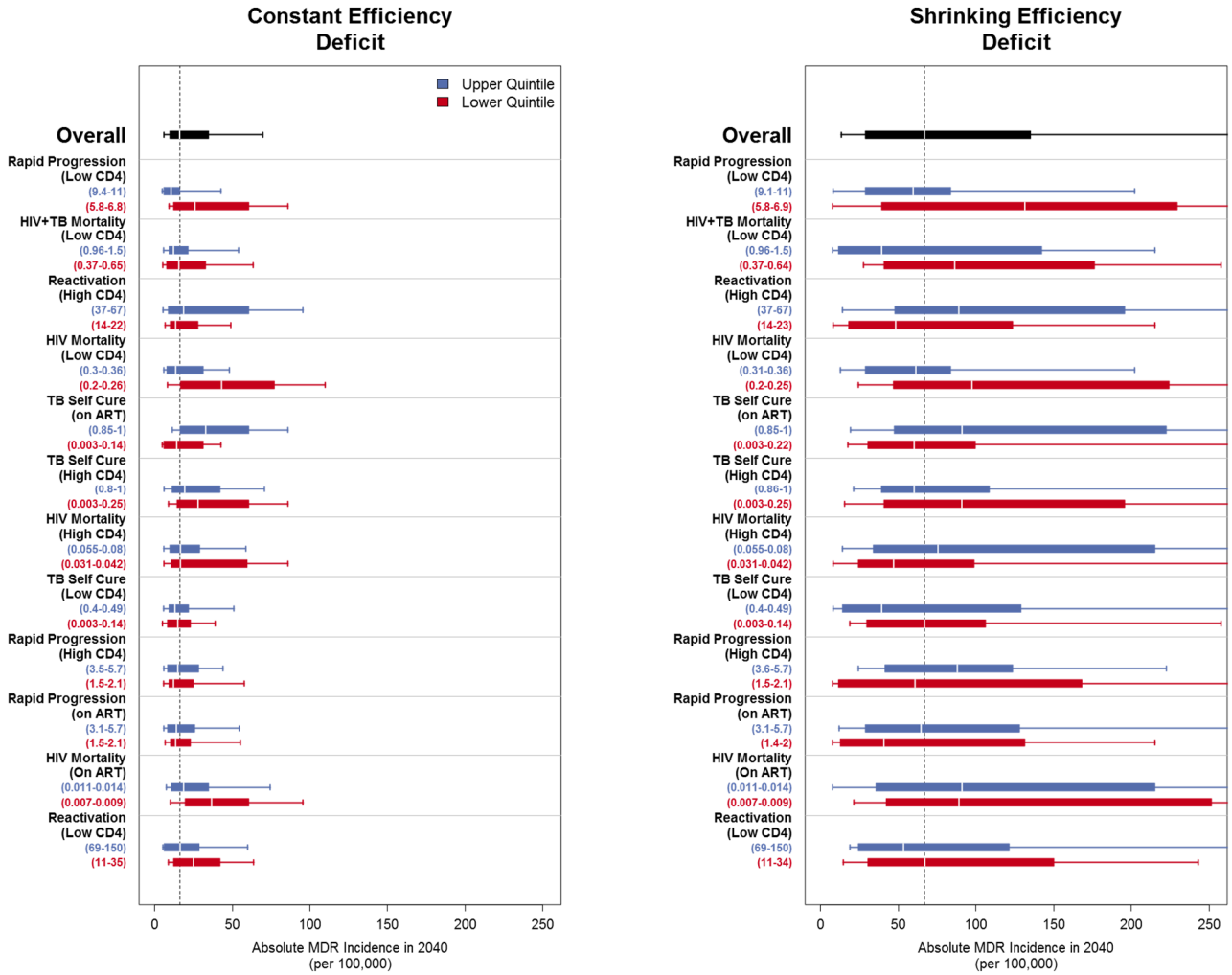

Figure S2.32 (Continued): Sensitivity Analysis – Absolute MDR-TB Incidence by HIV and HIV/TB Parameter Quintiles – Vietnam

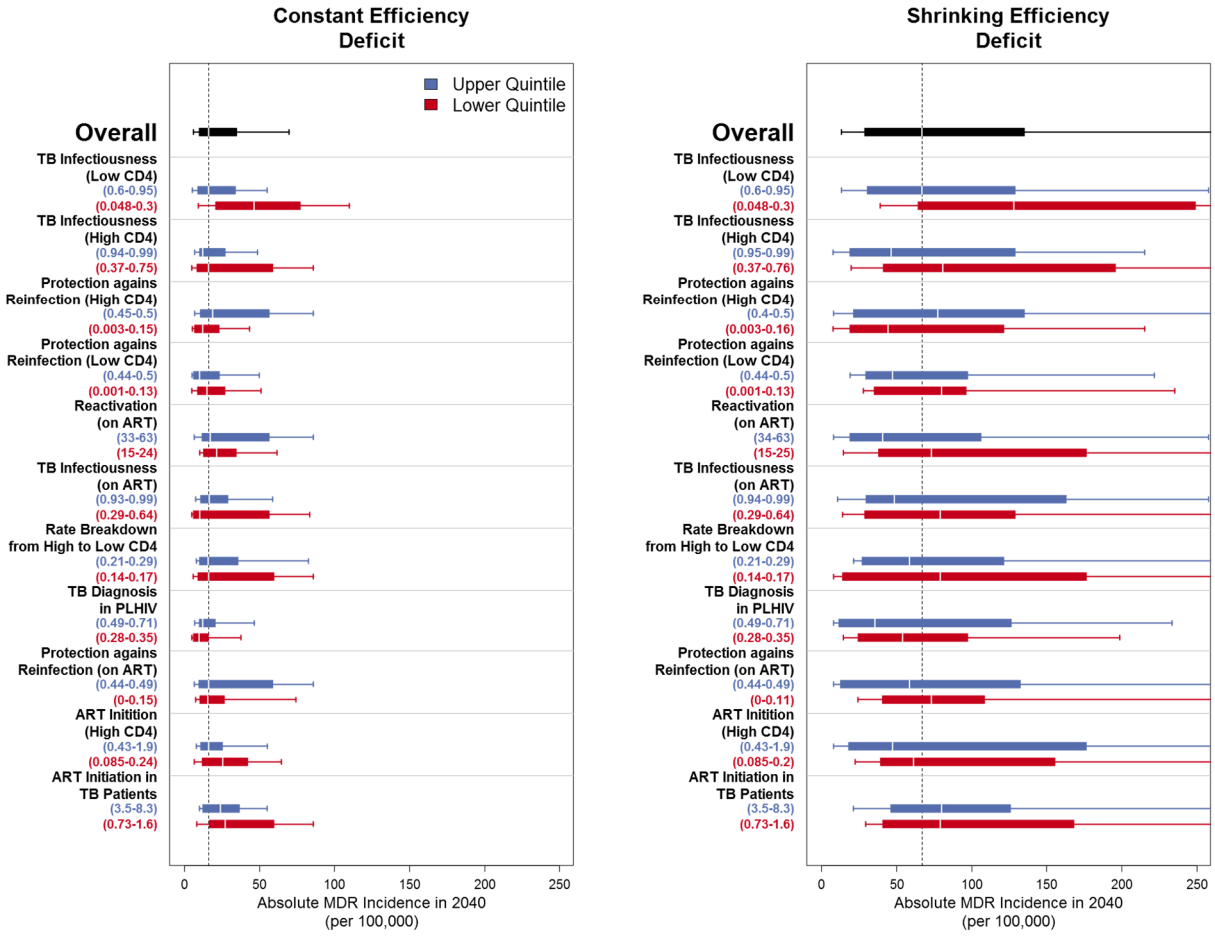

Figure S2.33: Sensitivity Analysis – PRCCs of MDR-TB Parameters and Absolute MDR-TB Incidence – Vietnam

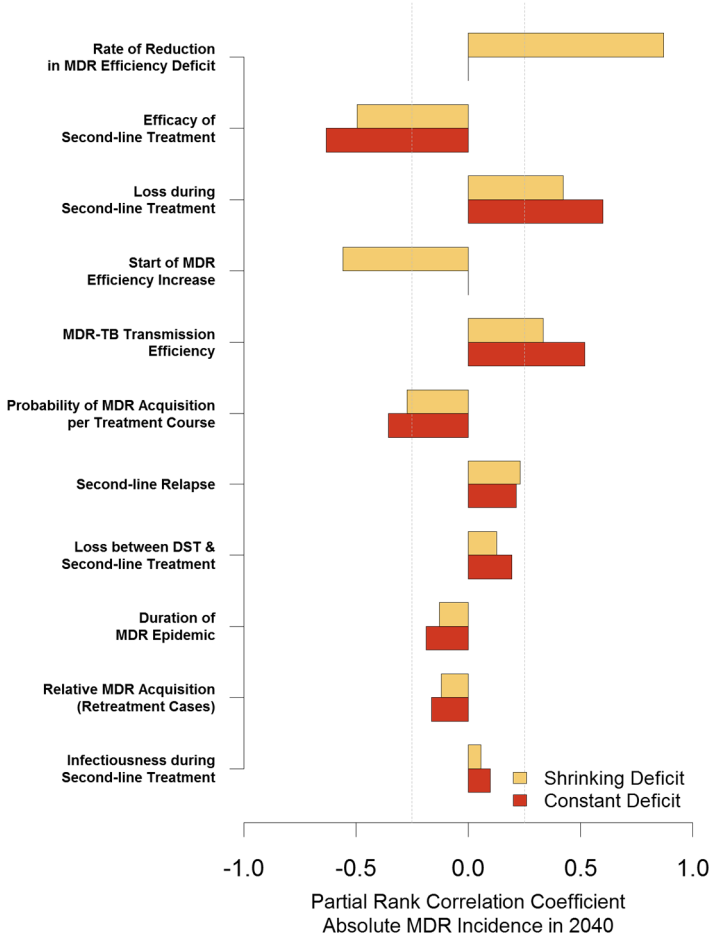

Figure S2.34: Sensitivity Analysis – Absolute MDR-TB Incidence by MDR-TB Parameter Quintiles – Vietnam

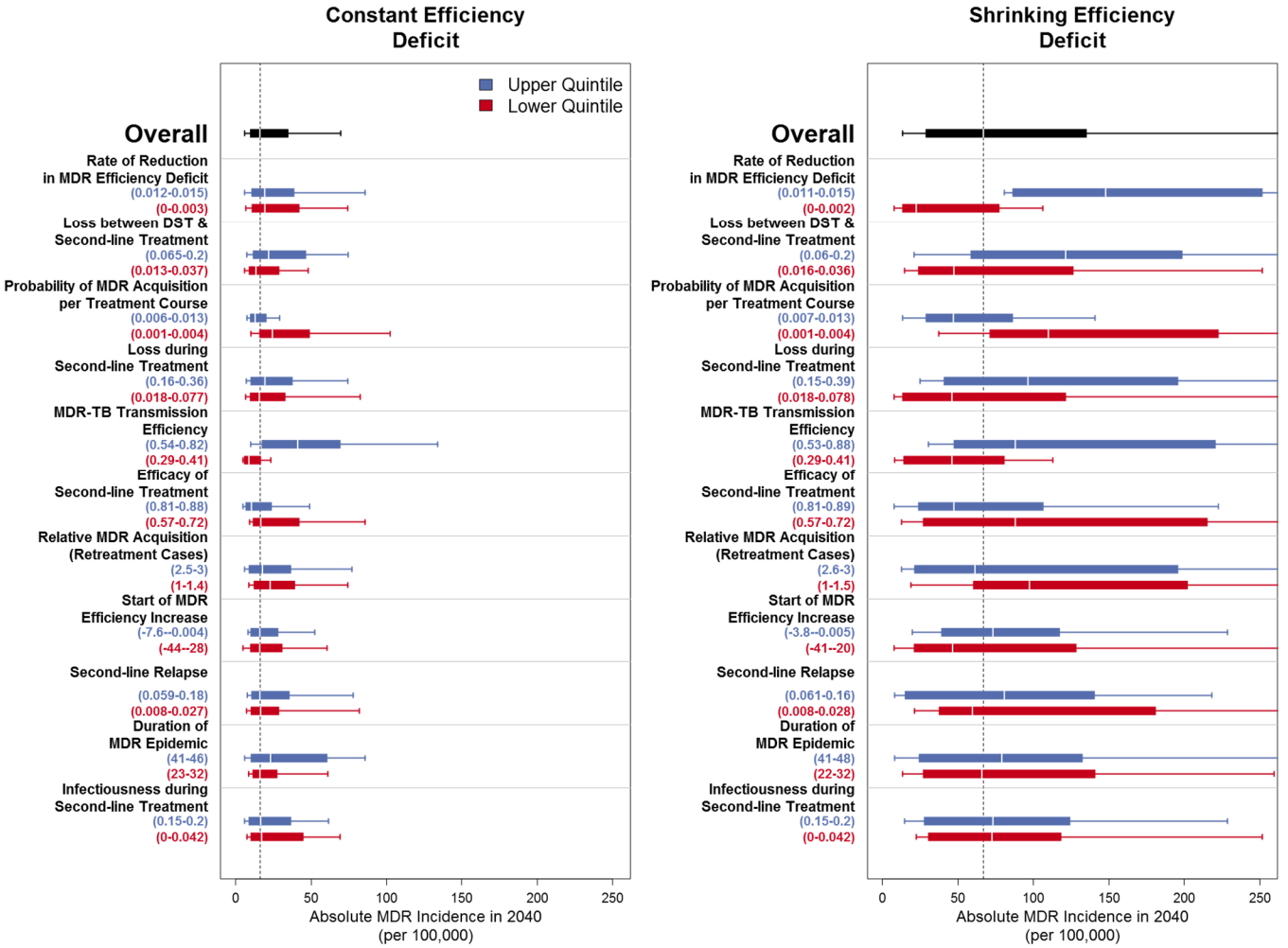

Figure S2.35: Sensitivity Analysis – PRCCs of TB Natural History Parameters and Change in Relative MDR-TB Incidence – Vietnam

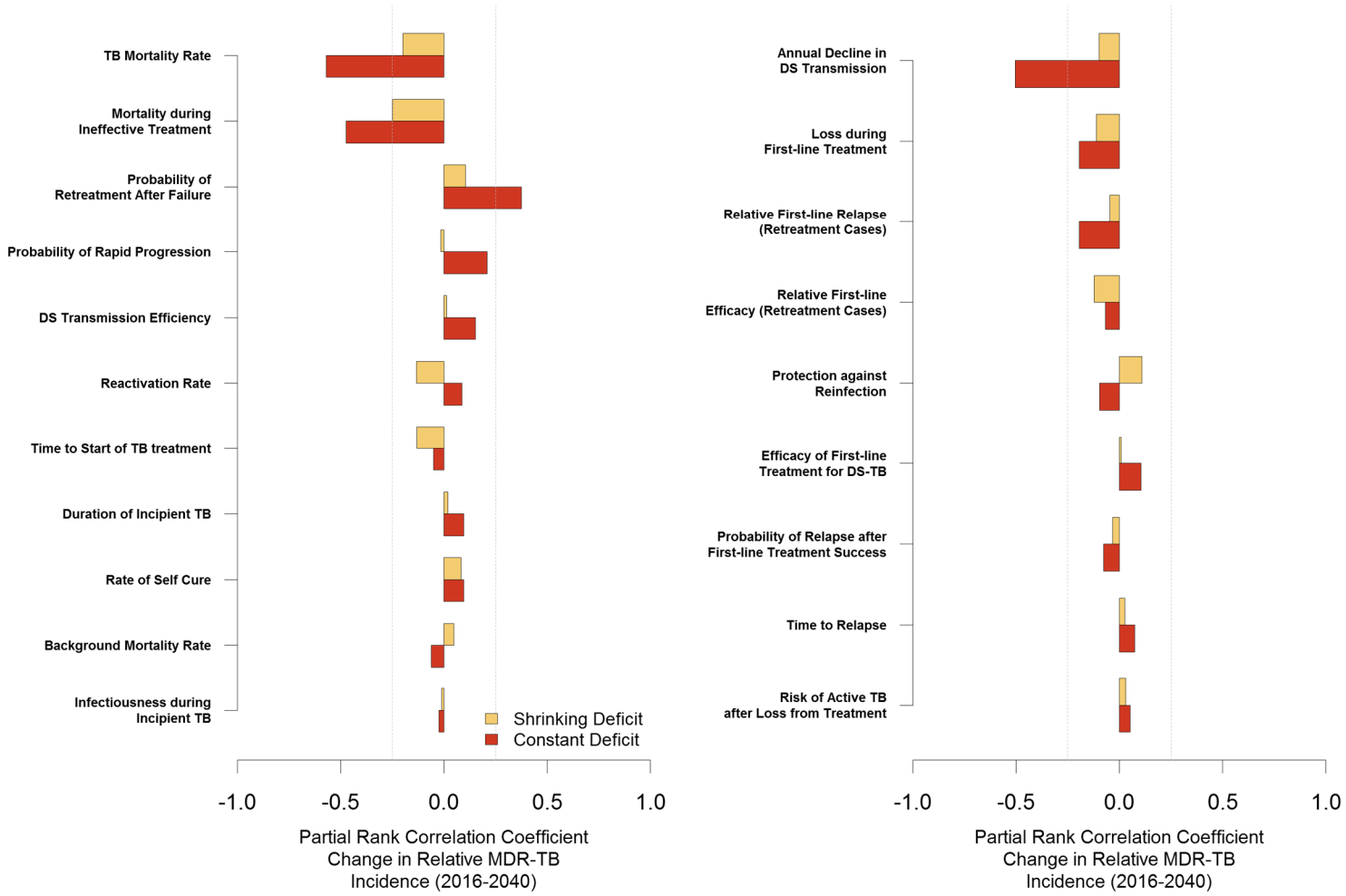

Figure S2.36: Sensitivity Analysis – Change in Relative MDR-TB Incidence by TB Natural History Parameter Quintiles – Vietnam

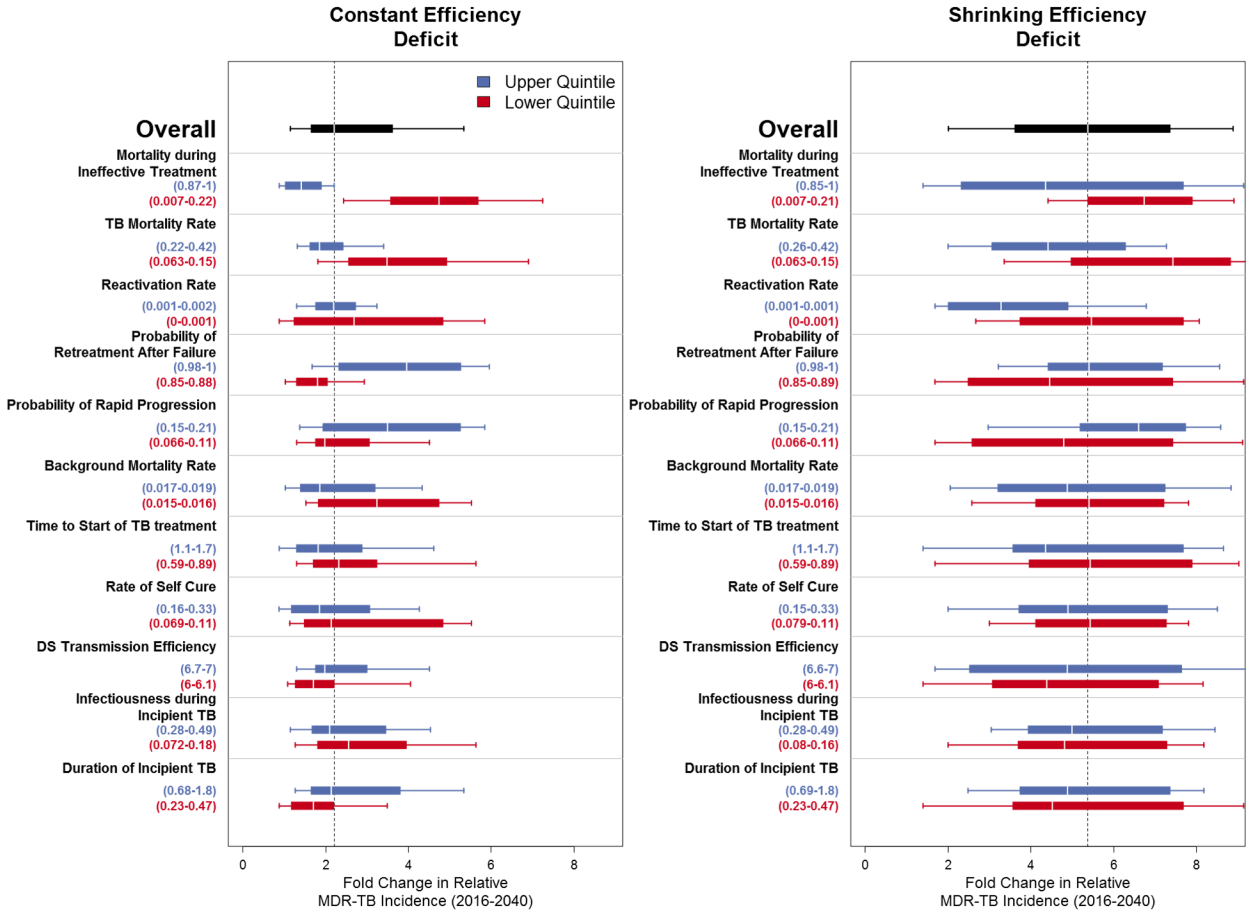

Figure S2.36 (Continued): Sensitivity Analysis – Change in Relative MDR-TB Incidence by TB Natural History Parameter Quintiles – Vietnam

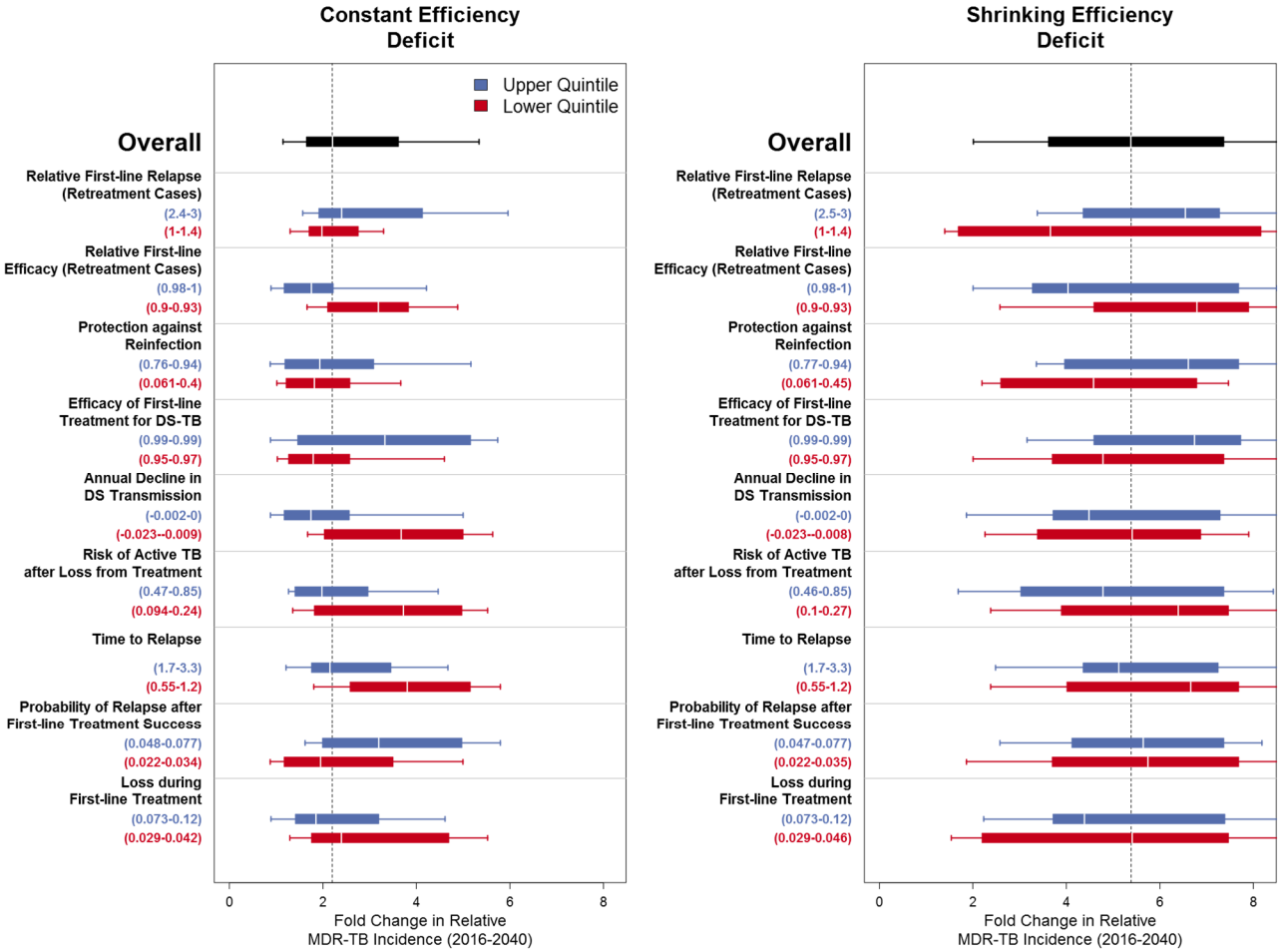

Figure S2.37: Sensitivity Analysis – PRCCs of HIV and HIV/TB Parameter and Change in Relative MDR-TB Incidence – Vietnam

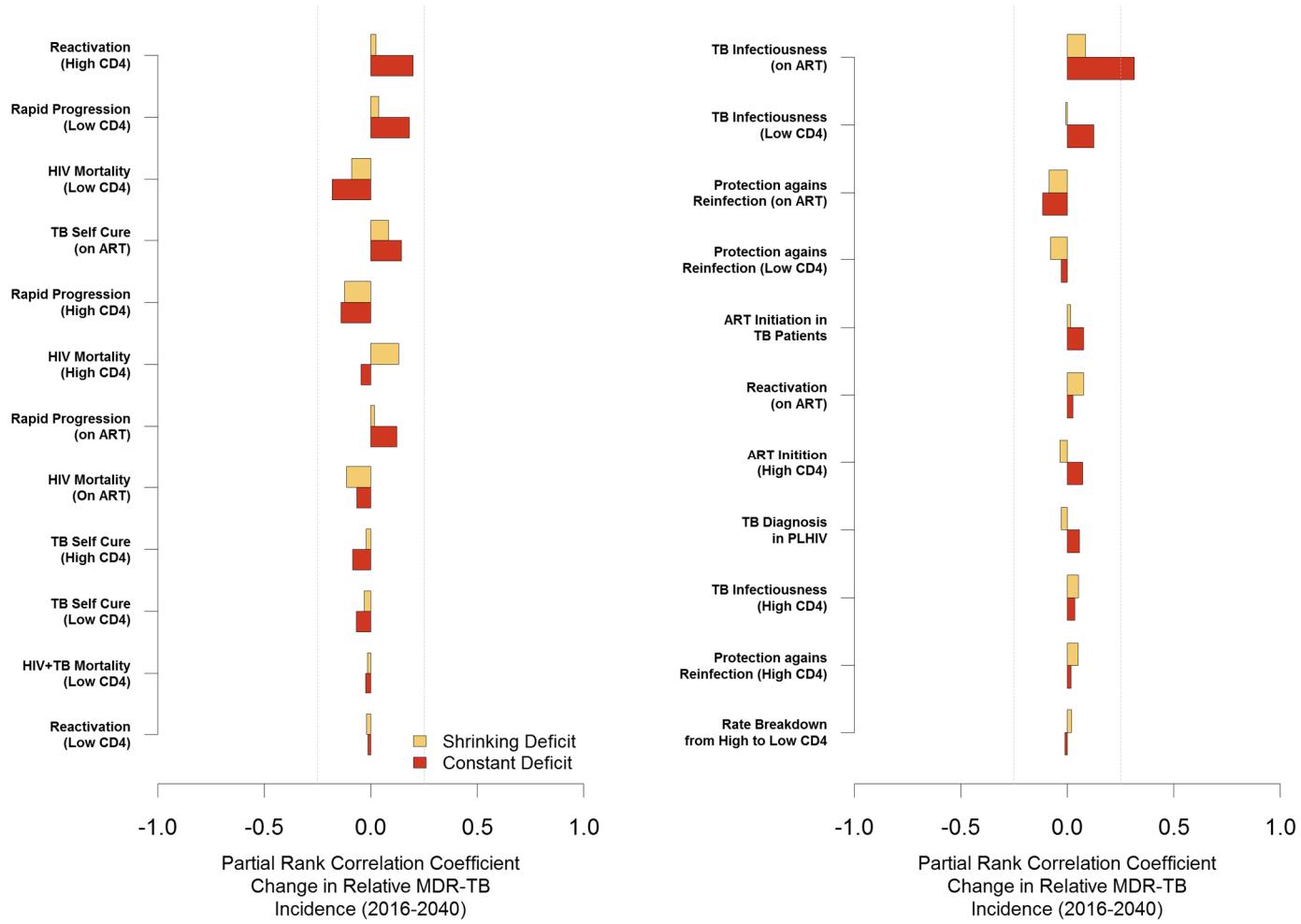

Figure S2.38: Sensitivity Analysis – Change in Relative MDR-TB Incidence by HIV and HIV/TB Parameter Quintiles – Vietnam

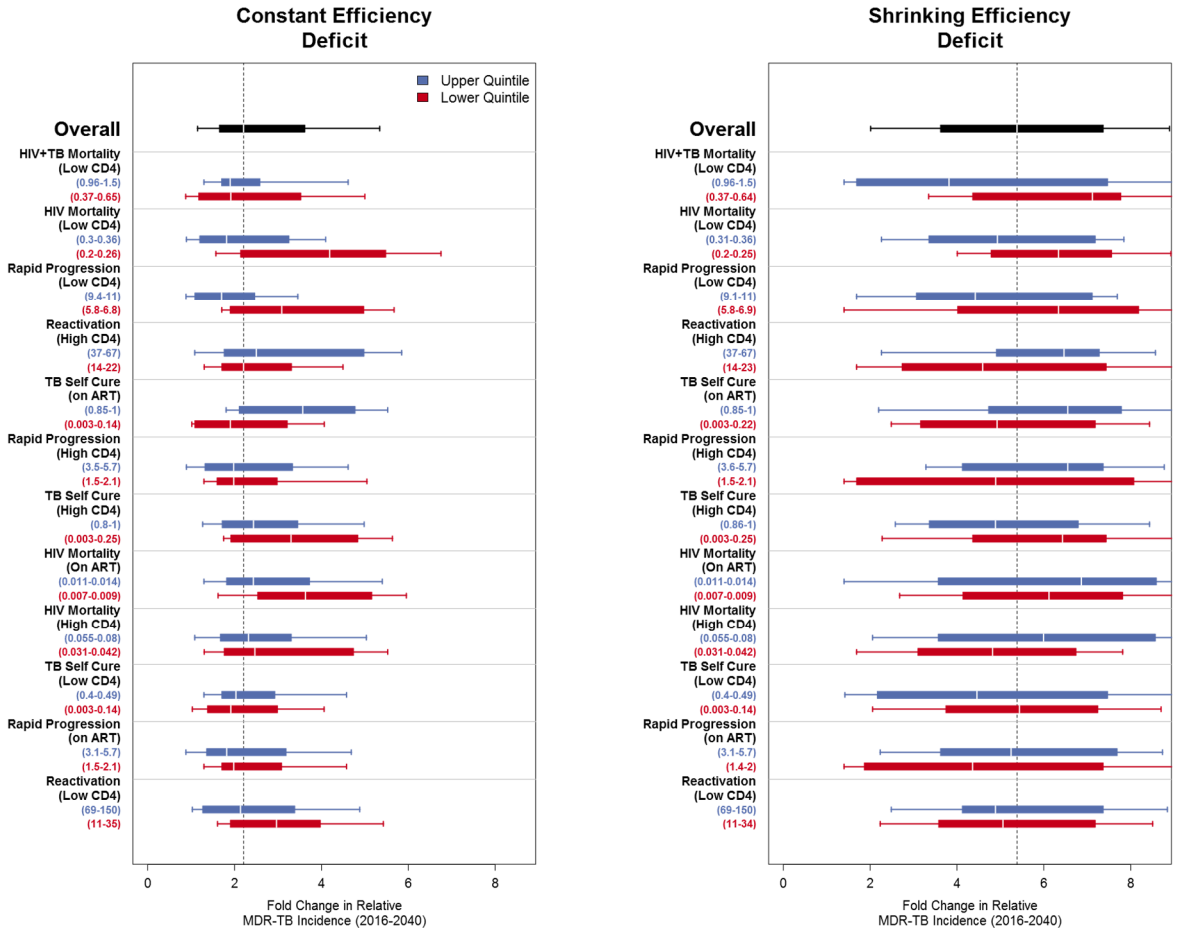

Figure S2.38 (Continued): Sensitivity Analysis – Change in Relative MDR-TB Incidence by HIV and HIV/TB Parameter Quintiles – Vietnam

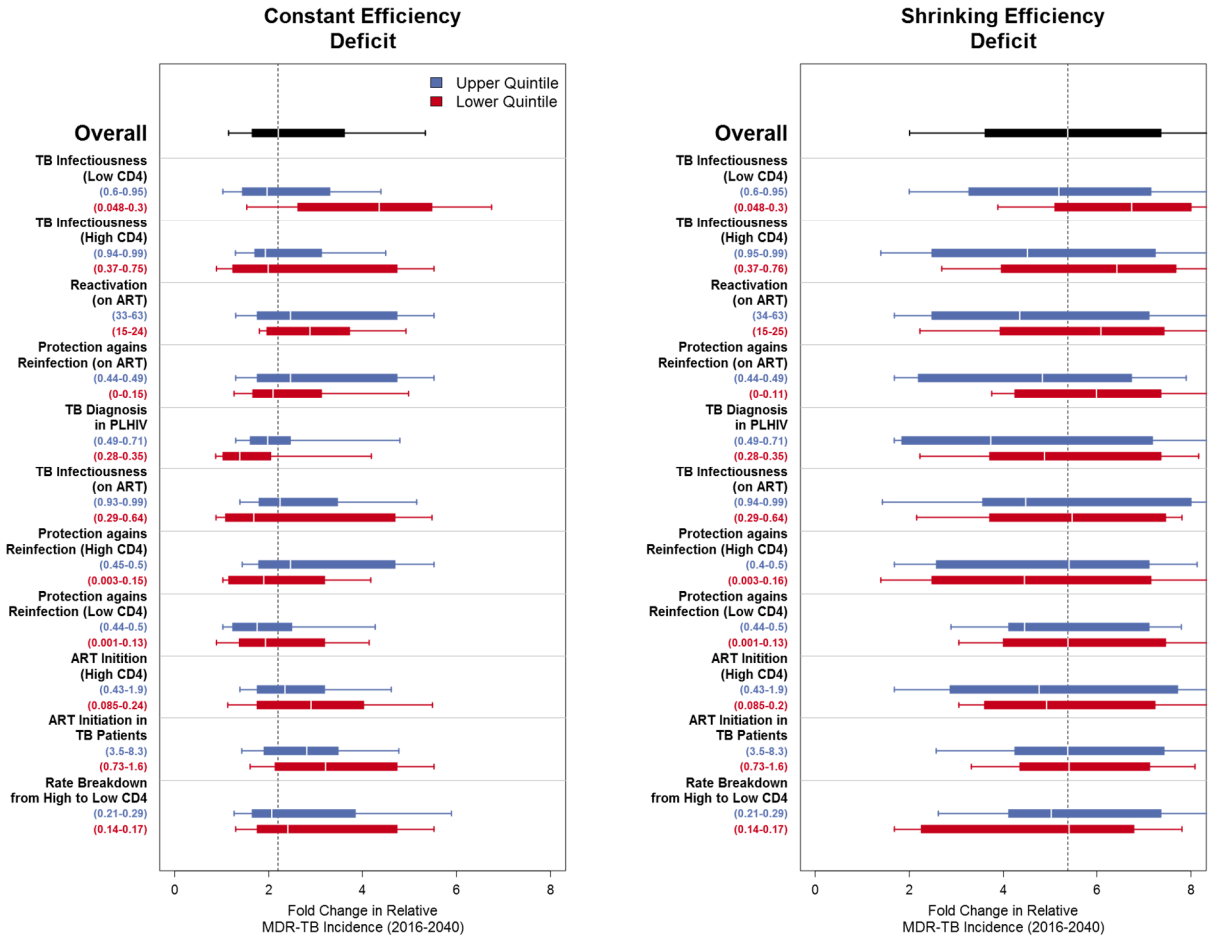

Figure S2.39: Sensitivity Analysis – PRCCs of MDR-TB Parameters and Change in Relative MDR-TB Incidence – Vietnam

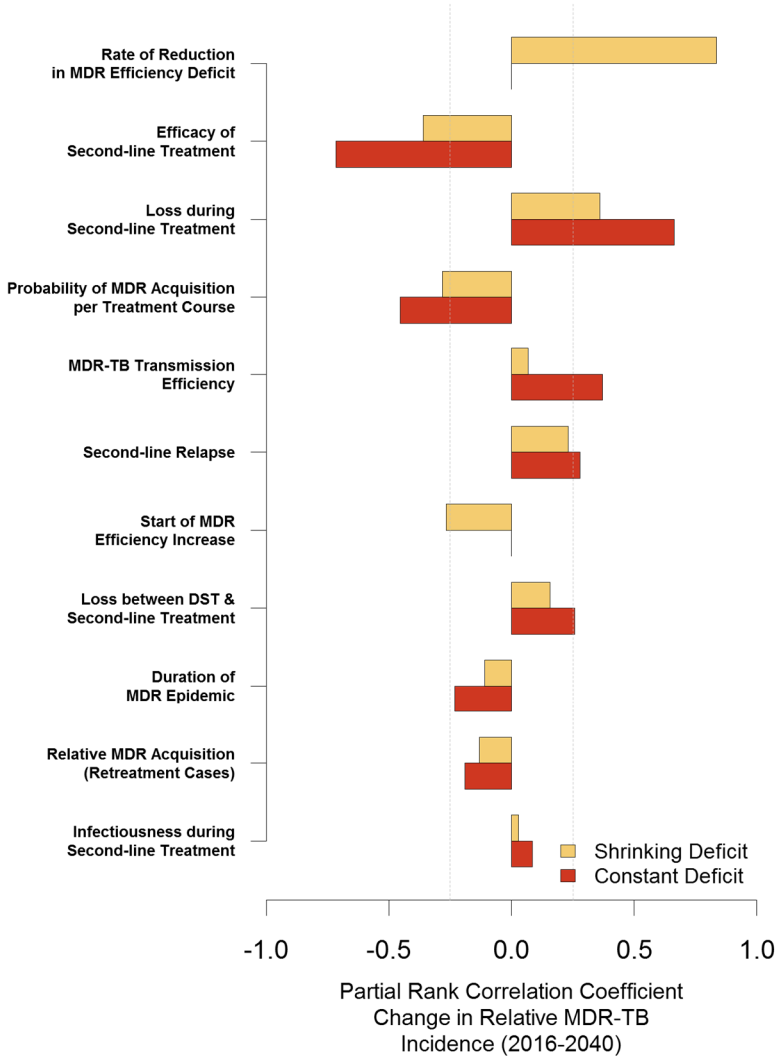

Figure S2.40: Sensitivity Analysis – Change in Relative MDR-TB Incidence by MDR-TB Parameter Quintiles – Vietnam

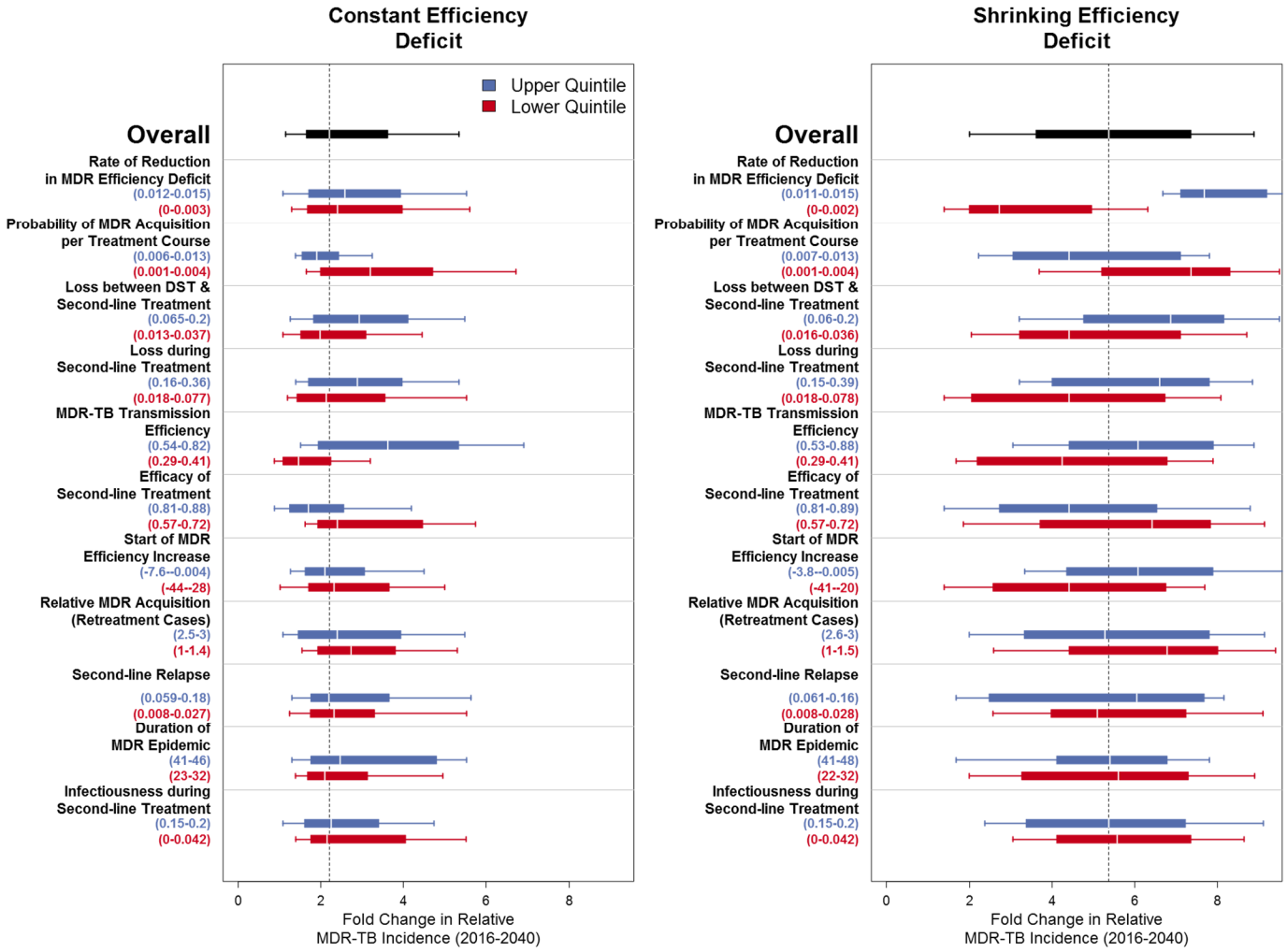

Sensitivity to Conditions at Initiation

To evaluate the behavior of the epidemic system of equations with varying initial conditions, the set of DS-TB parameters which produced the maximum likelihood simulation under standard conditions was used as a "base case" to compare the system's behavior. The incidence of DS-TB and the prevalence of TB infection in this "base case" simulation under standard initial conditions are presented in Figure S2.41.

Alternative simulations using the same parameter set were initiated under a variety of different conditions. The prevalence of active DS-TB was varied between 0.001% and 90%, and the prevalence of latent TB among those without active TB was varied between 0% and 99%. The behavior of the system was compared by examining time-trends in TB incidence (Figure S2.42) and the total prevalence of infection (Figure S2.43) in these alternative simulations before the introduction of MDR-TB or HIV. For reference the "base case" epidemic is plotted in red in each panel. While early behavior of the system is quite variable, in the decades preceding the introduction of MDR-TB and HIV all simulations approach the same equilibrium values of TB incidence (approximately 379 per 100,000) and prevalence of infection (approximately 71%). Additionally, the population of each state in each simulation in 1989 was compared to the population of each state in the "base case" simulation in 1989. Relative differences between the populations of each compartment in each simulation and those of the "base case" simulation are presented in Table S2.6. Regardless of the initial conditions of the system, the size of each compartment was within 7% of the value of the "base case" simulation by 1989, indicating that the differential equation system is stable with regard to the conditions of the system at the time of initiation.

Figure S2.41: Behavior of the "Base Case" DS-TB Simulation after Initiation

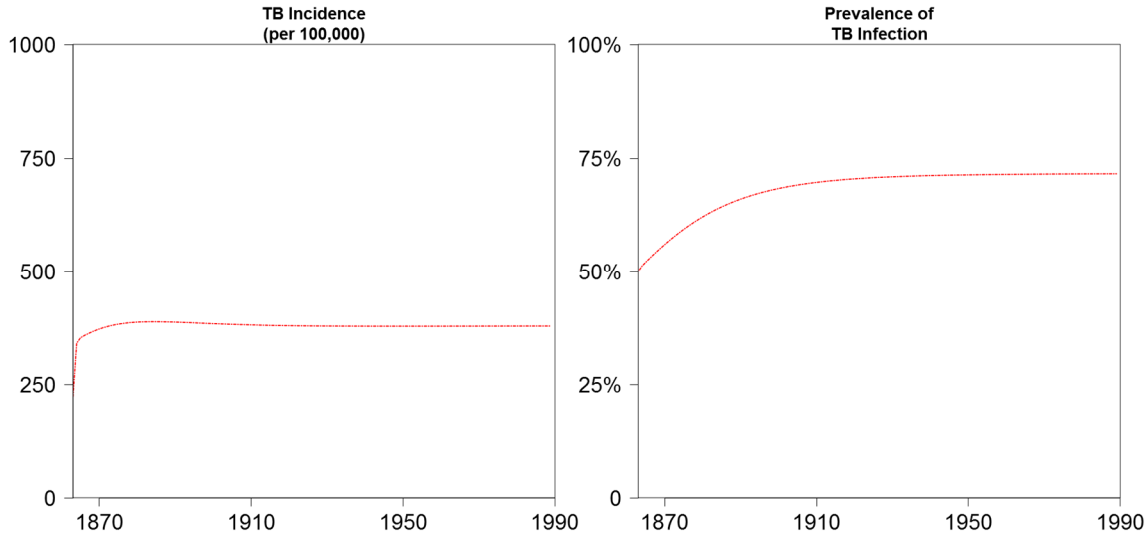

The parameter set which produced the maximum likelihood DS-TB epidemic (see Sampling & Calibration) was selected as a "Base Case" to evaluate the behavior of the ODE system under varying initial conditions. Here, the maximum likelihood epidemic was simulated using standard initial conditions (50% uninfected, 45.5% latently infected, 0.3% active TB, 0.2% early-active TB). The epidemic was initiated 150 years before the present and run without interruption until the introduction of either MDR-TB or HIV.

Figure S2.42: Impact of Initial Conditions on DS-TB Incidence

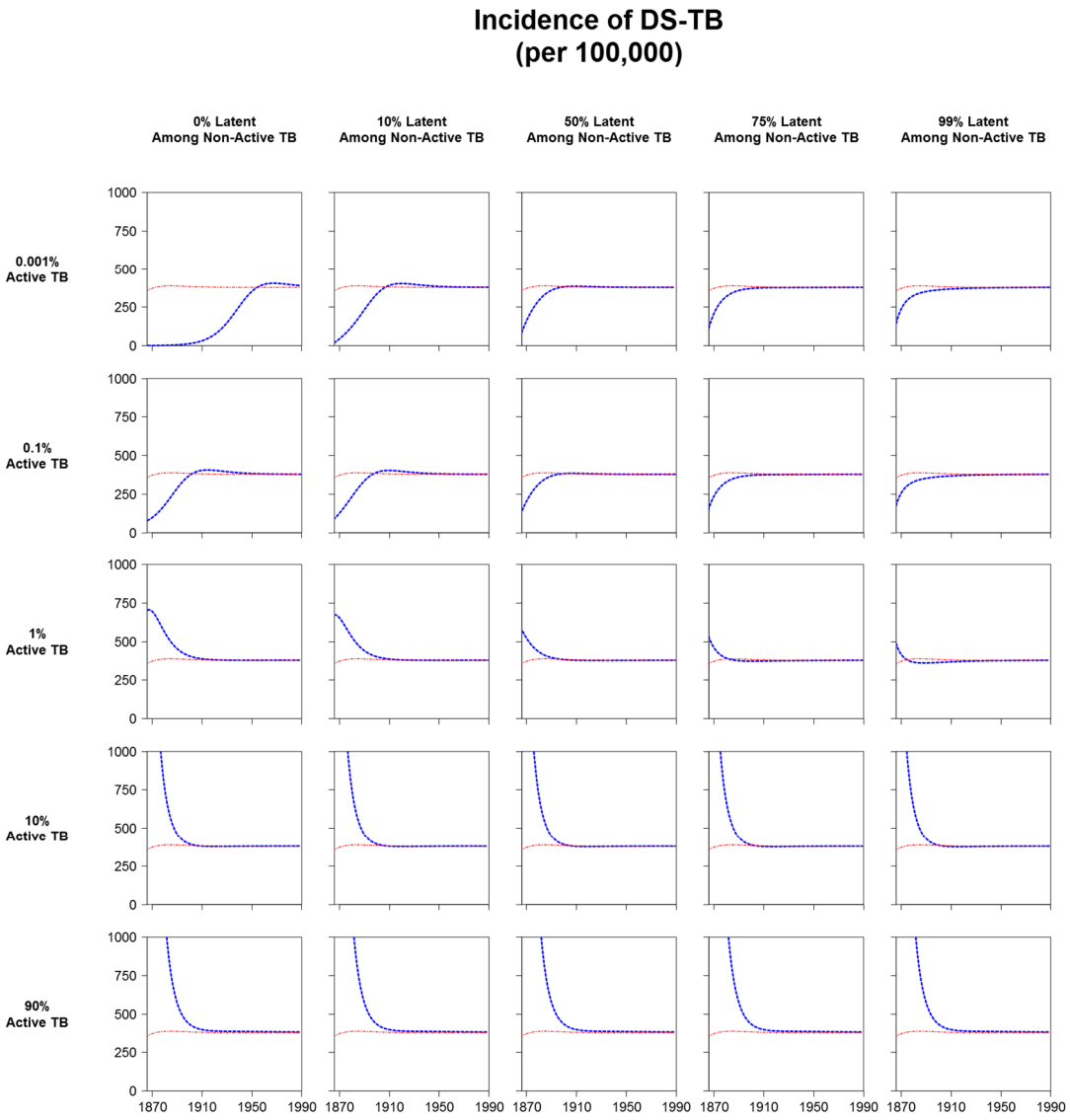

Plots represent the annual incidence of DS-TB cases since the time of simulation initiation (150 years before the present) until the introduction of MDR-TB or HIV. Curves in blue represent the behavior of the system under different combinations of the prevalence of active TB and latent TB infection at initiation. For comparison, in each panel the behavior of the "base case" simulation with standard initial conditions is plotted in red.

Figure S2.43: Impact of Initial Conditions on the Prevalence of TB Infection

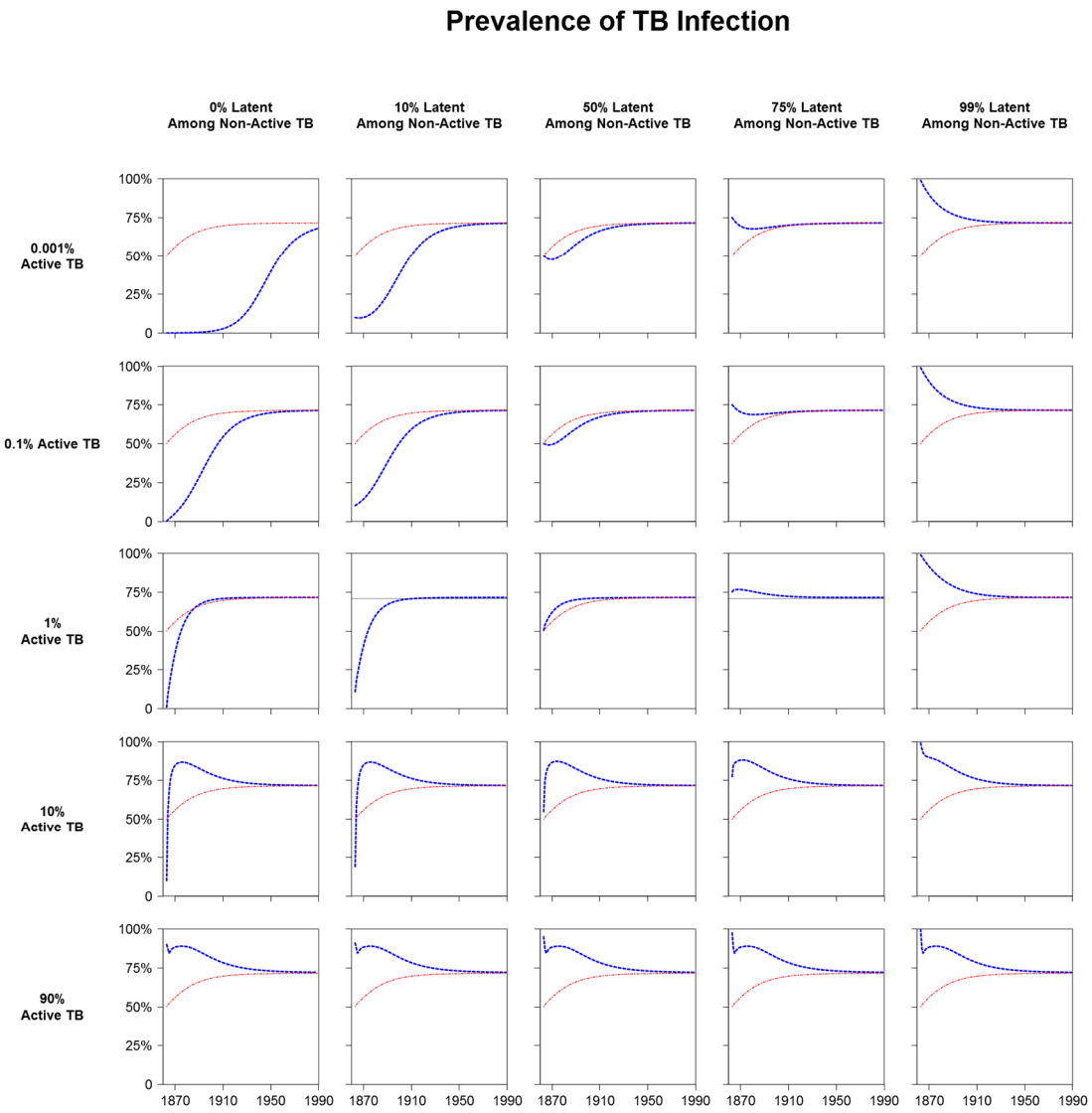

Plots represent the prevalence of all types of DS-TB infection and disease since the time of simulation initiation (150 years before the present) until the introduction of MDR-TB or HIV. Curves in blue represent the behavior of the system under different combinations of the prevalence of active TB and latent TB infection at initiation. For comparison, in each panel the behavior of the "base case" simulation with standard initial conditions is plotted in red.

Table S2.6: Percent Difference in State Sizes between Base Case and Alternative Initial Conditions in1989

Alternative Initial Conditions (150 years before the present)	S_N	S_P	L_N	L_P	E_N	E_P	A_N	A_P	B_{1eN}	B_{1eP}	B_{1iN}	B_{1iP}	W
0.001% Active TB, 0% Latent TB	4.10	0.37	0.68	3.00	0.02	0.01	0.01	0.01	0.01	<0.01	<0.01	<0.01	<0.01
0.001% Active TB, 10% Latent TB	0.24	0.02	0.35	0.56	<0.01	<0.01	<0.01	<0.01	<0.01	<0.01	<0.01	<0.01	<0.01
0.001% Active TB, 50% Latent TB	0.07	0.01	0.23	0.28	<0.01	<0.01	<0.01	<0.01	<0.01	<0.01	<0.01	<0.01	<0.01
0.001%Active TB, 75% Latent TB	0.04	0.02	0.27	0.29	<0.01	<0.01	<0.01	<0.01	<0.01	<0.01	<0.01	<0.01	<0.01
0.001% Active TB, 99% Latent TB	0.01	0.02	0.33	0.32	<0.01	<0.01	<0.01	<0.01	<0.01	<0.01	<0.01	<0.01	<0.01
0.1% Active TB, 0% Latent TB	0.17	0.01	0.21	0.37	<0.01	<0.01	<0.01	<0.01	<0.01	<0.01	<0.01	<0.01	<0.01
0.1% Active TB, 10% Latent TB	0.11	0.01	0.16	0.27	<0.01	<0.01	<0.01	<0.01	<0.01	<0.01	<0.01	<0.01	<0.01
0.1% Active TB, 50% Latent TB	0.05	0.01	0.18	0.22	<0.01	<0.01	<0.01	<0.01	<0.01	<0.01	<0.01	<0.01	<0.01
0.1% Active TB, 75% Latent TB	0.03	0.02	0.24	0.25	<0.01	<0.01	<0.01	<0.01	<0.01	<0.01	<0.01	<0.01	<0.01
0.1% Active TB, 99% Latent TB	0.01	0.02	0.31	0.29	<0.01	<0.01	<0.01	<0.01	<0.01	<0.01	<0.01	<0.01	<0.01
1% Active TB, 0% Latent TB	0.08	0.03	0.47	0.52	<0.01	<0.01	<0.01	<0.01	<0.01	<0.01	<0.01	<0.01	<0.01
1% Active TB, 10% Latent TB	0.07	0.02	0.41	0.45	<0.01	<0.01	<0.01	<0.01	<0.01	<0.01	<0.01	<0.01	<0.01
1% Active TB, 50% Latent TB	0.04	0.01	0.17	0.20	<0.01	<0.01	<0.01	<0.01	<0.01	<0.01	<0.01	<0.01	<0.01
1% Active TB, 75% Latent TB	0.03	<0.01	0.04	0.07	<0.01	<0.01	<0.01	<0.01	<0.01	<0.01	<0.01	<0.01	<0.01
1% Active TB, 99.% Latent TB	0.03	0.01	0.07	0.03	<0.01	<0.01	<0.01	<0.01	<0.01	<0.01	<0.01	<0.01	<0.01
10% Active TB, 0% Latent TB	0.33	0.08	2.30	2.60	0.01	0.01	0.01	0.01	<0.01	<0.01	<0.01	<0.01	<0.01
10% Active TB, 10% Latent TB	0.32	0.08	2.30	2.50	0.01	0.01	0.01	0.01	<0.01	<0.01	<0.01	<0.01	<0.01
10% Active TB, 50% Latent TB	0.30	0.08	2.10	2.30	0.01	0.01	<0.01	0.01	<0.01	<0.01	<0.01	<0.01	<0.01
10% Active TB, 75% Latent TB	0.28	0.07	1.90	2.10	0.01	0.01	<0.01	0.01	<0.01	<0.01	<0.01	<0.01	<0.01
10% Active TB, 99.% Latent TB	0.27	0.07	1.80	2.00	0.01	0.01	<0.01	<0.01	<0.01	<0.01	<0.01	<0.01	<0.01
90% Active TB, 0% Latent TB	0.75	0.19	6.40	6.90	0.02	0.02	0.01	0.02	0.01	0.01	<0.01	<0.01	<0.01
90% Active TB, 10% Latent TB	0.75	0.19	6.40	6.90	0.02	0.02	0.01	0.02	0.01	0.01	<0.01	<0.01	<0.01
90% Active TB, 50% Latent TB	0.75	0.19	6.40	6.90	0.02	0.02	0.01	0.02	0.01	0.01	<0.01	<0.01	<0.01
90% Active TB, 75% Latent TB	0.75	0.19	6.40	6.90	0.02	0.02	0.01	0.02	0.01	0.01	<0.01	<0.01	<0.01
90% Active TB, 99% Latent TB	0.75	0.19	6.40	6.90	0.02	0.02	0.01	0.02	0.01	0.01	<0.01	<0.01	<0.01

REFERENCES

1. Smith AFM, Gelfand AE. Bayesian statistics without tears: a sampling-resampling perspective. Am Stat. **1992**; 46(2):84–88.
2. John J, Draper N. An alternative family of transformations. Appl Stat. **1980**; 29(2):190–197.
3. World Health Organization. Global Tuberculosis Report 2017. 2017.
4. National Institute for Communicable Diseases (NICD). South African Tuberculosis Drug Resistance Survey 2012–14. 2016.
5. World Health Organization (WHO). Global Health Observatory data repository. http://apps.who.int/gho/data/?theme=main&vid=61830.
6. Tiemersma EW, Werf MJ van der, Borgdorff MW, Williams BG, Nagelkerke NJD. Natural history of tuberculosis: duration and fatality of untreated pulmonary tuberculosis in HIV negative patients: A systematic review. PLoS One. **2011**; 6(4):e17601.
7. Vynnycky E, Fine PE. The natural history of tuberculosis: the implications of age-dependent risks of disease and the role of reinfection. Epidemiol Infect. **1997**; 119(2):183–201.
8. Andrews JR, Noubary F, Walensky RP, Cerda R, Losina E, Horsburgh CR. Risk of progression to active tuberculosis following reinfection with Mycobacterium tuberculosis. Clin Infect Dis. **2012**; 54(6):784–791.
9. Horsburgh CR, O'Donnell M, Chamblee S, Moreland JL, Johnson J, Marsh BJ, et al. Revisiting rates of reactivation tuberculosis: a population-based approach. Am J

Respir Crit Care Med. **2010**; 182(3):420–425.

10. Fox GJ, Barry SE, Britton WJ, Marks GB. Contact investigation for tuberculosis: a systematic review and meta-analysis. Eur Respir J. **2013**; 41(1):140–156.
11. Sloot R, Schim Van Der Loeff MF, Kouw PM, Borgdorff MW. Risk of tuberculosis after recent exposure: a 10-year follow-up study of contacts in Amsterdam. Am J Respir Crit Care Med. **2014**; 190(9):1044–1052.
12. Onozaki I, Law I, Sismanidis C, Zignol M, Glaziou P, Floyd K. National tuberculosis prevalence surveys in Asia, 1990-2012: an overview of results and lessons learned. Trop Med Int Heal. **2015**; 20(9):1128–1145.
13. Dowdy DW, Basu S, Andrews JR. Is passive diagnosis enough? The impact of subclinical disease on diagnostic strategies for tuberculosis. Am J Respir Crit Care Med. **2013**; 187(5):543–551.
14. Behr MA, Warren SA, Salamon H, Hopewell PC, Ponce De Leon A, Daley CL, et al. Transmission of Mycobacterium tuberculosis from patients smear-negative for acid-fast bacilli. Lancet. **1999**; 353(9151):444–449.
15. Tostmann A, Kik S V., Kalisvaart NA, Sebek MM, Verver S, Boeree MJ, et al. Tuberculosis Transmission by Patients with Smear-Negative Pulmonary Tuberculosis in a Large Cohort in The Netherlands. Clin Infect Dis. **2008**; 47(9):1135–1142.
16. MacPherson P, Houben RM, Glynn JR, Corbett EL, Kranzer K. Pre-treatment loss to follow-up in tuberculosis patients in low- and lower-middle-income countries and high-burden countries: a systematic review and meta-analysis. Bull World Health Organ. **2014**; 92(2):126–138.

17. Gillespie SH, Crook AM, McHugh TD, Mendel CM, Meredith SK, Murray SR, et al. Four-month moxifloxacin-based regimens for drug-sensitive tuberculosis. N Engl J Med. **2014**; 371(17):1577–1587.

18. Merle CS, Fielding K, Sow OB, Gninafon M, Lo MB, Mthiyane T, et al. A four-month gatifloxacin-containing regimen for treating tuberculosis. N Engl J Med. **2014**; 371(17):1588–1598.

19. Jindani A, Harrison TS, Nunn AJ, Phillips PPJ, Churchyard GJ, Charalambous S, et al. High-dose rifapentine with moxifloxacin for pulmonary tuberculosis. N Engl J Med. **2014**; 371(17):1599–1608.

20. Menzies D, Benedetti A, Paydar A, Royce S, Pai M, Burman W, et al. Standardized treatment of active tuberculosis in patients with previous treatment and/or with mono-resistance to isoniazid: a systematic review and meta-analysis. PLoS Med. **2009**; 6(9).

21. Marx FM, Dunbar R, Enarson DA, Williams BG, Warren RM, Spuy GD Van Der, et al. The temporal dynamics of relapse and reinfection tuberculosis after successful treatment: a retrospective cohort study. Clin Infect Dis. **2014**; 58(12):1676–1683.

22. Menzies D, Benedetti A, Paydar A, Martin I, Royce S, Pai M, et al. Effect of duration and intermittency of rifampin on tuberculosis treatment outcomes: a systematic review and meta-analysis. PLoS Med. **2009**; 6(9):1–18.

23. Kruk ME, Schwalbe NR, Aguiar C a. Timing of default from tuberculosis treatment: a systematic review. Trop Med Int Heal. **2008**; 13(5):703–712.

24. Hong Kong Chest Service, Tuberculosis Research Centre Madras, British Medical

Research Council. A controlled trial of 2-month, 3-month, and 12-month regimens of chemotherapy for sputum-smear-negative pulmonary tuberculosis. Results at 60 months. Am Rev Respir Dis. **1984**; 130(1):23–28.

25. Badri M, Lawn SD, Wood R. Short-term risk of AIDS or death in people infected with HIV-1 before antiretroviral therapy in South Africa: a longitudinal study. Lancet. **2006**; 368(9543):1254–1259.

26. May M, Sterne J a C, Sabin C, Costagliola D, Justice AC, Thiébaut R, et al. Prognosis of HIV-1-infected patients up to 5 years after initiation of HAART: collaborative analysis of prospective studies. AIDS. **2007**; 21(9):1185–1197.

27. Menzies NA, Cohen T, Lin HH, Murray M, Salomon JA. Population health impact and cost-effectiveness of tuberculosis diagnosis with Xpert MTB/RIF: a dynamic simulation and economic evaluation. PLoS Med. **2012**; 9(11):e1001347.

28. Wolbers M, Babiker A, Sabin C, Young J, Dorrucci M, Chêne G, et al. Pretreatment CD4 cell slope and progression to AIDS or death in HIV-infected patients initiating antiretroviral therapy - The CASCADE collaboration: A collaboration of 23 cohort studies. PLoS Med. **2010**; 7(2):1–9.

29. Rodriguez B, Sethi AK, VCheruvu VK, Mackay W, Bosch RJ, Kitahata M, et al. Predictive Value of Plasma HIV RNA Level on Rate of CD4 T-cell decline in untreated HIV infection. JAMA. **2006**; 296(12):1498–1506.

30. Lessells RJ, Mutevedzi PC, Iwuji CC, Newell M-L. Reduction in early mortality on antiretroviral therapy for adults in rural South Africa since change in CD4+ cell count eligibility criteria. J Acquir Immune Defic Syndr. **2014**; 65(1):e17-24.

31. Dowdy DW, Chaisson RE. The persistence of tuberculosis in the age of DOTS:

reassessing the effect of case detection. Bull World Health Organ. **2009**; 87(4):296–304.

32. Selwyn P a, Hartel D, Lewis V a, Schoenbaum EE, Vermund SH, Klein RS, et al. A prospective study of the risk of tuberculosis among intravenous drug users with human immunodeficiency virus infection. N Engl J Med. **1989**; 320(9):545–50.

33. Gilks CF, Godfrey-Faussett P, Batchelor BIF, Ojoo JC, Ojoo SJ, Brindle RJ, et al. Recent transmission of tuberculosis in a cohort of HIV-1-infected female sex workers in Nairobi, Kenya. Aids. **1997**; 11(7):911–918.

34. Carvalho ACC, Deriemer K, Nunes ZB, Martins M, Comelli M, Marinoni A, et al. Transmission of Mycobacterium tuberculosis to Contacts of HIV-infected Tuberculosis Patients. Am J Respir Crit Care Med. **2002**; 164(12):2166–2171.

35. Huang CC, Tchetgen ET, Becerra MC, Cohen T, Hughes KC, Zhang Z, et al. The effect of HIV-related immunosuppression on the risk of tuberculosis transmission to household contacts. Clin Infect Dis. **2014**; 58(6):765–774.

36. Hermans SM, Castelnuovo B, Katabira C, Mbidde P, Lange JMA, Hoepelman AIM, et al. Integration of HIV and TB services results in improved TB treatment outcomes and earlier prioritized art initiation in a large urban HIV clinic in Uganda. J Acquir Immune Defic Syndr. **2012**; 60(2):29–35.

37. Ngamvithayapong J, Yanai H, Winkvist a, Diwan V. Health seeking behaviour and diagnosis for pulmonary tuberculosis in an HIV-epidemic mountainous area of Thailand. Int J Tuberc Lung Dis. **2001**; 5(11):1013–1020.

38. Cohen KA, Abeel T, Manson McGuire A, Desjardins CA, Munsamy V, Shea TP, et al. Evolution of extensively drug-resistant tuberculosis over four decades: whole

genome sequencing and dating analysis of Mycobacterium tuberculosis isolates from KwaZulu-Natal. PLoS Med. **2015**; 12(9):1–22.

39. Merker M, Blin C, Mona S, Duforet-Frebourg N, Lecher S, Willery E, et al. Evolutionary history and global spread of the Mycobacterium tuberculosis Beijing lineage. Nat Genet. Nature Publishing Group; **2015**; 47(3):242–249.

40. Lew W, Pai M, Oxlade O, Martin D, Menzies D. Initial Drug Resistance and Tuberculosis Treatment Outcomes: systematic review and meta-analysis. Ann Intern Med. **2008**; 149:123–134.

41. Johnston JC, Shahidi NC, Sadatsafavi M, Fitzgerald JM. Treatment outcomes of multidrug-resistant tuberculosis: a systematic review and meta-analysis. PLoS One. **2009**; 4(9).

42. Holtz TH, Sternberg M, Kammerer S, Laserson KF, Riekstina V, Zarovska E, et al. Time to sputum culture conversion in multidrug-resistant tuberculosis: predictors and relationship to treatment outcome. Ann Intern Med. **2006**; 144(9):650–659.

43. Ahuja SD, Ashkin D, Avendano M, Banerjee R, Bauer M, Bayona JN, et al. Multidrug resistant pulmonary tuberculosis treatment regimens and patient outcomes: an individual patient data meta-analysis of 9,153 Patients. PLoS Med. **2012**; 9(8).

44. Dharmadhikari AS, Mphahlele M, Venter K, Stoltz A, Mathebula R, Masotla T, et al. Rapid impact of effective treatment on transmission of multidrug-resistant tuberculosis. Int J Tuberc Lung Dis. **2014**; 18(9):1019–1025.

45. Toczek A, Cox H, Cros P Du, Cooke G, Ford N. Strategies for reducing treatment default in drug-resistant tuberculosis: systematic review and meta-analysis. Int J

Tuberc Lung Dis. **2013**; 17(3):299–307.

46. Ahmad Khan F, Gelmanova IY, Franke MF, Atwood S, Zemlyanaya NA, Unakova IA, et al. Aggressive regimens reduce risk of recurrence after successful treatment of MDR-TB. Clin Infect Dis. **2016**; 63(2):214–220.

47. Borrell S, Gagneux S. Infectiousness, reproductive fitness and evolution of drug-resistant *Mycobacterium tuberculosis*. Int J Tuberc Lung Dis. **2009**; 13(12):1456–1466.

48. Billington OJ, McHugh TD, Gillespie SH. Physiological cost of rifampin resistance induced in vitro in *Mycobacterium tuberculosis*. Antimicrob Agents Chemother. **1999**; 43(8):1866–9.

49. Grandjean L, Gilman RH, Martin L, Soto E, Castro B, Lopez S, et al. Transmission of multidrug-resistant and drug-susceptible tuberculosis within households: a prospective cohort study. PLoS Med. **2015**; 12(6):1–22.

50. Weyer K, Brand J, Lancaster J, Levin J, Walt M Van Der. Determinants of multidrug-resistant tuberculosis in South Africa : results from a national survey. South African Med J. **2007**; 97(11):1120–1128.

51. Nhung N V., Hoa NB, Sy DN, Hennig CM, Dean AS. The fourth national anti-tuberculosis drug resistance survey in Viet Nam. Int J Tuberc Lung Dis. **2015**; 19(6):670–5.

52. Marin J-M, Robert CP. Importance sampling methods for Bayesian discrimination between embedded models. Front Stat Decis Mak Bayesian Anal. **2010**; :513–527.

53. Sharma A, Hill A, Kurbatova E, Walt M van der, Kvasnovsky C, Tupasi TE, et al. Estimating the future burden of multidrug-resistant and extensively drug-resistant

tuberculosis in India, the Philippines, Russia, and South Africa: a mathematical modelling study. Lancet Infect Dis. Elsevier Ltd; **2017**; 17(7):707–715.

54. Fojo AT, Kendall EA, Kasaie P, Shrestha S, Louis TA, Dowdy DW. Mathematical modeling of "chronic" infectious diseases: unpacking the black box. Open forum Infect Dis. **2017**; 4(4):ofx172.

55. Asefa A, Teshome W. Total delay in treatment among smear positive pulmonary tuberculosis patients in five primary health centers, Southern Ethiopia: a cross sectional study. PLoS One. **2014**; 9(7):e102884.

56. Storla DG, Yimer S, Bjune GA. A systematic review of delay in the diagnosis and treatment of tuberculosis. BMC Public Health. **2008**; 8:1–9.

57. Sreeramareddy CT, Panduru K V, Menten J, Ende J Van den. Time delays in diagnosis of pulmonary tuberculosis: a systematic review of literature. BMC Infect Dis. **2009**; 9:91.

CURRICULUM VITAE

Phillip Salvatore, SM
PhD Candidate
Johns Hopkins School of Public Health
615 North Wolfe Street, E6039
Baltimore, Maryland 21205
psalvat1@jhu.edu
908.303.2317

Education

April 2018 — **Doctor of Philosophy (PhD) in Molecular Microbiology & Immunology**
Johns Hopkins Bloomberg School of Public Health (Baltimore, MD)
Thesis Title: "A multidisciplinary investigation of TB: mathematical and experimental studies of natural history, drug resistance biology, and MDR-TB transmission"

May 2014 — **Master of Science (SM) in Epidemiology**
Harvard School of Public Health (Boston, MA)
Thesis Title: "Fitness costs of drug-resistance mutations in multidrug resistant *M. tuberculosis*: a household-based case-control study"

May 2010 — **Bachelor of Arts (BA) in Molecular Biology**, magna cum laude with honors
Colgate University (Hamilton, NY)
Honors Thesis Title: "Epigenetic programming in alcoholism targets the amygdala and hippocampus"

Research Experience

8/2014 - 4/2018 — **PhD Candidate in Molecular Microbiology & Immunology**
Johns Hopkins Bloomberg School of Public Health (Baltimore, MD)
Lab of David Dowdy, MD, PhD

→ Investigated methods to mathematically link TB natural histories with population outcomes, the biological mechanisms of pyrazinamide antibiotic action, and future trends in MDR-TB epidemics

→ Executed and optimized laboratory assays using affinity chromatography, protein purification, recombinant genetics, antibiotic inhibition and tolerance, mass spectrometry, and DNA sequencing

→ Performed computational simulation of TB epidemics using individual-based stochastic and compartmental deterministic mathematical models and Bayesian calibration algorithms using R©, Python, and Linux Shell scripts

→ Authored two primary research manuscripts for publication (published in the Journal of Infectious Disease in 2017 and submitted to the Proceedings of the National Academies of Science, respectively) and one review manuscript for publication (published in the Biomedical Sciences Reference Database in 2017)

→ Collaborated with the TB Program Strategy Team of the Bill and Melinda Gates Foundation to generate projections of the future MDR-TB epidemic to guide the organization's policy and TB strategy

8/2012- 5/2014 **SM Candidate in Epidemiology**
Harvard School of Public Health (Boston, MA)
Lab of Ted Cohen, MD, DPH

→ Investigated the impact of drug resistance-conferring mutations on the transmission and generation of secondary cases of TB in Lima, Peru

→ Analyzed pathogen-, patient-, household-level clinical, demographic, and DNA sequence data generated from a matched case-control study of 196 households nested in a cohort of 810 patients using SAS© and Stata©

→ Authored a primary research manuscript for publication (published in the Journal of Infectious Disease in 2016)

7/2012 - 5/2013 **Research Assistant in Global Health Equity**
Brigham and Women's Hospital (Boston, MA)
Lab of Chunling Lu, PhD

→ Investigated top-down and bottom-up methods of health sector costs tracking data in 21 local health facilities in rural Rwanda funded with a $15 million grant

→ Designed econometric methods for evaluating baseline existing capital in rural health centers with minimal tracking and accounting capabilities using Microsoft Access, SAS©, and Stata®

→ Authored a primary research manuscript for publication (published in PLoS Medicine in 2014)

6/2009 - 12/2009 **Undergraduate Scholar and Laboratory Technician**
National Institute on Alcohol Abuse and Alcoholism (Bethesda, MD)
Lab of Markus Heilig, MD, PhD

→ Selected to participate in a six-month, full-time, off-campus study at the NIH intramural laboratories

→ Investigated associations between alcohol dependence and epigenetic modifications in the rat brain and the effects of an experimental therapeutic pharmaceutical compound

→ Authored a two-chapter thesis on the effects of epigenetic mechanisms in the brain modulating alcohol dependency through stress responses and recall memory

→ Awarded Honors in Molecular Biology for outstanding independent research performed at the NIH Main Campus and Clinical Center

5/2008 - 8/2008 **Summer Undergraduate Research Intern in Biochemistry and Molecular Biology**
Pennsylvania State College of Medicine (Hershey, PA)
Lab of Ira Ropson, PhD

→ Investigated mechanics of protein folding via residue nucleation sites using non-conservative point mutations in the intestinal fatty acid binding protein

→ Cloned and induced bacterial protein production using recombinant plasmids followed by triple chromatographic column purification

→ Characterized mutant protein nucleation stability using serial chemical denaturation and quantified by fluorescence, circular dichroism, and NMR

→ Presented findings at a research symposium composed of medical and graduate school faculty, staff, and students and hospital staff

Teaching Experience

2018 **Lecturer and Teaching Assistant**
"Practical Epidemiology for Basic Scientists" offered in the Department of Epidemiology
Johns Hopkins Bloomberg School of Public Health (Baltimore, MD)

→ Co-led and instructed 32 graduate students enrolled in the course required by graduate students in the departments of Molecular Microbiology & Immunology, Environmental Health & Engineering, and Biochemistry & Molecular Biology

→ Provided 9 lectures covering the following topics: Cohort Study Designs; Case-Control & Cross-Sectional Study Designs; Measures of Association; Bias; Confounding & Effect Modification; Infectious Disease Epidemiology; and Syntheses

→ Designed and conducted 8 weekly lab and review sessions to reinforce lecture materials and provide exposure to primary scientific literature in epidemiology

→ Manage all electronic course materials, the course website, responses to student inquiries, as well as all problem sets, quizzes, exams, assignments, and grades

2017 **Additional Lecturer and Teaching Assistant**
"Practical Epidemiology for Basic Scientists" offered in the Department of Epidemiology
Johns Hopkins Bloomberg School of Public Health (Baltimore, MD)

→ Instructed 49 graduate students from the departments of Molecular Microbiology & Immunology, Environmental Health & Engineering, Biochemistry & Molecular Biology, and Epidemiology

→ Provided 5 lectures covering the following topics: Clinical Trials; Measures of Association; Bias; and Confounding & Effect Modification

→ Designed and conducted 8 weekly lab and review sessions

2016 **Teaching Assistant**
"Practical Epidemiology for Basic Scientists" offered in the Department of Epidemiology
Johns Hopkins Bloomberg School of Public Health (Baltimore, MD)

→ Instructed 55 graduate students from departments of Molecular Microbiology & Immunology, Environmental Health & Engineering, Biochemistry & Molecular Biology, as well as the Masters in Public Health program and the Johns Hopkins School of Medicine

→ Provided 2 lectures covering Measures of Association

Awards and Distinctions

2016 **Trainee in the Molecular and Cellular Basis of Infectious Diseases**
Johns Hopkins Bloomberg School of Public Health (Baltimore, MD)

2015 - 2017 **Hegner, Cort, Root Memorial Fellow in Immunology and Infectious Disease**
Johns Hopkins Bloomberg School of Public Health (Baltimore, MD)

2012 - 2014 **Mary E. Wilson and Harvey V. Fineberg Fellow in Infectious Disease Epidemiology**
Harvard School of Public Health (Boston, MA)

2009 - 2010 **National Institutes of Health/Colgate University Off-Campus Study Awardee**
Colgate University (Hamilton, NY)

2009 **βββ Biology Honors Society Inductee**
Colgate University (Hamilton, NY)

2007 **ΦΗΣ First Year Honors Society Inductee**
Colgate University (Hamilton, NY)

Public Health Practice & Volunteer Experience

9/2011 - 2/2012 **Technical Advisor for Guinea Worm Eradication**
The Carter Center (Chari-Baguirmi, Chad)

→ Directed all Guinea Worm prevention, detection, and treatment activities for two health districts in Chad with two hospitals, 18 health centers, and 976 villages across nearly 10,000 sq. mi. at the epicenter of the Chadian dracunculiasis outbreak

→ Liaised with Chadian Ministry of Health officials at national, regional, district, and local levels to conduct trainings, public education, reporting, and clinical assessment

→ Conducted daily site visits to at-risk villages for outbreak case detection, filter distribution, larvicidal water treatments, and public education and discussion forums

→ Implemented action plan supervising three doctors, nine nurses, 552 volunteers, and an operating budget of over $56,000

2/2011 – 9/2011 **Curriculum Editor and Health Programs Volunteer**
Tostan International (Dakar, Senegal)

→ Managed all technical health programs for an international NGO acclaimed for facilitating new social norms to end Female Genital Mutilation

→ Wrote, revised, and edited a six-month health training curriculum for non-formal education in villages and development programs still used today

→ Formulated evaluation criteria of community-led development education programs implemented in over 3,000 villages across ten African countries

10/2010 – 1/2011 **Community Health Agent**
US Peace Corps (Dosso, Niger)
→ Trained to communicate health education curricula entirely in local languages and to utilize village social norms and traditions in articulating fundamental messages

→ Evacuated rapidly from village post to a safe-haven post in Morocco following repeated and continuing terrorist attacks and abductions throughout the country

9/2007 – 5/2010 **EMT Crew Chief**
Southern Madison County Ambulance Corps (Hamilton, NY)
→ Volunteered as an EMT requiring life-saving medical skills, quick thinking, and action under pressure

→ Supervised six ambulance shift crews as the senior EMT on duty, including the instruction and training of new responders

Editorial and Press Activities

2016 - 2017 **Scientific Peer Reviewer**
The International Journal of Tuberculosis and Lung Disease (Paris, France)

2016 **Scientific Peer Reviewer**
The European Respiratory Journal (Sheffield, United Kingdom)

2015 **Scientific Peer Reviewer**
Trends in Tropical Medicine (São Paulo, Brazil)

2015 **Invited Interview**
TheVerge.com article "Mutations that make bacteria resistant to antibiotics might also make them deadlier" by Arielle Duhaime-Ross
Accessible at <https://www.theverge.com/2015/7/22/9015505/antibiotic-resistant-bacteria-study-infection-deadliness>

Professional Memberships

2017 - Present **American Society for Tropical Medicine and Hygiene**

2016 - Present **The International Union against TB and Lung Disease**

2014 - 2017 **American Society for Microbiology**

Professional Development

Training & Certifications:

Biosafety Level 3
Respiratory Protection
Introduction to Incident Command System (FEMA ICS-100)
ICS for Single Resources and Initial Action Incident (FEMA ICS-200)
Animal Care and Use
Basic Human Subjects Research
Laboratory Safety Preparation
Bloodborne Pathogens
Conflict of Interest & Commitment
Title IX Harassment Prevention

Software & Programming Proficiency

R
SAS
Stata
Python
Linux Shell Scripting
Inkscape Vector Design
Microsoft Word, Excel, Access, PowerPoint, & Outlook

Language Skills

Fluent in English (native speaker)
Professionally proficient in French (used as the primary language of employment from October 2010 – January 2012)
Trained in Nigerien Zarma/Djerma (October 2010 – January 2011)

Publications

Salvatore PP, Proaño A, Kendall EA, Gilman RH, Dowdy DW. Linking individual natural history to population outcomes in tuberculosis. J Infect Dis. 2017; 217(1): 112-121. DOI: 10.1093/infdis/jix555.

Salvatore PP, Zhang Y. Tuberculosis: Molecular basis of pathogenesis. Ref Modul Biomed Sci. 2017; 1–15. DOI: 10.1016/B978-0-12-801238-3.95697-6.

Salvatore PP, Becerra MC, Abel zur Wiesch P, Hinkley T, Kaur D, Sloutsky A, Cohen T. Fitness costs of drug resistance mutations in multidrug resistant *Mycobacterium tuberculosis*: a household-based case-control study. J Infect Dis 2016; 213(1): 149-155. DOI: 10.1093/infdis/jiv347.

Lu C, Tsai S, Ruhumuriza J, Umugiraneza G, Kandamutsa S, **Salvatore PP**, Zhang Z, Binagwaho A, Ngabo F. Tracking rural health facility financial data in resource-limited settings: a case study from Rwanda. PLoS Med. 2014; 11(12): e1001763. DOI: 10.1371/journal.pmed.1001763.

Research Presentations

Salvatore PP. How might fitness costs impact MDR-TB transmission? A comparison of two mathematical models. Oral presentation, The Johns Hopkins Center for TB Research Clinical and Epidemiology Seminars. Baltimore, MD, March 8, 2018.

Salvatore PP. Projecting MDR-TB in South Africa and Vietnam: How the evolution of drug resistance can shape the future of tuberculosis. Poster presentation, American Society of Tropical Medicine and Hygiene 66th Annual Meeting (ASTMH 2017). Baltimore, MD, November 5-9, 2018.

Salvatore PP, Becerra MC, Abel zur Wiesch P, Hinkley T, Kaur D, Sloutsky A, Cohen T. The case-control study as a novel tool to quantify the fitness costs of drug resistance mutations. Oral presentation, The 13th International Conference on Molecular Epidemiology and Evolutionary Genetics of Infectious Diseases (MEEGID XIII). Antwerp, Belgium, May 10-13, 2016.

Salvatore PP. Epigenetic programming in alcoholism targets the amygdala and hippocampus. The 2010 Colgate University Molecular Biology Honors Research Seminar. Hamilton, NY, April 15, 2010.

Salvatore PP, Dalessio PM, Ropson IJ. Effects of a non-conservative mutation on folding in a β-sheet protein. Poster presentation, The 2008 Pennsylvania State College of Medicine Summer Research Forum. Hershey, PA, August 18, 2008.